THREE-DIMENSIONAL TISSUE-ENGINEERED CANCER MODELS FOR TUMORIGENIC STUDIES AND DRUG-TESTING APPLICATIONS

by

Shantanu Pradhan

A dissertation submitted to the Graduate Faculty of
Auburn University
in partial fulfillment of the
requirements for the Degree of
Doctor of Philosophy

Auburn, Alabama
August 6, 2016

Keywords: breast cancer, PEG-fibrinogen, microfluidics, ECM-mimetic, matrix stiffness, anti-cancer drug testing

Approved by

Elizabeth A. Lipke, Chair, Mary and John H. Sanders Endowed Associate Professor of Chemical Engineering
Mario R. Eden, Joe T. & Billie Carole McMillan Professor of Chemical Engineering
Allan E. David, John W. Brown Assistant Professor of Chemical Engineering
David J. Riese, Professor of Drug Discovery and Development
Robert D. Arnold, Associate Professor of Drug Discovery and Development

Abstract

Cancer is one of the most prevalent diseases, affecting millions of people throughout the world in various forms. Significant multidisciplinary efforts are being conducted to improve detection, diagnosis and treatment of the disease. One important research focus is to identify key disease mechanisms which can be exploited for the development of efficient drugs, thereby reducing cancer recurrence, improving patient mortality and ensuring progression-free survival. The emerging field of cancer tissue engineering aims to provide platforms whereby cancer tissue can be closely reproduced and simulated in a three-dimensional (3D) *in vitro* setup, facilitating the study of the disease outside the body and testing efficacy of different drugs prior to translation in clinical trials. This research focuses on the development of 3D *in vitro* models of breast cancer, amongst other cancer types, which closely mimic the microenvironmental conditions of native cancer tissue, and ultimately facilitate the investigation of specific tumorigenic mechanisms and testing anti-cancer drug efficacy.

This work highlights the use of biomimetic PEG-based hydrogels for the encapsulation and long-term 3D culture of various cancer cell types and subsequent investigation of cancer cell behavior and disease progression within 3D hydrogel scaffolds and subsequent testing of anti-cancer drug efficacy. Chapter 1 introduces the current state of cancer tissue engineering, the use of various biomimetic materials for mimicking the native tumor microenvironment and different biofabrication techniques employed for the development of tissue-engineered cancer models and drug-testing. In Chapter 2, generation of a millimeter-scale breast cancer model via a novel dual-phase, surface tension-based fabrication method for generation of poly(ethylene

glycol diacrylate) (PEGDA) hydrogel millibeads and tumor millibeads encapsulating breast cancer cells is presented. Chapter 3 provides background on the use of fibrinogen coupled with PEGDA (PEG-fibrinogen, PF), and its use in creating the tumor microsphere model for encapsulation of breast cancer cells and investigation of subsequent tumorigenic characteristics with relation to spontaneously aggregated tumor spheroids formed via the hanging droplet method. In Chapter 4, the effect of matrix stiffness and physical properties of PF-based hydrogels on the 3D growth and behavior of three breast cancer cell types is investigated. In Chapter 5, a study establishing a microfluidic oncomimetic model for co-culture of vascularized endothelium, breast cancer cells and fibroblasts and subsequent drug-testing is reported.

Acknowledgments

I would like to thank Dr. Elizabeth A Lipke for her direction, guidance and mentorship on the successful culmination of my Ph.D. project and in the preparation of this dissertation. I would like to thank members of my lab group, specifically, Dr. Wen (Aaron) Seeto, Dr. Alexander Hodge, Samuel Chang, Dr. Petra Kerscher and Iman Hassani, amongst others for their assistance and advice in various aspects of my project. My heartiest gratitude to my undergraduate students, Jacob Clary, Chloe Chaudhury, Stephen Lee, Kelsey Henderson and Nidhi Goel, who have helped me significantly in experiments and data analysis for this study. I would like to specially acknowledge help from Dr. Michael Miller and Dr. Michael Meadows for experimental advice for my projects. I am grateful to Dr. B. Prabhakarpandian and the CFDRC team at Huntsville and Dr. Robert Arnold for collaborative assistance. I would like to thank Dr. Mario Eden, Dr. Allan David and Dr. David Riese for their willingness to serve on my committee and their technical guidance and support.

Lastly, I would like to thank my parents, Dr. Chandan K. Pradhan and Mrs. Kanika Pradhan and my sister, Shreya Pradhan for providing mental support and encouragement throughout the course of my Ph.D. work.

Table of Contents

List of Figures

List of Abbreviations

2D	Two-dimensional
3D	Three-dimensional
ANOVA	One-way Analysis of Variance
BCA	Bicinchoninic Acid
bFGF	Basic Fibroblast Growth Factor
CA	Chitosan Alginate
CAFs	Cancer-associated Fibroblasts
DAPI	4',6-Diamidino-2-Phenylindole
DMEM	Dulbecco's Modified Eagle's Medium
DNA	Deoxyribonucleic Acid
ECM	Extracellular Matrix
ECs	Endothelial Cells
EHS	Engelbreth-Holm-Swarm
EMT	Epithelial-Mesenchymal Transition
EPCs	Endothelial Progenitor Cells
FITC	Fluorescin Isothiocyanate
GAG	Glycos-amino-glycans
HA	Hyaluronic Acid
hBTECs	Human Breast Tumor-associated Endothelial Cells
HIF-1α	Hypoxia-inducible Factor 1α

HMDS	Hexamethyldisilazane
HNSCC	Head and Neck Squamous Carcinoma Cells
HPC	High Perfusion Chip
HUVECs	Human Umbilical Vein Endothelial Cells
I651	Irgacure® 651
IC_{50}	Half maximal Inhibitory Concentration
IDC	Invasive Ductal Carcinoma
IL-8	Interleukin-8
IPN	Inter-penetrating Network
iPSCs	Induced Pluripotent Stem Cells
LPC	Low Perfusion Chip
MCTS	Multicellular Tumor Spheroids
MMP	Matrix metalloprotease
MSCs	Mesenchymal Stem Cells
NC	Nuclear:Cytoplasmic
NEAA	Non-essential Amino Acids
NMR	Nuclear Magnetic Resonance
NVP	1-Vinyl-2-Pyrrolidinone
PBS	Phosphate Buffered Saline
PBT	Poly(butylene terephthalate)
PCL	Poly(ε-caprolactone)

PDMS	Poly(dimethyl siloxane)
PEG	Poly(ethylene glycol)
PEGDA	Poly(ethylene glycol) Diacrylate
PEGMA	Poly(ethylene glycol) Monoacrylate
PEOT	Poly(ethylene oxide terephthalate)
PF	Poly(ethylene glycol) diacrylate-fibrinogen
PGA	Poly(glycolic acid)
pHEMA	Poly(2-hydroxyethyl methacrylate)
PLA	Poly(lactic acid)
PLGA	Poly(lactic-co-glycolic acid)
PlGF	Placental Growth Factor
PVA	Poly(vinyl alcohol)
PVA/G	Poly(vinyl alcohol)/gelatin
RAD	Rotating Aerial Disk
ROI	Regions of Interest
SEM	Scanning Electron Microscopy
SMCs	Smooth Muscle Cells
TCEP-HCl	Tris (2-carboxyethyl) phosphine Hydrochloride
TEOA	Triethanolamine
TICs	Tumor Initiating Cells
TM	Tumor Microspheres

TME	Tumor Microenvironment
TRITC	Tetramethylrhodamine Isothiocyanate
TS	Tumor Spheroids
UV	Ultraviolet
VEGF	Vascular Endothelial Growth Factor

1. INTRODUCTION

Breast cancer is the most frequently diagnosed and leading cause of death in women throughout the world accounting for 25% of all cancer cases and 15% of all cancer deaths among females with an estimated 1.7 million cases and 521,900 deaths in 2012 (Torre et al. 2015). It is also the second leading cause of cancer deaths among women in the United States (Keller et al. 2011). Incidence rates in many developed countries have fallen in recent years due to improved awareness and better treatment facilities. However, in many developing countries, the incidence rates continue to rise due to several factors like poor quality of life and inadequacies in detection, treatment and in health infrastructure. Thus, finding effective methods of preventing new incidences, controlling the progression of the disease and reducing the number of deaths through improved medication is of paramount importance.

Tissue engineering aims at applying the principles and methods of chemical and biomedical engineering in the field of life sciences for the study of normal and pathological mammalian tissue, and the development of biological substitutes to restore, maintain, or improve tissue function. In recent times, this field has progressed towards modeling of diseases and pathological conditions both *in vitro* and *in vivo*. Specifically, cancer tissue engineering, a sub-discipline of this field, has been developed to provide platforms where various physiological aspects of the disease can be studied both *in vitro* and *in vivo* (Ricci et al. 2013, Horch et al. 2013). Advances in this field have facilitated the development of different biomimetic models that can recapitulate various features of the tumor tissue and its microenvironment, thereby allowing investigators to better understand mechanisms of disease initiation and progression (Hutmacher et al. 2009, Burdett et al. 2010).

Cancer is a not a single disease, but a group of physiological anomalies collectively referred under the umbrella term ‘cancer’. These anomalies work in conjunction with each other to produce a cascade of physiological disorders ultimately resulting in malignant and metastatic diseases. Cancer tissue engineering aims at simulating these physiological disorders either individually or synergistically, through the combination of biomimetic materials and different biofabrication techniques. The main features of cancer tissue that are closely replicated are tumor initiation, epithelial-mesenchymal transition (EMT), malignant progression, cancer cell migration, angiogenesis, hypoxia and metastasis, amongst others (Hanahan and Weinberg 2000, Hanahan and Weinberg 2011).

Biomimetic tissue-engineered cancer models and technologies offer high degree of spatial, temporal and structural precision in controlling the physical parameters and components characteristic of the native tumor microenvironment. These technologies help to bridge the discontinuity existing between two-dimensional (2D) and *in vivo* models. 2D models are limited in their ability to explore specific biological phenomena due to inability to replicate tissue-specific pathophysiology. *In vivo* animal models are limited by cost and the challenge of precisely controlling experimental variables (spatial, molecular, and physical) of the tumor microenvironment. To address these limitations, well-characterized 3D tissue-engineered models that incorporate tissue pathophysiology and complexity are needed within the cancer model continuum. The objective of this work is the establishment of such 3D tissue-engineered cancer models using biomimetic hydrogel-based materials and employing various fabrication techniques, which result in tissue-mimetics with higher degree of pathophysiological structure and function and can recapitulate essential characteristics of the native tumor microenvironment.

Overall, cancer tissue engineering lies at the interface of tissue engineering, cancer biology and chemical and biomedical engineering, each field offering its own advantages and applications to the sub-discipline, as shown in Figure 1.0. Cancer biology provides the basic knowledge with regard to cellular growth, cell signaling, and morphological, phenotypic and genotypic expression of cancer cells and subsequent investigations in cancer-related phenomena like EMT, angiogenesis and metastasis. Based on information provided through cancer biology, tissue engineering establishes biomimetic three-dimensional (3D) models and various biofabrication techniques for investigation of the disease both *in vitro* and *in vivo*. Finally, chemical and biomedical engineering provide the basis of material design and synthesis (for use in tissue-engineered models), and platforms for the analysis of disease models and network pathways. Through the combination of these approaches, the resulting field of cancer tissue engineering broadly encompasses the knowledge gained from cancer biology, and engineering principles from tissue engineering and biomedical engineering to produce holistic systems where in-depth knowledge of disease mechanisms and efficacy of anti-cancer treatment strategies can be obtained, thereby leading to more efficient targeting of the disease.

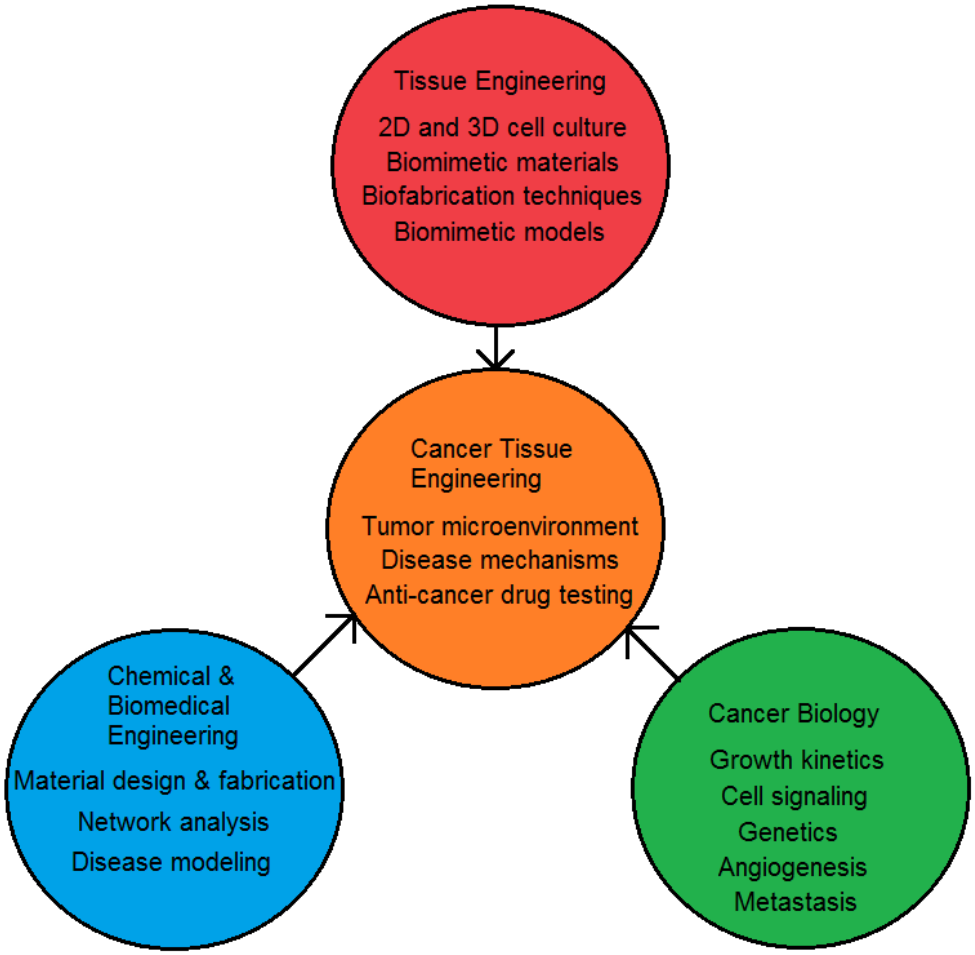

Figure 1.0: The broad scope of cancer tissue engineering. Schematic of the interface between three major fields of tissue engineering, cancer biology and chemical engineering that gives rise to cancer tissue engineering.

CHAPTER 1: Background

1.1 The Need for Tissue-engineered Cancer Models

Traditionally, cancer cells are cultured on 2D substrates for cellular investigations and drug-testing applications. However, due to inherent differences and poor physiological correlation between 2D cultured cells and cells *in vivo*, many candidate drugs fail to achieve the required standards of high efficacy and low toxicity (Imamura et al. 2015, Das et al. 2015). In 2D models, cancer cells lack microenvironmental cues and often, influence of other cell types typically found in the tumor microenvironment (TME) (Hutmacher et al. 2010). The presence of extracellular matrix (ECM) components and secondary cell types (e.g. fibroblasts, endothelial cells, immune cells etc.) lends increased chemo-resistance to cancer cells, both through intercellular signaling mechanisms and diffusion related mass transfer limitations (Kim and Tanner 2015). Incorporation of these factors in engineered tumor models provides better physiological context to cultured cells and helps obtain more relevant pre-clinical information with respect to drug testing (Hutmacher 2010). Figure 1.1 provides a comparative visualization of cancer cells cultured in 2D vs. 3D conditions. Specifically, the synergistic role of the range of factors present in the TME in influencing 3D cancer cell behavior and associated processes of epithelial-mesenchymal transition (EMT), tumor angiogenesis, cancer cell extravasation, intravasation and metastasis can be more accurately studied through the incorporation of biomimetic materials and associated cell types in the engineered models (Horch et al. 2013). In addition, the function of various factors of the TME in imparting chemo-resistance to cancer cells can also be studied using these tissue-engineered models (Hutmacher et al. 2010, Infanger et al. 2013).

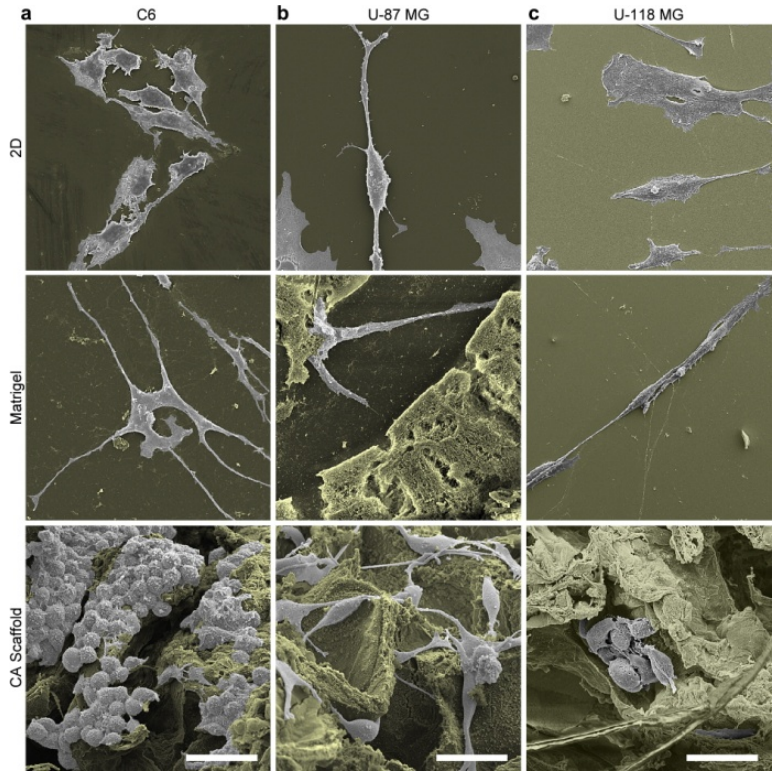

Figure 1.1: 2D and 3D cell culture. Differences in morphology of (a) C6, (b) U-87 MG and (c) U-118 MG glioma cells grown on 2D culture plates, Matrigel matrix, and CA scaffolds as visualized by SEM imaging. Cells in 2D cultured surfaces are flatter and more spread out while those in 3D culture are more rounded. Scale bars: 40 μm. Used with permission: (Kievit et al. 2010)

1.2 Biomimetic Materials for Cancer Cell Culture

The use of biomaterials and biomimetic scaffolds in 3D *in vitro* models has facilitated the bridging of the gap in correlation between 2D and *in vivo* models. These biomaterial-based models offer distinct advantages for cancer studies compared to 2D models, namely, 1) enabling of cell-matrix and cell-cell interactions, 2) induction of matrix mechanical stiffness effects on cancer cell growth characteristics, 3) incorporation of other cell types (e.g. fibroblasts, endothelial cells, immune cells and others) to recreate the tumor-stromal microenvironment,

4) involvement of specific cell-signaling mechanisms and related drug targets, 5) increase in tumor heterogeneity and 6) increase in drug-resistance. Each of these factors plays a critical role in simulating the pathophysiological complexities of native tumor tissue and ultimately providing clinically relevant information about anti-cancer drug efficacies (Alemany-Ribes and Semino 2014, Gill and West 2014, Seo et al. 2014, Chwalek et al. 2014, Yamada and Cukierman 2007). Biomaterials used in cancer research can be classified into three categories: 1) natural, 2) synthetic and 3) hybrid (combination of natural and/or synthetic materials). Natural polymers, obtained from animal or plant sources, include collagen, Matrigel, alginate and others; synthetic polymers include polylactide, polyglycolide, poly(ethylene glycol) (PEG) and their derivatives, while hybrid materials include PEG-conjugated proteins and biofunctionalized alginate amongst others. Each of these materials offers specific advantages which can be suitably employed to simulate the microenvironmental conditions of cancer tissue. One important category of biomaterials is hydrogels, which are cross-linked networks of chains of natural or synthetic polymers with the capability of high water absorption and facilitation of nutrient and cellular metabolite exchange. Mechanical and bio-chemical characteristics of hydrogels can be modulated by modifying either the individual polymer chains of the network or the cross-linking properties of the polymer chains in general (Nguyen and West 2002, Hoffman 2012). Specific bioactive moieties, including adhesive sites, growth factors and matrix metalloproteases (MMPs)-sensitive cleavage sites, can also be incorporated within hydrogel matrices to influence phenotype and growth of the encapsulated cancer cells *in vitro* (Nyga et al. 2011, Hutmacher 2010, Nguyen and West 2002). Overall, biomimetic hydrogels can be engineered chemically, mechanically and structurally, to modify cellular behavior with time and provide critical physiological context to 3D cultured cancer cells.

1.2.1 Natural Biomaterials

A number of naturally occurring proteins present in the tumor stroma contribute to the tumorigenic behavior of cancer cells via physico-mechanical interactions. These proteins include collagen, laminin, elastin and fibrinogen amongst others. In order to incorporate the biochemical properties of these natural ECM proteins, a number of naturally occurring biopolymers are used in 3D cancer models as described below.

Collagen I is the most abundantly occurring ECM protein found in the tumor stroma, imparting structural integrity and mechanical strength to the tissue mass. Collagen hydrogels, formed via physical crosslinking, have been used for the 3D encapsulation of various cell types including breast, prostate, endometrial and lung cancer cells (Szot et al. 2011a, Chen et al. 2012, Koutsilieris et al. 1994) (Fig. 1.2). In addition, collagen based gels have also been formed via enzymatic crosslinking with transglutaminase for the culture of breast, prostate and bone cancer cells (Fang et al. 2014). Metastatic MDA-MB-231 breast cancer cells within collagen I hydrogels demonstrated tissue-thickness dependent hypoxia and central necrosis when compared to standard 2D cultured cells (Szot et al. 2011a). In addition, breast and prostate cancer cells in collagen hydrogels for modeling bone metastasis exhibited higher MMP expression, symptomatic of enhanced metastatic potential (Koutsilieris et al. 1994, Bersini et al. 2014). Collagen hydrogels, due to their fibrillar nature, have also been used extensively for investigation of cancer cell migration via modulation of crosslinking density, fibril diameter and pore size. Increased stromal collagen density leads to higher tissue stiffness and is often predictive of malignant invasion. Elevated stromal collagen densities and associated fibrillar architecture promoted tumor formation, invasion and metastasis in *in vivo* mouse models (Provenzano et al. 2008), in *in vitro* mammary epithelial organoids (Cassereau et al. 2015) and in

self-aggregated tumor spheroids (Guzman et al. 2014). Specifically, modulation of fibrillar density and pore size was shown to impact directionality, cell displacement (Guzman et al. 2014, Bordeleau et al. 2013), persistence and morphological phenotype (Sapudom et al. 2015).

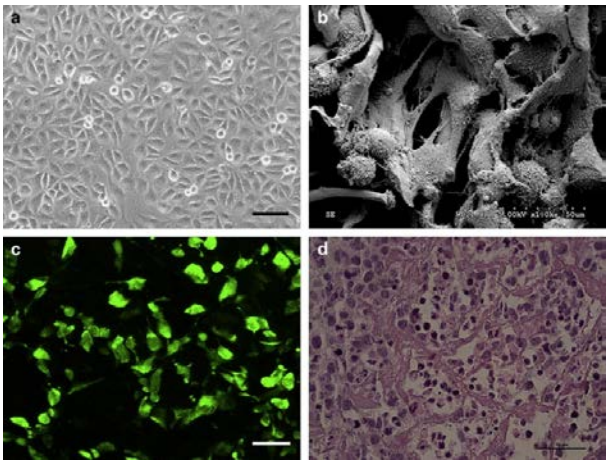

Figure 1.2: Collagen matrices for cancer cell culture. (a) Non-metastatic MCF7 cells cultured in 2D exhibit epithelial sheet-like morphology. In contrast, (b) SEM and (c) confocal images indicate diversified morphologies of MCF7 cells when cultured in 3D collagen scaffolds. (d) Hematoxylin-eosin staining of 3D collagen scaffolds cultured with cells show a multi-layer cell structure. Scale bar: 50 μm. Used with permission: (Chen et al. 2012).

Matrigel, a basement membrane composite secreted by Engelbreth-Holm-Swarm (EHS) mouse sarcoma cells, has also been extensively used as a biomaterial for cancer cell culture (Kleinman and Martin 2005, Benton et al. 2014). Primarily comprised of collagen type IV, laminin, perlecan, entactin and other proteases and growth factors, Matrigel significantly promoted tumorigenic growth and invasive morphologies of various cancer cell types both *in vitro* (Yeung et al. 2010, Sasser et al. 2007) and *in vivo* (Topley et al. 1993, Olsen et al. 2010). Specifically, Matrigel enhanced breast cancer cell invasion in co-culture with human bone marrow stromal cells (Sasser et al. 2007) and stromal fibroblasts (Pinto et al. 2014). Another useful application of Matrigel is in invasion-based assays for investigation of cancer cell

migration (Yu and Machesky 2012, Zhu, Liang, et al. 2015, Kramer et al. 1986) and morphological aggressiveness (Bae et al. 1993).

Alginate, derived from seaweed, is another natural biopolymer used in cancer cell studies. Alginate is composed of repeating units of α-L-guluronic acid and β-D-mannuronic acid and has been used as a thermally stable cold setting gel for cancer cell encapsulation (Workman et al. 2014, Kingsley et al. 2013). It exhibits a high water holding capacity and high porosity, and its physico-chemical properties like pH, molecular weight, mechanical and ionic strength can be tuned via modulation of relative concentration of the two monomer units (Draget et al. 1997, Xu and Burg 2007). Alginate was used for the 3D hydrogel encapsulation of lung cancer cells (Godugu et al. 2013), human leukemic cells (Thao et al. 2012), mouse breast cancer cells (Raof et al. 2011) and for enrichment of cancer stem cells from hepatocellular and squamous cell carcinoma cell lines (Xu, Liu, et al. 2014). In addition, alginate hydrogels with modulated mechanical stiffness (soft (21 kPa), moderate (70 kPa) and hard (105 kPa)) were used to investigate tumor-initiating features of head and neck squamous cell carcinoma cells (Liu, Liu, Xu, et al. 2015) and tumorigenic characteristics in hepatocellular carcinoma cells (Liu, Liu, Xie, et al. 2015). Agarose, a biopolymer similar to alginate and composed of D-galactose and 3,6-anhydro-L-galactopyranose, has also been used for the 3D encapsulation of mouse renal carcinoma cells (Smith, Gazda, Conn, Jain, Asina, Levine, Parker, Laramore, Martis, Vinerean, David, Qiu, Cordon-Cardo, et al. 2011, Smith, Gazda, Conn, Jain, Asina, Levine, Parker, Laramore, Martis, Vinerean, David, Qiu, North, et al. 2011) and MCF7 breast cancer cells (Vantangoli et al. 2015).

Hyaluronic acid (HA), a prominent member of the GAGs family, has also been investigated for its role in cancer progression. Composed of repeating units of D-glucuronic acid

and D-N-acetylglucosamine, it is known for its high molecular weight and presence in a wide range of tissue ECM (Laurent and Fraser 1992). HA hydrogels were used for the 3D culture of renal carcinoma cells for bone metastasis (Pan et al. 2015), study of invasive behavior of prostate cancer cells (Gurski et al. 2012), recapitulation of prostate cancer spheroid microenvironment (Xu et al. 2012) and 3D invasion of a wide range of cancer cell types from both primary and metastatic tumors (David et al. 2004). Low molecular weight HA promoted invasion and metastasis of breast cancer cells and represented a good prognostic indicator of breast cancer progression (Wu, Cao, et al. 2015). U87 astrocytoma cells grown in 3D HA hydrogel displayed enhanced expression of cancer stem cell markers including Nestin, CD44 and CD133 (Martinez-Ramos and Lebourg 2015).

Silk fibroin, usually obtained from silk worm species *Antheraea mylitta* and *Bombyx mori*, have been established as a suitable biomaterial for the culture of different cancer cell types including those from breast, prostate (Talukdar et al. 2011), osteosarcoma (Tan et al. 2011) and hepatocellular carcinomas (Kundu et al. 2013) (Fig. 1.3). Silk fibroin scaffolds were used for investigation of breast and prostate cancer metastasis to bone, lung and liver (Seib et al. 2015, Kwon et al. 2010a). Silk fibroin was also electrospun into cryogenic scaffolds for 3D culture of squamous carcinoma cells (Bulysheva et al. 2013).

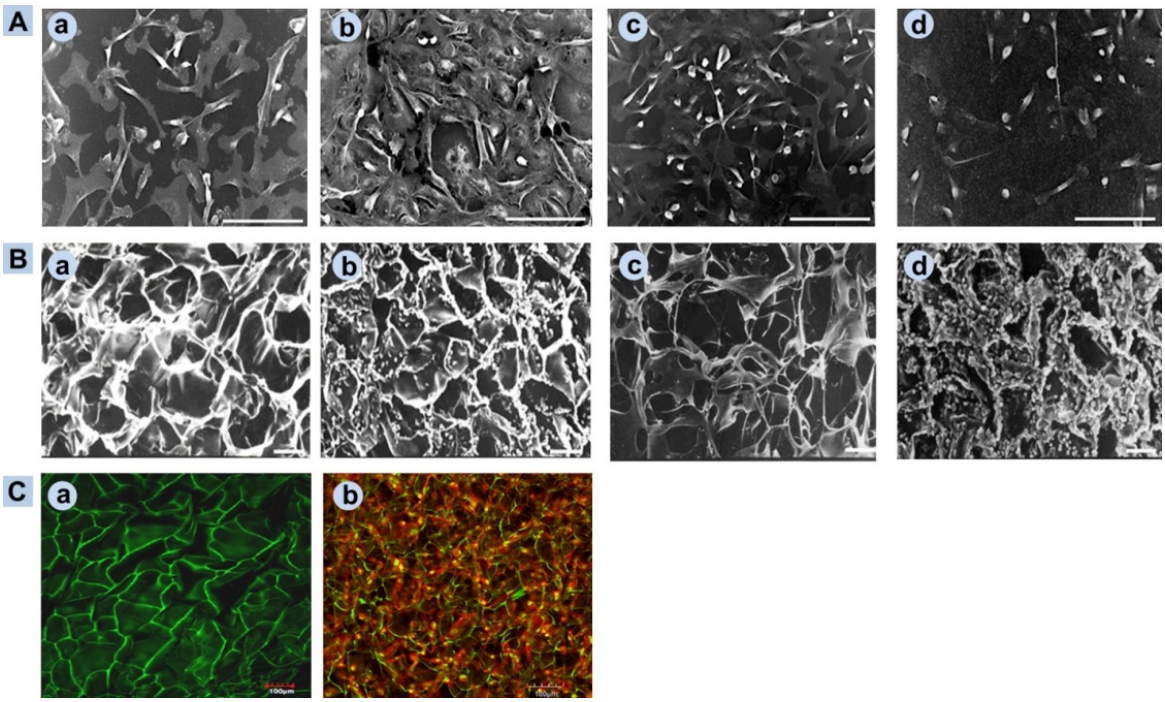

Figure 1.3: Silk fibroin matrices for cancer cell culture. (A) Metastatic MDA-MB-231 human breast adenocarcinoma cells cultured on different 2D matrices: a) tissue culture plate, b) 2D Matrigel, c) *A. mylitta* silk fibroin 2D film, d) *B. mori* fibroin 2D film; (B) a) *B. mori* fibroin scaffold without cells, b) *B. mori* scaffold seeded with MDA-MB-231 cells, c) *A. mylitta* fibroin scaffold without cells, d) *A. mylitta* fibroin scaffold seeded with MDA-MB-231 cells cultured for 5 days. (C) Confocal images of a) *A. mylitta* 2% silk fibroin scaffold, b) scaffold with MDA-MB-231 cells cultured with actin filaments (red) and nuclei (green). Scale bars represent 100 μm. Used with permission: (Talukdar et al. 2011).

Other natural biomaterials used in 3D cancer cell culture include chitosan and fibrin. Chitosan scaffolds were used for the 3D culture of MCF7 cells, with a higher degree of swelling and acetylation of chitosan polymer promoting cell attachment and growth kinetics (Dhiman et al. 2004). Fibrin gels of low stiffness (90 Pa), obtained by crosslinking of naturally occurring fibrinogen with thrombin, were used for the 3D culture of various human and mouse cancer cell

types, which promoted cancer stemness and formation of tumor spheroids with upregulation of stem cells markers including CD133, Nestin, Bmi-1 and c-kit (Liu et al. 2012, Tan et al. 2014).

Overall, a wide range of natural materials obtained both from plant and animal sources have been utilized for 3D culture of cancer cells and subsequent investigation of tumorigenic phenomena including invasiveness, metastasis and expression of stem cell-like characteristics, thereby providing reliable and scalable culture platforms for cancer research.

1.2.2 Synthetic Biomaterials

Though natural biomaterials provide good physiological context and facilitate biological signaling mechanisms in 3D cultured cancer cells, they suffer from certain limitations including batch-to-batch variability, low mechanical stiffness (0.1-10 kPa) and inconsistency in presentation of bioactive ligands in 3D matrices. In order to overcome these limitations, synthetic biopolymers have been developed as a substitute for natural materials. These polymers include poly(ethylene glycol) (PEG), poly(ε-caprolactone) (PCL), poly(vinyl alcohol) (PVA), poly(glycolic acid) (PGA), poly(lactic acid) (PLA) and their derivatives. Due to lack of bioactive sites, some synthetic materials including PEG need to be conjugated with biomimetic ligands such as short peptide sequences or larger proteins to provide sites for cell adhesion and matrix degradation and to facilitate cell-ECM interactions.

Conjugated PEG-based hydrogels can be fabricated via photo-polymerization and their physico-chemical properties (mechanical strength, pore size, porosity and cell attachment sites) altered by changing the molecular weight, cross-linking density, concentration and chemical modifications of PEG chains (Zustiak and Leach 2010, Kloxin et al. 2010, Kloxin et al. 2009a). PEG provides a “blank slate” into which various bioactive moieties can be incorporated via

covalent coupling to individual PEG chains. These moieties include specific peptide sequences mimetic of fibronectin (RGDS, REDV), laminin (YIGSR, IKVAV) and collagen (DGEA) for cellular adhesion (Nguyen and West 2002, Zhu 2010) and proteolytically-degradable sequences such as KCGPQG↓IWGQCK, GCYK↓YNRCG (derived from Collagen Type I, sensitive to MMP-1, -2, -3, -7, -8, and -9) (Leight et al. 2015, Raeber et al. 2005, Gill et al. 2012, Singh et al. 2014). Unmodified PEG hydrogels were used for the 3D encapsulation and culture of MCF7 human breast cancer and 4T1 mouse breast cancer cells (Pradhan et al. 2014, Yang et al. 2013b). Further, PEG hydrogels with conjugated CD44-binding peptide and modulated matrix stiffness were used for investigation of cancer stem cell markers and tumorsphere formation for various cancer cell types (Jabbari et al. 2015, Yang et al. 2013a). RGD- and YIGSR-conjugated PEG hydrogels supported the growth and tumorigenic signaling of normal and cancerous mammary epithelial cells (Weiss et al. 2012). Relative combination of adhesive PEG-RGDS and degradable PEG-PQ-PEG hydrogels, with modulated stiffness (21-55 kPa), degradability and adhesion were used for 3D culture of lung adenocarcinoma cells and subsequent investigation of epithelial morphogenesis and EMT (Gill et al. 2012). Biofunctionalized PEG hydrogels were also used for mimicking tumorigenic microenvironment of glioblastoma (Wang et al. 2014) and prostate cancer (Sieh et al. 2012), and for investigation of cell migration characteristics of fibrosarcoma cells (Singh et al. 2014).

In addition to PEG-based hydrogels, synthetic materials including PGA, PLA, PVA and PCL have also been used in cancer cell studies. The components of these polymers are derived from natural metabolites; hence, they are biodegradable, biocompatible *in vitro* and able to provide critical biological cues to encapsulated cells. Also, PGA has a higher rate of degradation compared to PLA, hence PGA is used as a co-monomer with PLA to form

poly(lactic-co-glycolic acid) (PLGA) to control the rate of degradation of the fabricated scaffolds (Xu and Burg 2007). Porous PLGA and PLA microparticles were fabricated via a solvent evaporation technique for use as scaffolds for MCF7 breast cancer cell culture, with incorporation of PVA demonstrating improved cell adhesion and growth (Sahoo et al. 2005). In addition, PLGA was also used for making cryopreservable, tumorigenic 3D scaffolds using a water-oil emulsion technique for culture of MCF7 cells (Kang and Bae 2009) and porous sponges using a supercritical CO_2 gas-foaming method for culture of Hep3B hepatocellular carcinoma cells (Zhu et al. 2008) (Fig. 1.4). In another model, 3D Ewing sarcoma tumors were formed in porous electrospun PCL scaffolds to mimic the bone microenvironment, with cancer cells exhibiting morphology, growth kinetics, and protein expression profiles close to native tumors (Fong et al. 2013).

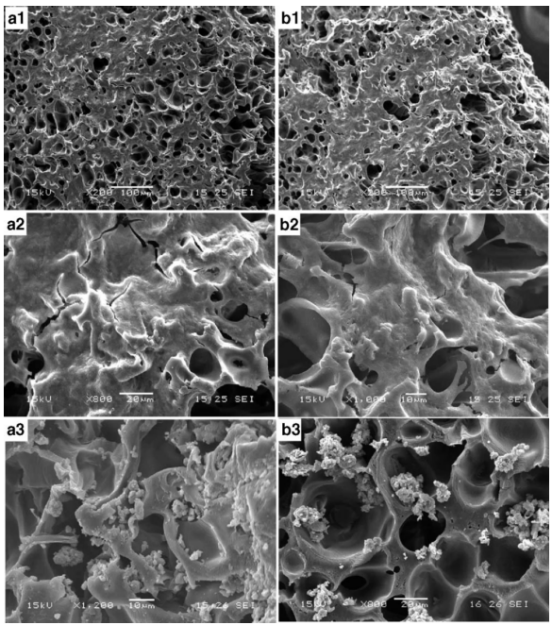

Figure 1.4: Synthetic PLGA scaffolds for cancer cells culture. SEM images of Hep3B cells cultured on (a) PLGA 50:50 and (b) PLGA 85:15 sponges; (a1 and b1) cells grown on the outer surfaces of the PLGA sponges; (a2 and b2) magnified images of the cells grown on the outer

surfaces; and (a3 and b3) cells grown on the inner pores of the PLGA sponges. Used with permission: (Zhu et al. 2008)

Overall, synthetic biomaterials have significantly facilitated the 3D culture and investigation of a wide range of cancers, by providing a uniform, controlled platform with modulated substrate characteristics and devoid of heterogeneity arising from biological factors.

1.2.3 Hybrid Biomaterials

Although natural and synthetic biomaterials provide important biological context to 3D cultured cancer cells, due to specific inherent limitations, these materials independently lack the ability to accurately present true tumor microenvironmental cues. For example, alginate by itself lacks adhesive moieties for cellular attachment; hence it is coupled with chitosan (Phan-Lai et al. 2013, Florczyk et al. 2012) or fibronectin-mimetic peptide sequence RGD (Fischbach et al. 2009) to provide a more cell-permissive matrix for cancer cell culture. Specifically, chitosan-alginate (CA) scaffolds were used for the 3D culture of mouse and human glioma cells, demonstrating enhanced tumorigenic growth *in vitro* and *in vivo* (Kievit et al. 2010) and enrichment of CD133+ glioblastoma stem cells with associated expression of stem cell markers (Kievit et al. 2014). In addition, RGD-alginate scaffolds promoted tumorigenic morphology and angiogenic expression of oral squamous cell carcinoma cells via integrin engagement (Fischbach et al. 2009) and further regulation of hypoxia and global changes in gene expression (DelNero et al. 2015). Alginate has also been combined with Matrigel to form interpenetrating network (IPN) structured hydrogels for investigation of malignant progression of normal mammary epithelium. The stiffness of the IPN matrix was controlled by modulation of relative Matrigel concentration or enhanced calcium crosslinking of alginate without affecting pore structure or ligand

accessibility. Addition of RGD ligands to alginate-Matrigel IPN matrix was used to alter ECM composition. Increasing matrix stiffness induced malignant phenotype of normal mammary epithelial cells which was abrogated by addition of adhesive ligands via β4 integrin-mediated mechanotransduction (Chaudhuri et al. 2014).

Synthetic PEG and its derivatives have been combined with other natural materials such as collagen and Matrigel for the fabrication of hybrid scaffolds. By reinforcing collagen fibers with poly(ethylene glycol) di-(succinic acid N-hydroxysuccinimidyl ester), hydrogels of higher stiffness (4.0 kPa vs 0.7 kPa) were obtained demonstrating proliferation, morphology and proangiogenic activity of HepG2 hepatocellular carcinoma cells (Liang et al. 2011). Matrigel combined with poly(ethylene glycol) diacrylate (PEGDA) and poly(ethylene glycol) monoacrylate (PEGMA) in varying concentrations supported differential growth and branching morphology of normal and tumor mammary epithelial organoids. Addition of α-CDYRGDS adhesive ligand to PEG-Matrigel promoted dissemination of single cells from the epithelial cluster and increasing stiffness with additional PEG moieties prevented branching morphogenesis of both normal and tumor organoids (Beck et al. 2013). Matrigel was also combined with another synthetic polymer, poly(2-hydroxyethyl methacrylate) (pHEMA) to form sphere-templated scaffolds for the culture of various prostate cancer cell types (Long et al. 2014).

Examples of other hybrid biomaterials include chitosan coupled with silk-fibroin for the culture of hepatocellular carcinoma cells (She et al. 2008) and with gelatin for 3D culture of lung carcinoma, breast adenocarcinoma, cervical carcinoma and osteosarcoma cells (Arya et al. 2012). Collagen hydrogels reinforced with increasing concentrations of agarose were used to modulate elasticity of bioengineered scaffolds for the culture of glioblastoma cells. Incorporation of agarose introduced dense mesh-like structures within collagen fibers that ultimately induced

mesenchymal-to-amoeboid transition in cell motility and reduced invasion of glioma cells (Ulrich et al. 2010). In another study, the effect of micro-scale scaffold architecture on the growth and function of pancreatic ductal adenocarcinoma was also investigated. Poly(vinyl alcohol)/gelatin (PVA/G) and poly(ethylene oxide terephthalate)/poly(butylene terephthalate) (PEOT/PBT) copolymers were used to form scaffolds using three different techniques: emulsion and freeze-drying, compression molding followed by salt leaching, and electrospinning. In comparison to PEOT/PBT fiber scaffolds, PVA/G and PEOT/PBT sponge-like scaffolds promoted higher aggregate formation and MMP secretion similar to native cancer tissue, thereby demonstrating the role of matrix architecture on cancer cell morphology and aggressiveness (Ricci et al. 2014).

Overall, hybrid biomaterials provide combinatorial advantages of both natural and synthetic materials in the fabrication of bioengineered scaffolds of 3D cancer cell culture. While incorporating the biomimetic characteristics of natural materials essential for cellular growth, morphology and function, hybrid materials also retain the ease of synthesis, reproducibility and low batch-to-batch variability of synthetic materials. Thus, hybrid biomaterials can be suitably produced in a scalable manner and applied for use in 3D cancer studies.

1.3 Tissue-engineered Cancer Models

Several aspects of native tumors need to be replicated in *in vitro* models for achieving close physiological relevance, the chief among them being metastasis and angiogenesis, which can be achieved by the modulation of the cell-cell and cell-ECM interactions *in vitro* (Morales and Alpaugh 2009, Kwon et al. 2010b, Wang et al. 2005). Metastasis is initiated by cancer cells with a high proliferation rate and high matrix degradation abilities which are able to invade

through the surrounding stroma and extravasate into blood capillaries (Langley and Fidler 2011). The matrix stiffness, incorporation of specific biological moieties, the tumorigenic nature and invasive potential of the cancer cells can be enhanced by altering the biochemical and mechanical properties of the surrounding ECM, thereby influencing their metastatic potential.

Hypoxia and angiogenesis experienced in tumor tissue are also correlated with each other. As a result of altered cell phenotype and cell metabolism, high cell proliferation rates, and non-uniformity in nutrient and waste exchange, hypoxia is frequently experienced by many cells found within the tumor tissue. This triggers a cascade of events whereby hypoxia-inducible factor (HIF)-1α is released by the cells in response to the hypoxic environment, causing the release of angiogenic growth factors and cytokines including VEGF (vascular endothelial growth factor) (Roskoski 2007) (Shweiki et al. 1995), bFGF (basic fibroblast growth factor) (Farhat et al. 2012), IL-8 (interleukin 8) (Xu et al. 2012) and others, both by cancer cells and surrounding stromal fibroblasts (Li and Lu 2011) (Kalluri and Zeisberg 2006, Räsänen and Vaheri 2010). The release of angiogenic factors leads to the migration of endothelial cells (ECs) (Oudar 2000) and endothelial progenitor cells (EPCs) (Bourhis et al. 2010, Ehrbar et al. 2005) towards the cancer tissue resulting in the formation of blood vessel-like structures (Melero-Martin and Dudley 2011). Simulating these phenomena, either individually or in conjunction with each other, is one of the main challenges of cancer tissue modeling. In the following sections, the current state-of-the-art 3D models developed to investigate the different hallmarks of cancer and related phenomena including angiogenesis, invasion and metastasis are presented.

1.3.1 Cancer Cell Culture using 3D models

Conventional 3D models can be grouped into two major categories: 1) cells embedded within a layer of bioactive matrix and 2) cells organized as multicellular aggregates or spheroids. Combinations of the two groups have also been explored. Cells encapsulated within biomimetic matrices can also self-assemble into multicellular aggregates within these scaffolds during culture over time. These models can be fabricated with a single cancer cell line or with secondary cell lines co-cultured with cancer cells (Kimlin et al. 2011). With recent advances in technology, newer models are being developed to extend the limits and capabilities of conventional 3D tumor models beyond those classified above.

In pseudo 3D models, where cells are cultured on the surface of a bioactive matrix, valuable information can be obtained regarding the invasive and metastatic potential of tumor cells, migration mechanism and their cellular interactions. In an invasion assay, intra-epithelial tumor cells migrated through HEK cell layers grown on the surface of human de-epidermalized dermis. (Alt-Holland et al. 2008). Cancer cells cultured on the surface of biomimetic matrices can provide information regarding integrin-mediated cell-matrix interactions and influence of matrix stiffness on cancer cell behavior. Most commonly, polyacrylamide gels, coated with collagen, and with controlled stiffness have been used for investigation of 3D cancer cell behavior (Fischer et al. 2012). In addition, micropatterning of ECM surfaces for obtaining spatial control of 3D cancer cell culture has also provided important information regarding cell adhesion, migration and cell-matrix interactions (Théry 2010).

The first category involves encapsulation of cells within a bioactive matrix for 3D cell culture. As discussed earlier, a variety of biomimetic materials have been used to fabricate scaffolds for 3D growth and culture of cancer cells, whereby the cells are able to migrate through

the interstitial spaces of the porous scaffolds. The scaffolds also typically contain MMP-sensitive sites allowing cells to degrade the matrix, proliferate and gradually fill the internal spaces of the scaffolds. As before, encapsulation can either include cancer cells alone or in co-culture with tissue-specific cell types. Using these models, investigators can study the interactions of cancer cells with the surrounding microenvironment and characterize their growth and phenotypic behavior.

Models that enable co-culture of multiple cell types allow for the study of the potential role of the secondary cells (Hanahan and Coussens 2012, Miki et al. 2012) and tumor stroma (Pietras and Ostman 2010, Shieh 2011) in the promotion or inhibition of the tumorigenic activity of the cancer cells. To study the process of blood vessel formation, endothelial cells can be co-cultured with cancer cells and formation of branching networks of tubules, indicative of the early angiogenic process, can be quantified. In one study, the process of vascular morphogenesis in decellularized ECM obtained from the co-culture of breast cancer cell lines and fibroblasts was investigated; the presence of fibroblasts with metastatic cells was found to have a stimulatory role in formation of capillary-like structures with improved angiogenic properties (Hielscher et al. 2012). Co-culture of basal and luminal non-invasive breast cancer cells with mammary fibroblasts induces their conversion to a more malignant invasive phenotype through reorganization of deposited extracellular collagen fibrils (Dang et al. 2011). Heterotypic adhesions between cancer cells and fibroblast mediated by atypical cadherins may also play a role in early metastasis (Apostolopoulou and Ligon 2012). Fibroblasts also regulate morphological features and provide increased chemoresistance to cancer cells in co-culture (Li and Lu 2011). Co-culture with embryonic stem cells or embryonic stem cell-conditioned medium

have been shown to have an inhibitory effect on the proliferation, migration and spheroid forming ability of metastatic breast cancer cells (Raof et al. 2011).

The second category involves culturing cancer cells as multicellular tumor spheroids (MCTS). MCTS are either grown in culture media or embedded within a bioactive matrix to simulate the microenvironmental tumor conditions *in vivo* (Ho et al. 2010, Carlsson and Nederman 1989). They can be formed with cancer cells only or in conjunction with other cell types found in the vicinity of the native tumor tissue. MCTS are able to replicate many of the cellular and histological characteristics found in native tissue. For example, Ewing tumor cells cultured as spheroids were better able to replicate the signaling mechanism of primary tumors as compared to 2D cultured cells with respect to morphology, proliferation and expression of ERK1/2, AKT and cyclin D1 (Lawlor et al. 2002).

Different methods have been developed for the formation of tumor spheroids including spontaneous cell aggregation both in liquid overlay culture and in spinner flasks, and biomaterial encapsulation (Kim et al. 2004, Hirschhaeuser et al. 2010a). Continuous research is being conducted to develop advanced models and fabrication methods for 3D cell culture. One recent method involves the use of a rotating wall vessel under simulated microgravity with micro-carrier beads, where cancer cell alone or in co-culture with multiple cell types can be used to form aggregates (Jessup and Frantz 2000, Rhee et al. 2001). Human prostate cancer cells co-cultured with bone fibroblasts showed significant chromosomal changes, altered growth profiles, changes in response to androgens, estrogens, growth factors with enhanced tumorigenicity and metastatic potential (Rhee et al. 2001). Another recently developed method is a novel mini-bioreactor with a rotating aerial disk (RAD) design. Its enhanced cell culture media-recirculation properties allowed improved oxygen diffusion and faster re-organization of

mouse lymphoma cells into 3D colonies, resulting in decreased mitochondrial activity in the cultured cells, indicating a quiescent cytoplasmic activity more similar to native tumor cells (Thouas et al. 2008).

1.3.2 Modeling of Tumor Angiogenesis

Some of the prominent methods of modeling tumor angiogenesis involve the use of PEG-based hydrogels, alginate and/or other materials which can conditionally release entrapped growth factors that stimulate the encapsulated cells to undergo early angiogenic processes. Spatio-temporal simulation of angiogenesis can be achieved by varying the combination and concentration of growth factors delivered as well as the scaffolding design. This enables investigation of multiple angiogenic aspects of the cellular microenvironment, including chemotactic cell migration through the matrix, interaction between multiple cell types, response of cancer cells to gradient-driven differences in specific factors and biological mechanisms driving cancer cell migration and invasion (Verbridge, Chandler, et al. 2010). Endothelial cells encapsulated within 3D scaffolds can also be studied for the phenomena of cell adhesion, migration towards cancer cells, organization into tubular structures and vessel stabilization and maturation.

In one study, human microvascular endothelial cells were co-cultured with MDA-MB-231 breast cancer cells within bilayered, collagen I hydrogels to observe for angiogenic sprouting (Szot et al. 2013). Co-culture of HUVECs with oral cancer cells in alginate hydrogels in a controlled oxygen environment helped modulate hypoxic conditions within the engineered tumors. VEGF and IL-8 levels in this model were dependent upon oxygen levels in environment, location within the tumors and their size (Verbridge, Choi, et al. 2010).

Thus angiogenesis can be modeled in 3D cultures by exploiting the cooperative interaction between cancer cells and their surrounding microenvironment. Varying tumor cells' distances from surrounding microvasculature to create cultures in different series of progression with spatio-temporal variation can shed light on the invasive and angiogenic capability of the tumor cells. The composition of the ECM can also be altered to incorporate different proteins and related peptide sequences to help understand the specific interactions between cytokines and secreted factors in the progression of disease, including angiogenesis and subsequent metastasis (Ghajar and Bissell 2010).

1.3.3 Modeling of 3D Metastasis

Metastasis has been widely modeled in 2D and 3D cultures and extensive knowledge has been gained about the mechanisms by which tumor cells detach from the primary site, traverse to distant locations in the body, adhere and invade into the secondary site through matrix degradation and repopulate the site with newly proliferating cells, especially in the bone, brain, liver and lungs (Langley and Fidler 2011). 3D extravasation models have been developed which can help identify highly metastatic and motile cancer cells and their interactions with endothelial cells and the basal matrix during transendothelial migration (Brandt et al. 2005). These models have also provided extensive insight into the underlying cellular mechanisms related to epithelial-mesenchymal transition (EMT), thereby providing a platform for drug screening processes (Li et al. 2011).

MCF7 and MDA-MB-435 breast cancer cells cultured in a modified Boyden chamber were observed for cell migration and invasion. The ability of cells to migrate through control (migration) or invade through Matrigel-coated filters (invasion) was measured within the Boyden

chamber. N-cadherin-expressing cells migrated more efficiently, with increased invasion of Matrigel, and adhered more efficiently to endothelial cell monolayers (Hazan et al. 2000). To study the bone metastasis of prostate cancer, different options available for the 3D co-culture of prostate cancer cells and osteoblasts, have been surveyed (Wang et al. 2005). Prostate cancer PC3 cells cultured within 3D matrices made of silk fibroin and coupled with BMP-2 showed significant increase in DNA content and gene expression indicative of cell proliferation and metastatic phenotype of the cultured cells in the presence of BMP-2 (Kwon et al. 2010a). A 3D spheroid culture of MCF7 cells and a xenograft cell type established from a human inflammatory breast cancer (IBC) revealed that the IBC cells overexpress E-cadherin and exhibit high degree of cellular polarity with similar architectural features as observed *in vivo*. Also, with progress of time, there was degeneration of the cytoplasmic membrane and nuclear translocation of cytoplasmic domain of E-cadherin which are early signals for EMT and hence metastasis (Morales and Alpaugh 2009).

Thus it is evident that 3D models play a very important role in elucidating many of the key mechanisms related to cancer. By recreating the microenvironmental conditions of the native tumor tissue on a lab bench scale, they provide a suitable transition platform between the traditional 2D monolayer culture and the more complex *in vivo* or animal models. The continuous effort to improve the suitability of these models for the study of specific cancer-related phenomena will lead to the generation of new knowledge and will give better insight into the drug-targeting therapies for the disease.

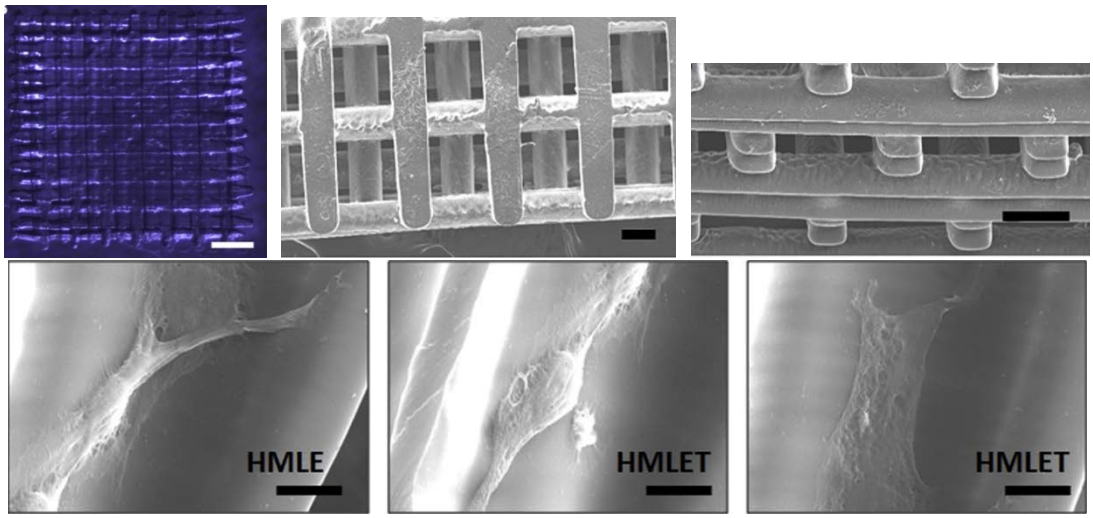

Figure 1.5: Modeling metastasis in 3D scaffolds. (Top) PEGDA scaffolds having 2D slab and 3D log-pile structures and (bottom) cancer cells migrate through the successive layers of the above construct. Scale bar: 100 µm. Used with permission: (Soman et al. 2012)

1.4 Fabrication Techniques for 3D Cancer Models

1.4.1 Fabrication of Multicellular Tumor Spheroids

A number of different techniques for the fabrication and investigation of tumor cell aggregates or MCTS have been developed. This is particularly useful as some cancer cell lines do not tend to spontaneously form tightly packed aggregates when cultured *in vitro*, hence requiring special means to encapsulate cells in a spherical mass and establish cell-cell contact within them. Traditionally, tumor spheroids have been generated using spontaneous aggregation from cell suspensions on non-adhesive surfaces (Sutherland and Durand 1984, Smalley et al. 2006), hanging droplets (do Amaral et al. 2010, Yuhas and Li 1978, Kelm et al. 2003b) and spinner flasks (Sutherland and Durand 1984). However, these methods are time dependent and the spheroids obtained are variable in size and packing density depending upon the cell type.

The review by Achilli, et al. demonstrates the different methods for tumor spheroid culture that have been developed, their relative advantages and limitations, analysis methods and their applications (Achilli et al. 2012). HeLa human cervical cancer cells encapsulated within duplex microcapsules composed of gelatin gel surrounded by an alginate shell were made to form spheroids and showed higher proportion of G_0/G_1 cells than tumor spheroids formed by self-aggregation (Sakai et al. 2011). MCF7 tumor spheroids were formed within alginate-oligochitosan microcapsules were found to be more resistant to photodynamic therapy as compared to cells grown in monolayers (Zaytseva-Zotova et al. 2011).

Tumor spheroid formation has also been facilitated by photolithography and micromachining of structures on the surface of poly(dimethyl siloxane) (PDMS) and silicon yielding homogenous spheroids at a higher throughput. MCF7 and HepG2 spheroids were formed in pyramid-like holes on a silicon chip surface overlaid with PDMS microchannels and cell culture media was perfused through the microchannels, enabling long-term culture (Torisawa et al. 2007). MCF7 spheroids were also formed in hexagonal patterned microwells coated with polyHEMA formed using photolithography and UV light embossing (Markovitz-Bishitz et al. 2010). In another similar technique, microwells were molded on photo-crosslinkable chitosan hydrogels using PDMS molds where HepG2 cells were grown as spheroids in the microwells while NIH 3T3 fibroblasts were grown in monolayer co-culture on the chitosan surface around the HepG2 spheroids (Fukuda et al. 2006).

Nanoprinting technology has been used to fabricate structures that minimize cell-surface interactions and help in the formation of tumor spheroids. Tumor spheroids of multiple cell types were formed on nano-culture plates (NCPs), in which nanoscale rectangular grids were printed

on transparent synthetic resinous bases, the cultured spheroids being examined for tumor-specific gene expression and morphological analysis (Yoshii et al. 2011).

Microfluidic systems have also been developed for high-throughput production of tumor spheroids. These systems provide for the controlled formation of spheroids of uniform shape and size and also facilitate their interaction with the surrounding microenvironment. LCC6/Her-2 breast tumor cells were entrapped within alginate hydrogels while flowing through microfluidic channels, cell culture media being perfused through the microfluidic pathway bordering the hydrogel (Chen et al. 2010). Similar alginate hydrogels encapsulating tumor spheroids were formed on a specially designed cell culture microfluidic chip containing uniformly sized microsieves to capture the cell spheroids (Yu et al. 2010). MCF7 spheroids of uniform shape, size and cellular density was formed by hydrodynamic trapping cells in PDMS microtraps, the trapped cells forming spheroids through the boundary restrictions imposed by the walls of the traps (Wu et al. 2008). A PDMS microfluidic spheroid formation array was fabricated for the production of size-controlled spheroids that allowed for the perfusion of desired components between the tumor spheroids and the surrounding flowing media (Ota and Miki 2011). Colon and breast tumor spheroids were formed within PDMS microbubbles with opened tops spheroids by flowing culture media across the microbubbles (Agastin et al. 2011).

These techniques have been helped further our understanding of the formation and culture of cancer cells in spheroids while also allowing them to be created at a faster pace and higher throughput volume as compared to traditional methods of culture. Hence they can be used for the testing and screening of a large number of candidate drugs. Though these culture methods require specialized techniques and equipment, the advances of modern fabrication technology have made it possible for many researchers to develop suitable platforms with relative ease.

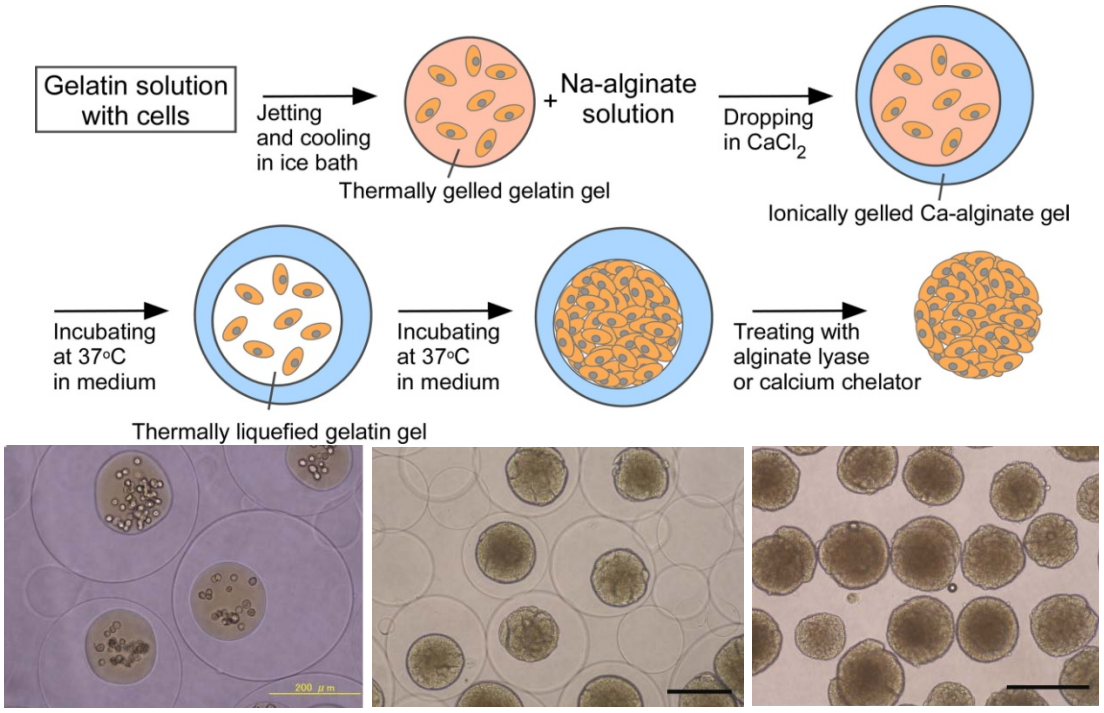

Figure 1.6: Tumor spheroids formed in calcium alginate microcapsules. Schematic of tumor spheroids formed within calcium alginate microcapsules with spherical liquid cores template by gelatin microparticles with each stage showing the gradual formation and retrieval of tumor spheroids. Used with permission: (Sakai et al. 2010)

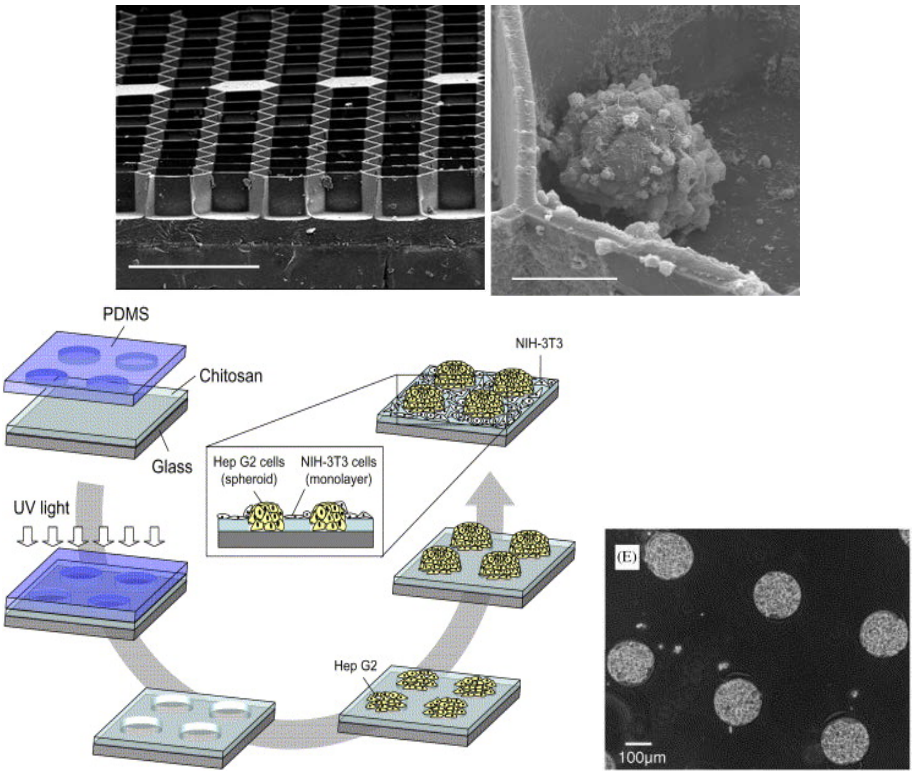

Figure 1.7: Microfabrication methods for tumor spheroid generation. (Top) A PDMS microstructure array and (Bottom) a chitosan-PDMS microarray for high-throughput spheroid production. Used with permission: (Top) (Markovitz-Bishitz et al. 2010) and (Bottom) (Fukuda et al. 2006)

1.4.2 Fabrication of Biomaterial-based Cancer Models

A number of innovative fabrication methods have been developed by investigators for 3D cancer cell culture and cancer models (Nikkhah et al. 2011, Chung et al. 2012, Cuchiara et al. 2010, Tan and Desai 2005). These models can also be used for the investigation of anti-angiogenic therapy and targets for drug delivery (Schneider and Miller 2005, Stroock and Fischbach 2010).

An extensive review by Chung, et al. describes different microfluidic fabrication methods using natural and synthetic biomaterials adopted for tissue engineering applications (Chung et al.

2012). An integrated microfluidic system for the co-culture of HeLa cells and HUVECs to study the cell migration and dynamic cell interactions between the two lines has been developed (Zheng et al. 2012). A versatile, automated microfluidic cell culture system with tunable culture conditions has also been fabricated (Gomez-Sjoberg et al. 2007), which could potentially be used for long-term cancer cell culture.

Microfabricated and micropatterned constructs have also been used for the study of cell adhesion, growth, migration and cellular interactions with the microenvironment (Liu and Chen 2005, Miller et al. 2012). In a recent study, perfusable 3D engineered tissue was formed by the rapid casting of patterned vascular networks using carbohydrate glass as a sacrificial template. This method is compatible with a wide number of natural and synthetic biomaterials and facilitates ample vascularization of the fabricated construct to support cell viability and function (Miller et al. 2012). A water-in-oil emulsion technique for the rapid formation of PEG-based hydrogel microspheres encapsulating cells has been developed and could be extended towards cancer cell culture (Franco et al. 2011). Peptide-coupled PEG-based hydrogels can also be micropatterned to provide spatial cues that drive endothelial morphogenesis (Moon et al. 2009). Microvasculature formation can also be guided within these hydrogels by the use VEGF-mimetic peptides amongst others (Leslie-Barbick, Saik, et al. 2011, Leslie-Barbick, Shen, et al. 2011). In one study, cancer and other cell types suspended in Matrigel were seeded on chromatography paper, which was later stacked as multiple layers to simulate *in vivo* tissue, thereby allowing the study of hypoxia, nutrients gradients (for cancer cells) and tubulogenesis (for HUVECs) (Derda et al. 2009). In a co-culture study of cancer cells, macrophages and myofibroblasts, cancer cell migration was inhibited due to the secretion of TNF-α by macrophages, leading to subsequent reduction in TGF-β secretion by myofibroblasts (Hsu et al. 2012).

Photolithography has facilitated the fabrication of microchannels in PDMS templates filled with collagen gels to simulate endothelial tubulogenesis (Raghavan, Nelson, et al. 2010). Confocal images from tissue samples coupled with two-photon laser scanning lithography has been used for the patterning of microchannel networks in hydrogels coupled with peptides (Culver et al. 2012, Hahn et al. 2005) or proteins (West 2011) for promotion of vascular tubulogenesis. These techniques can also be used for the simulation of tumor microvasculature and angiogenic growth by co-culturing cancer and endothelial cells. Breast cancer cells in HA micromolded hydrogels spatially co-cultured with ECFCs in fibrin hydrogels were investigated for the tumor angiogenic process (Dickinson et al. 2012).

Significant studies have been conducted to elucidate the role of micropatterned environments on cell phenotype and morphology (Leslie-Barbick, Saik, et al. 2011). Various methods have been developed to micropattern adhesive regions onto substrates and generate well defined surface chemistry that can suitably promote specific cellular phenotype expression, cellular interactions (Fukuda et al. 2006) and cell migration (Raghavan, Desai, et al. 2010). Lithographically patterned microarrays facilitate the co-culture of different cell types and study of their mutual interactions (Felton et al. 2012). Co-culture of endothelial cells and fibroblasts using multilayer micropatterning of cell sheets for studying neovascularization has been investigated (Asakawa et al. 2010, Muraoka et al. 2013, Tsuda et al. 2007). These models can be extended for the study of cancer cell behavior and interactions with fibroblasts, endothelial cells and other cell types.

CHAPTER 2: Dual-phase, Surface Tension-based Fabrication of PEG-based Hydrogel Millibeads and Tumor Millibeads

2.1 Introduction

Poly(ethylene glycol) (PEG)-based hydrogels have been extensively used for controlled delivery of drugs (Lee and Feijen 2012, Knop et al. 2010, Fu and Kao 2009) and macromolecules (Yonet-Tanyeri et al. 2013, Bal et al. 2013), cell-delivery for tissue regeneration (Moon et al. 2010, Kraehenbuehl et al. 2009, Mooney et al. 2011), and two-dimensional (2D) and three-dimensional (3D) culture of cells *in vitro* and *in vivo* (Soman et al. 2012, Sieh et al. 2012, Yang et al. 2013b). Some of the chief advantages of using PEG are its high water content and porous nature, ability to crosslink at physiological temperature and pH, covalent binding and controlled release of bioactive molecules (Bal et al. 2013), controlled proteolytic degradation of bioactive sites (Lutolf et al. 2003), tunable mechanical properties (Deforest et al. 2010) and permeability to oxygen and nutrients (Engberg and Frank 2011, Cruise et al. 1998). Numerous techniques have been developed to fabricate PEG-based hydrogels by both physical and chemical modifications (Kloxin et al. 2009b, Sant et al. 2010, Tibbitt and Anseth 2009). By developing additional techniques to control the specific size and geometry of PEG-based hydrogels, 3D tissues can be engineered that better replicate healthy and diseased physiological microenvironments and be used in *in vitro* drug testing.

The suitability of PEG-based hydrogels in tissue-engineering applications has facilitated the fabrication of 3D *in vitro* cancer models. These models aim to closely simulate the native tumor microenvironment which can be further used for drug-testing applications. In previously established methods, *in vitro* 3D cancer models are usually formed by spontaneous aggregation of cancer cells (called tumor spheroids) (Hirschhaeuser et al. 2010b, Kong et al. 2011, Zhang et

al. 2005) or encapsulation of cancer cells within biomimetic materials and scaffolds (Yang et al. 2013b, Szot et al. 2011b, Ho et al. 2010). Both techniques impose the desired limitations on oxygen and nutrient diffusion to the cancer cells, leading to hypoxia and cell death at the core of the aggregate and higher cellular viability and proliferation at the periphery. This phenomenon of hypoxic core formation is observed in native and *in vivo* tumors and has been widely emulated *in vitro* as a means of increasing physiological relevance (do Amaral et al. 2011, Fischbach et al. 2007, Kim et al. 2004).

A number of methods have been previously established to produce hydrogel microstructures via photolithography, emulsification, microfluidics and micromolding (Chung et al. 2012, Smith et al. 2012, Bing et al. 2013, Ren et al. 2012, Elbert 2011, Revzin et al. 2001). Specifically, PEG-based hydrogel microspheres have been investigated for various applications, with special focus placed on fabrication techniques to achieve desired specificity in size distribution (King et al. 2011, Wohl-Bruhn et al. 2013, Nichols et al. 2009). However, majority methods aim at creating relatively small hydrogel microparticles and microspheres (sub-500 μm scale) for efficient release of entrapped biomolecules or for ensuring good diffusion of nutrients and oxygen to maintain high viability of encapsulated cells (King et al. 2011, Elbert 2011). The method reported in this study is the first to fabricate large-sized (millimeter-scale) PEG-based hydrogel millibeads for the 3D culture of encapsulated cancer cells, called ‘tumor millibeads’. The larger size is critical for replicating key aspects of the native tumor microenvironment *in vitro* and thereby recapitulating the cellular characteristics in a 3D *in vitro* context.

In this study, we demonstrated a novel fabrication method of creating PEG-based hydrogel millibeads using a dual-phase water-in-oil system. By exploiting the differences in the surface tensions of air, aqueous and oil phases, large, uniform and size-controlled hydrogel

millibeads were formed. Encapsulation of cancer cells in the hydrogel millibeads ('tumor millibeads') and maintenance in 3D culture was demonstrated, followed by assessment of cell viability. This technique potentially facilitates the creation of a 3D tissue-engineered cancer model that could be used for the investigation of tumorigenic phenomena occurring in the cancer microenvironment in an *in vitro* setup. The fabricated millibeads were comparatively larger in size as compared to hydrogel microspheres reported in other liquid-liquid emulsion systems and the resulting tumor millibeads could effectively simulate larger, millimeter-scale tumors occurring in the human body. In addition, the hydrogel millibeads could also be used for the entrapment and controlled delivery of desired therapeutics at the site of delivery and thereby prove useful in the field of drug-delivery.

2.2 Materials and Methods

All chemicals were obtained from Sigma-Aldrich (St. Louis, MO) unless mentioned otherwise.

2.2.1 PEGDA Synthesis

Poly(ethylene glycol) diacrylate (PEGDA) was prepared as described previously (DeLong et al. 2005). Briefly, PEG (Molecular weight: 10 kDa) was reacted with acryloyl chloride (1:4 molar ratio) in anhydrous dichloromethane with triethylamine (1:2 molar ratio) under argon overnight at 25°C. The resulting PEGDA was purified by phase separation using 2M K_2CO_3. The organic phase containing PEGDA was dried using anhydrous $MgSO_4$ and filtered. Finally, PEGDA was precipitated in diethyl ether, filtered and dried overnight under vacuum. The degree of acrylation was characterized by ^{1}H-NMR and the PEGDA was stored at -20°C.

2.2.2 Cell Culture and Maintenance

MCF7 human breast adenocarcinoma cells were kindly provided by Dr. Richard C. Bird, College of Veterinary Medicine, Auburn University. MCF7 cells were cultured in DMEM (GIBCO®, Carlsbad, CA) supplemented with 10% fetal bovine serum (Atlanta Biologicals, Atlanta, GA), 1% (v/v) non-essential amino acids (NEAA) (Lonza, Walkersville, MD), 1% (v/v) Penicillin/Streptomycin (GIBCO®), 1% (v/v) Glutamax (GIBCO®) and 1% (v/v) sodium pyruvate (GIBCO®). The cells were maintained in tissue-culture flasks in a humidified atmosphere of 5% CO_2 and constant temperature of 37°C. Cell passages of 6-20 were used for all experiments. Cells cultured in 2D were enzymatically dissociated with 0.25% Trypsin/2.21 mM EDTA (Corning Cellgro®, Manassas, VA) and used for 3D encapsulation.

2.2.3 Hydrogel Millibead and Tumor Millibead Fabrication

A dual photoinitiator, water-in-oil system was used for making hydrogel millibeads with and without cells (Olabisi et al. 2010). The aqueous phase hydrogel precursor solution was made by dissolving 10% (w/v) PEGDA in sterile PBS with 1.5% (v/v) triethanolamine (TEOA), 37 mM 1-vinyl-2-pyrrolidinone (NVP), and the aqueous phase photoinitiator, 0.1 mM Eosin Y in PBS. PEGDA precursor was crosslinked into hydrogels by free-radical visible light photo-polymerization. To make the oil phase solution, 1.5% (v/v) triethanolamine and 3 µl/ml of oil phase photoinitiator (300 mg/ml Irgacure® 651 (Ciba®) in NVP) was mixed with mineral oil in a Petri dish. Microspheres were fabricated using a novel method: a set volume of precursor solution (2, 5 or 10 µl) was pulled up and then pipetted down slowly to form a droplet at the end of the pipette tip. Droplets were then carefully placed on the surface of the oil, so that the aqueous phase droplet remained floating at the oil-air interface. The floating droplets were crosslinked by exposure to light (365-700 nm wavelength) for 10 seconds (Fig. 2.1). Upon

completion of crosslinking, the newly formed hydrogel millibeads were removed from the oil phase, washed with PBS and centrifuged at 200g for 2 minutes twice to remove all residual oil. The millibeads were then allowed to swell in PBS and reach equilibrium state (swelling occurs due to hydrophilic interactions between PEGDA chains and water molecules, causing absorption of water).

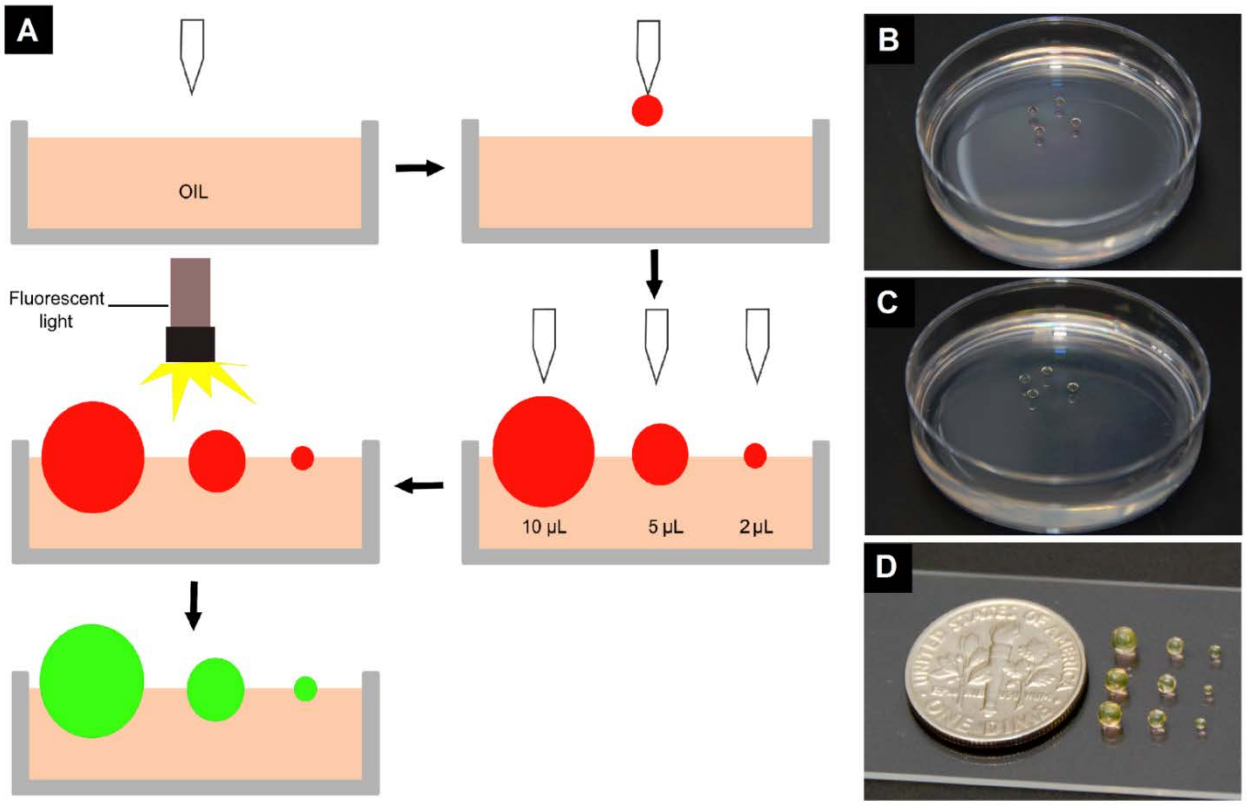

Figure 2.1: Hydrogel millibeads formation. (A) Aqueous polymer precursor is pipetted onto the surface of the oil phase, where it remains suspended at the air-oil interface due to surface tension and is photocrosslinked to yield hydrogel millibeads. (B) Uncrosslinked polymer precursor floating at the air-oil interface. (C) Crosslinked hydrogel millibeads after light exposure. (D) Size comparison of hydrogel millibeads of three different pipetted volumes.

For cell encapsulation, trypsinized MCF7 cells were mixed with the aqueous phase hydrogel precursor solution at 60×10^6 cells/ml. Tumor millibeads were then formed as described above. The millibeads containing cells were harvested, washed with DMEM and incubated in cell culture media at 37°C, 5% CO_2 atmosphere for 5 days (Figure 2.2A)

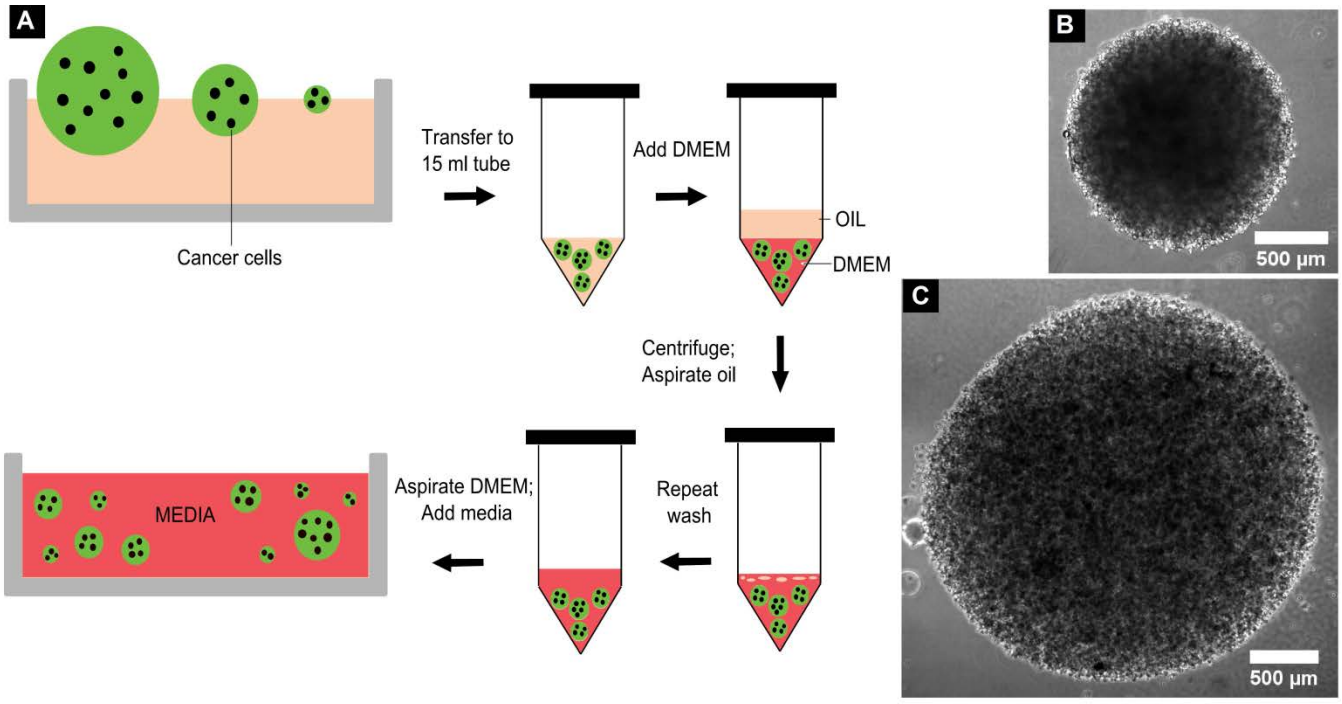

Figure 2.2: Tumor millibead formation. (A) Cells are mixed with the polymer precursor. Suspension is crosslinked to form tumor millibeads at the air-oil interface. The tumor millibeads are harvested, washed twice in DMEM to remove all oil and cultured in media. Photomicrographs of cancer cells encapsulated within (B) 2 µl and (C) 5 µl tumor millibeads.

2.2.4 Image Acquisition and Analysis

For each of the three different groups (2, 5 and 10 µl millibeads), two experimenters made 20 millibeads in 3 different batches (a total of 60 millibeads per condition). For each group, fabricated millibeads were pooled together and selected randomly for microscopic imaging and quantitative analysis. Phase contrast images of hydrogel millibeads with and

without cells were acquired using an inverted Nikon Eclipse Ti microscope fitted with an Andor Luca S camera. For each millibead, the perimeter, P, the geometric mean diameter (D) and the projected area (A) were determined using ImageJ version 1.48a software (NIH). For each size group, 20 millibeads were analyzed. Data was exported to MS Excel and a shape factor describing the sphericity of the millibeads (Φ) was calculated as described earlier (Kelm et al. 2003b):

$$\Phi = \frac{\pi \times \sqrt{\frac{4A}{\pi}}}{P} \qquad (1)$$

The mean geometric diameter calculated from the major (a) and minor (b) axes of the fitted region of interest (ROI) around the millibeads is given by:

$$D = \sqrt{a \times b} \qquad (2)$$

The spherical volume of the millibeads, based on the projected area, was calculated as follows:

$$V = \frac{4\pi}{3}\left(\frac{D}{2}\right)^3 \qquad (3)$$

The shape factor corrected volume, V′, is given by:

$$V' = \Phi V \qquad (4)$$

2.2.5 Hydrogel Swelling

To assess hydrogel millibead swelling, size and percentage increase of volume were evaluated with time. Acellular hydrogel millibeads were allowed to swell in PBS and images of swollen hydrogels were acquired at 5, 30, 60 and 120 minutes after incubation in PBS. The images were analyzed using ImageJ to determine geometric mean diameter, volume, and sphericity of swollen millibeads as described in the previous section. For each size group 30 millibeads were analyzed. The percentage increase in volume of hydrogel millibeads due to swelling was calculated using the following formula:

$$\% \text{ Increase in volume} = \frac{\text{Final volume-Initial volume}}{\text{Final volume}} * 100 \qquad (5)$$

2.2.6 Diffusional Release from Hydrogel Millibead

The release profile of entrapped TRITC-dextran from the hydrogel to the surrounding buffer was analyzed. Hydrogel millibeads entrapped with 5 mg/ml of (Molecular Weight: 4400 Da) were formed as described above. After removal of residual oil, the millibeads were allowed to incubate in 50 µl of PBS (for each millibead) to ensure that the entire millibead is completely submerged and to facilitate the diffusion of the entrapped TRITC-dextran from within the hydrogel matrix to the surrounding PBS. The PBS was collected at specific time points in a 96 well plate and 50 µl of fresh PBS was immediately added to the hydrogel millibeads. The collected PBS containing the TRITC-dextran was analyzed through a plate reader at 540/25 excitation wavelength and 590/35 emission wavelength. Known concentrations of TRITC-dextran in PBS were used for the standard curve and fresh PBS without TRITC-dextran was used as the blank. This procedure was continued until there was no detectable signal in the collected PBS. The absolute fluorescence intensity obtained from the plate reader was converted into concentration based on the standard curve and was reported as the percentage of the total TRITC-dextran that diffused out over the entire period of observation. For each size group 10 samples were analyzed for each time point.

2.2.7 SEM Imaging

Hydrogel millibeads with and without cells were visualized through scanning electron microscopy (SEM). First, the samples were fixed in 3% glutaraldehyde for 2 hours at room temperature and then post-fixated in 2% osmium tetroxide for 2 hours, each step being followed by 2 PBS washes. The fixed samples were dehydrated in graded ethanol series sequentially and

made to undergo chemical drying by hexamethyldisilazane (HMDS) for 30 minutes, followed by air drying (Braet et al. 1997). Finally, the dry samples were sputter-coated with gold (EMS 550X Auto Sputter Coating Device), mounted on aluminum stubs and imaged using SEM (Zeiss EVO 50 SEM). The average size of cells encapsulated within tumor millibeads was also evaluated from the obtained micrographs using ImageJ. Dehydration of samples in ethanol may cause undesired shrinkage of molecules, hence care must be taken to dehydrate in a graded series of 30%, 50%, 70%, 80%, 90% and 100% with 15 minutes incubation at room temperature at each step to minimize shrinkage and maintain the intact structures of the samples.

2.2.8 Fluorescence Staining and Analysis

Cancer cells were encapsulated within hydrogel millibeads and maintained in 3D culture. They were subsequently washed with PBS and incubated in the Live/Dead® Cell viability stain (Invitrogen, Carlsbad, CA) for 1 hour. The samples were washed with PBS again and imaged under an inverted Nikon Ti microscope. Tumor millibeads were washed with PBS to remove all media and fixed with 4% paraformaldehyde for 1 hour at room temperature. They were subsequently washed and permeabilized with 0.5% Triton X-100 for 15 minutes. The millibeads were blocked with blocking buffer for 3 hours. They were subsequently stained with Alexa Fluor® 568 Phalloidin and DAPI (Invitrogen) in blocking buffer overnight. The millibeads were washed in PBS and dehydrated using graded ethanol series. After air-drying, they were mounted on coverslips and imaged using confocal microscopy to observe encapsulated cell morphology and distribution (Nikon AI Confocal Scanning Laser Microscope).

2.2.9 Statistical Analysis

All statistical analysis was performed using Minitab 16 Statistical Software (Minitab Inc.). One-way analysis of variance (ANOVA) with Tukey's family error rate of 5% was used to

evaluate statistical significance between multiple groups. An assumption of equal variances between groups was made, based on the large, equal and independent sample size for each group, low variance ratio (<4) and effectively negligible difference in sampling variance (σ^2/n) between different groups, thereby maintaining the robustness of the ANOVA test. A minimum of 10 replicates of each category was used for statistical analysis. Unless otherwise indicated, $p<0.05$ was considered statistically significant.

2.3 Results and Discussion

A novel method for the fabrication of millimeter-scale hydrogel beads using a dual-phase, dual photoinitiator system to crosslink hydrogels at the air-water-oil interface is presented. The resulting hydrogel millibeads were characterized for size, swelling behavior and diffusion characteristics. Using this fabrication method, cells were then encapsulated within the millibeads and cell viability and morphology was evaluated. SEM analysis was conducted on millibeads with and without cells to visualize the microstructure of fabricated millibeads.

2.3.1 Tight Control of Millibead Shape and Size

To demonstrate the feasibility and capabilities of this technique, three different initial volumes for the fabrication of hydrogel millibeads, 2, 5 and 10 µl, were tested to demonstrate the ability of this technique for creation of large millimeter-scale hydrogel constructs over a range of sizes (2-15 mm^3). These volumes were selected based on the final desired sizes of the resulting hydrogel millibeads. Physiologically, tumors in the absence of vasculature are typically limited to 1-2 mm in diameter (1-2 mm^3 in volume). Though the hydrogel millibeads encapsulating cancer cells are larger in size compared to avascular tumors, these tumor-mimic millibeads could be further encapsulated in larger matrices with pre-formed vasculature to mimic advanced, vascularized tumors. The millibeads formed were imaged and analyzed for mean geometric

diameter, sphericity and volume. The average geometric mean diameters for the 2, 5 and 10 µl millibeads were 1670 ± 35 µm, 2370 ± 12 µm and 3089 ± 56 µm, respectively. The average volumes of the 2, 5 and 10 µl hydrogel millibeads after complete swelling in PBS were 2.44 ± 0.15 µl, 6.94 ± 0.08 µl and 15.06 ± 0.81 µl, respectively (Fig. 2.3). Mean geometric diameter and volume were significantly different between the three size groups of hydrogel millibeads ($p<0.001$, $n=20$). Importantly, the standard deviations of both mean geometric diameter (2.09%, 0.49% and 1.80% of the means for the 2, 5 and 10 µl millibeads respectively) and volume (6.15%, 1.15% and 5.38% of the means for the 2, 5 and 10 µl millibeads respectively) for each of the size groups were also minimal, indicating good size-control of millibeads using the established technique.

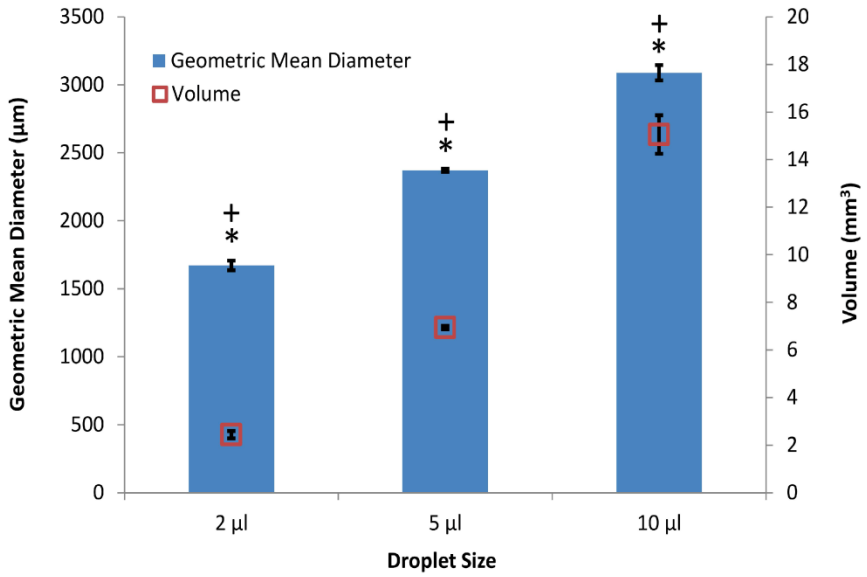

Figure 2.3: Size-controlled fabrication of hydrogel millibeads. Hydrogel millibeads of different sizes were generated by pipetting three different volumes (2, 5 and 10 µl) of the polymer precursor. The final volumes of the hydrogel millibeads after swelling correlated well with the initial pipetted droplet volume. The geometric mean diameters (+ $p<0.001$) and volume (* $p<0.001$) were significantly different for all tested droplet sizes ($n=20$ per condition). Low

standard deviation of the same pipetted volume reflects the tight control over millibead size and volume.

The average sphericities of the 2, 5 and 10 µl millibeads were 0.990 ± 0.002, 0.983 ± 0.016 and 0.974 ± 0.002, respectively (0.000 being perfectly linear and 1.000 being perfectly spherical), indicating that the millibeads formed using the technique were consistent and close to perfectly spherical in shape (Fig. 2.4). Additionally, there was no significant statistical difference in the sphericity between the three groups, indicating uniformity of the resulting millibeads. The millibead size range achieved using this technique is substantially larger than that obtained by similar liquid-liquid emulsion techniques with tight control of size.

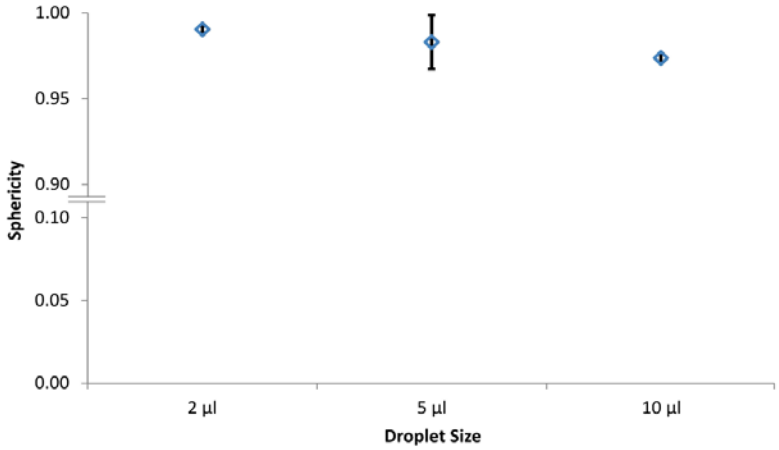

Figure 2.4: Sphericity of hydrogel millibeads. Hydrogel millibeads of three different droplet sizes (2, 5 and 10 µl) showed sphericity very close to 1, where 1 indicates a perfect sphere. No significant difference ($p<0.001$, $n=20$ per condition) was found in the sphericity of millibeads between the three sizes, demonstrating the usefulness of the fabrication technique over a range of sizes. Also, the small standard deviation (< 0.02) between millibeads indicates the uniformity and repeatability of the process.

2.3.2 Swelling of Hydrogels

Hydrogels are characterized by the uptake of water and swelling to an equilibrium size, post fabrication. Hydrogels encapsulating cells also undergo swelling after incubation in culture media due to hydrophilic interactions between polymeric functional groups and water molecules, causing absorption of water. This behavior was anticipated in the case of hydrogel millibeads and hence, the swelling behavior and final size of the swollen hydrogel millibeads was quantified for each initial polymer precursor volume. The swelling behavior of the hydrogel millibeads was studied by allowing the millibeads to incubate in PBS for 5, 30, 60 and 120 minutes and subsequent imaging of swollen hydrogels. Hydrogel millibeads started swelling immediately and reached a plateau phase within 2 hours of incubation time. For the 2 µl millibeads, there was no significant difference in mean geometric diameter between time points. However, for the 5 and 10 µl millibeads, there was significant increase in mean geometric diameter between the initial and final time points (Fig. 2.5). The small standard deviations in the diameters for each of the size groups indicated that final swollen millibead sizes for each initial droplet volume remained tight. Understanding millibead swelling and final size is critical for their use in future applications, including cell encapsulation and long-term culture.

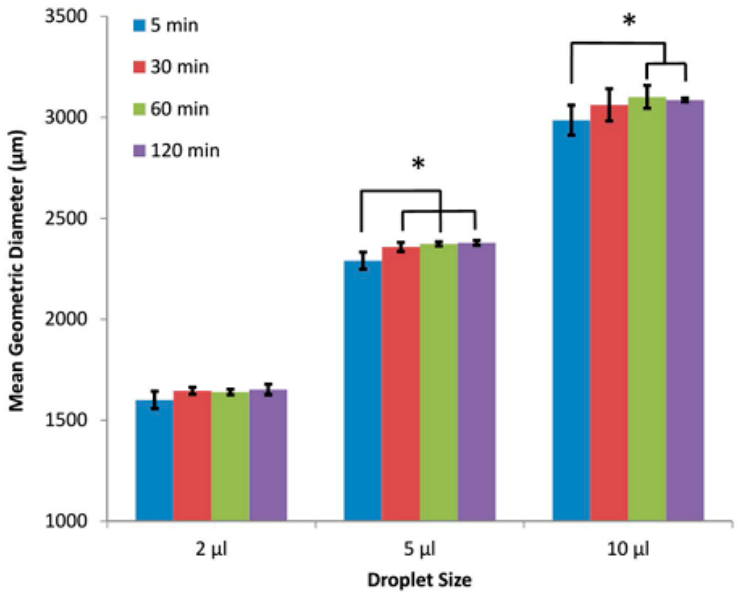

Figure 2.5: Swelling behavior of hydrogel millibeads. Hydrogel millibeads of three different sizes (2, 5 and 10 µl) were swollen in PBS and their increase in sizes was quantified. Uniformity and size differences were maintained throughout the swelling process. Millibead diameter increased significantly between the initial and final time points for the 5 and 10 µl size millibeads (* $p<0.05$, $n=20$).

2.3.3 Size-dependent Release from Hydrogel Millibeads

PEG-based hydrogels have been extensively used for the controlled release of entrapped bioactive molecules in drug-delivery applications. Hence, investigating the release behavior of our established hydrogel millibead system was deemed important. By entrapping TRITC-dextran (Molecular weight: 4.4 kDa, Concentration: 5 mg/ml) into the millibeads at the time of crosslinking and measuring the cumulative release with time, the differences in release behavior between the three sizes of hydrogel millibeads were evaluated. The 2 µl hydrogel millibeads showed the fastest release with no further release detected after 60 minutes, whereas the 10 µl millibeads showed the slowest release of the entrapped TRITC-dextran, with the 5 µl millibeads

being intermediate (Fig. 2.6, 2.7). The rate of change of fluorescence intensity (indicative of rate of release from the millibeads) was also observed to decrease with time, possibly due to reduction in the mass transfer driving force (Fig. 2.8).

These observations indicate that release of entrapped molecules from the hydrogel matrix is dependent on millibead size; larger hydrogel millibeads offer greater mass transfer resistance to entrapped molecules, whereas smaller millibeads facilitate faster release of molecules. Therefore, control over the time-course of diffusion can be achieved by varying the size of the fabricated millibeads. In addition, the rate of release from the hydrogel millibeads would also be dependent of the nature (molecular weight, hydrophilicity/hydrophobicity etc.) of the entrapped molecules and the initial concentration difference between the millibead interior and the surrounding buffer. Higher molecular weight molecules would be released from hydrogel millibeads at a much slower rate compared to low molecular weight molecules, possibly due to differences in interactions with PEGDA microarchitecture. Further work would be required to ascertain the rates of diffusion of oxygen, carbon dioxide, glucose, lactic acid and other physiologically relevant molecules in the hydrogel millibead model and associated diffusion coefficients. It can be surmised that diffusion of gaseous molecules like oxygen and carbon dioxide would also be dependent on their relative solubility in the culture media. Glucose (molecular weight: 180 Da) and lactic acid (molecular weight: 90 Da) would be expected to exhibit higher diffusion rates compared to the TRITC-dextran (molecular weight: 4400 Da) used in this study. When cells are encapsulated within the millibeads, understanding and controlling the time-course of diffusion is important for understanding the exchange of oxygen, nutrients and cellular metabolites through the hydrogel matrix. Limiting diffusion to differing degrees is anticipated to provide control over size of the hypoxic core within tumor millibeads; cells

encapsulated within larger millibeads would be expected to undergo greater nutritional deprivation, leading to the formation of a larger central hypoxic core (and larger region of cell death) as compared to smaller millibeads. In addition, knowledge of the diffusion properties could also be exploited for drug-delivery applications by entrapping suitable bioactive molecules within the millibeads to facilitate controlled release at desired delivery sites.

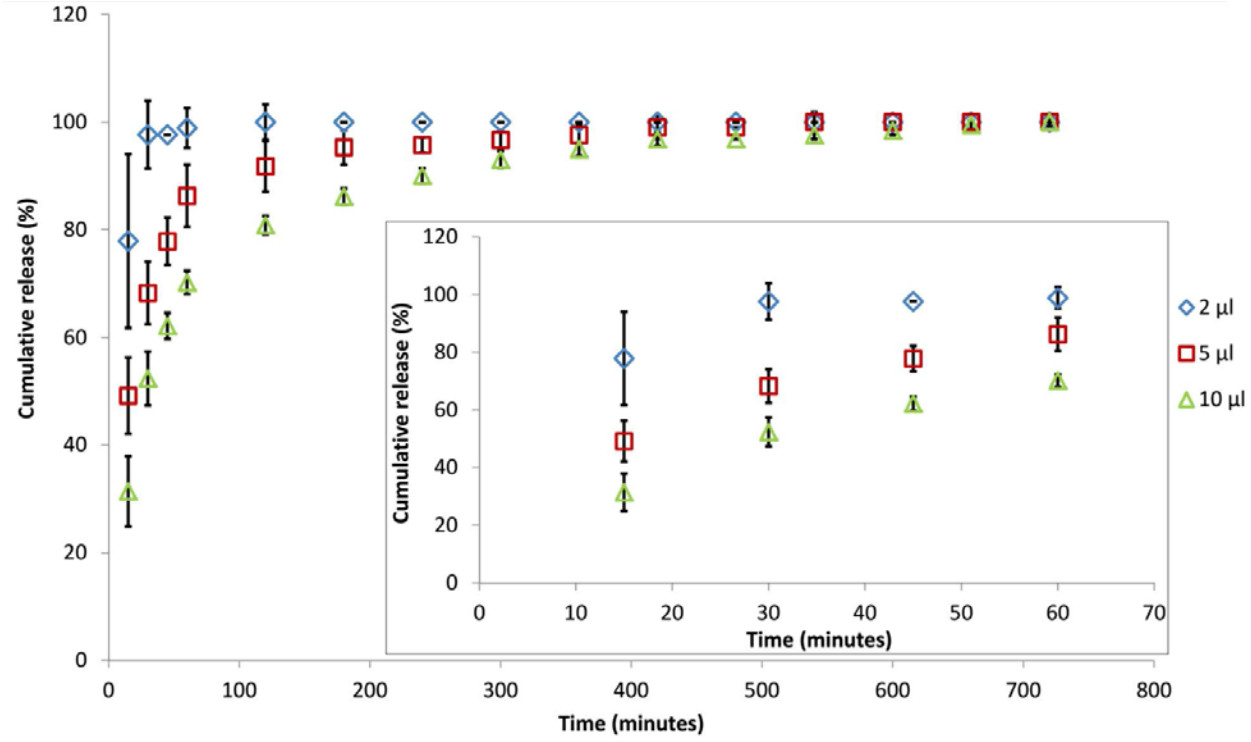

Figure 2.6: Size-dependent release profile from hydrogel millibeads. The release of TRITC-dextran is dependent on the diameter and volume of the millibeads, due to the diffusion resistance presented by the millibead size. Cumulative release was significantly different between 2, 5 and 10 µl millibeads for time points up until 360 minutes ($p<0.005$, $n=10$). (Inset) Expanded view of the diffusion profile for the initial 70 minutes of study.

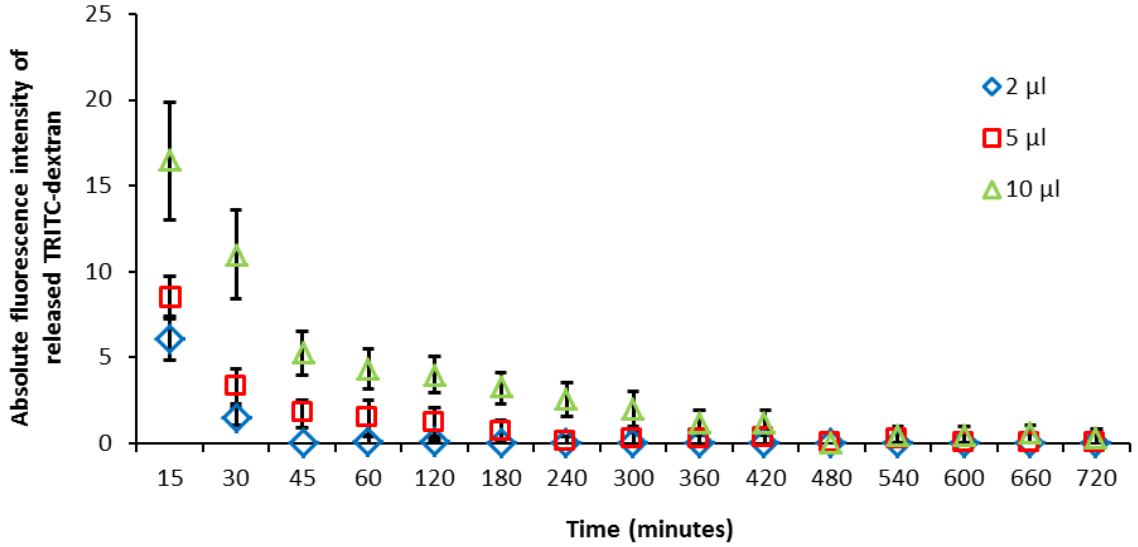

Figure 2.7: TRITC-dextran release profile from hydrogel millibeads. The concentration of TRITC-dextran released from hydrogel millibeads at each time point and rate of release over time is dependent on the diameter/volume of the millibeads.

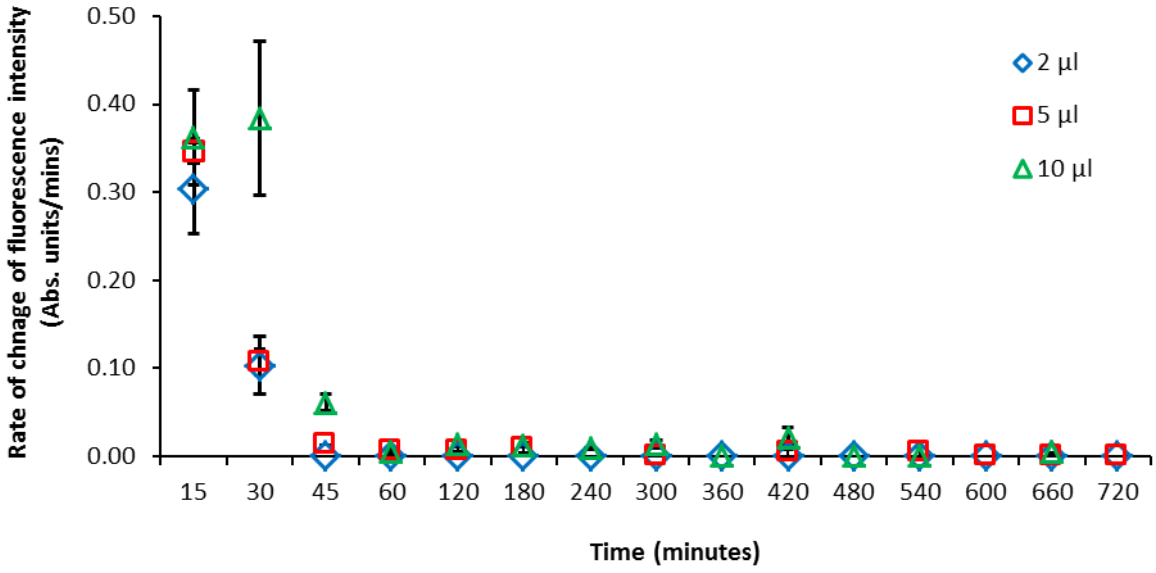

Figure 2.8: Rate of TRITC-dextran release from hydrogel millibeads. The rate of release of TRITC-dextran from hydrogel millibeads gradually decreases with time due to decreasing concentration gradient from the hydrogel millibead to the surrounding buffer.

2.3.4 Replication of Native Morphology and Viability in Tumor Millibeads

MCF7 breast cancer cells were encapsulated in the hydrogel millibeads to form ‘tumor millibeads (Fig. 2.2B, C). The MCF7 cells within these tumor millibeads were visually observed through phase contrast and fluorescence microscopy to study their distribution, morphology and growth. Initially and also over 5 days in culture, cells were evenly distributed throughout the entire volume of the tumor millibeads and had a rounded morphology as revealed by fluorescence imaging (Fig. 2.9). Based on these observations, we can support the hypothesis that cancer cells can be cultured for several days within the 3D environment provided by the PEGDA tumor millibeads. The increase in contrast observed beyond Day 3 might indicate proliferation in the cell colonies. However, it is also possible to have been caused by the onset of cell death due to diffusional limitations of oxygen and other nutrients. Fluorescence staining of nuclei and actin filaments and confocal imaging was used to examine the 3D morphology of the cells within the millibead matrix (Fig. 2.9). Cells were found to be uniform distributed with evidence of cell-cell contact. Actin filaments were found to be uniformly surrounding the nucleus, thereby revealing the rounded cytoskeletal structure of the cells. This rounded nature of the cells within the 3D culture environment of the tumor millibeads more closely replicates the native morphology of cancer cells *in vivo* as compared to those in 2D culture where cells appear flatter and more spread out.

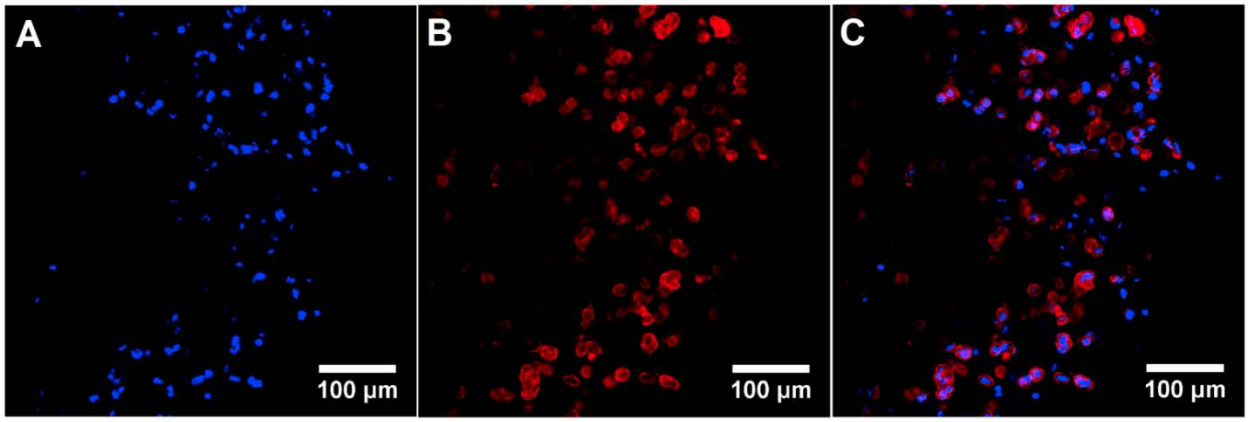

Figure 2.9: Morphology of MCF7 cells within tumor millibeads. Confocal fluorescence imaging of cancer cells on Day 5 showed uniform cell distribution and rounded cell morphology within the 3D matrix. (A) Cell nuclei (DAPI, blue), (B) Actin filaments (Phalloidin, red) and (C) overlay.

To observe the ultrastructure of hydrogel millibeads with and without cells and the arrangement of the cells in the 3D matrix, we visualized the millibeads using SEM. Hydrogel millibeads displayed a much smoother surface compared to those with cells, with closer inspection revealing the presence of grooves and ridges (Fig. 2.10A,B). It is possible that ethanol dehydration steps may have introduced surface artifacts and shrinkage of samples during preparation. Tumor millibeads with cells (Day 3) showed the random distribution of cells on the surface of the millibeads. The cells appeared to be rounded and well-encapsulated within the PEGDA matrix, with their diameter ranging from 8-13 µm (Figure 2.10C,D). Most of the cells appeared to have projections on their surface and hollow cavities leading into the interior regions were visible in many of the cell encapsulated millibeads (Figure 2.11). Although the PEGDA used to establish this technique is not readily degradable by the encapsulated cells, this fabrication method can be readily used with other photocrosslinkable PEG co-polymers containing cell adhesion and enzymatic degradation sites, which would likely result in a less

rounded cell morphology. Overall, the tumor millibead ultrastructure revealed the presence of well-established cell-cell and cell-matrix interactions.

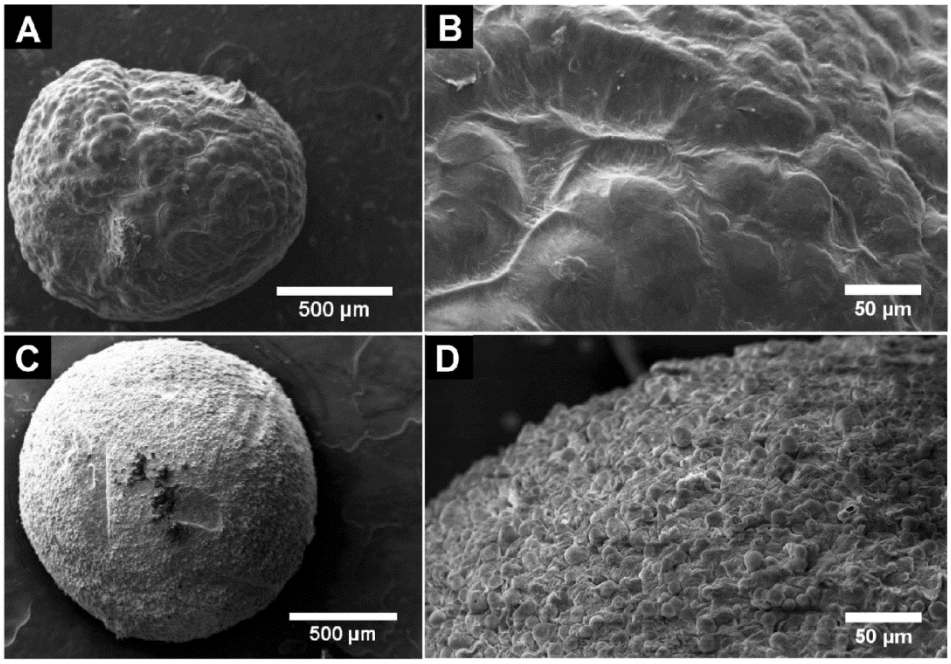

Figure 2.10: Ultrastructure of hydrogel and tumor millibeads. Hydrogel millibeads without (A,B) and with (C,D) encapsulated cancer cells were observed through SEM. (A) Millibeads without cells displayed a smoother surface. (B) Closer inspection reveals the presence of grooves and ridges possibly caused by sample preparation. (C) Tumor millibeads appear dotted with cells at the surface. (D) Magnified view of tumor millibead reveals the uniform distribution of round-shaped cells on the surface.

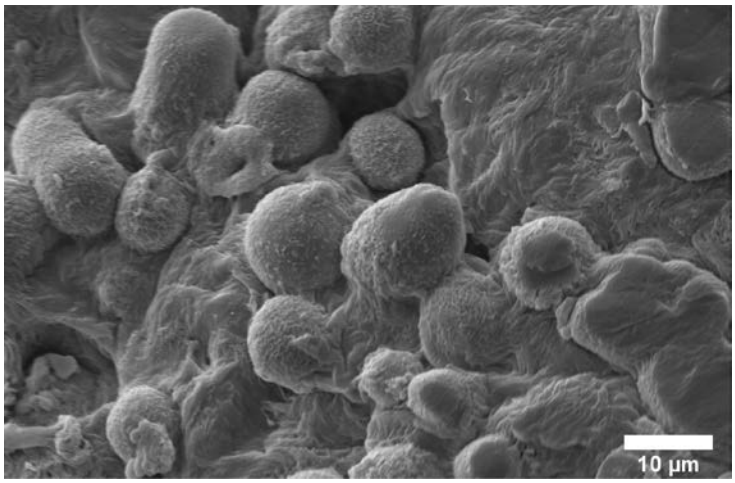

Figure 2.11: Ultrastructure of tumor millibeads. Visualization of cell distribution on tumor millibead surface. Cancer cells encapsulated within tumor millibeads are observed through SEM at high magnification. The ultrastructure reveals the presence of cell surface projections and hollow cavities leading into the interior of the millibeads. The cells appear rounded with well-established cell-cell junctions.

Native tumors found in the human body are characterized by the presence of a region of cell death at the core surrounded by viable, proliferative cells at the outer regions. This phenomenon occurs, in part, due to the diffusional limitations of oxygen and other nutrients, which cannot diffuse beyond a distance of a few hundred microns into the tumor mass. In addition, the presence of concentration gradients of various biomolecules from the peripheral regions to the inner regions also exerts survival pressure on cancer cells. Most current tumor models strive to achieve a heterogeneous population of cells within the fabricated constructs thereby better replicating the native microenvironment. By using our novel fabrication technique to create tumor millibeads over 1 mm in diameter, we anticipated being able to create tumor millibeads that developed a core region of cell death and viable cells at the periphery. Importantly, cell viability 3 hours post-encapsulation was high and uniform throughout the tumor

millibeads as visualized by fluorescence-based live/dead staining, where live cells appear green and dead cells appear green (Fig. 2.12A,B,C). These results indicate that the cells survived encapsulation using this technique and that regional differences in viability were not initially present. However, live/dead staining of tumor millibeads after 5 days in culture showed the presence of a large number of dead (red) cells in the central region of tumor millibeads surrounded by green-stained cells at the periphery (Fig. 2.12D,E,F).

Some key aspects related to diffusion need to be considered in the case of hydrogel millibeads and tumor millibeads. Though complete release of entrapped molecules can be achieved in hydrogel millibeads without cells when maintained over a sufficiently long time period, the same may not hold true for the case of tumor millibeads with encapsulated cells. The presence of the cells themselves may pose mass transfer resistances to the diffusion of molecules (media reagents, oxygen, carbon dioxide, drugs) and hence establish a diffusion gradient from the periphery to the core regions of the millibeads. A comparative study of diffusion in millibeads with and without cells is necessary to investigate this hypothesis in more details. In addition, the size of the core region of dead cells might also be affected by the size of the fabricated millibeads. Smaller millibeads (2 μl) might exhibit smaller regions of cell death while larger millibeads (5 or 10 μl) might exhibit larger regions of cell death in the core of the millibeads due to differences in diffusion gradients. Another interesting aspect for investigation would be the penetration of drugs within the tumor millibeads. The ability of drug molecules to diffuse within the millibead structure would depend on the molecular weight and molecular characteristics of the drug compound, the density of the encapsulated cells and the overall size of the tumor millibeads, amongst other factors. The diffusion gradient of drug molecules and resulting cancer cell death need to be investigated in future work.

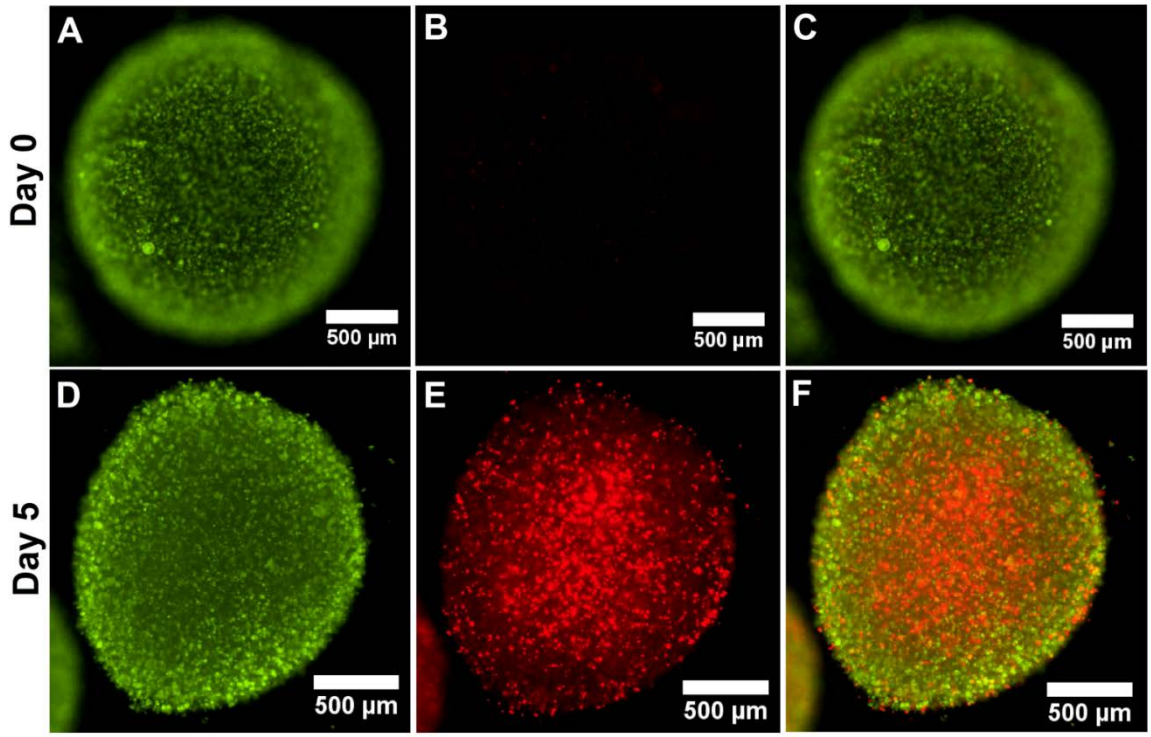

Figure 2.12: Native tumor conditions replicated in tumor millibeads. Cancer cells encapsulated within tumor millibeads were stained for live (green)/dead (red) cells on Day 0 (A,B,C) and Day 5 (D,E,F). (A) On Day 0, majority of cells were viable with (B) the presence of few dead cells that are uniformly distributed as seen in (C) overlay. (D) However, on Day 5, cells viability was no longer uniform, with a high percentage of cells in the outer regions remaining viable and (E) a region of high cell death having formed in the center of the tumor millibead as seen in (F) overlay, thereby closely replicating the heterogeneous viability patterns in native and *in vivo* tumor masses.

2.4 Conclusions

This study demonstrates the ability to fabricate large-sized hydrogel millibeads using a novel surface-tension based liquid-liquid system. Crosslinking was achieved using a dual photoinitiator system. The hydrogel millibeads formed using this system were consistent between batches, uniform in size and shape, and substantially larger than those obtained using

similar methods reported earlier. In addition, the pipetted droplet volumes correlated well with the final volumes of the hydrogel millibeads. Good control over the size, and thereby volume, of the resulting hydrogel millibeads was demonstrated. Hydrogel millibeads were characterized in terms of size, shape, swelling behavior and diffusion properties. Additionally, cancer cells were also encapsulated within the hydrogel millibeads and were maintained in 3D culture for multiple days. The ability to fabricate large millibeads facilitated the formation of a necrotic core of cells surrounded by healthy, proliferative cell layers within the tumor millibeads; *in vivo* and native tumor tissues also display this type of tumor morphology. By creating a reproducible fabrication method, this system paves the way for generation of large hydrogel millibeads that could potentially be used for future drug-delivery applications and in the creation of *in vitro* tumor models that better the native tumor microenvironment for use in drug testing and cancer research.

CHAPTER 3: Development of a Three-dimensional Spheroidal Cancer Model via Water-in-oil, Emulsion-based Fabrication of PEG-fibrinogen Tumor Microspheres

3.1 Introduction

The tumor microenvironment (TME), composed of various extracellular matrix (ECM) proteins and supporting cell types, plays an influential role in the tumorigenic progression of breast cancer cells, including malignant growth, loss of epithelial polarity and disorganization of normal cellular architecture in the breast tissue (Allen and Louise Jones 2011, Krause et al. 2010, Bissell et al. 2002). Specific components of the ECM (*e.g.* collagen, laminin, fibrinogen, and others) have been implicated in these changes, involving abnormal production and deposition of ECM proteins in the TME, dysregulation in integrin-mediated cell-matrix interactions and subsequent uncontrolled cellular signaling mechanisms (Oskarsson 2013, Staton et al. 2003, Costantini et al. 1991, Kolodziejczyk and Ponczek 2013). Specifically, fibrinogen has been shown to be assembled, secreted, and deposited in the breast TME by MCF7 breast adenocarcinoma cells (Rybarczyk and Simpson-Haidaris 2000). In addition, fibrinogen and its related fragments also promote tumor angiogenesis through interaction with fibroblast growth factor-2 (FGF-2), vascular endothelial growth factor (VEGF) and subsequent activation and proliferation of endothelial cells (Sahni and Francis 2000, Sahni et al. 2008). In this study, a biosynthetic hydrogel material, PEG-fibrinogen (PF), obtained by covalent coupling of PEGDA and fibrinogen, is employed to maintain MCF7 cells in long-term three dimensional (3D) culture and, evaluate the growth and tumorigenic phenotype of cells within the 3D matrix.

Development of tissue-engineered breast cancer models requires a good understanding of the biophysical and biochemical interactions between cancer cells and the TME. Traditionally, 2D models have been used in cancer research for candidate drug screening due to their ease of

handling, observation and analysis. However, 2D cultured cells are unable to replicate the native TME conditions due to significant differences in the cellular morphology, gene expression at the RNA level, intracellular signaling, and drug resistance between 2D cultured cells and those in *in vivo* tumors (Smalley et al. 2006, Pickl and Ries 2009). Hence, various 3D models have been established to improve upon 2D models and better recapitulate *in vivo* animal models (Baker and Chen 2012). 3D models combine the advantages of both 2D models (*in vitro* controllable conditions, relative ease of handling and analysis compared to animal models) and xenograft models (recapitulation of physiological complexities of the TME) (Yamada and Cukierman 2007). The tumor spheroid model, formed by spontaneous self-aggregation of tumor cells on a non-adhesive surface such as agar or in hanging droplets (Kelm et al. 2003a, Sutherland et al. 1971), replicates specific features of *in vivo* tumors including central hypoxic conditions, heterogeneity in phenotype and gene expression and altered cellular metabolism (Carlsson and Acker 1988, Hirschhaeuser et al. 2010a), but suffers from some limitations as well. Aggregate forming tendencies in different cancer cell lines vary widely, especially with respect to time-length of aggregation, cell-cell adhesion, and size, shape and consistency of resulting spheroids (Rainaldi et al. 1999, Wu et al. 2008, Elliott and Yuan 2011, Lin and Chang 2008). Tumor spheroids are susceptible to dissociation during handling and experimentation and the microenvironmental conditions (*e.g.* presence of ECM, cell-matrix interactions, mechanical stiffness) in tumor spheroids cannot be controlled (Markovitz-Bishitz et al. 2010). Moreover, mass transport limitations imposed by ECM components on exchange of cellular metabolites and delivery of anti-cancer drugs in native or *in vivo* tumors cannot be accurately replicated in tumor spheroids.

Thus, as an improvement over the tumor spheroid model, current methods employ the use of various biomimetic materials (natural, synthetic or a hybrid of both) coupled with novel fabrication techniques (microfluidics, photolithography and others) to develop *in vitro* tissue-engineered models of breast cancer that closely mimic native tissue characteristics. A number of different natural and synthetic materials have been used for cancer cell encapsulation including collagen (Szot et al. 2011a), calcium alginate (Sakai et al. 2010), poly(D,L-lactic-co-glycolic acid) (PLGA) (Kang and Bae 2009), polylactic acid (PLA) (Xu and Burg 2007), silk fibroin (Talukdar et al. 2011) and PEG-based hydrogels (Liang et al. 2011). These models aim to simulate the microenvironmental conditions of native breast tumors in order to provide more accurate and clinically relevant information about molecular mechanisms of breast cancer progression and to obtain more physiologically relevant drug-efficacy results. Biomaterial-incorporated engineered cancer models have distinct advantages over traditional spheroid models of cancer; biomaterials enable regulation of the microenvironmental conditions surrounding the cancer cells and provide the ability to establish and maintain tissue heterogeneity and complexity.

To this end, the naturally occurring ECM protein fibrinogen has been covalently coupled with synthetically prepared PEGDA to produce PF, to investigate its potential suitability in supporting cancer cell proliferation and facilitating tumorigenic expression in 3D culture. PF has been previously used for the 3D culture of smooth muscle cells (SMCs) (Lee, Tin, et al. 2014), induced pluripotent stem cells (iPSCs) (Bearzi et al. 2014), fibroblasts (Kesselman et al. 2013), mesenchymal stem cells (MSCs) (Xu et al. 2015) and others, but its applicability in cancer models is yet to be investigated. The mechanical and biochemical properties of the PF hydrogels can be modulated to recapitulate that of native cancer tissue by controlling the relative

concentrations of PEGDA and fibrinogen in the hydrogel precursor (Bearzi et al. 2014). Covalently coupled PEGDA renders PF photocrosslinkable at physiological temperature and pH and provides sustained mechanical stiffness and architecture to the 3D matrix. Fibrinogen facilitates critical integrin-mediated signaling mechanisms required for cell attachment, spreading, and proliferation (Mosesson 2005). Thus, PF provides both biological functionalities required for cell survival and proliferation and the ability to control the cellular microenvironment to simulate native tumor conditions. In addition, the ability of PF to be fabricated into spheroidal hydrogel constructs of consistent size and shape enables ease of translation towards existing drug-testing platforms and assays.

In this study, the ability to encapsulate MCF7 cells within PF hydrogel microspheres using a dual-photoinitiator, water-in-oil emulsion technique, and to maintain the resulting "tumor microspheres" in long-term 3D culture is demonstrated. To establish PF tumor microspheres as an improved spheroidal 3D cancer model, the size and shape distribution of tumor microspheres (TM) and self-aggregated tumor spheroids (TS) formed using the hanging droplet method is compared. Further, the growth rate, viability, ultrastructure and 3D morphological features of cells within TM and TS is compared, and thereby the advantages of incorporating PF as a biomimetic matrix on the tumorigenic growth and morphology of encapsulated MCF7 cells is investigated. Finally, the ability to culture a range of cancer cell types (metastatic and non-metastatic) within PF microspheres is demonstrated, thereby establishing the applicability of using the tumor microsphere model to study diverse types of cancer.

3.2 Materials and Methods

All chemicals were obtained from Sigma-Aldrich (St. Louis, MO) unless mentioned otherwise.

3.2.1 Cell Culture and Maintenance

MCF7 human breast adenocarcinoma cells were kindly provided by Dr. Richard Bird, College of Veterinary Medicine, Auburn University and cell passages of 6-20 were used in all experiments. Cells were cultured in DMEM (GIBCO®, Life Technologies, Carlsbad, CA) supplemented with 10% fetal bovine serum (Atlanta Biologicals, Norcross, GA), 1% (v/v) non-essential amino acids (NEAA) (Lonza, Walkersville, MD), 1% (v/v) penicillin/streptomycin (GIBCO®), 1% (v/v) Glutamax (GIBCO®) and 1% (v/v) sodium pyruvate (GIBCO®). MDA-MB-231 breast cancer cells were provided by Dr. Robert Arnold (Harrison School of Pharmacy, Auburn University) and were maintained in the same media as MCF7 cells. SK-BR-3 breast cancer cells were provided by Dr. David Riese (Harrison School of Pharmacy, Auburn University) and were maintained in McCoy's 5a Modified media (VWR, Radnor, PA) with 10% FBS and 1% (v/v) Pen-Strep. HT29 colon cancer cells were obtained from Dr. Michael Greene (Department of Nutrition, Auburn University) and were maintained in the same media as SK-BR-3 cells. PC-3 and PC-3-Met (a metastatic variant of the wild-type PC-3 cells) were obtained from Dr. Allan David (Department of Chemical Engineering, Auburn University) and were maintained in F-12K (Kaighn's Modified Media) media (VWR) with 10% FBS and 1% (v/v) Pen-Strep.

3.2.2 Tumor Spheroid Formation and Culture

MCF7 cells were made to aggregate into tumor spheroids (TS) using the hanging droplet technique. Briefly, cells obtained after trypsinization were resuspended in cell culture media at a

density of 0.15×10^6 cells/ml. 150 mm Petri dishes were filled with 20 ml autoclaved deionized water to provide humidification to the hanging droplets. To form the TS (day 0), 20 µl droplets (3000 cells/drop) of the cell suspension were formed on the lids with a multichannel pipettor, which were then inverted over the dishes and allowed to incubate for 3 days. Due to gravity, the cells aggregated at the apex of each hanging droplet to form tumor spheroids. The spheroids were harvested (day 3) and maintained in suspension culture using poly(2-hydroxy ethyl methacrylate) (Poly-HEMA)-coated Petri dishes for 28 days following initial formation of droplets.

3.2.3 PF Synthesis and Characterization

Poly(ethylene glycol) diacrylate (PEGDA) was prepared as described previously (Pradhan et al. 2014). Bovine fibrinogen was covalently coupled to PEGDA according to established protocols (Plotkin et al. 2014). Briefly, fibrinogen was dissolved in an 8 M solution of urea in 10 mM PBS at a concentration of 7 mg/ml. Tris (2-carboxyethyl) phosphine hydrochloride (TCEP-HCl) was added at a molar ratio of 1.5:1 TCEP to fibrinogen cysteines to the above solution, the final pH being adjusted to 8.0. PEGDA was dissolved in the 8 M urea-PBS buffer at 280 mg/ml (300% excess), centrifuged and the clear PEGDA solution was slowly added to the fibrinogen solution. The reaction was allowed to proceed for 3 hours at 25°C in the dark. The solution was then diluted with an equal volume of urea-PBS buffer and precipitated by adding it into acetone (J.T. Baker, Center Valley, PA) at a volumetric ratio of 4:1 of acetone to product solution. The precipitate was separated, centrifuged and the supernatant acetone was removed. After air-drying, the precipitate was weighed and re-dissolved in urea-PBS buffer at 2.2 ml of buffer/g of precipitate. The product was dialyzed against 1 L sterile

PBS over 24 hours (with three changes of PBS) at 4°C in the dark. The final product was aliquoted into sterile centrifuge tubes and stored at -80°C.

To characterize the synthesized PF, the protein concentration and the net solid weight of the dry product was determined. Briefly, the protein content of the final PF solution was measured using a standard Pierce™ BCA Protein Assay Kit (Thermo-Scientific, Rockford, IL). In order to measure relative PEG content, PF solution was aliquoted in glass vials, lyophilized, and the net weight of the dry solid was determined. The PEGylation efficiency was calculated according to the previously established formula (Dikovsky et al. 2006) as given below in Equation (1).

$$\varepsilon_{PEGylation} = \frac{[PEG]}{[Fibrinogen]} \times \text{theoretical}\left\{\frac{MW_{Fibrinogen}}{29 \times MW_{PEG}}\right\} \qquad (1)$$

3.2.4 PF Hydrogel Microsphere Fabrication

PF hydrogel microspheres were formed using a dual-photoinitiator, water-in-oil emulsion based method adapted with some modifications from that described by Franco, et al. for PEG-peptide hydrogel microspheres (Franco et al. 2011). Briefly, trypsinized cells were resuspended at the desired initial cell density (20×10^6 or 60×10^6 cells/ml of PF) in a hydrogel precursor consisting of PF dissolved in PBS, with 1.5% (v/v) triethanolamine (TEOA), 37 mM 1-vinyl-2-pyrrolidinone (NVP), 1% (v/v) Pluronic F68 (10% (w/v) solution in PBS) and 0.1 mM Eosin Y in PBS. 100 µl of the above cell-laden aqueous phase suspension was added to an oil phase solution in a glass test tube consisting of 1 ml mineral oil and 5 µl Irgacure® 651 (I651) (Ciba Specialty Chemicals, Tarrytown, NY) photoinitiator solution (300 mg/ml of I651 in NVP). The aqueous and oil phases were simultaneously vortexed (for 2 seconds) and photocrosslinked (for 28 seconds) in the presence of a light source of wavelength 365-700 nm to obtain hydrogel

microspheres encapsulating cancer cells. The emulsion was resuspended with washing buffer, DMEM, and centrifuged at 200g for 3 minutes to separate the aqueous and oil phases. The oil phase was aspirated and the remaining aqueous phase was resuspended, washed with DMEM and centrifuged again. The tumor microspheres (day 0) were finally resuspended in media and maintained in culture in PolyHEMA-coated dishes for 28 days. As a negative control, MCF7 cells were also encapsulated within PEGDA hydrogel microspheres (polymer precursor concentration: 100 mg/ml) and maintained in 3D culture for at least 21 days.

A similar protocol was followed for microsphere encapsulation of other cell types. MDA-MB-231, SK-BR-3, HT29, PC-3 and PC-3-Met cells were encapsulated within the PF microspheres at an initial density of 10×10^6, 10×10^6, 20×10^6, 10×10^6 and 10×10^6 cells/ml respectively and maintained in the respective culture media for at least 14 days.

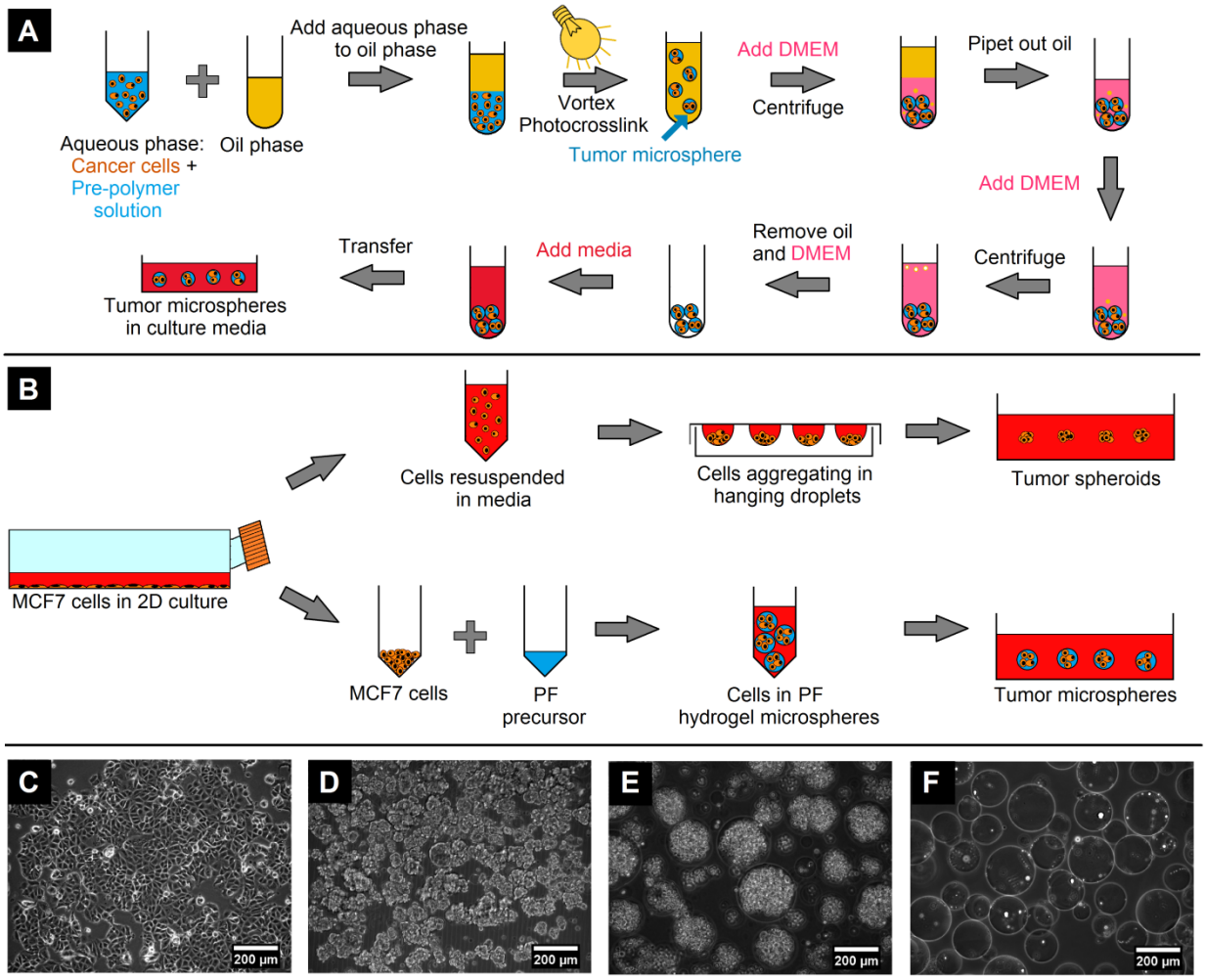

Figure 3.1: Schematic of fabrication processes for PF tumor microsphere (TM) and tumor spheroid (TS) models. (A) Dual-phase, water-in-oil emulsion technique for the 3D encapsulation of cancer cells in PF hydrogel microspheres. (B) Comparative fabrication technique for TS and TM. MCF7 cells (C) in 2D culture, (D) cultured as TS or (E) in TM. (F) PF microspheres formed without cells.

3.2.5 Image Acquisition and Analysis

Phase contrast images of the hanging droplet tumor spheroids (TS) and the PF hydrogel tumor microspheres (TM) with "low" (20×10^6 cells/ml) and "high" (60×10^6 cells/ml) cell densities were acquired using an inverted Nikon Eclipse Ti microscope fitted with an Andor

Luca S camera on days 3, 7, 14, 21 and 28 (for TS) and days 0, 7, 14, 21 and 28 (for TM). The images were analyzed using ImageJ software, version 1.48q (NIH), to obtain size and shape characteristics. Briefly, regions of interest (ROI) were drawn around TS and TM, major and minor axes and circularity were evaluated and the data was exported to MS Excel. The mean geometric diameter (D) was calculated from the major (a) and minor (b) axes of the fitted ROI according to Equation (2) as described previously (Pradhan et al. 2014).

$$D = \sqrt{a \times b} \qquad (2)$$

A minimum of 100 individual TS and TM were analyzed at each time point for each of 3 individual batches.

3.2.6 SEM Imaging

Hanging droplet tumor spheroids (TS) and PF tumor microspheres (TM) were imaged through scanning electron microscopy to visualize their ultrastructure. Briefly, TS and TM were washed with PBS to remove all culture media and fixed in 3% glutaraldehyde (Electron Microscopy Sciences, Hatfield, PA) for 2 hours at 25°C. After two PBS washes, the TS and TM were postfixated with 2% osmium tetroxide for 2 hours. The fixed samples were dehydrated in graded ethanol series sequentially and made to undergo chemical drying by hexamethyldisilazane (HMDS) for 30 minutes, followed by air drying. Finally, the dry samples were mounted on aluminum stubs, sputter-coated with gold (EMS 550X Auto Sputter Coating Device) and imaged using SEM (Zeiss EVO 50 SEM).

3.2.7 Viability Staining and Quantification

Cell viability and growth in tumor spheroids (TS) and tumor microspheres (TM) were visualized and quantified through fluorescence staining and imaging. Briefly, TS and TM were washed in PBS to remove media and incubated in the Live/Dead® cell viability stain (Invitrogen,

Carlsbad, CA) for 30 minutes. The samples were washed with PBS again and imaged under an inverted Nikon Ti microscope. Acquired images (z-stacks) were analyzed using ImageJ software. For each individual TS and TM, the number of live and dead cells and the mean geometric diameter (as described in Section 2.4) were quantified manually. The volume of individual TS and TM was computed according to the formula:

$$V = \frac{1}{6}\pi D^3 \qquad (3)$$

The total number of cells (live and dead) was quantified and the cell density was calculated based on the volume of each individual TS and TM. This analysis was carried out on days 3, 7, 14, 21 and 28 (for TS) and days 0, 7, 14, 21 and 28 (for TM). A minimum of 15 individual TS and TM from each of 3 independent batches (for both TS and TM) were analyzed for each time point.

3.2.8 Fluorescence Staining and Quantification

In order to visualize and quantify the 3D morphology of MCF7 cells in tumor spheroids (TS), PF tumor microspheres (TM) and PEGDA microspheres, the cells were fluorescently stained and imaged via confocal microscopy. Briefly, TS and TM were washed with PBS and encapsulated within larger PEGDA hydrogel discs (diameter: 5 mm, thickness: 500 μm) to ensure sharp focus in the interior regions of the 3D samples. The encapsulated samples were fixed with 4% paraformaldehyde (Electron Microscopy Sciences) for 1 hour at 25°C, washed with PBS, permeabilized with 0.5% Triton X-100 for 15 minutes followed by incubation with blocking buffer (2% bovine serum albumin and 5% FBS in PBS) for 3 hours. They were subsequently stained with Alexa Fluor 568 Phalloidin and DAPI (Invitrogen) in blocking buffer for 3 hours, mounted on coverslips and imaged using confocal microscopy (Nikon AI Confocal Scanning Laser Microscope) to obtain z-stacks. Fluorescence images were analyzed using

ImageJ software and the data was exported to MS Excel. A minimum of 20 images were analyzed for each group (TS and TM). For morphometric analysis, several parameters were quantified including percentage of polar cells, nuclear area, cellular area, nuclear:cytoplasmic ratio (Equation 4), nuclear volume density (Equation 5) (Nandakumar et al. 2011, White et al. 1997), cell-cell junction length and normalized junction length (Equation 6).

$$\text{Nuclear volume density} = \frac{\text{Nuclear area}}{\text{Cellular area}} \quad (4)$$

$$\text{Nuclear:cytoplasmic ratio} = \frac{\text{Nuclear area}}{\text{Cellular area-Nuclear area}} \quad (5)$$

$$\text{Normalized cell-cell junction length} = \frac{\text{Cell-cell junction length}}{\text{Total junction length of corresponding cells}} \quad (6)$$

3.2.9 Statistical Analysis

All statistical analysis was performed using Minitab 17 Statistical Software (Minitab Inc.). After checking for normality of distribution, One-way Analysis of Variance (ANOVA) with Tukey's family error rate of 5% was used to evaluate statistical significance between multiple groups, assuming equal variance and equal sample size of compared groups. In case of unequal variance between groups, the Games-Howell post-hoc test was employed following the ANOVA analysis. Unless otherwise indicated, $p < 0.05$ was considered statistically significant. For analysis of diameter and circularity of tumor spheroids and tumor microspheres, at least 100 spheroids and microspheres were evaluated in 3 independent batches. For analysis of viability and growth rate of cells within tumor spheroids and microspheres, at least 15 spheroids or microspheres were evaluated for each of 3 independent batches. For morphological analysis, a minimum of 100 cells were analyzed from each group.

3.3 Results

3.3.1 Characterization of Synthesized PF

In order to confirm the quality and consistency of the synthesized PF, the degree of acrylation of PEGDA, evaluated using NMR spectroscopy, was found to be 96.50%. The concentration of fibrinogen in the PF precursor, evaluated using the BCA assay, was found to be 9.94 mg/ml. After lyophilization, the net weight of PEGDA in the precursor was calculated as 21.01 mg/ml with a PEGylation efficiency of 120.78%. Subsequent synthesis batches yielded product with a fibrinogen content of 9-11 mg/ml and a PEGylation efficiency of 85-110%, thereby demonstrating a tight control over the quality of the final product and low batch-to batch variability. The resulting hydrogel, formed via visible light exposure in the presence of Eosin Y photoinitiator, was also subject to degradation by collagenase type II (1 mg/ml, 200 units/mg), where it underwent complete degradation within 30 minutes at 37°C, thereby demonstrating its suitability for degradation by cell-secreted MMPs. These results are consistent with previous observations reported in literature (Dikovsky et al. 2006, Almany and Seliktar 2005).

3.3.2 3D Culture of MCF7 Cells in Tumor Microspheres

In order to create a biomaterial-based spheroidal tumor model that could overcome certain limitations of the standard tumor spheroid (TS) model, the PF tumor microsphere (TM) model was fabricated using a dual-phase, emulsion-based technique for encapsulation and 3D culture of MCF7 cells (Fig. 3.1A). Initially, microspheres without cells were fabricated (Fig. 3.1F) to optimize the vortexing speed, photocrosslinking time and intermediate wash steps with DMEM. Next, the optimum initial cell encapsulation density was determined by testing the initial cell density within the TM at 20×10^6 cells/ml (“low” density) and 60×10^6 cells/ml (“high” density). Through 28 days in culture, cells appeared to proliferate, forming dense colonies. This

led to increased darkening and reduction of transparent void space within the TM, as observed through phase contrast microscopy. Subsequently, the effect of low and high cell encapsulation densities on the size and shape of microspheres were evaluated.

3.3.3 Influence of Initial Cell Density on Microsphere Size and Shape Characteristics

The cell density of engineered bio-constructs is an important consideration for the close replication of native tissue. Cancer tissues from different sources have been reported to have cell densities on the order of 10^8 cells/ml (Elliott and Yuan 2012). The initial cell encapsulation density within hydrogel microspheres is of importance in achieving subsequent cell densities on this order of magnitude. Hence, the initial cell densities within the PF precursor were varied between 20×10^6 and 60×10^6 cells/ml with the goal of obtaining a final density on the order of 10^8 cells/ml in the microspheres within the culture period. The initial cell density was observed to have a profound effect on the cell encapsulation and formation of the hydrogel microspheres, specifically with respect to diameter and circularity of the final constructs. At a the "low" density of 20×10^6 cells/ml, the encapsulation efficiency was quite high with nearly 100% of cells being encapsulated within the microspheres (Fig. 3.2B). A small number of microspheres (<1%) less than 50 μm in diameter were observed to form without any encapsulated cells (Fig. 3.2B), which were subsequently eliminated with ease during subsequent media changes (Fig. 3.2E, H). With time, cells were observed to form local colonies, with eventual darkening of colonies and reduction of transparent void space within the microspheres. Additionally, the cell colonies remained completely confined within the boundaries of the microspheres even on day 28 with very little protrusion outside the microsphere edge (Fig. 3.2H). In contrast, when the cell density was raised to a "high" value of 60×10^6 cells/ml, a large number of cells were observed to remain unencapsulated outside the microspheres, suspended in the culture media (Fig. 3.2C). With

subsequent culture time, these cells either adhered to the outer surface of the microspheres or formed independent cellular aggregates (tumor spheroids) (Fig. 3.2F). In addition, the cells on the outside surfaces of microspheres adhered with those on surrounding microspheres, thereby leading to adhesion and aggregation of individual microspheres and formation of larger, heterogeneous structures (Fig. 3.2F,I). Both low and high cell density PF microspheres supported the growth and maintenance of cells in the 3D hydrogel matrix.

In comparison to tumor microspheres, cells grown in self-aggregated tumor spheroids were highly heterogeneous in terms of growth and size distribution (Fig. 3.2A,D,G). The harvesting process of tumor spheroids from the hanging droplets three days post-formation led to disaggregation of some spheroids, resulting in individual cells remaining suspended along with aggregated spheroids (Fig. 3.2A). With time, the spheroids appeared to grow darker in contrast, indicating increased cell density, and with more condensed bodies on day 28 as compared to loose aggregates on day 3 (Fig. 3.2A,G). In addition, individual spheroids were also observed to adhere to one another over time, leading to formation of larger and more irregular spheroid bodies (Fig. 3.2D, G).

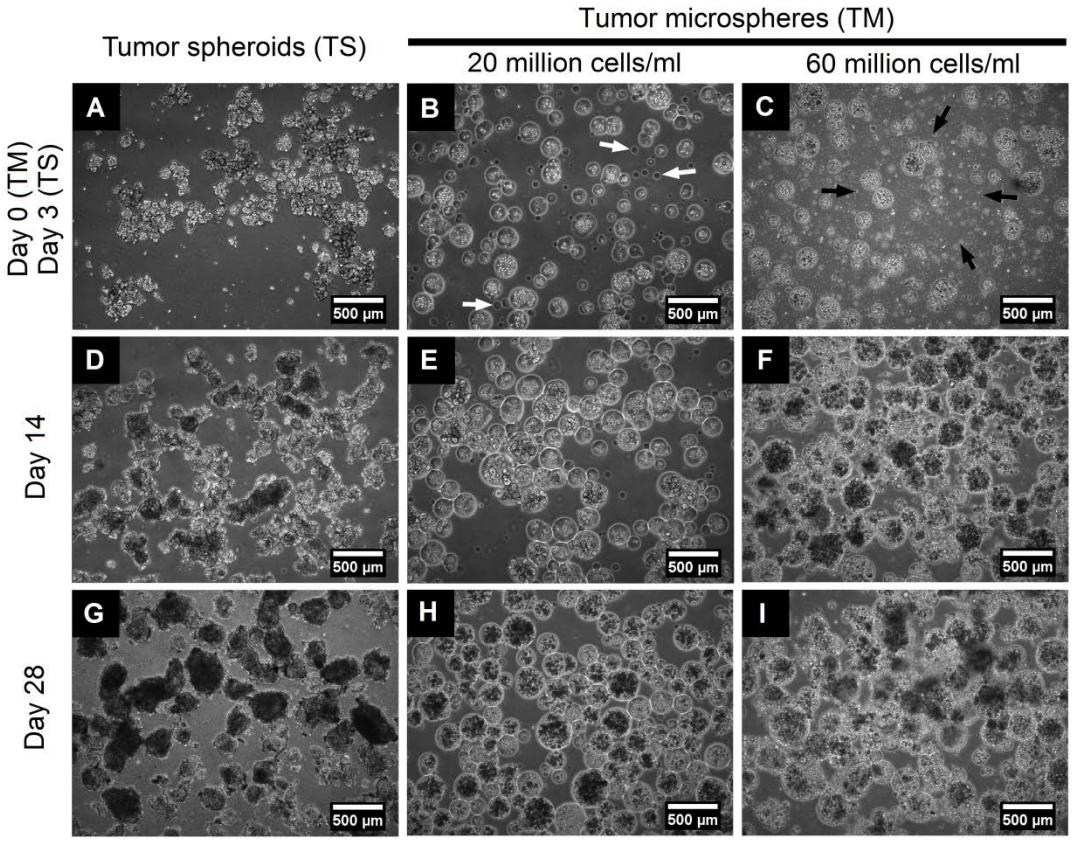

Figure 3.2: Long-term culture of tumor spheroids (TS) and tumor microspheres (TM). Representative images of TS (A,D,G) and TM (B,C,E,F,H,I) from 3 independent batches. Tumor spheroids (A,D,G) displayed heterogeneous growth in size and shape with increasing cell density. Tumor microspheres with lower cell density (B,E,H) resulted in a more uniform range of size and circular shape profile with the presence of some microspheres without any encapsulated cells (solid arrows). Size and shape homogeneity were progressively lost in microspheres with higher cell density (C,F,I) due to presence of unencapsulated cells (black arrows).

Uniform size and shape characteristics of bio-engineered tumor constructs are critical in obtaining relevant and comparable information in high-throughput drug screening assays. Hence, analysis of diameter and circularity (metrics for size and shape respectively) of fabricated tumor microspheres was important in determining the potential of the model in generating uniform

constructs. Examination of the size and shape of engineered constructs revealed broad differences in the distribution ranges among the 3 groups (self-aggregated tumor spheroids, PF tumor microspheres with 20×10^6 cells/ml and those with 60×10^6 cells/ml) (Fig. 3.3). Tumor spheroids were highly polydisperse with respect to diameter and circularity with a significant fraction being less than 50 μm in diameter and less than 0.75 in circularity (1.00 being perfectly circular). With time, the fraction of spheroids in the 100-400 μm range increased due to cell proliferation and subsequent spheroid growth (Fig. 3.3A). Circularity of tumor spheroids was heterogeneous with a significant fraction remaining less than 0.75 throughout the 28 day culture period. This trend can be attributed to non-uniform and loose aggregation of cells in the hanging droplets, adherence of individual spheroids to form larger irregular bodies (highly elongated in some cases) and spatial heterogeneity of growth within individual spheroids. The size of the hanging droplet tumor spheroids and the PF hydrogel microspheres in this study were usually within 500 μm in diameter, hence diffusion gradients of nutrients, oxygen and other metabolites were not pronounced enough to cause any core hypoxic or cell death regions. Whereas this small size scale is not appropriate for investigating the effects of hypoxic core formation and resulting effects on cell behavior, this size range is appropriate for ready adoption for assays already established for tumor spheroids (Ho et al. 2012, Kenny et al. 2015, Gong et al. 2015, Kunz-Schughart et al. 2004) (including MTT assay, LDH cytotoxicity assay). Creating tumor microspheres of this size provides the ability to have 3D tumor microenvironmental control while still employing established experimental approaches.

In comparison to tumor spheroids, in low cell density tumor microspheres (20×10^6 cells/ml) the size and shape distributions were significantly more uniform; a large fraction were between 100-300 μm in diameter and 0.95-1.00 in circularity throughout the

culture period, with a very small fraction having a diameter below 50 μm or above 300 μm (Fig. 3.3A, B). Increasing the cell encapsulation density to 60×10^6 cells/ml in the microspheres introduced a certain degree of heterogeneity, with a higher fraction being above 300 μm in diameter and less than 0.90 in circularity over time. The variance and coefficient of variation in distribution was lower for the tumor microsphere groups compared to tumor spheroids, both in terms of diameter and circularity (Fig. 3.4).

Overall, tumor microspheres with 20×10^6 cells/ml cell encapsulation density provided the tightest control of size and shape characteristics with least variance amongst the three groups. Regulation of the cell density resulted in formation of more uniform microsphere constructs, which were able to maintain this uniformity (with respect to diameter and circularity) throughout the culture period. Adherence between individual microspheres was also greatly reduced at the lower cell encapsulation density. These characteristics are important for maintaining homogeneity in bio-engineered tumor models for further scalability towards high-throughput platforms. Though the fabricated hydrogel microspheres with diameter of 100-300 μm are representative of very small tumors which may not be physiologically relevant when considering advanced or aggressive tumors, the ultimate objective of this study is to establish a geometrically similar model to the established self-aggregated tumor spheroid model and subsequent comparative investigation of the biomaterial matrix effect on cancer cell growth and morphology.

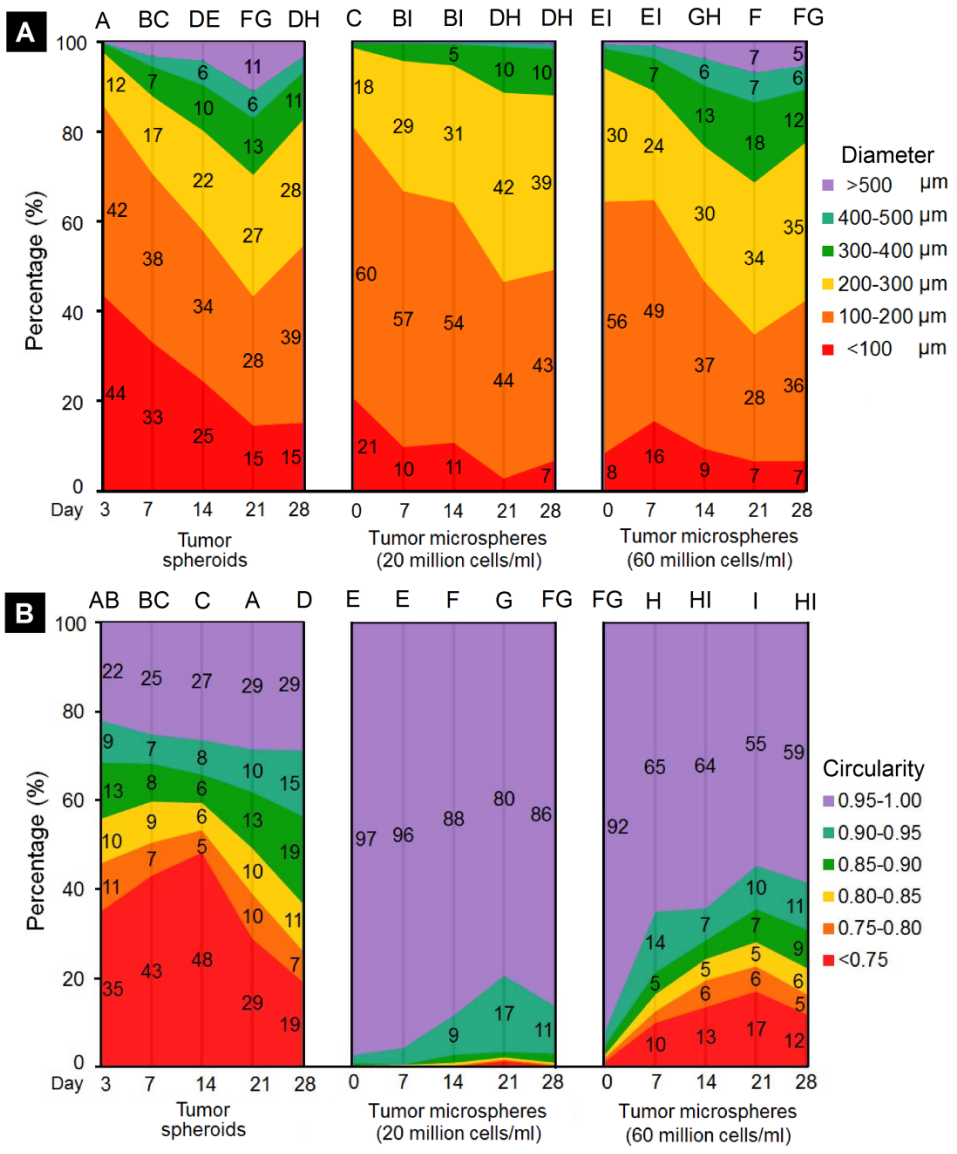

Figure 3.3: Size and shape characteristics of tumor spheroids (TS) and PF tumor microspheres (TM). TM displayed higher uniformity in size and shape distribution compared to TS. TM with lower cell density had (A) the most uniform distribution of diameter (100-300 µm) and (B) the highest degree of circularity (close to 1.00), compared to TS and TM with higher cell density. Individual numbers represent percentage and individual letters represent significance grouping obtained from statistical analysis. Groups not sharing a common letter have significantly different means. (n>300 TS or TM in 3 independent batches, $p<0.05$)

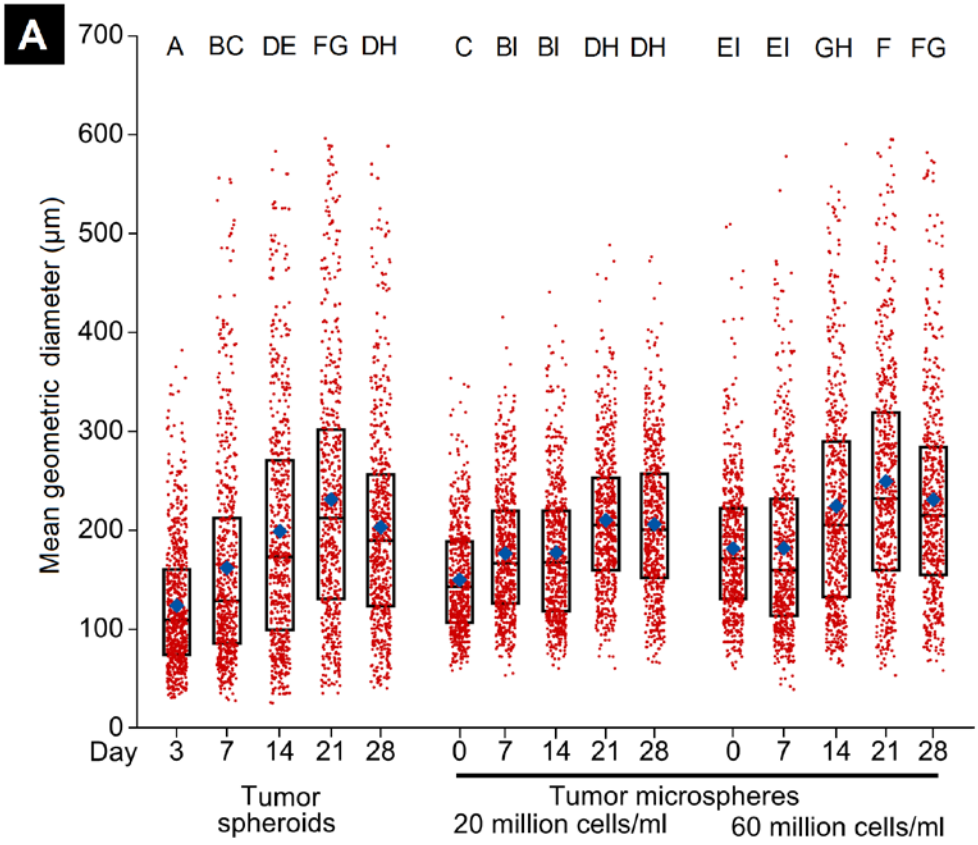
A
Mean geometric diameter (µm)
700
600
500
400
300
200
100
0
A BC DE FG DH C BI BI DH DH EI EI GH F FG
Day 3 7 14 21 28 0 7 14 21 28 0 7 14 21 28
Tumor spheroids
Tumor microspheres
20 million cells/ml
60 million cells/ml

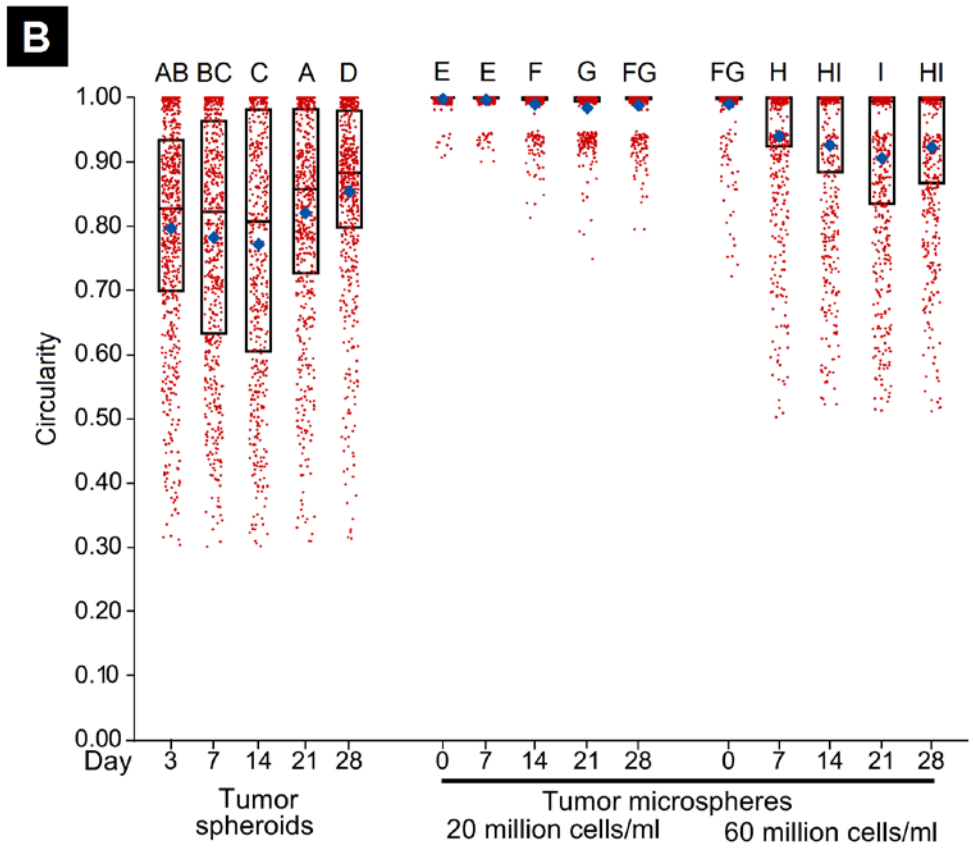
B
Circularity
1.00
0.90
0.80
0.70
0.60
0.50
0.40
0.30
0.20
0.10
0.00
AB BC C A D E E F G FG FG H HI I HI
Day 3 7 14 21 28 0 7 14 21 28 0 7 14 21 28
Tumor spheroids
Tumor microspheres
20 million cells/ml
60 million cells/ml

Figure 3.4: Size and shape distribution of tumor spheroids (TS) and tumor microspheres (TM). (A) Mean geometric diameter and (B) circularity of TS and TM, with low and high initial cell encapsulation densities, at different time points of culture. Blue diamonds denote mean while rectangular boxes represent lower quartiles, medians and upper quartiles. Groups not sharing a common letter have significantly different means ($n>300$ TS or TM in 3 independent batches, $p<0.05$).

3.3.4 Viability and Cell Proliferation within Spheroids and Microspheres

Maintenance of high viability and continued proliferation of cells are important criteria in engineering 3D cancer models for subsequent drug-testing studies. We hypothesized that cells in the tumor microspheres would demonstrate high viability and time-dependent growth consistent with observations from phase contrast images. Both tumor spheroids and tumor microspheres demonstrated high cellular viability (close to 90%) throughout the entire culture period with minimal batch-to-batch variability (Fig. 3.5A,B). Although initial viability in tumor microspheres on day 0 was marginally lower, it recovered to above 90% in subsequent days with cellular growth (Fig. 3.5B). Considering that the diameters of the vast majority of spheroids or microspheres did not exceed 500 μm, mass transfer limitations were not pronounced enough, in general, to cause hypoxic cell death. However, with further optimization of the fabrication technique, this model is could be transitioned to platforms currently being established to employ tumor spheroids. The use of biomimetic PEG-fibrinogen in the tumor microsphere model provides added physiological complexity, tumor microenvironmental influences and cell-matrix interactions which would be difficult to achieve in the traditional tumor spheroid model.

Tumor spheroids demonstrated a high cellular density (on the order of 10^8 cells/μm^3), consistent with that observed in native cancer tissues of different origins (Fig. 4C). It can be

inferred that in the absence of any exogenous ECM, the cells were tightly confined in close proximity to each other in order to form individual spheroids. The cell packing density within the tumor spheroids was 91 ± 16 cells/10^6 μm^3 ($91\times10^6 \pm 16\times10^6$ cells/cm^3) on day 0 and 124 ± 29 cells/10^6 μm^3 ($124\times10^6 \pm 29\times10^6$ cells/cm^3) on day 21 (Fig. 3.5C). In contrast, cell packing density in tumor microspheres increased from 20 ± 4 cells/10^6 μm^3 ($20\times10^6 \pm 4\times10^6$ cells/cm^3) on day 0 to 106 ± 12 cells/10^6 μm^3 ($106\times10^6 \pm 12\times10^6$ cells/cm^3) on day 21 (Fig. 3.5D). Initial cell density evaluated on day 0 was consistent with cell concentration in the PF polymer precursor during the microsphere fabrication process; the final cell density obtained on day 21 was similar to that in tumor spheroids. Batch-to-batch variability in average cell density was minimal for both tumor spheroids and tumor microspheres; however, the coefficient of variation of cell density at all the time points was significantly lower in tumor microspheres as compared to that in tumor spheroids (Fig. 3.6).

Overall, encapsulation of MCF7 cells in the PF hydrogel microspheres promoted cell proliferation while maintaining high viability throughout the culture period. These results corroborate our initial assumption about cell growth based on increase in colony formation and gradual reduction in void space within the microspheres. Thus, the importance of incorporating biomimetic PF as a cell-permissive ECM in spheroidal cancer models is validated.

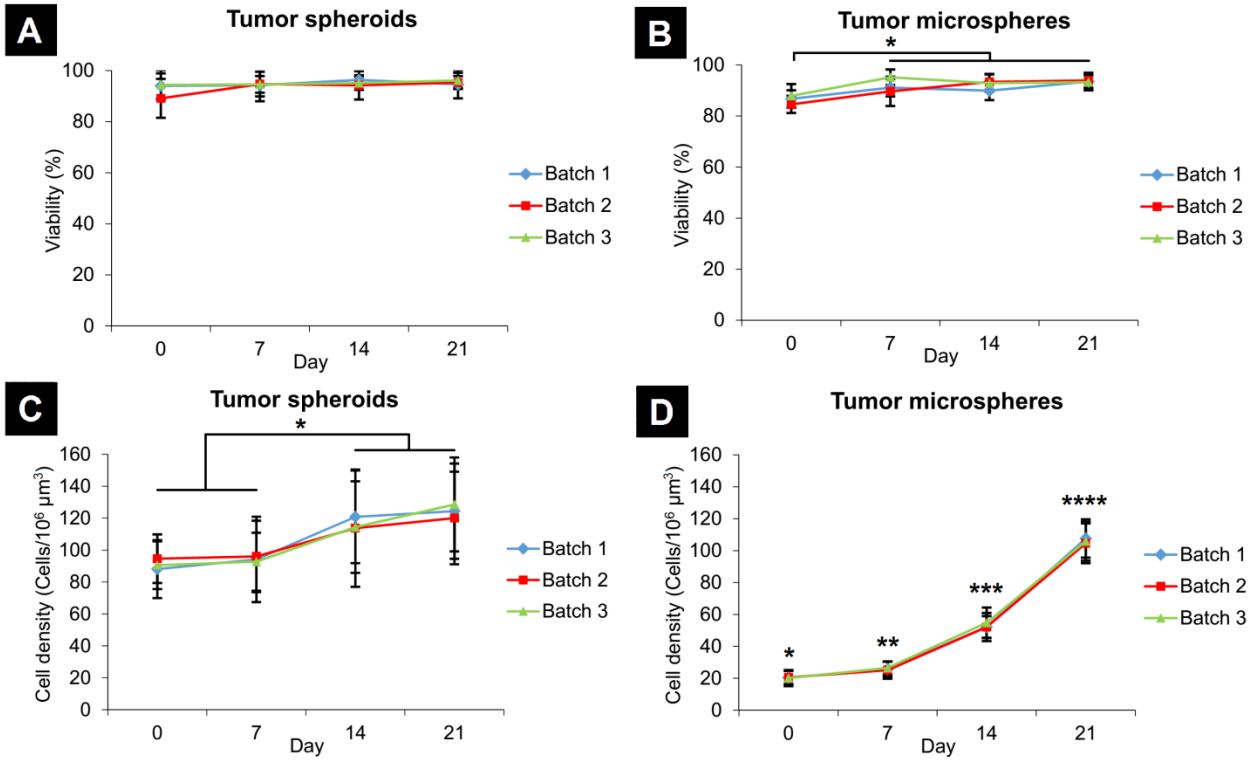

Figure 3.5. Comparison of cell viability and growth within the TS and TM models. High cell viability is maintained in both (A) TS and (B) TM through 21 days in culture ($p<0.05$, $n=45$ in 3 independent batches). Cell density was relatively higher in TS (C) compared to that in TM (D), where rapid increase in density is observed through 21 days ($p<0.05$, $n=45$ in 3 independent batches).

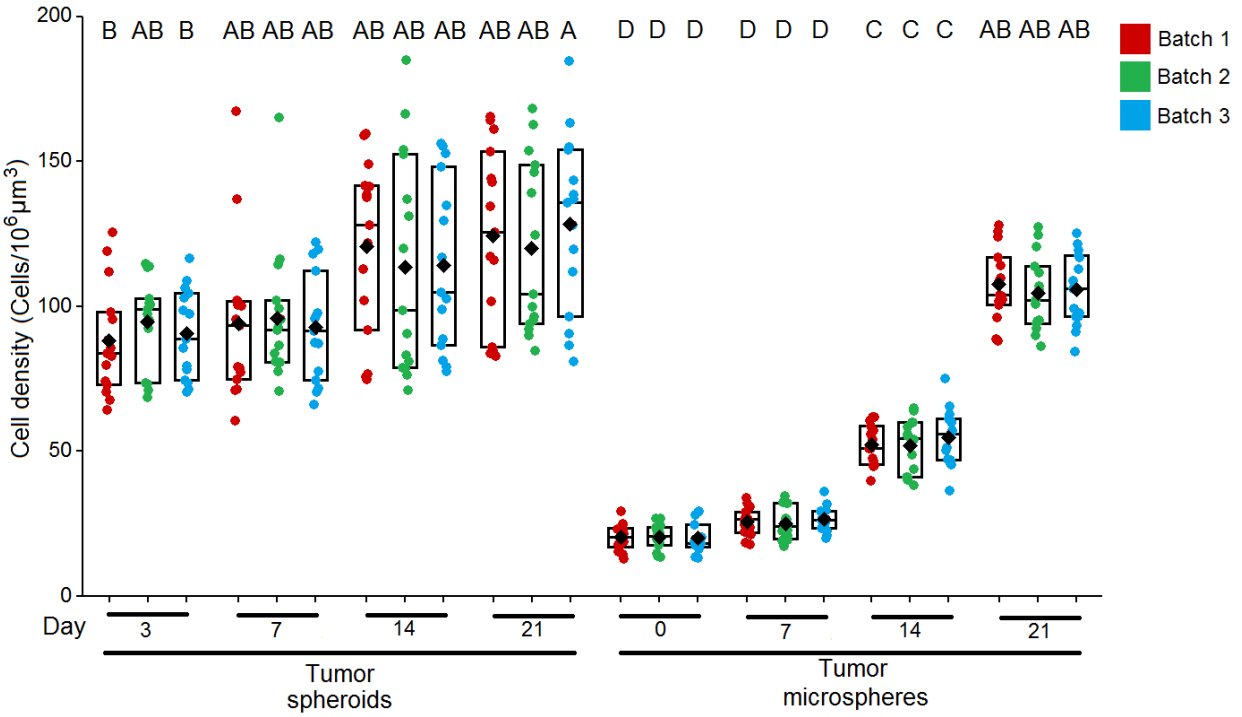

Figure 3.6: Growth rate of cells in tumor spheroids (TS) and tumor microspheres (TM). Comparison of cell density within individual TS and TM from 3 independent batches through 21 days in culture. Black diamonds denote means while rectangular boxes represent lower quartiles, medians and upper quartiles. Groups not sharing a common letter have significantly different means (n=15 TS or TM per batch per time point, $p<0.05$).

3.3.5 Ultrastructural Differences between Tumor Spheroids and Microspheres

In order to view the ultrastructural matrix properties and determine differences in cellular morphology and tissue structure, SEM imaging was conducted on tumor spheroids and tumor microspheres (with and without cells). In general, cells within tumor spheroids appeared to be larger in size with numerous cell surface projections, tight cell-cell adherens junctions, and more uniform organization reminiscent of the epithelial polar morphology found in normal breast tissue (Fig. 3.7A,B). In some loosely aggregated tumor spheroids, cells seemed to lack these

tight junctions and appeared more spherical in morphology, while still remaining firmly adherent within the spheroids. In contrast, cells within tumor microspheres appeared more randomly organized, heterogeneous in orientation, smaller in size and well-distributed throughout the hydrogel matrix (Fig. 3.7C,D). Presence of cell adherens junctions was markedly absent in tumor microspheres. In addition, numerous pore-like structures leading to the interior of microspheres were also noticed on the surface and immediate interior of microspheres (Fig. 3.8E,F). A cross-sectional view of the tumor microsphere interior revealed dense cellular packing with cells homogenously interspersed within the PF matrix (Fig. 3.8F). Tumor microspheres without cells revealed a porous, mesh-like architecture both on the surface and in the interior regions of the PF hydrogel microspheres (Fig. 3.8A, B).

In general, SEM imaging revealed broad differences in the ultrastructural morphology and organization of cells within tumor spheroids and tumor microspheres. Cells within tumor microspheres appeared to have a more disorganized and random structure compared to those in spheroids, reminiscent of the disorganized structure in native breast cancer tissue. Loss of epithelial polarity and tight adherens junctions of cells in tumor microspheres were also indicative of departure from epithelial morphology of these cells in 3D culture, possibly due to selective pressure exerted by the matrix on the encapsulated cancer cells. Another interesting aspect of investigation would be ultrastructural variations between different breast cancer cell lines. Specifically, MDA-MB-231 cells, being metastatic and aggressive in nature, would be expected to exhibit elongated morphologies and cellular protrusions when cultured within PF hydrogel microspheres.

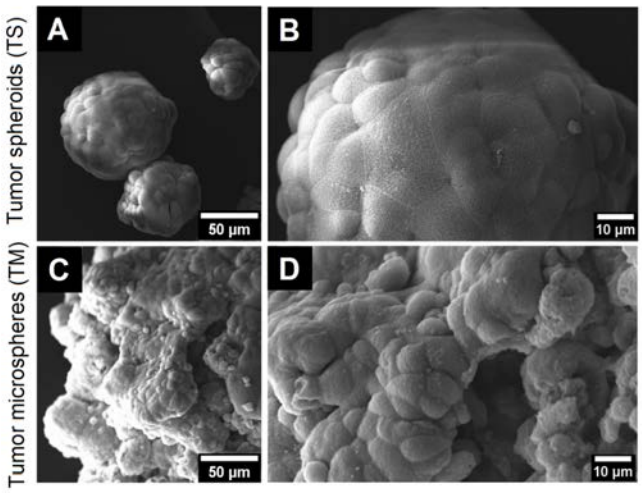

Figure 3.7: Ultrastructural differences between tumor spheroids (TS) and tumor microspheres (TM). TS (A,B) display higher degree of uniformity in cellular architecture with distinct adherens cell-cell junctions and apico-basal polarity. TM (C,D) exhibit a more disorganized arrangement of cells with loss in polarity and reduced cell size.

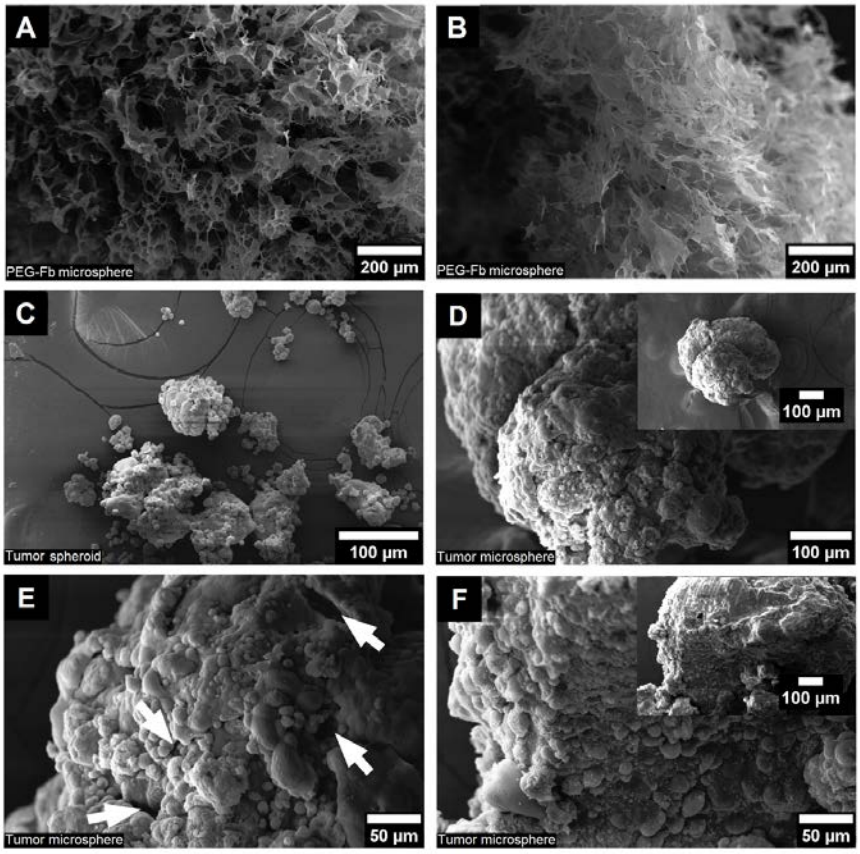

Figure 3.8: Ultrastructural features of tumor spheroids and tumor microspheres. PF microspheres without any cells display a porous mesh-like matrix both on the outside (A) and inside (B) of microspheres. (C) High degree of size and shape heterogeneity of tumor spheroids. (D) Magnified view of a tumor microsphere (inset) with disorganized cellular architecture at the surface. (E) Pore-like structures visible at the surface of a tumor microsphere (denoted by white arrows). (F) Dense cell packing and random presentation of cells in the interior region of a tumor microsphere (inset).

3.3.6 Promotion of Tumorigenic Morphology within Microspheres

In order to understand the influence of the biomaterial matrix on key tumorigenic characteristics of MCF7 cells cultured as spheroids or in hydrogel microspheres, 3D

morphometric analysis was conducted on three fabricated models, tumor spheroids, PF tumor microspheres and PEGDA microspheres. PEGDA microspheres were specifically chosen as the non-bioactive, control group as PEGDA is not known to support cell adhesion or cell-matrix interactions. 3D morphological characteristics of cells in all groups were quantified using fluorescence images of cellular nuclei and actin filaments. Cells in tumor spheroids displayed a more organized, oriented arrangement with sharp, distinct and rounded nuclei and actin filaments being concentrated at the periphery of cells (Fig. 3.9A). Cells in PF tumor microspheres were observed to be disorganized with lack of specific orientation and diffuse appearance of cell nuclei. In addition, cells in microspheres seemed compressed and were significantly smaller in size, so that the nuclei occupied a major fraction of the cell itself (Fig. 3.9B). Cells in PEGDA microspheres appeared to be further rounded, confined and restricted to local regions, possibly due to lack to cell-matrix interactions (Fig. 3.9C). These observations could be attributed in part to the spatial limitations imposed by the surrounding hydrogel matrix on the cells.

Quantification of these distinct morphological differences was conducted by evaluation of specific parameters including apico-basal polarity, nuclear area, cellular area, nuclear:cytoplasmic ratio (NC ratio), nuclear volume density and cell-cell junction length for both tumor spheroids and tumor microspheres. Cell polarity is a distinguishing feature of the normal mammary epithelium, with cells displaying a broader apical surface and tapering down to a narrower basal surface in conjunction with adjacent cells while maintaining tight cell-cell junctions with each other. The percentage of cells displaying this apico-basal polar morphology was significantly lower in the non-bioactive, control group of PEGDA microspheres (11 ± 4%) than in tumor microspheres (51 ± 9%) or in spheroids (85 ± 9%) (Fig. 3.9D). Nuclear area (PEGDA microspheres: 87 ± 45 μm^2, PF tumor microspheres: 92 ± 42 μm^2 and tumor spheroids:

150 ± 46 μm^2) and cellular area (PEGDA microspheres: 175 ± 92 μm^2, PF tumor microspheres: 194 ± 97 μm^2 and tumor spheroids: 451 ± 148 μm^2) were significantly reduced in cells in the presence of biomaterial matrix (Fig. 3.9E, F). Interestingly, the NC ratio (PEGDA microspheres: 1.16 ± 0.59, PF tumor microspheres: 0.97 ± 0.35 and tumor spheroids: 0.55 ± 0.20) and nuclear volume density (PEGDA microspheres: 0.51 ± 0.11, PF tumor microspheres: 0.48 ± 0.08 and tumor spheroids: 0.34 ± 0.08) were significantly different in all three groups (Fig. 3.9G, H). This observation can be attributed in part to the restrictive forces exerted by the surrounding 3D matrix on the cells and possibly higher nuclear activity of cells within PF tumor microspheres. In the absence of an initial supporting matrix in the tumor spheroids, cells appeared to have a higher degree of freedom in arranging themselves into organized architectures within the spheroids, while those in PF tumor microspheres were spatially restricted, growing outward from local colonies and gradually forming local niches of cellular growth as permitted by the 3D matrix. Further, analysis of cell-cell junction length revealed significantly lower junction lengths between cells in PEGDA and PF microspheres (PEGDA microspheres: 13 ± 4 μm, PF tumor microspheres: 13 ± 4 μm and tumor spheroids: 17 ± 5 μm) possibly due to lower cell size (Fig. 3.9I). When normalized with respect to the total length of the cell periphery, junction length as a percentage of total cell length was found to be higher in the PEGDA microspheres compared to the other two groups (PEGDA microspheres: 0.16 ± 0.04 μm, PF tumor microspheres: 0.13 ± 0.04 μm and tumor spheroids: 0.14 ± 0.04 μm) (Fig. 3.9J).

In summary, cells in PF tumor microspheres, although smaller in cellular size, had higher nuclear mass, a greater degree of disorganization and enhanced tumorigenic morphology compared to those in tumor spheroids. Though cells displayed tight junctions in all three models, cells in tumor spheroids were more similar to the normal mammary epithelial morphology as

compared to those in tumor microspheres. The induction of tumorigenic characteristics of MCF7 cells within PEG-fibrinogen microspheres in comparison to those grown without any biomaterial (tumor spheroid model) can be attributed to a number of factors including the inherent 3D selective pressure on the encapsulated cells, influence of matrix stiffness, specific integrin-mediated cell-matrix interactions amongst others. The specific role of each of these factors on the promotion of tumorigenic characteristics of MCF7 cells could be investigated in more details in future studies. Overall, these morphometric analyses demonstrate the important advantages of employing an exogenous, biomimetic matrix within 3D spheroidal tumor constructs. Though MCF7 cells are not highly tumorigenic *in vivo*, these investigations primarily concern with establishing a 3D biomimetic model to demonstrate the role of PEG-fibrinogen in modulating 3D cancer cell characteristics and morphology in comparison to the traditional method of forming self-aggregating tumor spheroids. In future, this technique can be extended towards modeling of more phenotypically aggressive tumors that are more physiologically relevant compared to that presented in this study. Certain highly aggressive cell lines are unable to form spontaneous tumor spheroids due to weak cell-cell interactions and hence cannot be investigated consistently using the approaches designed for the tumor spheroid model. However, with the established tumor microsphere model, this limitation can be overcome as multiple cell lines of varying degrees of aggressiveness can be cultured within biomimetic microspheres in future cancer studies.

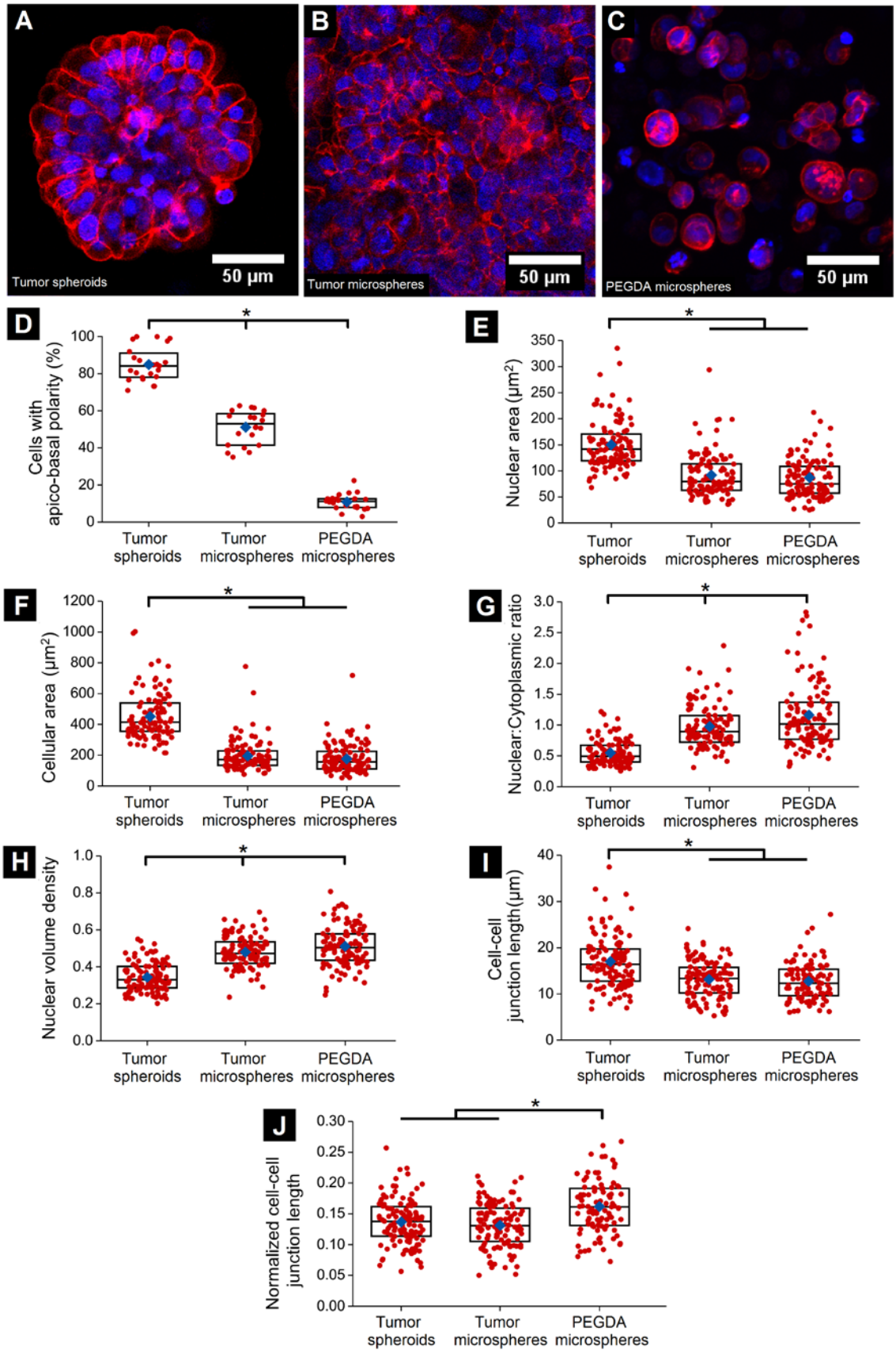
A
Tumor spheroids
50 µm
B
Tumor microspheres
50 µm
C
PEGDA microspheres
50 µm
D
Cells with apico-basal polarity (%)
E
Nuclear area (µm²)
F
Cellular area (µm²)
G
Nuclear:Cytoplasmic ratio
H
Nuclear volume density
I
Cell-cell junction length (µm)
J
Normalized cell-cell junction length
Tumor spheroids
Tumor microspheres
PEGDA microspheres
*

Figure 3.9: Enhanced morphometric tumorigenicity of cells in PF tumor microspheres. Confocal image slice of (A) tumor spheroids (TS), (B) tumor microspheres (TM) and (C) PEGDA microspheres (PEGDA-TM) stained for nuclei (DAPI, blue) and actin filaments (phalloidin, red). Compared to TS, TM and PEGDA-TM exhibit (C) reduced polarity ($n>20$ representative images, $p<0.05$), (D, E) reduced nuclear and cellular area ($n>100$ cells, $p<0.05$), (F, G) elevated nuclear cytoplasmic ratio and nuclear volume density ($n>100$ cells, $p<0.05$) and (H) reduced cell-cell junction length. (I) TS and TM have lower normalized cell-cell junction length compared to PEGDA microspheres ($n>100$ cells, $p<0.05$). Blue diamonds denote mean while rectangular boxes represent lower quartiles, medians and upper quartiles.

3.3.7 3D culture of other cancer cell types in PF hydrogel microspheres

Finally, it was of general interest to investigate the applicability of extending the tumor microsphere model for encapsulation of other cancer cell lines. Cancer cells lines of different origins tend to exhibit differential growth characteristics between 2D and 3D culture (Ivascu and Kubbies 2007). Specifically, cells of epithelial origin display a tendency to grow in local colonies with a higher degree of cell-cell adhesion and cellular circularity in 2D culture (Loessner et al. 2010). In contrast, metastatic and more aggressive cancer cell lines display a mesenchymal phenotype where cells appear more elongated, with visible protrusions and with significantly lower cell-cell adhesion tendencies (Neve et al. 2006). Further, the lack of strong adhesion capabilities of these cell lines prevents them from forming dense cellular aggregates in 3D culture, thereby making the formation of tumor spheroids severely challenging (Rainaldi et al. 1999). Hence, comparative investigation of cancer cell lines of epithelial and mesenchymal phenotypes using tumor spheroids is technically challenging.

In order to address this issue, we encapsulated cancer cells from different tissue origins, displaying a range of phenotypes and exhibiting differential growth characteristics in 2D culture, within PF hydrogel microspheres. We hypothesized that cells grown in 2D culture would display specific phenotypic differences from those in 3D microsphere culture. For breast cancer, two additional cell types, SK-BR-3 and MDA-MB-231 were chosen for 3D encapsulation within microspheres. SK-BR-3 cells displayed tight cell-cell junctions bearing an epithelial morphology in 2D culture (Fig. 3.10A). Upon encapsulation in microspheres, these cells formed local spherical colonies initiating from single cells (Fig. 3.10B, C). In contrast, MDA-MB-231 cells displayed an invasive, mesenchymal phenotype with highly elongated cells in 2D culture (Fig. 3.10D). Interestingly, when encapsulated within PF microspheres at the same initial density, these cells spread out rapidly and occupy the entire volume of microspheres within just 7 days of culture (Fig. 3.10B, C). Colon cancer HT29 cells grew as local colonies with tight cell-cell junctions in 2D culture, reminiscent of the intestinal epithelia (Fig. 3.10G). In 3D PF microspheres, they were observed growing in dense local clusters arising from single cells, becoming larger with time and eventually occupying the previously unoccupied void space within microspheres (Fig. 3.10H, I). For prostate cancer, two cell lines, PC-3 and a metastatic variant, PC-3-Met, were chosen. In 2D culture, PC-3-Met cells were observed to be more elongated and displayed a more aggressive phenotype compared to PC-3 cells (Fig. 3.10J,M). In 3D PF microspheres, the PC-3-Met cells displayed faster and denser colony formation and invasion through the 3D matrix compared to the PC-3 cells, thereby demonstrating the differences in aggressiveness between the two variant cell lines (Fig. 3.10K, L, N, O).

Overall, we have demonstrated the ability to encapsulate a large variety of cancer cell types, both of epithelial and mesenchymal phenotype, and maintain them in culture through at

least 14 days within PF hydrogel microspheres. This capability provides significant advantages over the tumor spheroid self-aggregation technique, where certain cell lines do not have a tendency to spontaneously form multicellular aggregates or form very loose aggregates at best. In addition, encapsulation of multiple cancer cell types provides us previously unknown information about the nature of 3D growth, aggressiveness and morphology in comparison with each other and stark differences from that observed in 2D cell culture. Hence, the PF microsphere model can be generally extended for use in 3D spheroidal culture of cancer cells, further investigation of tumorigenicity and drug-testing applications.

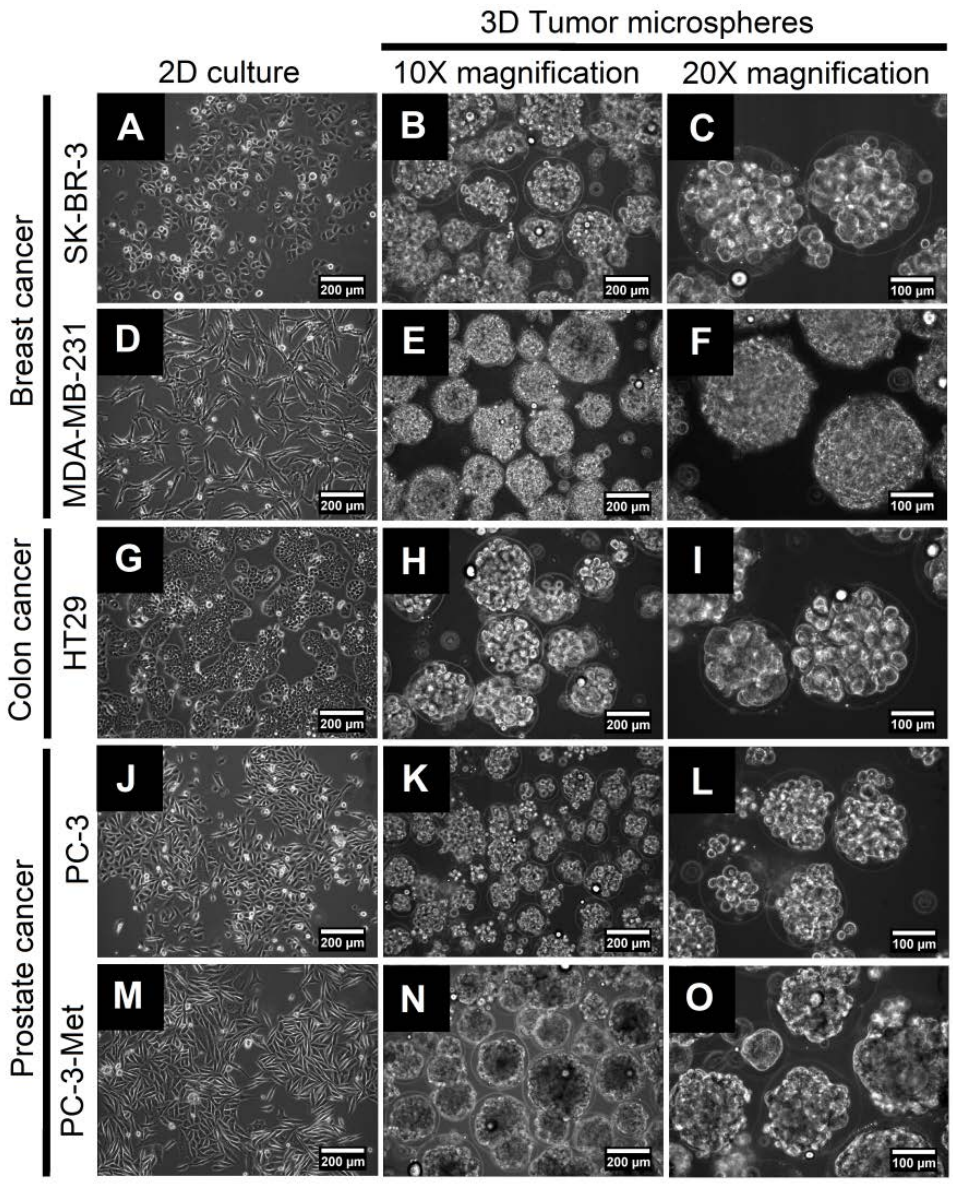

Figure 3.10: Culture of other cancer cell types in tumor microspheres. A wide range of metastatic and non-metastatic cancer cells displaying either epithelial or mesenchymal morphology in 2D culture were successfully cultured within PF microspheres including breast cancer SK-BR-3 (A-C), MDA-MB-231 (D-F), colon cancer HT29 (G-I) and prostate cancer PC-3 (J-L) and PC-3-Met (M-O) cells with representative images at day 14 of culture.

3.4 Discussion

Microenvironmental regulation of tumorigenic progression is a vital consideration in the development of bioengineered 3D tumor models. Various ECM components such as collagen, laminin and fibrinogen, found in the TME, have been implicated in aiding the progression of pre-cancerous cells towards more malignant and metastatic growth. Hence, incorporation of these ECM cues into 3D tumor models for investigation of biological mechanisms of disease progression is of vital importance. To this end, collagen, Matrigel, hyaluronic acid, calcium alginate, PLA, PLGA and other materials have been widely used for encapsulation and 3D culture of cancer cells. However, the role of fibrinogen in the tumorigenic progression of cancer cells has not received much attention. In this study, the ability of fibrinogen to support and promote phenotypic tumorigenicity of MCF7 cells and other cancer cell types is demonstrated, thereby addressing in part, the lack of application of fibrinogen in 3D cancer models.

Multicellular aggregates or tumor spheroids are regarded as the “gold standard” in 3D cancer models and have been widely used for testing anti-cancer drug efficacies. Numerous investigations have been conducted to improve the suitability of the tumor spheroid model for use in high-throughput screening assays. Novel fabrication methods and techniques have been developed to generate uniform, size-controlled and robust tumor spheroids; some of these methods include the use of ice lithography for fabrication of quasi-spherical microwells on hydrophobic substrates (Liu et al. 2014), microfluidic self-assembly (Wu et al. 2008), nanoimprinted scaffolds for spontaneous cellular aggregation (Yoshii et al. 2011) and polymer microstructure arrays for high-throughput generation of tumor spheroids (Markovitz-Bishitz et al. 2010). However, the majority of these techniques are limited by the inherent inability to control and investigate the influential role of ECM components in regulating 3D morphological

characteristics of cancer cells, exchange of cellular metabolites, and diffusion of drugs. In addition, the varying propensity of different cancer cell lines to form highly heterogeneous multicellular aggregates also imparts non-uniformity in further drug-testing results and hinders the ability to obtain clinically-relevant information about drug toxicity and efficacy. Therefore, a platform enabling the high-throughput generation of bioengineered spheroidal tumor constructs that incorporate a biomimetic ECM and provide a tumorigenic microenvironment, would be a significant improvement over current tumor spheroid technologies.

In previous studies, comparative analyses have been conducted between 2D cultured cancer cells and those in 3D self-aggregated spheroids or in novel biomaterial matrices (Xu, Sabanayagam, et al. 2014, Chen et al. 2012, Huang and Hsu 2014). However, comparative analysis between 3D spheroids and a geometrically similar model incorporating the effects of a biomaterial matrix has been lacking. In order to address this issue, a novel tumor microsphere model for the encapsulation and 3D culture of cancer cells was developed and comparative analyses with the traditional tumor spheroid model to determine the influence of a biomimetic matrix, PF, on the 3D tumorigenic growth characteristics of MCF7 cells were conducted. The mere presence of a permissive, exogenous, fibrinogen-based matrix in the cellular microenvironment was demonstrated to have a drastic effect on the tumorigenic growth and morphology of 3D cultured cells. Specific parameters of the dual-phase, water-in-oil emulsion technique used for the fabrication of tumor microspheres, including vortexing speed, cross-linking time and initial cell encapsulation density, were carefully optimized for the high-throughput generation of PF hydrogel microspheres, with high encapsulation efficiency, high initial cell viability, low batch-to-batch variability and a high degree of uniformity of cell density within individual microspheres, while eliminating any microsphere agglomeration. For

comparison, the hanging droplet method was chosen for the generation of tumor spheroids due to its relative ease in spheroid formation and harvesting, higher degree of spheroid uniformity compared to the non-adhesive agar plate method and rapid rate of aggregate formation. The initial cell density per hanging droplet and spheroid formation time were optimized for the generation of tight cellular aggregates of controlled size. However, a certain degree of heterogeneity inherent to the fabrication and handling of the tumor spheroid model could not be eliminated. Analysis of diameter and circularity (descriptors of size and shape respectively) revealed the higher degree of uniformity and lower variance of PF tumor microspheres (particularly with the lower initial cell encapsulation density) compared to tumor spheroids. Overall, the fabrication method for generation of tumor microspheres yielded highly superior bioengineered tumor constructs as compared to those obtained via the hanging droplet method. In addition, the size range obtained with the microsphere fabrication method could potentially be narrowed further by adopting a microfluidics approach to generate more homogenous and monodisperse microspheres. The significant improvement in uniformity in size and shape distribution of the microsphere method over the hanging droplet technique merits attention and further investigation in the future.

In the present study, the growth profiles of MCF7 cells revealed broad differences between cells cultured as multicellular tumor spheroids and those within PF microspheres. Cells in tumor spheroids displayed a higher cell density throughout the 21 day culture period with moderate increase in density at later time points. This observation could be attributed to the absence of significant ECM components in the tumor spheroids, thereby leading to the dense packing of the cells in tight conjunction with one another. However, it can be surmised that the cells produced endogenous ECM components, albeit in relatively minute quantities, that might

have enabled initial aggregate formation and subsequent cell proliferation. Additionally, if the increase in tumor spheroid diameter over time is taken into account, it can be implied that as new cells were produced within spheroids, the spheroids themselves grew radially outwards, with the cells gradually arranging themselves into a regulated architecture with moderate increase in cell packing density. In sharp contrast, cells within tumor microspheres appeared individually and uniformly dispersed within the 3D matrix, with subsequent local colony formation, increasing colony size and merging of individual colonies, thereby leading to a substantial rise in cell density over time. The lower cell density at the initial time point corresponded to the optimized cell concentration in PF precursor used for generation of tumor microspheres and the final cell density obtained was comparable to that in tumor spheroids and those found in native tumor tissues. It is worthwhile to mention that the overall size of tumor microspheres remained fairly constant through 21 days along with progressive increase in cell density within the microspheres. Beyond 28 days, some cell colonies seemed to protrude beyond the spherical edges of the microspheres and escape the 3D matrix environment imposed by the hydrogel material. Hence, our investigations were limited to the culture period where the cells colonies were completely restricted within the hydrogel matrix. Comprehensively, we demonstrate the ability of the PF matrix to support the rapid proliferation and maintenance of MCF7 cells in 3D culture, thereby establishing the suitability of the tumor microsphere system as a 3D model for further investigation into mechanisms of tumorigenic progression.

3D morphometric analyses revealed stark differences between cells in self-aggregated tumor spheroids and those within PF tumor microspheres. Initially observed via SEM and further confirmed through fluorescence imaging, apico-basal polarity of cells appeared to be drastically reduced in tumor microspheres compared to tumor spheroids. Apico-basal polarity is a

distinguishing feature of the normal mammary epithelium; departure from this polar organization and architecture represents the first step in epithelial-mesenchymal transition and subsequent malignant transformation (Huebner and Ewald 2014, Chen et al. 2013, Godde et al. 2010). Cells in tumor spheroids displayed a high degree of organization and self-assembly, forming structures reflective of normal mammary acini. In sharp contrast, cells within tumor microspheres displayed a disorganized and abnormal arrangement, reminiscent of aggressive tumor growth. Though both nuclear and cellular area were significantly reduced in cells within tumor microspheres, possibly due to spatial limitations imposed by the surrounding hydrogel matrix, the nuclear cytoplasmic ratio (NC ratio) and nuclear volume density were highly elevated in the tumor microspheres compared to tumor spheroids. In addition, cells in tumor microspheres also displayed higher degree of cellular and nuclear atypia, consistent with cancerous growth. The NC ratio has been frequently used in histopathological analyses and gradation of tumors and to differentiate regions of cancerous growth from normal tissue (White et al. 1997, Nandakumar et al. 2012, Nandakumar et al. 2011). Pre-malignant and cancerous cells are characterized by scant cytoplasm, larger nuclear size, higher NC ratio and higher nuclear volume density compared to normal cells, possibly due to chromosomal abnormalities and poor cellular differentiation state (Pienta and Coffey 1991, Ladekarl 1995). Specifically, for breast DCIS (ductal carcinoma in situ), NC ratio was found to increase from 0.4 to 0.8 with increased hypoxic load and decreased cellular differentiation stage (Helczynska et al. 2003). Therefore, our observations led to the conclusion that MCF7 cells in tumor microspheres display enhanced tumorigenic morphology compared to those in tumor spheroids. Further in-depth investigations at the genomic and proteomic level would be required to establish the tumorigenic capabilities of the MCF7 cells cultured both within PF hydrogel microspheres and those grown as self-aggregated spheroids.

Further analysis of tight cell-cell junctions revealed prominent differences between the cellular architecture and organization within tumor spheroids and tumor microspheres. Tight junctions play an important role in maintenance of apico-basal polarity, with specific demarcation of apical and basolateral membrane domains of cells, inhibition of cellular migration and preservation of tissue architecture. Malignant transformation of cells is characterized by loss of tight junction proteins (claudins and zona occludens), reduction in cell-cell adhesion capacity and increased ability of cellular migration and invasion into surrounding stromal tissue (Le Bras et al. 2012, Martin and Jiang 2009). In general, cells in tumor spheroids displayed higher cell-cell junction lengths, specifically those arranged in an apico-basal architecture. However, the junction length was significantly reduced for cells in tumor microspheres with a corresponding loss of polarity, indicative of the malignant progression within the hydrogel matrix. Interestingly, when the cell-cell junction length was normalized to the total cell perimeter, the observations were reversed, with cells in tumor microspheres displaying higher normalized junction length compared to those in tumor spheroids. This could be attributed in part to the reduced cellular size and reduced perimeter of individual cells, thereby leading to an overall increase in normalized junction length. Overall, the 3D morphometric analyses revealed the increased phenotypic tumorigenicity and proclivity towards malignant transformation of cells within tumor microspheres compared to those within tumor spheroids. These observations reinforce the importance of incorporating a cell-permissive biomimetic ECM matrix in the cellular microenvironment when designing and fabricating bioengineered cancer models.

This study specifically focuses on the impact of PEG-fibrinogen as a biomimetic matrix on the morphological and growth features of MCF7 cells. Though the MCF7 cell line is

representative of a non-aggressive breast tumor subtype, its use in this study is meant to provide a preliminary proof-of-concept of the suitability of PEG-fibrinogen for 3D cancer cell culture. Further work would be needed to elucidate the role of PEG-fibrinogen on the tumorigenicity of MCF7 cells and other more aggressive cell types at the genomic and proteomic levels. In addition, this work primarily deals with the fabrication and optimization of micron-scale tumor constructs. Future work will focus on the addition of more complex and intricate microstructures associated with small tumors, for example, basement membrane surrounding the micro-scale tumors. In addition, these tumor microspheres can also be encapsulated within larger PEG-fibrinogen hydrogels encapsulating secondary cell types including cancer-associated fibroblasts and endothelial cells.

The differences in growth trends between the tumor microsphere model and *in vivo* models could possibly result from inherent differences between 3D *in vitro* systems, which are more simplistic in nature compared to *in vivo* models, which involve higher degrees of physiological complexities that are challenging to incorporate in 3D *in vitro* systems. MCF7 cells are non-aggressive in nature and do not form spontaneous tumors in *in vivo* models. Additionally, since MCF7 cells exhibit hormone responsiveness, their proliferation and invasiveness can be hormonally stimulated under specific conditions. When MCF7 cells are exposed to culture media under 2D and 3D conditions, the cells are exposed to basal levels of hormonal stimulation from the serum components of the culture media itself. However, due to increasing physiological complexities of *in vivo* models and absence of sufficient hormonal stimulation, MCF7 cells are unable to form spontaneous tumors *in vivo*. A similar growth trend is observed in the tumor microsphere model as well. Since cells cultured in the PEG-fibrinogen tumor microspheres are maintained in the same culture media as 2D cells, it can be surmised that

the cells are also exposed to certain levels of hormonal stimulation from the serum components of the culture media, similar to those cultured in 2D. In addition, MCF7 cells encapsulated within the PEG-fibrinogen microspheres also experience greater spatial freedom for local colony formation within the structure of individual microspheres than is potentially available in vivo. In comparison, MCF7 cells cultured as tumor spheroids are more tightly packed throughout the culture period and only the outermost layer of cells enjoy the spatial freedom of outward growth. These differences, in part, can explain the growth trends of MCF7 cells in the tumor microsphere and the tumor spheroid model.

In general, the tumor microsphere model presents distinct advantages over the currently popular tumor spheroid model, namely: (a) Presence of a cell-permissive fibrinogen matrix that supports tumorigenic growth and morphology of encapsulated cancer cells, (b) Ability to uniformly encapsulate a wide variety of cancer cell types and potentially co-encapsulate secondary cell types along with cancer cells within microspheres and (c) High-throughput generation of homogeneous spheroids with ease of analysis for investigation of biological mechanisms associated with tumor progression. In addition, this model could potentially aid in testing drug-efficacy on cancers at different growth stages. For example, drugs could be tested immediately after encapsulation of cells to study the cytotoxic effects on individual cells or at a later time point, where cells have formed large colonies and display advanced tumorigenic growth features. Additionally, individual microspheres could be encapsulated in co-culture with other cell types (*e.g.* stromal fibroblasts, endothelial cells, immune cells and others) within larger hydrogel constructs to generate a more recapitulative, 3D bioengineered tumor model. Based on the results of the current study, the established tumor microsphere model could be employed for evaluation and screening of anti-cancer drug compounds in future investigations.

3.5 Conclusions

A novel fabrication technique for the high-throughput generation of PF hydrogel microspheres and the ability to encapsulate and maintain a range of different cancer cell types within these 3D spheroidal constructs for long culture periods has been demonstrated. Comparative size and shape analysis established the higher uniformity and lower variability in diameter and circularity of the tumor microspheres over self-aggregated tumor spheroids. Cell viability was high in both models with tumor microspheres having a higher cellular growth rate. Investigation of the ultrastructural and 3D morphological features of cells within both systems revealed the superiority of the tumor microsphere model in supporting and enhancing the morphometric tumorigenicity of encapsulated cancer cells. It is anticipated that continued adaptation and improvement of microsphere fabrication techniques could facilitate the application of the tumor microsphere model in high-throughput assays designed for multicellular tumor spheroids.

CHAPTER 4: PEG-fibrinogen Based Hydrogels For 3D Breast Cancer Cell Culture

4.1 Introduction

The development of three-dimensional (3D) tissue-engineered biomimetic cancer models for 3D cell culture is an important step towards modeling of the disease for investigations of tumorigenic mechanisms and drug-testing applications (Estrada et al. 2016, Bray et al. 2015, Chen et al. 2012, Szot et al. 2011a). Traditionally in high-throughput screening (HTS) assays, cancer cells cultured on two-dimensional (2D) 96- or 384-well plates are used for testing efficacies of large numbers of potential candidate drugs. However, due to inherent differences between 2D cultured and native cancer cells, many tested drugs fail to achieve desired results in clinical studies (Bray et al. 2015, Edmondson et al. 2014, Hickman et al. 2014). In order to bridge this gap in correlation, bioengineered cancer models are developed via 3D culture of cancer cells within biomimetic hydrogels that closely mimic native tissue characteristics under *in vitro* conditions (Gu and Mooney 2015, Carvalho et al. 2015). These scaffolds used for simulating native extracellular matrix (ECM) characteristics are usually obtained from natural (*e.g.* collagen, Matrigel, agarose) (Provenzano et al. 2008, Sapudom et al. 2015, Sasser et al. 2007, Pinto et al. 2014, Vantangoli et al. 2015), synthetic (*e.g.* poly(ethylene glycol), poly(lactic-co-glycolic acid)) (Pradhan et al. 2014, Gill et al. 2012, Yang et al. 2013b) or hybrid (combination of natural and synthetic) sources (Fischbach et al. 2009, Kievit et al. 2010).

One of the components of the native tumor ECM is fibrinogen, which is known to be secreted and deposited by cancer cells (Simpson-Haidaris and Rybarczyk 2001, Rybarczyk and Simpson-Haidaris 2000). Fibrinogen (Fb) is a hexameric, nodular protein with a molecular weight of approximately 340 kDa and consisting of two sets of α, β and γ chains, linked by disulfide bonds (Hall and Slayter 1959). Fibrinogen can be covalently conjugated with PEGDA

to form PF (PF) via Michael-type addition reaction between thiol groups on cysteine sites in the fibrinogen molecule and PEGDA polymeric chains (Almany and Seliktar 2005). PF precursor, mixed with Eosin Y, can be photocrosslinked to form hydrogels using visible light under physiological temperature and pH (Kerscher et al. 2016), which renders it suitable for 3D culture of a wide variety of cell types including smooth muscle cells (SMCs), induced pluripotent stem cells (iPSCs), chondrocytes and others (Peyton et al. 2008, Bearzi et al. 2014, Appelman et al. 2011).

3D cell behavior and function within PF-based hydrogels can be influenced by modulation of matrix stiffness and other physical characteristics of the hydrogel matrix. Specific modifications of the PF precursor (variation in PEGDA chain length, incorporation of Pluronic F127 micelles) resulted in significant changes in the microarchitecture and overall bulk properties of the resulting hydrogels and subsequent cellular morphology and function (Frisman et al. 2012, Almany and Seliktar 2005). Specifically, addition of excess PEGDA in the PF precursor led to increase in crosslinking densities in hydrogel matrices, increase in storage moduli, and differences in morphology, viability and cardiac function of encapsulated PlGF-MMP9-engineered iPSCs (Bearzi et al. 2014). Overall, the bulk and microstructural features of PF hydrogels can be suitably modulated to study cellular responses to changes in microenvironmental stiffness.

In recent studies, breast cancer models have been developed using various biomimetic materials for the investigation of tumorigenic phenomena such as cellular migration, angiogenesis, and metastasis and for anti-cancer drug testing (Peela et al. 2016, Estrada et al. 2016, Seib et al. 2015, Zhu, Wang, et al. 2015, Dhiman et al. 2005, Subia et al. 2015). Generally, breast cancer can be classified into three distinct molecular subtypes: luminal subtype (estrogen

receptor positive (ER+)/progesterone receptor positive (PR+)/human epidermal growth factor receptor negative (HER2-)), HER-2 subtype (ER-, PR-, and HER2+), and triple negative subtype (ER-, PR-, HER2-). Some comparative studies have been conducted between representative cell lines of these subtypes (Kenny et al. 2007, Subik et al. 2010, Ivascu and Kubbies 2007, Feng et al. 2013, Bray et al. 2015, Hakanson et al. 2012, Peela et al. 2016, Rijal and Li 2016); however, the role of matrix stiffness and physical properties in modulating the morphology and behavior of multiple breast cancer molecular subtypes in an *in vitro*, tunable 3D model needs to be investigated in more detail.

In this study, a comparative investigation of three different cancer cell lines, representing the major breast cancer subtypes, cultured within PF hydrogels is presented and 3D cell behavior (morphology, growth) in response to varying physical properties is examined. Hydrogel stiffness was modulated by the addition of excess PEGDA, which resulted in microarchitectural differences and variation in growth and morphological characteristics of the encapsulated cell lines. In addition, high viability and rates of proliferation were also observed for all cell lines within the tumor models. Interestingly, within these models, variation in colony size with distance from periphery was observed, which is reminiscent of native tumor heterogeneity. Overall, these findings can be useful in engineering tumor microenvironments *in vitro* and for comparative analysis of cancer cell behavior in modulated microenvironments. These tumor models can be further extended for the investigation of tumorigenic phenomena (e.g. epithelial-mesenchymal transition, angiogenesis and metastasis) and for anti-cancer drug testing applications. Investigation of the role of the tumor microenvironment, its characteristics and its influence on the growth and 3D behavior of cancer cells can provide valuable information on cell-matrix interactions and could reveal potential targets for the development of anti-cancer therapeutics. Aspects of

cellular biomechanics, 3D behavior and cell-matrix interactions can be recapitulated in 3D *in vitro* models, hence providing researchers with opportunities to discover these targets.

4.2 Materials and Methods

All chemicals were obtained from Sigma-Aldrich (St. Louis, MO) unless mentioned otherwise.

4.2.1 Cell Culture and Maintenance

MCF7 (ER+, PR+, HER2-) breast cancer cells were kindly provided by Dr. Richard Bird, College of Veterinary Medicine, Auburn University. SK-BR-3 (ER-, PR-, HER2+) breast cancer cells were obtained from Dr. David Riese, Harrison School of Pharmacy, Auburn University. MDA-MB-231 (ER-, PR-, HER2-, metastatic) breast cancer cells were provided by Dr. Robert Arnold, Harrison School of Pharmacy, Auburn University. All cells were cultured as described previously in Section 3.2.1.

4.2.2 PEG-fibrinogen Synthesis and Characterization

PEGDA was prepared as described previously (Pradhan et al. 2014). Bovine fibrinogen was covalently coupled to PEGDA according to established protocols (Almany and Seliktar 2005). Briefly, fibrinogen was dissolved in an 8 M solution of urea in 10 mM PBS at a concentration of 7 mg/ml. Tris (2-carboxyethyl) phosphine hydrochloride (TCEP-HCl) was added at a molar ratio of 1.5:1 TCEP to fibrinogen cysteines to the above solution and the final pH was adjusted to 8.0. PEGDA was dissolved in the 8 M urea-PBS buffer at 280 mg/ml, centrifuged, and the clear PEGDA solution was slowly added to the fibrinogen solution. The reaction was allowed to proceed for 3 hours at 25°C in the dark. The solution was then diluted with an equal volume of urea-PBS buffer and precipitated by adding it into acetone (J.T. Baker,

Center Valley, PA) at a volumetric ratio of 4:1 of acetone to product solution. The precipitate was separated from the acetone by centrifugation, weighed and re-dissolved in urea-PBS buffer at 2.2 ml of buffer/g of precipitate. The product was dialyzed against 1 L sterile PBS over 24 hours (with three changes of PBS) at 4°C in the dark. The final product was aliquoted into sterile centrifuge tubes and stored at -80°C. The synthesized PF was characterized similarly as described earlier in Section 3.2.3.

4.2.3 Cell Encapsulation in PF Hydrogels

Poly(dimethyl siloxane) (PDMS) molds were prefabricated for hydrogel formation by preparing a PDMS sheet of thickness 600 μm between two glass slides separated by spacers. The sheets obtained were then punched using a biopsy punch (diameter: 4 mm, maximum height: 700 μm) to obtain cylindrical shaped molds. These PDMS sheets with cylindrical shaped molds were affixed tightly to the bottom of a 6 well plate to prevent leakage of cell-hydrogel precursor. Hydrogel precursor was prepared by mixing PF solution in PBS with 1.5% (v/v) triethanolamine (TEOA), 37 mM 1-vinyl-2-pyrrolidinone (NVP), and 0.1 mM Eosin Y in PBS as photoinitiator. A volume of 10 μL of the precursor was pipetted into each PDMS mold affixed in a well-plate and crosslinked via visible light exposure (Light intensity: 203 mW/cm^2) for 2 minutes. After 2 minutes, the PDMS sheet was peeled off from the well plate leaving behind cylindrical shaped, photo-crosslinked hydrogels. Media was added to the well plates and hydrogel constructs were maintained in the well plate for further analysis (Fig. 4.1). In order to modulate hydrogel stiffness, additional PEGDA (250 mg/ml in PBS) was added to the PF precursor at a volumetric ratio of 96:4 (PF+1%P) or 92:8 (PF+2%P) prior to photocrosslinking. In order to encapsulate cancer cells within PF hydrogels, cells maintained in 2D flasks were trypsinized, counted, and

resuspended in polymer precursor at 20×10^6 cells/ml prior to photocrosslinking. The resulting tumor constructs were maintained in their respective culture media through the duration of study.

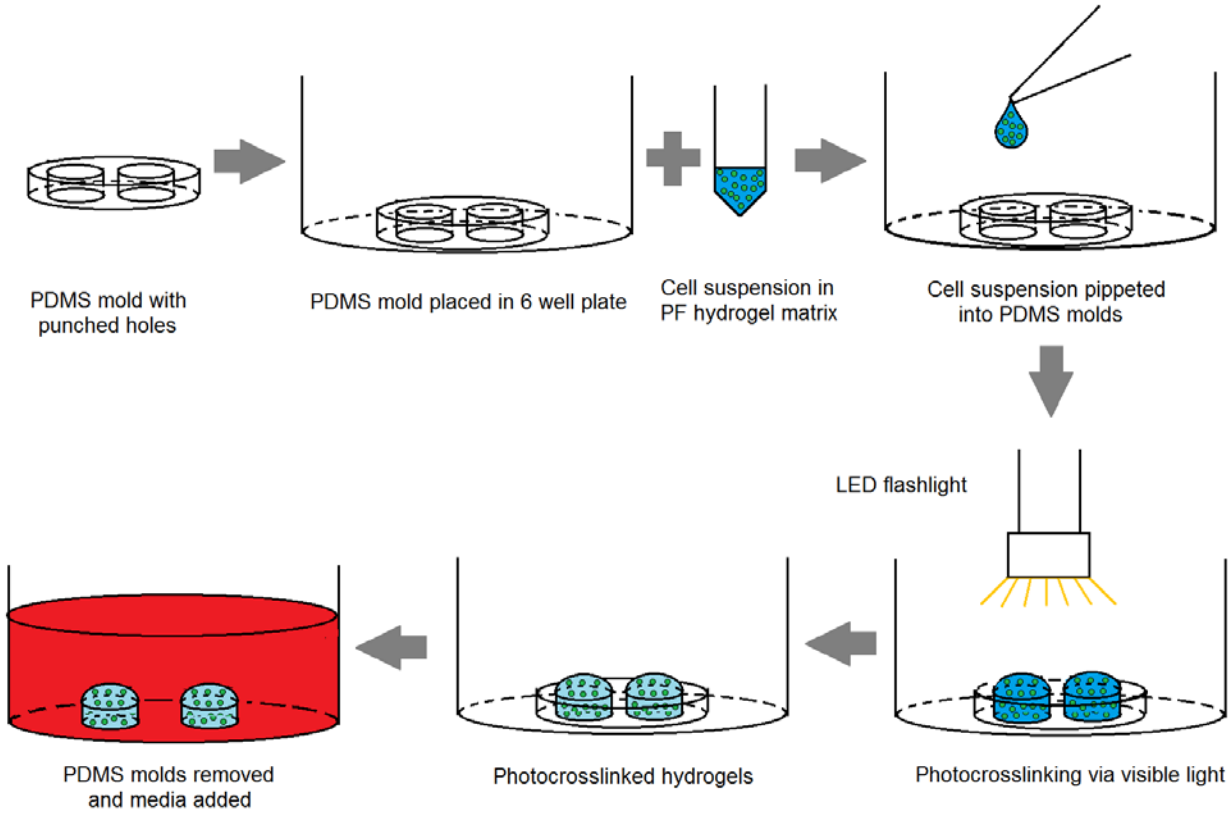

Figure 4.1: Schematic of PF-based hydrogel formation. PDMS molds (thickness: 700 μm) are affixed on a 6 well plate and hydrogel precursor (10 μl) mixed with cells is pipetted within the molds. The precursor-cell mixture is crosslinked via visible light for 2 minutes and the PDMS molds are removed to obtain hydrogels encapsulating cells which are then maintained in culture media.

4.2.4 Mechanical Characterization

In order to measure the Young's modulus of the tumor constructs, constructs were subjected to parallel-plate compression testing under physiological conditions using a CellScale Microsquisher® system and associated SquisherJoy software. Briefly, MCF7 cells were

encapsulated within hydrogels of varying PEGDA concentrations at 20×10^6 cells/ml and maintained in 3D culture for 5 days prior to mechanical testing. These tumor constructs (4 mm in diameter and 700 μm in thickness) were then loaded onto the Microsquisher® platform and maintained at 37°C in PBS, preconditioned for compression testing and made to undergo cycles of compression and relaxation at a rate of 5 μm/s for a minimum of 20% strain. The force-displacement data obtained from the compression test were converted to stress-strain curves and the lower portion of the curve (5-15% strain) was used to obtain a linear regression line and estimate the Young's moduli of the bioengineered tumor constructs. A minimum of 3 samples were measured for each condition.

4.2.5 SEM Imaging

The ultrastructural features of acellular hydrogel constructs and cell-laden tumor constructs were visualized through SEM. Acellular hydrogel constructs were washed in PBS, cryo-frozen in liquid nitrogen and dried using lyophilization for 3 hours. Tumor constructs were first washed with PBS, fixed with 4% glutaraldehyde for one hour, and then post-fixated with 2% osmium tetroxide for one hour, all at 25°C. The fixed constructs were dehydrated gradually in increasing concentrations of ethanol (30%, 50%, 70%, 90% and 100%, 10 minutes for each concentration) and finally chemically dried using hexamethyl disilazane (HMDS, Electron Microscopy Sciences, Hatfield, PA) for 3 hours. Dried samples were mounted on carbon taped-aluminum stubs, sputter-coated with gold (Pelco SC-6 sputter coater) and imaged using scanning electron microscope (JEOL JSM-7000F). SEM images of the acellular hydrogel constructs were analyzed for pore size, pore density and porosity using ImageJ software (NIH, version 1.48q). A minimum of 50 pores per condition were analyzed for pore size determination and 5 representative images per condition were analyzed for pore density and porosity quantification.

Individual pores in the representative SEM images were outlined manually in the ImageJ software and their mean geometric diameters were considered as pore size. The number of pores in specific sections of the SEM images (2500 μm^2 area) were manually counted and extrapolated on a per mm^2 area basis. For porosity analysis, the SEM images were converted to binary masks with pores appearing black in color and 'non-pore' regions appearing white. The total area covered by the black regions (pore regions) was measured and the divided by the total area of the image field of view (entire hydrogel area) to obtain the percentage porosity for the respective conditions.

4.2.6 Morphological Analysis

Morphological features representative of cancer cell growth and cell spreading were quantified via phase contrast microscopy and image analysis through 15 days in culture. Post-encapsulation of cancer cells, tumor constructs maintained in 3D culture were imaged using a Nikon Ti inverted microscope equipped with an Andor Luca S camera every three days. Z-stacks obtained above were analyzed using ImageJ software to determine colony area, diameter, circularity, and aspect ratio (for MCF7 and SK-BR-3 cells) and cellular area, diameter, circularity, aspect ratio, and elongation length (for MDA-MB-231 cells). Specifically, colony/cellular morphologies were quantified by focusing through individual planes in a sequential manner from top to bottom of the z-stacks. Since, individual planes contain both in-focus and out-of-focus regions of interest, quantification of morphological features was conducted at only those planes where edges and boundaries of cells/colonies appeared sharpest and most distinct. A minimum of 50 colonies (for MCF7 and SK-BR-3 cells) or cells (for MDA-MB-231 cells) were analyzed for each time point and each condition.

4.2.7 Cell Viability Analysis

Viability of cells within the PF hydrogel tumor models were observed and quantified via fluorescence microscopy and image analysis. Briefly, tumor constructs were washed with PBS and incubated in Live/Dead® cell viability stain (Invitrogen, Carlsbad, CA) for 30 minutes. Excess Live/Dead stain was washed with PBS and z-stack images of the samples were acquired under an inverted Nikon Ti microscope. The images (z-stacks, thickness: 200 μm) were analyzed using ImageJ software by manually counting the cells in each slice of the z-stack. A minimum of 5 z-stack images were quantified for each time point and each condition.

4.2.8 Immunostaining and Fluorescence Microscopy

The 3D morphology and proliferation of cancer cells within bioengineered tumor constructs were visualized by immunostaining and confocal fluorescence microscopy and quantified via digital image analysis. Briefly, tumor constructs maintained in 3D culture were washed with PBS, fixed with 4% paraformaldehyde (Electron Microscopy Sciences) for 1 hour at 25°C, permeabilized with 0.5% Triton-X for thirty minutes followed by incubation with blocking buffer (2% bovine serum albumin and 5% FBS in PBS) overnight. On the following day, the constructs were incubated with primary antibody against Ki67 (rabbit polyclonal, Abcam, Catalog# ab15580, 1:100 dilution) for 3 hours followed by incubation with secondary antibody against Ki67 (Alexa Fluor 488 goat anti-rabbit polyclonal, Thermo-Fisher, Catalog# A-11008, 1:200 dilution) and Alexa Fluor 568 Phalloidin (Thermo-Fisher, Catalog# A12380, 1:200 dilution) for 3 hours. Finally, the constructs were stained with Hoechst 33342 (1:200 dilution) for one hour and washed with PBS. Immunostained constructs were mounted on coverslips and imaged using confocal microscopy (Nikon AI Confocal Scanning Laser Microscope) to obtain z-stacks. Fluorescence images were analyzed using ImageJ software by

manually counting the number of cells in the field of view positive for Ki67 expression. A minimum of 5 z-stacks were analyzed for each condition.

4.2.9 Statistical Analysis

All statistical analysis was performed using Minitab 17 Statistical Software (Minitab Inc.). After checking for normality of distribution, One-way ANOVA with Tukey's family error rate of 5% was used to evaluate statistical significance between multiple groups, assuming equal variance and equal sample size of compared groups. In case of unequal variance between groups, the Games-Howell post-hoc test was employed following the ANOVA analysis. Unless otherwise indicated, $p < 0.05$ was considered statistically significant.

4.3 Results

4.3.1 Modulation of Hydrogel Stiffness via Relative PEGDA content

A number of techniques were used to determine specific characteristics of the PF-based hydrogels. The degree of acrylation of PEGDA, measured via ^{1}H NMR spectroscopy, was determined to be 96.0%. The fibrinogen concentration and the dry weight of PEGDA in the synthesized PF solution obtained after dialysis were determined to be 16.6 mg/ml and 21.5 mg/ml, respectively. The PEGylation efficiency was calculated as 74.0%. Addition of 1.0% and 2.0% PEGDA in the PF precursor resulted in protein concentration of 16.0 mg/ml and 15.3 mg/ml, respectively, and PEGDA concentration of 30.6 mg/ml and 39.8 mg/ml, respectively. The final composition of the three hydrogel formulations used were: PF: % Mass of total polymer = 3.8% w/v, Molar ratio of PEG: fibrinogen = 44:1; PF+1%P: % Mass = 4.7% w/v, Molar ratio = 65:1 and PF+2%P: % Mass = 5.5% w/v, Molar ratio = 88:1.

Mechanical characterization of tumor constructs (diameter: 4 mm, thickness: 700 μm) 5 days post cell encapsulation revealed significant differences in stiffness of the constructs. The stress-strain curves for all three hydrogel compositions were linear and elastic in the 15% strain range (Fig. 4.1A). The Young's moduli for the three hydrogel compositions were evaluated as 3.2 ± 0.5 kPa (PF), 5.4 ± 0.5 kPa (PF+1%P) and 9.0 ± 1.4 kPa (PF+2%P), which were significantly different from each other (Fig. 4.1B). Thus, modulation of mechanical stiffness, amongst changes in other parameters (e.g. pore characteristics), can be achieved by incorporation of excess PEGDA within the PF precursor and can be subsequently used for detailed investigation of 3D cancer cell behavior. Specifically, differences in diffusion coefficients that might result from the addition of excess PEGDA needs to be investigated in details in future studies.

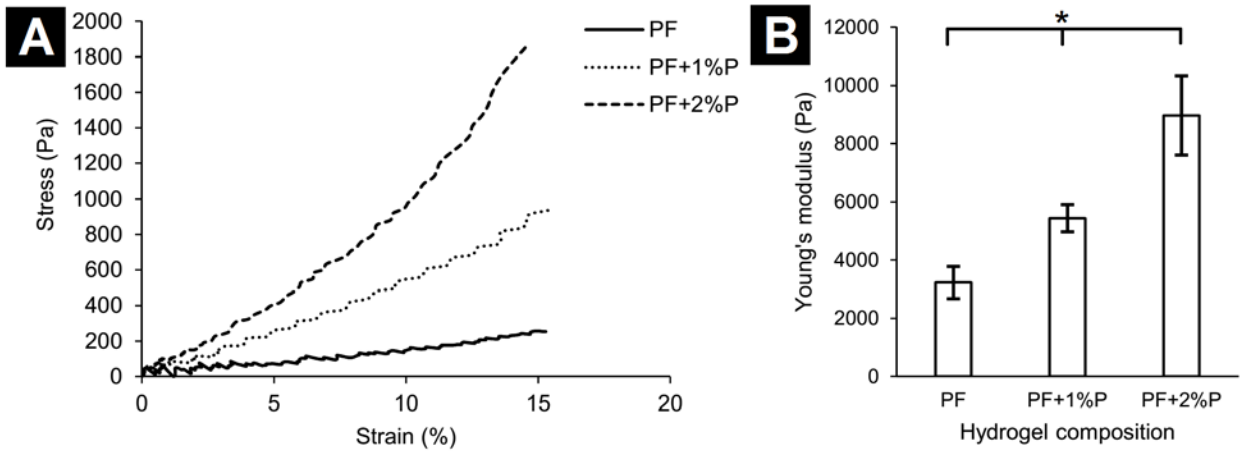

Figure 4.2: Mechanical characterization of tumor constructs. (A) Stress-strain behavior of hydrogel constructs of PEG-fibrinogen (PF), PF with 1% excess PEGDA (PF+1%P) and with 2% excess PEGDA (PF+2%P) demonstrates the influence of PEGDA moieties in hydrogel characteristics. (B) Incorporation of excess PEGDA results in increasing Young's modulus of bioengineered tumor constructs (n=3 hydrogels, *$p<0.05$).

4.3.2 Ultrastructural Variations in PF-based Tumor Constructs

Acellular hydrogel constructs were fabricated and visualized via SEM to observe stiffness-dependent ultrastructural differences. All three hydrogel compositions (PF, PF+1%P, PF+2%P) displayed a uniform, porous architecture with good pore interconnectivity (Fig. 4.2A, B and C). PF hydrogels exhibited a rougher surface with the presence of microgrooves and sub-micron pores, while PF+2%P hydrogels had a smoother and more structured appearance, indicating that the excess PEGDA promotes a firmer matrix with self-supporting microarchitectural features (Fig. 4.2D, E and F). Quantification of pore size of these PF-based hydrogel matrices revealed the average pore size of PF, PF+1%P and PF+2%P hydrogels to be 4±1 μm, 8±3 μm and 16±4 μm respectively, which were significantly different from each other (Fig. 2G). In addition, the pore density of PF hydrogels (50000 ± 4000 pores/mm^2) was significantly higher than that of PF+1%P hydrogels (39000 ± 5000 pores/mm^2) and PF+2%P hydrogels (20000 ± 5000 pores/mm^2) (Fig. 4.2H). Interestingly, the porosity of the three different hydrogel compositions (PF: 49 ± 3%, PF+1%P: 50 ± 5% and PF+2%P: 52 ± 2%) were comparable with each other (no significant difference), indicating that as the relative PEGDA concentration increases, the pores become larger in size but less numerous, thereby maintaining relative consistency in the overall porosity of the PF-based hydrogels.

Ultrastructural visualization of tumor constructs revealed prominent cell line-dependent variations in tumor constructs. In general, for all the three cell lines, uniform cell distribution in the field of view was observed. MCF7 cells in PF hydrogels formed distinct colonies with possible presence of tight and adherens cell-cell junctions, particularly at the edges of the tumor constructs (Fig. 4.3A and D), while cells in the middle regions appeared more isolated (Fig. 4.3G). Closer inspection of the MCF7 cell surface revealed the presence of numerous

microvilli and other cell-surface projections that potentially play a significant role in cell-cell and cell-matrix interactions (Fig. 4.31J and M).

SK-BR-3 cells also displayed a similar ultrastructural morphology in PF hydrogels. The cells formed local colonies with visible cell-cell junctions, potentially tight and adherens junctions, though the colonies were of smaller size compared to MCF7 cells (Fig. 4.3B). As observed earlier with MCF7 cells, SK-BR-3 cells at the edge of tumor constructs formed larger colonies compared to those in the middle regions which appeared more isolated (Fig. 4.3E and H). At higher magnification, the mesh-like nature of the matrix was visible and cell-surface projections of SK-BR-3 cells appeared grossly different from those of MCF7 cells (Fig. 4.3K and N).

MDA-MB-231 cells appeared to be distributed as single cells within the hydrogel matrix without the presence of major cell-cell junctions (Fig. 4.3I and L), as is characteristic of their metastatic nature. On closer inspection at the edges and middle regions of the bioengineered tumor constructs, some cells appeared to be elongated or have cellular extensions while other appeared more rounded (Fig. 4.3F and I). At higher magnifications, the mesh-like appearance of the hydrogel matrix and microvilli and filopodia at the cell surface interacting with the surrounding matrix were distinctly visible (Fig. 4.3L and O), which were consistent with observations in a previous study with fibroblasts cultured in collagen scaffolds (Masci et al. 2016).

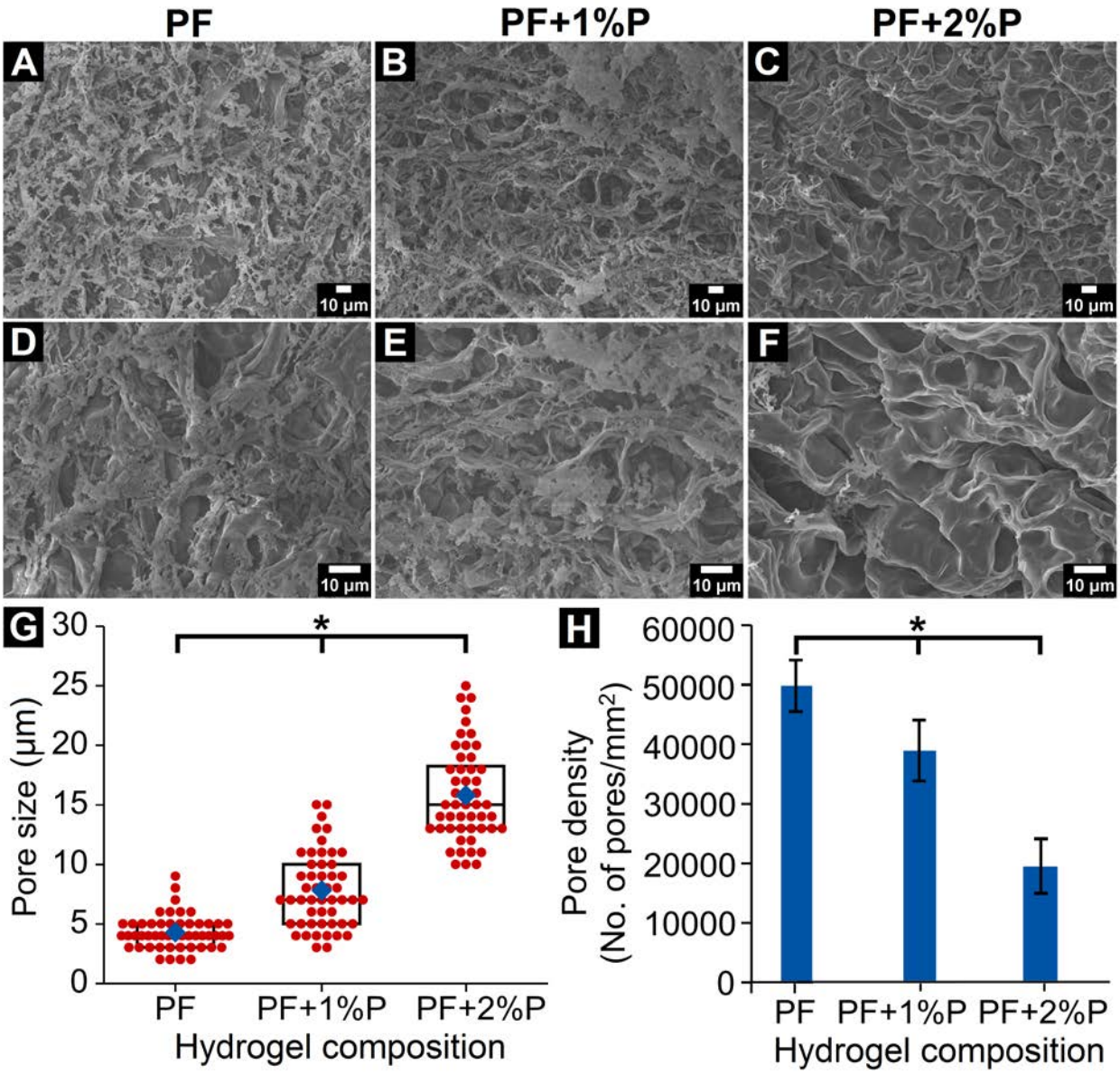

Figure 4.3: Stiffness-dependent ultrastructural differences in PF-based hydrogels. (A and D) PF hydrogels exhibit a greater degree of surface roughness due to the presence of microgrooves and sub-micron pores and a higher degree of pore interconnectivity. (B and E) PF+1%P hydrogels reveal an increasing degree of groove-like features. (C and F) PF+2%P hydrogels display a smoother pore surface and a greater degree of self-supporting features indicative of higher stiffness imparted by excess PEGDA. Quantification of ultrastructural characteristics of

PF-based hydrogels revealed (G) increased pore size and (H) decreased pore density with increasing relative PEGDA content. Red points denote individual pore measurements, blue diamonds denote mean of respective group and black boxes represent the upper quartile, median, and lower quartile of each respective group (Pore size: n=50 pores, Pore density: n=5 representative regions of interest, *p<0.05).

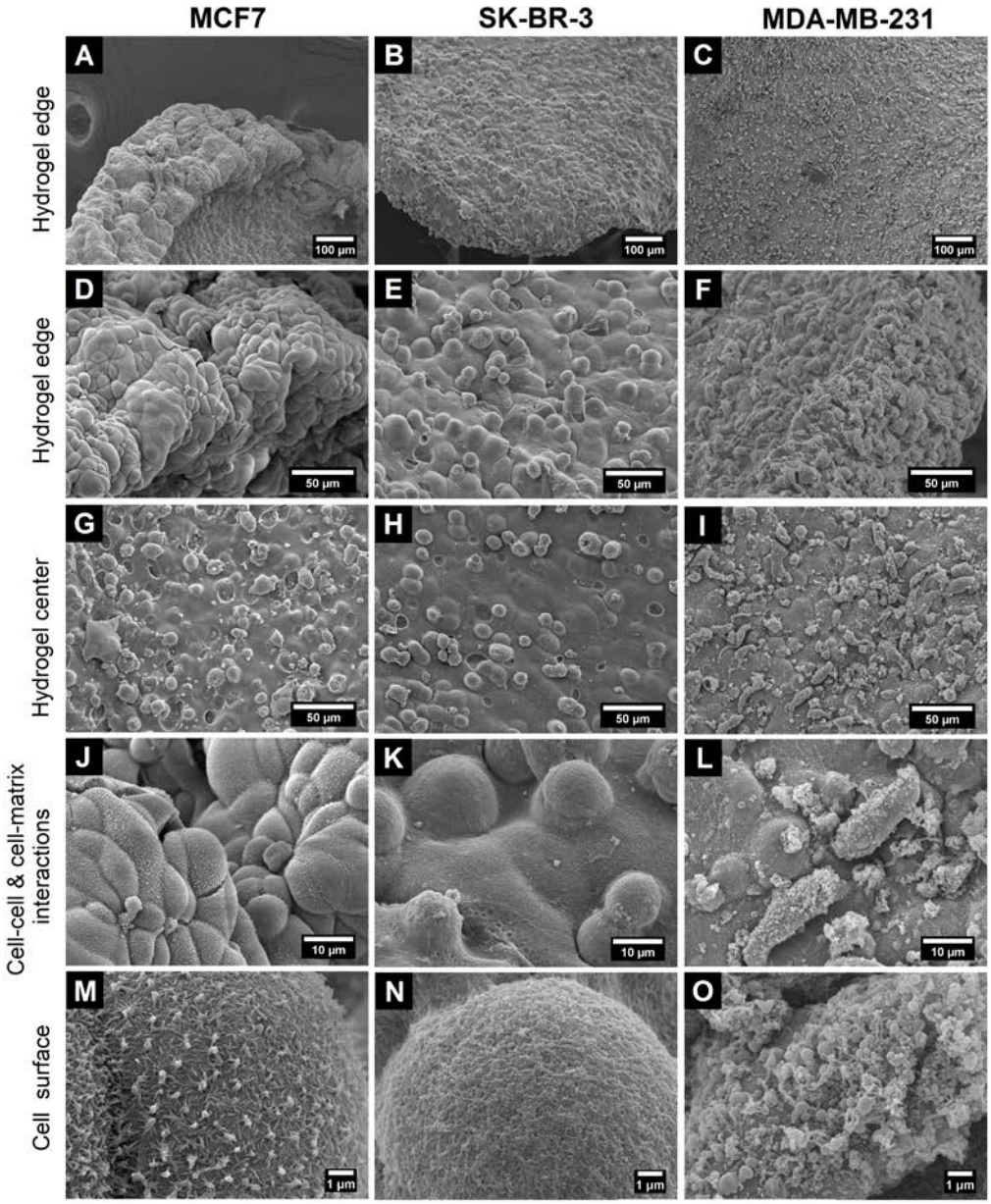

Figure 4.4: Ultrastructural features of tumor constructs. MCF7 cells within PF hydrogels display (A, D) a greater degree of colony formation at the edge compared to (G) the center of the hydrogel constructs and also exhibit (J) cell-cell interactions (denoted by white arrows) through (M) numerous cell-surface microvilli. SK-BR-3 cells display smaller colony formation compared to MCF7 cells which are (B, E) more numerous at the hydrogel edge compared to (H) the center regions. (K, N) Cell-cell and cell-matrix interactions are visible through surface microvilli-like features. MDA-MB-231 cells exhibit (C) more elongated and invasive morphology with (F) higher cell density at the hydrogel edge compared to (I) the center of hydrogel constructs. (O) Elongated cells exhibit distinct cell-surface projections of varying shapes and dimensions. (M, N, O) Cell-surface projections are markedly different for the three cell types indicating heterotypic cell-matrix interactions.

4.3.3 Influence of Hydrogel Matrix Modifications on Cancer Cell Morphology

In order to assess the impact of hydrogel stiffness on encapsulated cancer cells, PF-based hydrogels were visualized and phase-contrast images were analyzed for morphological features indicative of cancer cell growth and migration. In general, irrespective of stiffness variations, MCF7 cells encapsulated within bioengineered tumor constructs appeared as individual cells on day 0 which progressed to form distinct locally distributed colonies through day 15 of culture, especially near hydrogel construct edges (Fig. 4.5A-D). The cell colonies formed by MCF7 cells increased in area and diameter through 15 days. Cells in PF+2%P hydrogels (highest stiffness) formed significantly larger colonies (based on colony area and diameter) compared to cells in PF hydrogels (lowest stiffness) (Fig. 4.5E and F). However, colony circularity and colony aspect ratio (indicative of invasiveness (Chaudhuri et al. 2014, Jimenez Valencia et al. 2015, Wu, Phillip, et al. 2015, Geum et al. 2016)) remained fairly comparable among the three groups (Fig.

4.5G and H). Cells in phase contrast images appear different from those in SEM images due to differences in magnification and artifacts of SEM sample preparation.

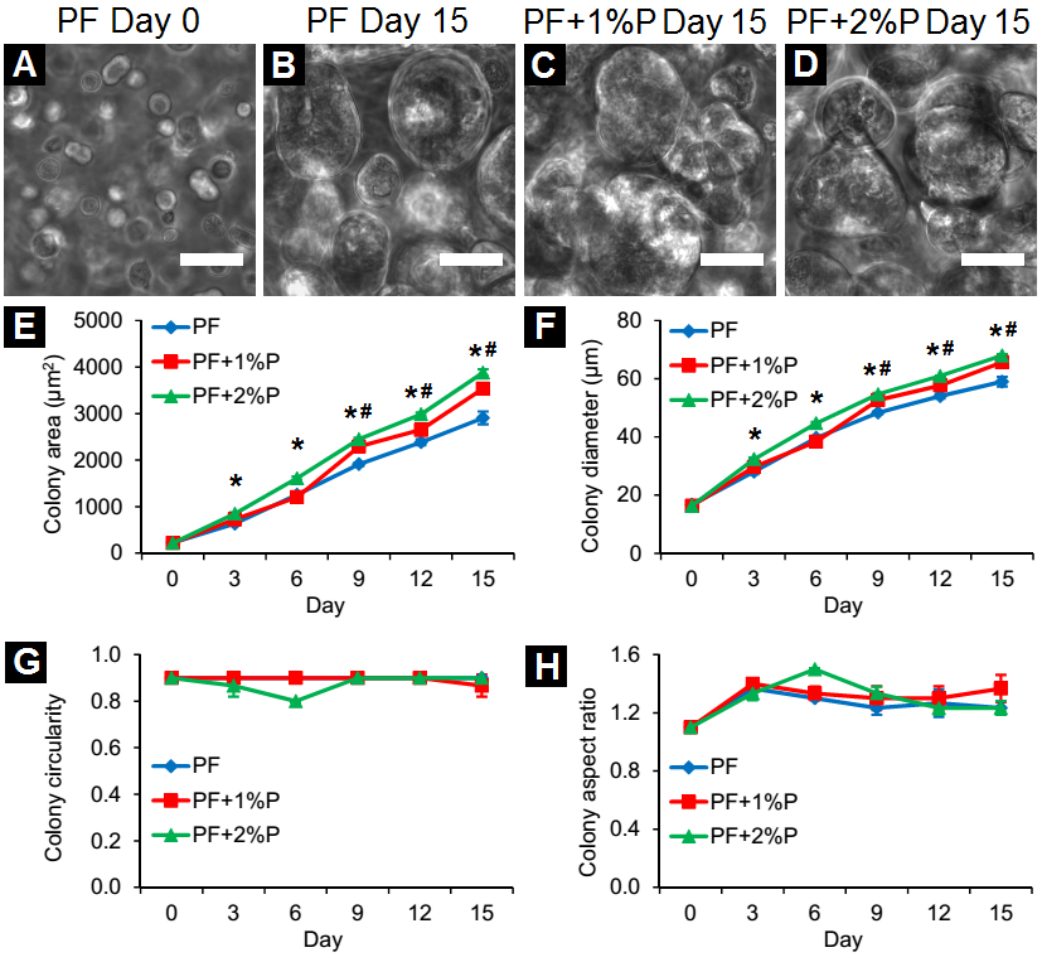

Figure 4.5: Characterization of MCF7 colonies over time. (A-D) MCF7 cells display tight cell colonies within PF-based hydrogels. (E) Colony area and (F) colony diameter of MCF7 cells increase with time, with PF+2%P hydrogels promoting larger colony formation. (G) Colony circularity and (H) colony aspect ratio remain fairly constant among the three groups (n= 50 colonies in 3 hydrogels per condition, * Significant difference between PF and PF+2%P, # Significant difference between PF and PF+1%P, $p<0.05$). Scale bar = 50 μm.

SK-BR-3 cells also showed similar morphological characteristics with single cells on day 0 forming distinct cell colonies through day 15 (Fig. 4.6A-D). SK-BR-3 cells exhibited increases in colony area and diameter through 15 days of culture. However, no significant difference was observed in colony area or diameter among the three hydrogel groups, suggesting that SK-BR-3 cells may be less responsive to changes in matrix stiffness compared to MCF7 cells. Notably, SK-BR-3 cells formed smaller colonies in the hydrogel constructs compared to MCF7 cells for all the three hydrogel compositions (~2000 μm^2 area for SK-BR-3 cells vs. ~3000 μm^2 for MCF7 cells) (Fig. 4.5 E-F and Fig. 4.6 E-F). As reported above for MCF7 cells, colony circularity and aspect ratio remained fairly constant throughout the culture period (Fig. 4.7C and D).

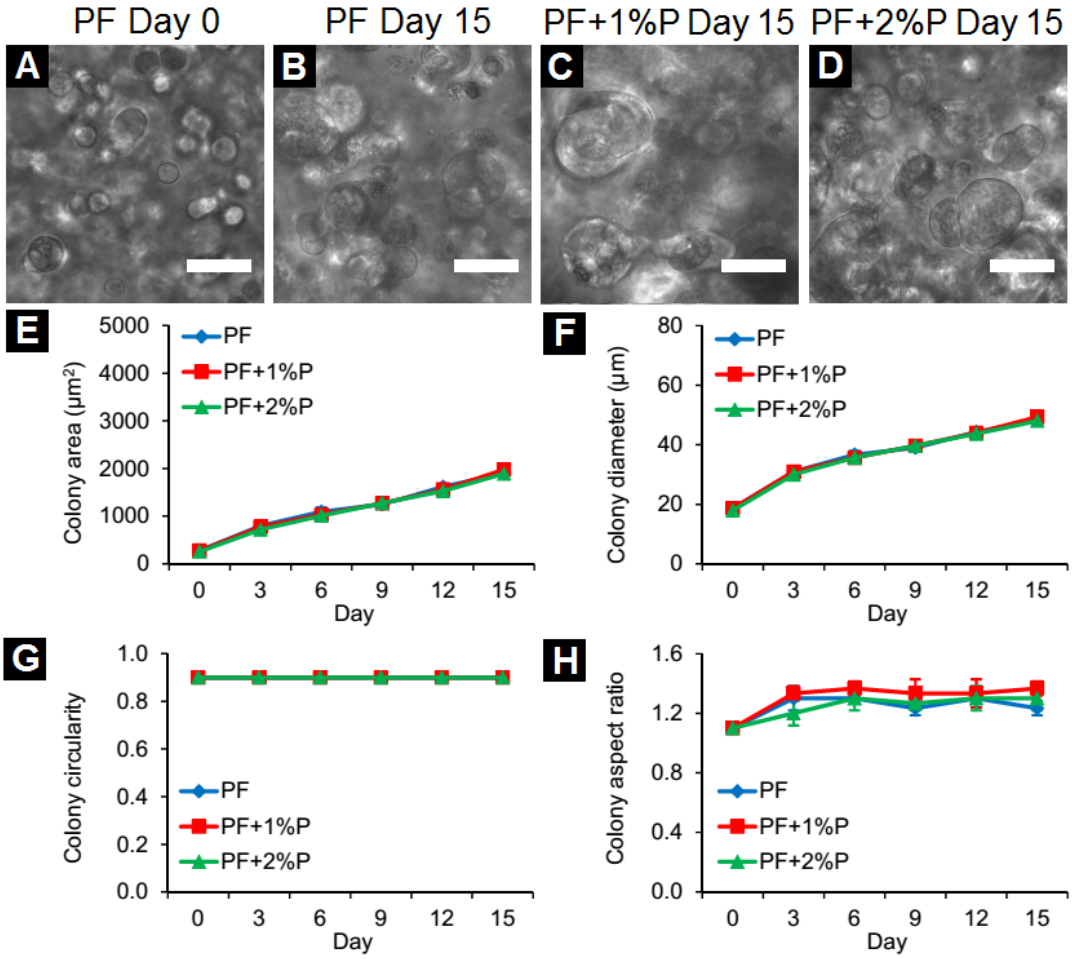

Figure 4.6: Characterization of SK-BR-3 colonies over time. (A-D) SK-BR-3 cells display tight cell colonies within PF-based hydrogels. (E) Colony area and (F) colony diameter of SK-BR-3 cells increase with time, with no significant effect of matrix stiffness on morphological features. (G) Colony circularity and (H) colony aspect ratio remain fairly constant among the three groups (n= 50 colonies in 3 hydrogels per condition, no significant difference between groups). Scale bar = 50 μm.

MDA-MB-231 cells, being metastatic in nature, formed cellular protrusions with gradual elongation of cells and subsequent apparent migration and invasion of individual cells within the hydrogel matrix (Fig. 4.7A-D). Elongated cells were also observed to form cellular interconnections with each other via protrusions (Fig. 4.7B). Interestingly, a distinct proportion of MDA-MB-231 cells were observed to remain spherical in shape throughout the 15 day culture period, without committing to an invasive morphology (Fig. 4.7C and D). Cellular area and diameter remained fairly constant over time; however, cells in the lowest stiffness hydrogels displayed significantly higher cellular area and diameter (Fig. 4.7E and F). Cellular circularity and aspect ratio (indicative of invasiveness) were also significantly different between hydrogels with the highest and lowest stiffness (Fig. 4.7G and H). Average elongation length was significantly higher in hydrogels of lowest stiffness (Fig. 4.8). These observations can be attributed to PF hydrogels (lowest stiffness) potentially having lower crosslinking density, higher pore interconnectivity, higher average pore diameter and lower stiffness compared to PF+2%P hydrogels (highest stiffness), thereby allowing a higher number of cellular protrusions and greater degree of invasion. Notably, standard deviations of measured parameters were considerably higher for MDA-MB-231 cells compared to the other two cell lines. This can be attributed to the presence of a distinct sub-population of cells that remained spherical in shape,

potentially quiescent in behavior, without displaying any invasive phenotype through the entire culture period.

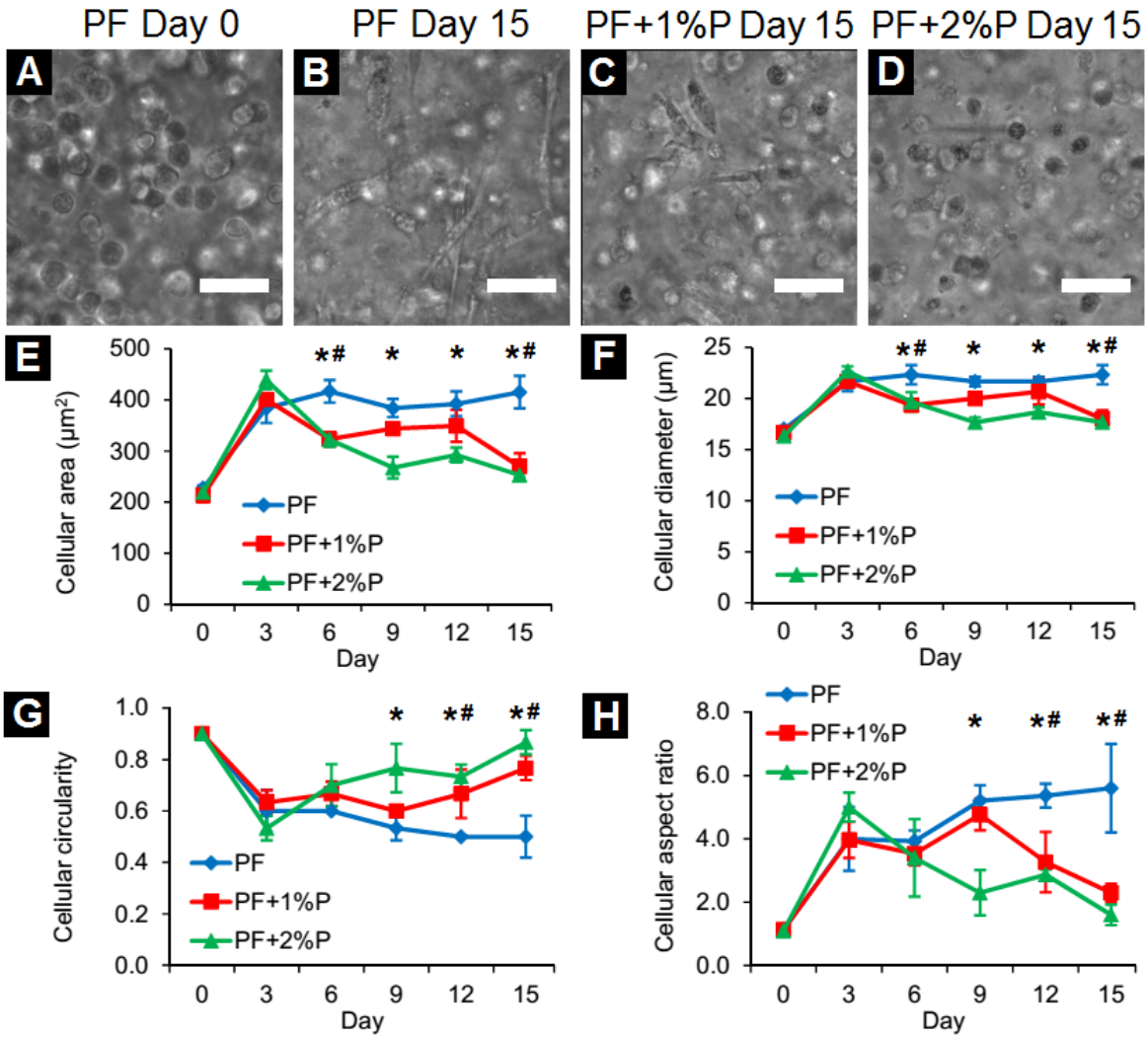

Figure 4.7: Characterization of MDA-MB-231 cells over time. (A-D) MDA-MB-231 cells exhibit an invasive and elongated morphology within hydrogel matrix while some cells remain spherical in shape and non-committed towards an invasive morphology. (E) Cellular area and (F) cellular diameter of MDA-MB-231 cells vary over time, with PF hydrogels promoting higher cellular size. (G) Colony circularity and (H) colony aspect ratio are also significantly different between hydrogels of the lowest and highest stiffness. (n= 50 cells in 3 hydrogels per condition,

* Significant difference between PF and PF+2%P, # Significant difference between PF and PF+1%P, $p<0.05$). Scale bar = 50 μm.

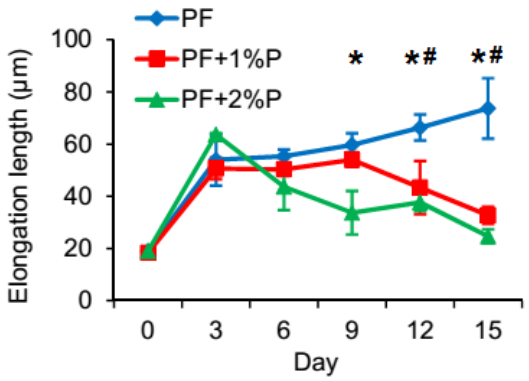

Figure 4.8: Elongation of MDA-MB-231 cells over time. MDA-MB-231 cells in the PF hydrogels are more elongated compared to those in PF+1%P and PF+2%P hydrogels. (n= 50 cells in 3 hydrogels per condition, * Significant difference between PF and PF+2%P, # Significant difference between PF and PF+1%P, $p<0.05$).

Overall, morphological features of encapsulated cancer cells in PF-based hydrogels of varying stiffness are primarily dependent on cell type. Cells of epithelial phenotype (MCF7, SK-BR-3) displayed tight colony formation and local growth while cells of mesenchymal phenotype (MDA-MB-231) exhibited invasive morphologies. In addition, increased matrix stiffness and decreased matrix porosity also had cell type-dependent effect on cellular morphology. These morphological trends are a result of the synergistic effect of changes in matrix stiffness and pore characteristics, rather than individual influences of matrix characteristics. The individual role of stiffness and pore characteristics on 3D cell behavior needs to be investigated in more details.

4.3.4 High Cell Viability in Tumor Models

In order to assess the viability of the encapsulated cancer cells in 3D culture, the tumor constructs were stained with Live/Dead dye and cell viability was evaluated via fluorescence imaging. On day 0 immediately after encapsulation, all cell lines displayed high viability (>90%) irrespective of matrix stiffness. No significant effect of stiffness or trend was observed on viability for any cell line and viable cells appeared to be fairly well-distributed throughout the entirety of the bioengineered tumor constructs, with no obvious locational differences (Fig. 4.9A-L). Interestingly, MDA-MB-231 cells that appeared rounded in shape within PF-based hydrogels also demonstrated high viability, indicating that these cells were non-invasive and potentially quiescent in terms of proliferative and metabolic behavior (Fig. 4.9J, K and L). In some cases, at the final time point on day 15 of culture, there was a significant reduction in cell viability compared to day 0 values across the three cell lines and three matrix stiffnesses; however, these day 15 values still remained relatively high (>80%), indicating good viability of cells within bioengineered tumor constructs over time (Fig. 4.9M). As future work, the effects of diffusion coefficients of bioactive molecules, if any, on the viability of encapsulated cells need to be investigated in more detail.

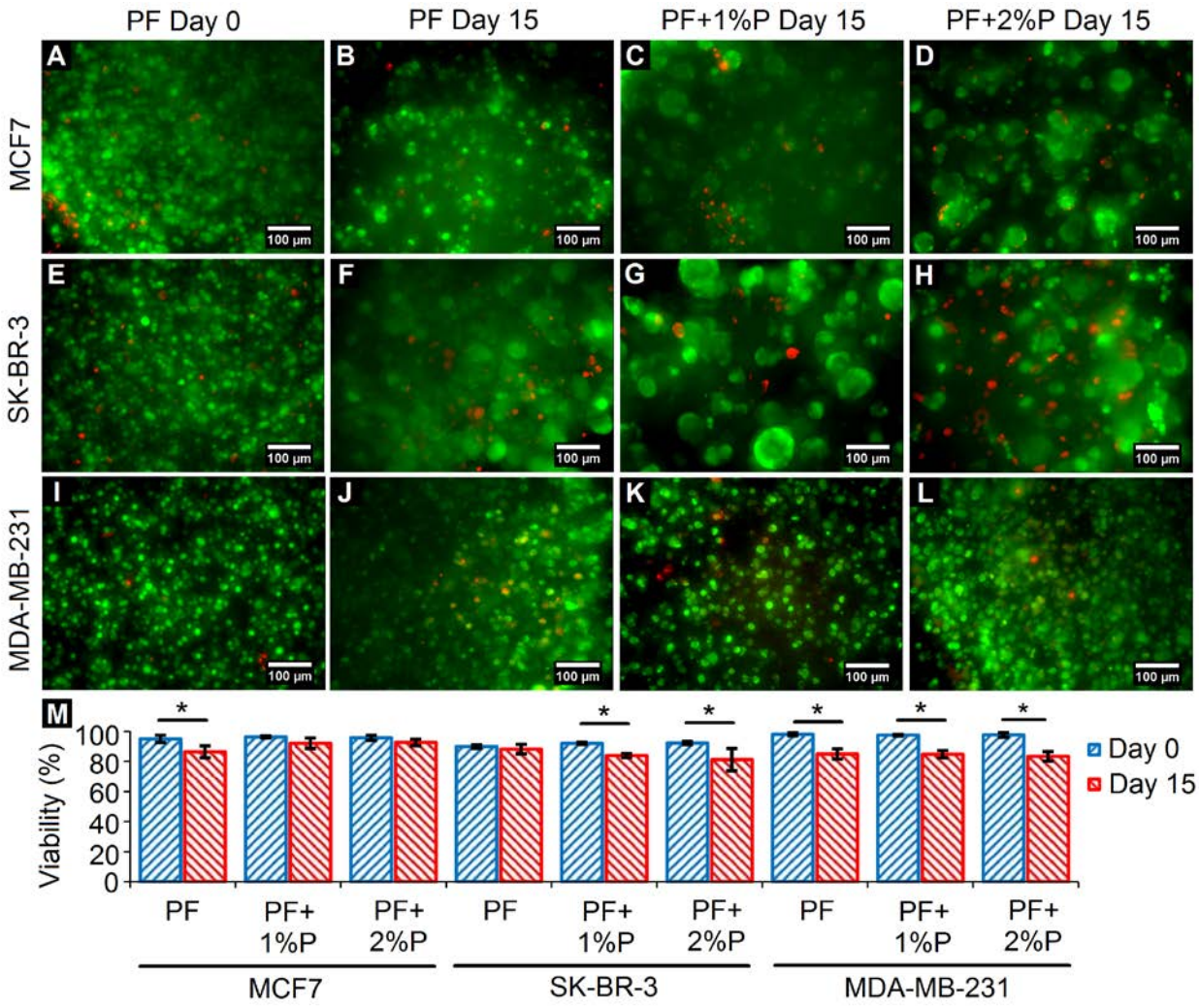

Figure 4.9: Cell viability in 3D tumor models. (A-L) Representative fluorescence images of cells within 3D bioengineered tumor constructs (combined Z- stack of thickness 200 µm) stained with calcein AM (Live, green) and ethidium homodimer (Dead, red) on days 0 and 15 demonstrate uniform distribution of live cells. (M) MCF7, SK-BR-3 and MDA-MB-231 cells exhibit relatively high cell viability through 15 days of culture, irrespective of matrix stiffness, thereby demonstrating that matrix stiffness does not influence cell viability; temporal changes in viability were observed in some conditions (n = 5 z-stacks from at least 3 separate constructs, *$p<0.05$).

4.3.5 3D Morphology and Proliferation in Tumor Models

In order to characterize 3D morphology and quantify proliferation of cancer cell lines, the bioengineered tumor constructs of varying stiffness were stained with phalloidin to visualize actin filaments and for Ki67 to identify proliferating cells and imaged under fluorescence confocal microscopy. MCF7 cells were observed to form local, circular colonies with prominent cell-cell junctions and actin filaments localized at the periphery of cells. Approximately 70% of cells stained positively for Ki67 in hydrogels of varying stiffness (subcellular location: nuclei), indicating relatively high cell proliferation irrespective of matrix stiffness (Fig. 4.10A-C, J).

SK-BR-3 cells also showed similar behavior within the bioengineered tumor constructs. These cells also appeared as local colonies with tight cell-cell junctions replicative of their native morphology with approximately 80% of the cells staining positive for Ki67 (Fig. 4.10D-F, J). Majority of cells displayed nuclear localization of Ki67 while some cells displayed cytoplasmic/membranous localization of Ki67. No stiffness-dependent differences in cellular proliferation were observed in the bioengineered tumor constructs.

MDA-MB-231 cells displayed an invasive morphology with cellular extensions within the 3D hydrogel matrix. Cells within PF hydrogels (lowest stiffness) displayed higher degree of filopodial extensions and elongations, which were gradually reduced in hydrogels with increasing PEGDA concentrations and increasing stiffness (Fig. 4.10G-I, J). Interestingly, a significant proportion of MDA-MB-231 cells remained circular in shape without displaying an invasive phenotype and this proportion gradually increased with increasing stiffness. In addition, cells with an invasive morphology exhibited nuclear Ki67 expression while those with a rounded morphology exhibited cytoplasmic Ki67 expression (Fig. 4.10G-I). Cytoplasmic/membranous staining of Ki67 has been previously reported and has been correlated with high grade,

ER- tumors with HER2 amplification (Faratian et al. 2009, Grzanka et al. 2000). Possible explanations for this observation include cross-reactivity with other analogous proteins or relocalization of Ki67 within cells (Faratian et al. 2009). It could also be attributed to the five different isoforms of the Ki67 protein (α, β, γ, δ and ε) which have been reported in literature; although their functional roles have not been investigated in detail (Schmidt et al. 2004). It is possible to surmise that Ki67 positivity alone may not be sufficient to comprehensively describe the proliferation status of MDA-MB-231 cells and further investigation is necessary to distinguish truly proliferative cells from quiescent ones.

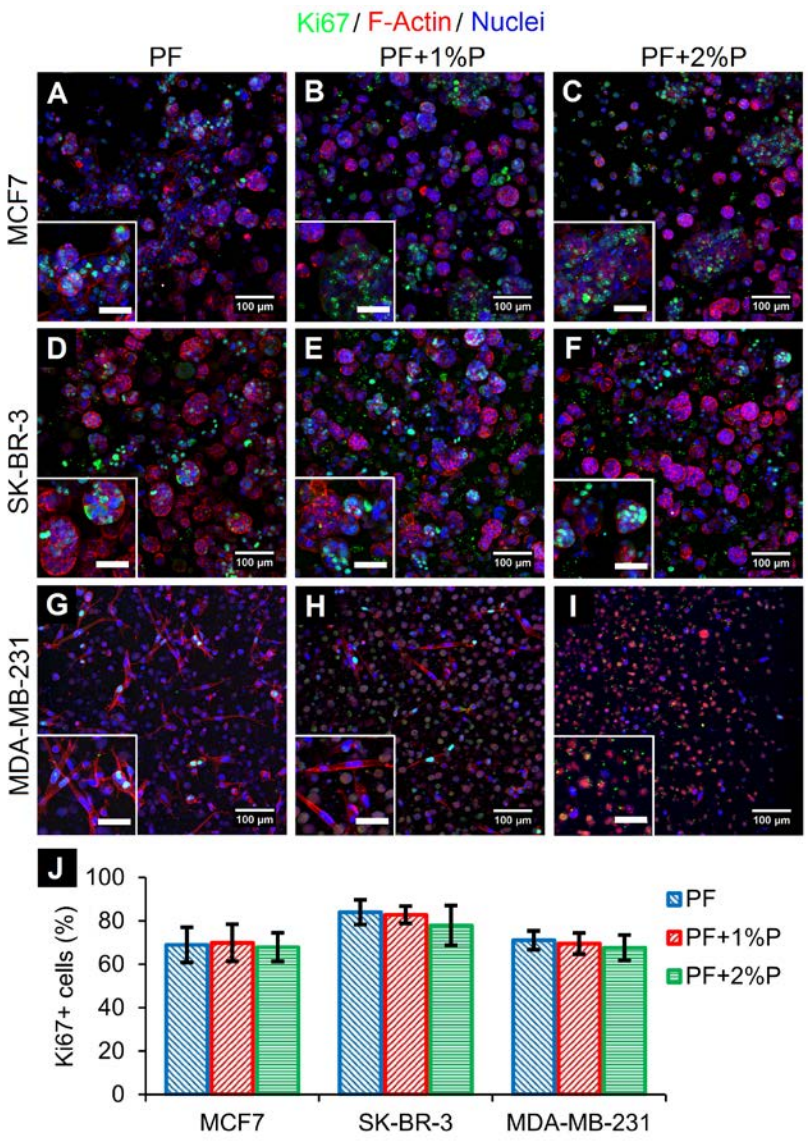

Figure 4.10: Cell line- and stiffness-dependent morphology and proliferation within PF-based hydrogels. On day 15 post-encapsulation, (A-C) MCF7 and (D-F) SK-BR-3 cells display local colony formation with cells stained for actin filaments (red, cell morphology), Ki67 (green, cell proliferation), and nuclei (blue). (G-I) MDA-MB-231 cells display elongated morphology which is decreased with increasing stiffness. (J) Relative percentage of Ki67 positive cells for cancer cell lines in PF-based hydrogels of varying stiffness (n= 5 z-stacks from at least 3 separate constructs).

4.3.6 Locational Growth Heterogeneity in Tumor Models

Cancer cells found in native tumor tissue exhibit significant heterogeneity in growth characteristics, proliferation, metabolism, hypoxia and other cellular signaling mechanisms. In this context, we observed locational growth heterogeneity in the tumor constructs, specifically with MCF7 and SK-BR-3 cells, via analysis of cell colony size on days 0, 7 and 15. After encapsulation on day 0, MCF7 and SK-BR-3 cells appeared as single cells distributed uniformly throughout the tumor constructs (Fig. 4.12A and B). However, when observed on day 7, cells close to the edge of the tumor constructs formed larger colonies compared to those located in the further interior regions (Fig. 4.12C and D). This difference in colony area was even more conspicuous on day 15 when colonies near the hydrogel edge appeared distinctly larger indicative of extensive cell growth while those farther away from the edge appeared isolated and relatively quiescent in behavior (Fig. 4.12E and F, Fig. 4.13). The decrease in colony area was either exponential or according to the power law with increasing distance from the hydrogel edge (Fig. 4.12). However, no distinct effect of matrix characteristics on cellular heterogeneity was observed, with cells in different stiffness hydrogels exhibiting similar trends in growth heterogeneity (Fig. 4.12). Further investigation of cell proliferation revealed that more Ki67+ cells were localized near the tumor construct periphery and gradually decreased in number beyond a distance of ~ 400 μm from the hydrogel edge (Fig. 4.13E). Spatial variation in the density of Ki67+ cells and colony size were well-correlated, with higher numbers of proliferative cells and larger colonies at the construct periphery and lower numbers of proliferative cells and smaller colonies in the interior regions of the construct (Fig. 4.13F,G).

These observations can be attributed to the assumption that cancer cells near the edge have better access to nutrients and oxygen from media diffusing near the edge of the hydrogel;

however, as the diffusion distance increases, mass transfer resistance prevents cells in the interior regions from being proliferative or metabolically active. In addition, as the cell colonies near the edge become larger with time, the colonies themselves impart intrinsic resistance to the diffusion of nutrients to cells located in the interior regions of the hydrogels, further enhancing the locational differences in colony area. The effect of additional PEGDA incorporation on the diffusional gradients of nutrients and cellular metabolites and resulting 3D cell behavior and morphology should be investigated in more detail.

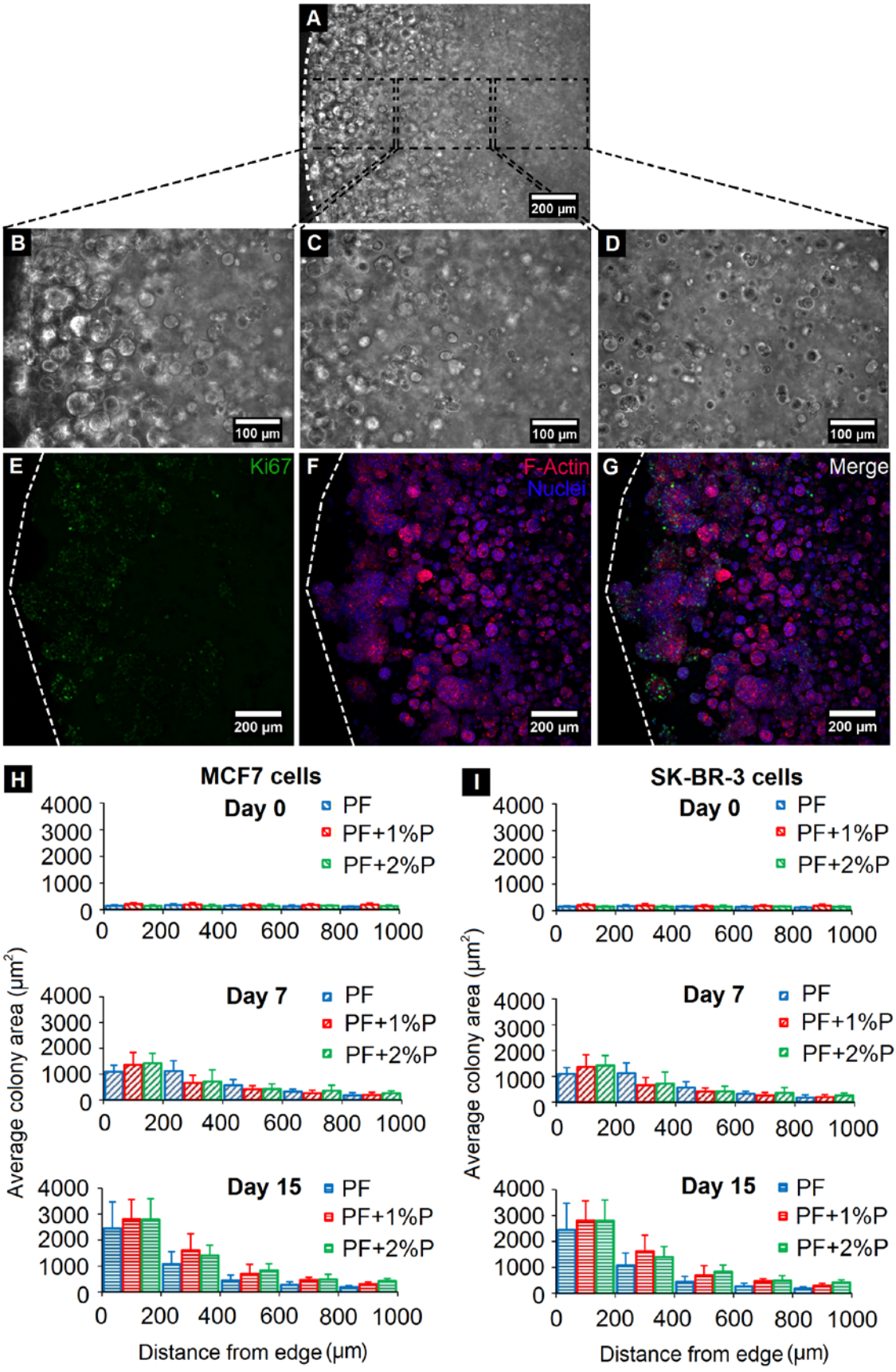
A
200 μm
B
100 μm
C
100 μm
D
100 μm
E
Ki67
200 μm
F
F-Actin
Nuclei
200 μm
G
Merge
200 μm
H
MCF7 cells
Day 0
PF
PF+1%P
PF+2%P
Day 7
Day 15
Average colony area (μm²)
Distance from edge (μm)
I
SK-BR-3 cells
0
200
400
600
800
1000
1000
2000
3000
4000

Figure 4.11: Spatial variations in proliferation and colony area. (A) MCF7 cells cultured within PF hydrogels (white arrow represents hydrogel edge) and imaged on day 15 exhibit locational differences in colony size with (B) those near the edge being largest in size, (C) those in the intermediate zone being smaller, and (D) those in the innermost zone being most isolated and smallest in area. (E, F, G) MCF7 cells positive for Ki67 (proliferative cells) are located closer to the hydrogel edge (represented by dotted lines) while those in the hydrogel center appear non-proliferative and quiescent. (H) MCF7 and (I) SK-BR-3 cells are uniformly sized throughout hydrogel constructs on day 0, but locational differences in colony area are observed on day 7 and become more prominent by day 15.

4.4 Discussion

This study establishes a 3D *in vitro* model of three molecular subtypes of breast cancer and investigates the effect of matrix stiffness on the growth, morphology and heterogeneity of encapsulated cells maintained in long-term 3D culture. Establishing 3D biomimetic microenvironments in tissue-engineered cancer models is essential for recapitulating intrinsic tumorigenic characteristics of cancer cells including cellular mechanobiology, cell-cell and cell-matrix signaling. Towards this end, PF has been employed as a suitable biomaterial for establishing 3D tumor models. Previously, a number of natural and synthetic materials have been used for establishing 3D cancer models including collagen, Matrigel, agarose, alginate, silk fibroin, peptide-conjugated PEG and others (Rijal and Li 2016, Xu and Burg 2007). However, the use of fibrinogen as a potential ECM scaffold for cancer cell studies has not been investigated in detail. The native breast tissue ECM is composed mainly of fibrillar collagens, laminin, tenascin, fibronectin and other proteins (Oskarsson 2013, Lu et al. 2012). In addition to these proteins, fibrinogen has also been found to be an important constituent of the ECM matrix

in normal and malignant breast stroma, promoting tumorigenic progression not only through integrin-mediated cancer cell-matrix interactions, but also by stimulating angiogenic growth via endothelial cell communications (Costantini et al. 1991, Kolodziejczyk and Ponczek 2013, Simpson-Haidaris and Rybarczyk 2001, Palumbo and Degen 2001). Hence, detailed investigation of the biochemical interactions between breast cancer cells and ECM fibrinogen is of potential interest in discovering novel therapeutic targets for drug treatment strategies.

In addition to cell-matrix signaling mechanisms, the bulk stiffness of the breast tissue (imparted by the cells and ECM matrix components) is also a driving factor towards malignant and metastatic behavior (Fenner et al. 2014, Butcher et al. 2009). In an investigation of normal and cancerous breast tumor clinical samples, it was found that normal fat and fibroglandular tissue exhibited Young's moduli of ~3 kPa and fibroadenoma and low grade IDC (invasive ductal carcinoma) exhibited a moduli of 6-10 kPa. However, with evolution of tumor stage to DCIS (ductal carcinoma in situ) and intermediate grade IDC, the moduli increased to ~15-20 kPa and in the case of high grade IDC, the modulus was ~ 40 kPa (Samani et al. 2007). Bioengineered tumor models employing other biomaterials also exhibit a wide range of stiffness values. Soft fibrin gels used for culturing B16-F1 melanoma cells demonstrated higher tumorigenicity in 100 Pa gels compared to 400 Pa or 1000 Pa gels (gel stiffness corresponding to initial measurements of cellular constructs) (Liu et al. 2012). Human head and neck squamous carcinoma cells (HNSCC) cultured within alginate beads of wide stiffness range demonstrated higher enrichment of tumor initiating cells (TICs) in moderate stiffness (70 kPa) hydrogels compared to soft (20 kPa) or hard (105 kPa) stiffness hydrogels (stiffness being measured in acellular constructs) (Liu, Liu, Xu, et al. 2015). Specifically, acellular PF hydrogels have been shown to be relatively soft in terms of stiffness (~0.01-0.10 kPa), with the Young's moduli

dependent on molecular weight of PEGDA crosslinkers (4-20 kDa) and the relative weight of the PEGDA fraction (10-20% w/v) in the polymer precursor (Almany and Seliktar 2005). Shear storage moduli (G') of acellular PF, PF with additional 1% PEGDA and PF with additional 2% PEGDA hydrogel were reported as ~120 Pa, ~350 Pa, and ~700 Pa respectively (Bearzi et al. 2014). Similarly, the compressive moduli of acellular PF hydrogels with 0%, 1% and 2% additional PEGDA were reported as 448 Pa, 1008 Pa and 2306 Pa respectively (Peyton et al. 2008).

When reporting stiffness of hydrogel constructs, it is important to consider the presence of encapsulated cells and their ability to dynamically modulate bulk stiffness when maintained under long-term 3D culture. In this study, we observed that the incorporation of breast cancer cells within tumor constructs significantly increased the stiffness range to ~3-9 kPa, as compared the stiffness of acellular PF hydrogels (reported earlier in literature). At the high cell encapsulation density of 20 million cells/ml used in this study, the encapsulated cells themselves were a major contributor to the stiffness of tumor constructs, in addition to the hydrogel matrix per se. Although the Young's moduli of the tumor models were closer to that of low-grade IDC than that of intermediate or high-grade IDC, even these moderate variations in matrix stiffness and microarchitectural properties elicited a prominent response in breast cancer cells. In this study, encapsulated MCF7 cells were allowed to acclimatize in the 3D PF-based matrix and start expressing their characteristic morphology for 5 days prior to mechanical testing. The stiffness of PF-based tumor models is expected to further increase with time, as was demonstrated earlier with fibroblasts (Kesselman et al. 2013), and vary with the morphology and phenotype of encapsulated cancer cells as the cells proliferate in long-term culture, exerting cellular stress on the surrounding ECM matrix and also secreting and depositing endogenous ECM components in

the surrounding microenvironment. Reciprocally, the dynamic changes in stiffness could potentially affect cancer cell-matrix signaling mechanisms and induce genetic, proteomic and morphological changes at the cellular and tissue scales.

Matrix stiffness and porosity are important factors affecting the cellular fate of encapsulated cancer cells within engineered tissue constructs (Lu et al. 2012, Levental et al. 2009). In this study, the stiffness and pore characteristics of PF-based hydrogels are coupled with each other, which is a limitation of this hydrogel platform. Addition of excess PEGDA leads to increasing stiffness while at the same time, increase in pore size and reduction in pore density. Detailed investigation of material design and fabrication are necessary to uncouple the effect of one parameter from the other and study the resulting effects on 3D cell behavior. In a previous study, interpenetrating networks of reconstituted basement membrane matrix and alginate were used to independently modulate matrix stiffness, composition and architecture for the culture of normal mammary epithelial cells (Chaudhuri et al. 2014). In addition, the responsiveness of encapsulated cells to independently modulated matrix stiffness, ECM chemistry and ligand density has also been investigated (Peyton et al. 2006). The matrix stiffness of tumor models in this study could be further increased by incorporation of bioactive PEG-peptide moieties into the PF precursor prior to crosslinking in order to match it to intermediate or high-grade IDC. The peptide sequences that could be conjugated to PEGDA macromer include RGDS or YIGSR (for cellular adhesion) and GGGPQG↓IWGQGK or KCGPQG↓IWGQCK or GCYK↓YNRCG (for enzymatic degradation) (Leight et al. 2015, Raeber et al. 2005, Gill et al. 2012, Singh et al. 2014). However, it must be noted that incorporation of these sequences in PF precursor would also alter the ultrastructural characteristics, and biochemical composition of the engineered scaffolds in terms of bioactive moieties available for cellular adhesion and degradation; hence,

care must be taken to suitably match these characteristics with that of native and *in vivo* tumors to maintain physiological relevance. Specifically, it has been demonstrated that the compressive modulus of bioactive PEG hydrogels could be varied in the range of ~20-55 kPa, independent of tunable biochemistry, by modulated incorporation of adhesive RGDS and degradable GGGPQG↓IWGQGK sequences and controlled PEGDA macromer concentration in the polymer precursor. These biomolecular variations eventually led to changes in epithelial morphogenesis and induction of epithelial-mesenchymal transition (EMT) in a lung adenocarcinoma cell line (Gill et al. 2012). Incorporation of these bioactive moieties within PF-based hydrogels in a physiologically relevant context could potentially reveal more interesting differences in cancer cell morphology, proliferation rates and EMT. Additionally, the incorporation of additional PEGDA moieties could also lead to changes in the diffusion rates of specific bioactive molecules like glucose, lactic acid, oxygen, carbon dioxide and others. The role of pore characteristics and porosity of the hydrogel matrices in influencing the diffusion phenomena and the resulting effects on 3D cell behavior also needs to be investigated in details.

Future investigations of the tumor models established in this study could incorporate higher degrees of complexity such as inclusion of secondary cell types (e.g. fibroblasts, endothelial cells, macrophages etc.) to more closely replicate native tumor conditions. Fibroblasts are known to exert contractile stresses on the surrounding ECM matrix due to their tendency of cell spreading and have the ability to dynamically stiffen hydrogel constructs over time (Frisman et al. 2011). Hence, fibroblast-ECM interactions could also have a significant reciprocal effect on cancer cell growth and malignant progression. Specifically, cancer-associated fibroblasts (CAFs), known to upregulate tumorigenicity, malignancy and metastasis, co-cultured with cancer cells could reveal important information about mechanisms of disease

progression and anti-cancer drug resistance (Liao et al. 2009, Orimo et al. 2005). In addition, testing of specific anti-cancer drugs could be conducted on the tumor constructs to evaluate their cytotoxic effectiveness. These tumor models offer an advantage over other traditional 3D tumor models through their ability to recapitulate the heterogeneity that is inherent to native tumors. Specifically, cells located at the native tumor periphery are in close proximity to neo-vasculature and hence richly supplied with nutrients and oxygen. However, cells located in the interior regions of the tumor tissue experience diffusional gradients of oxygen (leading to hypoxia) and nutrients (leading to accumulation of waste metabolites and acidic pH). When cancer cells are cultured within *in vitro* 3D biomimetic models, some of the key features related to tumor heterogeneity such as hypoxia and cell proliferation can be more closely recapitulated than is achievable in typical 2D culture conditions. Previously, we have shown that MCF7 cells cultured within spheroidal PEGDA hydrogel millibeads (2 mm diameter) exhibit viable cell layers in the hydrogel periphery, but undergo significant cell death in the interior regions of the millibeads (Pradhan et al. 2014). A previous study of MDA-MB-231 cells encapsulated within transglutaminase-crosslinked gelatin hydrogels also displayed growth and morphological heterogeneity due to onset of hypoxia in the central regions of the hydrogel constructs (Fang et al. 2014). Likewise, since a distinct sub-population of MCF7, SK-BR-3 and MDA-MB-231 cells in the central regions of PF-based bioengineered tumor constructs appear to be non-proliferative or non-committed towards phenotypic invasive morphology, the effect of anti-cancer drugs on these cells could be studied with special focus. These cells within the PF-based tumor constructs could also be investigated for potential cancer stem cell-like characteristics.

Overall, the established bioengineered breast tumor models provide a reliable and effective method for investigation of 3D cancer growth and morphology in the presence of a

biomimetic matrix of tunable stiffness with future applications in cancer cell studies and drug-testing platforms.

4.5 Conclusions

In this study, tumor models based on PF hydrogels with varying physical characteristics representing three distinct molecular subtypes of breast cancer have been developed. Incorporation of additional PEGDA in the PF matrix led to an increase in the Young's moduli of constructs and prominent differences in ultrastructural architecture as observed through SEM. Cancer cells encapsulated within these hydrogels exhibited cell type-dependent and matrix-dependent variation in morphology, cell spreading and growth. High viability of cell lines was maintained in 3D culture. 3D morphology was visualized and proliferation was quantified within the tumor models. Additionally, locational variation of colony size, indicative of tumor heterogeneity, was quantified within the tumor models. These tumor constructs can be used in the future for designing improved biomimetic models that can recapitulate key characteristics of the native breast tumor microenvironment and facilitate further investigation of tumorigenic phenomena *in vitro*.

CHAPTER 5: Investigation of Anti-cancer Drug Testing on a 3D Microfluidic Cancer-on-a-chip Platform

5.1 Introduction

The tumor microenvironment (TME) consists of diverse elements in addition to cancer cells, most notably, cancer-associated fibroblasts (CAFs), endothelial cells, immune cells and stromal ECM proteins like collagen, laminin and others (Mao et al. 2013, Soysal et al. 2015). The complex milieu of these entities acting synergistically through cell-cell and cell-matrix signaling mechanisms gradually leads to malignant and metastatic progression. In addition to these elements, some other contributing factors of the TME in tumorigenic progression include the mechanical stiffness of the tissue, factors secreted by the cancer and other cell types that induce paracrine signaling and abnormal deposition and arrangement of ECM proteins within the ECM. Understanding the role and influence of each of these factors independently and also synergistically with each other is critical in constructing the mechanistic timeline of disease progression. Further, recognition of important signaling and tumorigenic mechanisms is valuable in finding new therapeutic targets for drug discovery and development.

Current *in vitro* 3D tissue-engineered cancer models incorporate particular elements of the TME in various degrees of complexity that faithfully recapitulate specific tumorigenic phenomena like angiogenesis, epithelial-mesenchymal transition (EMT), cancer cell migration and metastasis (Bischel et al. 2013). Incorporation of ECM-mimic biomaterials within these models helps provide important information of cancer cell behavior in 3D matrices in response to ECM composition, porosity, microarchitecture and stiffness, amongst other parameters. In addition to these models, microfluidic chip-based platforms have also been developed to investigate the interactions of cancer cells with the surrounding stroma in the presence of an

endothelial vasculature (Lee, Park, et al. 2014, Sung and Beebe 2014, Bischel et al. 2015). These cancer-on-a-chip platforms facilitate investigation of specific tumorigenic mechanisms like cancer cell migration, EMT, extravasation and metastasis, in addition to cancer-endothelial interactions and cancer-fibroblast interactions (Boussommier-Calleja et al. 2016, Bersini et al. 2014, Jeon et al. 2015, Bruce et al. 2015). However, these platforms also suffer from some limitations; many of them incorporate very simplistic vasculature designs that may not mimic native physiological blood flow in the TME while others feature too few elements of the TME that may not achieve the required level of complexity as *in vivo* or native systems.

In order to address these challenges and to improve upon currently existing systems, a novel 3D microfluidic platform has been developed that incorporates the following key features: 1) an intricate network of lumenized endothelial vasculature originally obtained from an *in vivo* source, 2) a central chamber consisting of cancer cells and fibroblast co-encapsulated within a 3D biomimetic PEG-fibrinogen (PF) matrix, 3) a well-established perfusable connection between cancer-fibroblast region and surrounding vasculature and 4) inlet and outlet ports for introduction of cells, culture media and anti-cancer agents in a dynamic and continuous manner. Using this cancer-on-a-chip platform, specific interactions of cancer cells with surrounding endothelial vasculature including cancer cell extravasation and migration to secondary sites were investigated. In addition, cancer cells and fibroblasts were maintained in long-term 3D co-culture and morphological progression of cancer cells was quantified. Diffusion of fluorescently-tagged TRITC-dextran from the vascular channels to the cancer-fibroblast region was evaluated and the resulting tumor heterogeneity was visualized. Finally, two anti-cancer drugs, doxorubicin and paclitaxel, were perfused from the vascular channels and their cytotoxic effects on the cancer cells as well as the endothelial cells were quantified, thereby demonstrating the ability of this

system in assessing anti-cancer drug efficacy in the presence of multiple physiological factors of the tumor stroma.

5.2 Materials and Methods

5.2.1 Design and Fabrication of Microfluidic Platform

Two specific microvascular designs (C002 and D002) were used in this study. They will henceforth be referred to as “high perfusion chip” (HPC, for C002 design) and “low perfusion chip” (LPC, for D002 design). These designs were obtained from digitized images of mouse vasculatures. Briefly, a fluorescent probe (FITC-dextran, Molecular weight: 4 kDa) was injected into mouse vasculature and confocal microscopy images were obtained in the local area of perfusion. These images were then digitized using the software package Arc-Info (ESRI) into AutoCAD-MAP format. The “arc-node topology” feature in Arc-Info was used to digitize the microvascular network to map the vessels. Flow directions in these networks as observed *in vivo* served as guidelines for defining inlet and outlet ports in the digitized network. Layouts of the digitized network images were rendered in AutoCAD LT (AutoDesk, San Rafael, CA). The AutoCAD designs were printed at high resolution on Mylar film (CADArt, Poway, CA). The Mylar film was then used as a photomask for ultra-violet (UV) light (365 nm) for patterning an 8 μm thick layer of positive SU-8 photoresist (AZ P4620, Clariant, Somerville, NJ) spun on top of a silicon wafer. After development of the photoresist, the layer was removed using a developer solution. PDMS (Sylgard 184) was prepared according to manufacturer’s (Dow Corning, Midland, MI) instructions, added on top of the photoresist mold and allowed to cure for 4 hours at 70°C. Through holes, defining the inlets and outlets, were punched using a beveled 25-gauge needle. The bonding surfaces of the PDMS and a pre-cleaned 1×3 in. glass slide (Fisher Scientific, Pittsburgh, PA) were treated with oxygen plasma (150 mTorr, 50 W, 20 s)

produced in the parallel plate plasma asher (March Inc., Concord, CA), to produce a tight bond between the two surfaces. Tygon microbore tubing with an outside diameter of 0.6 in. and inner diameter of 0.2 in. connected to 24 gauge stainless steel needle served as the connecting port to the syringe mounted on a programmable syringe pump. All the studies for this work were performed on networks with vessel diameters of 100 μm.

5.2.2 Cell Culture and Maintenance

MCF7 and MDA-MB-231 breast cancer cells were obtained and cultured as described in Section 4.2.1. BJ-5ta normal human foreskin immortalized fibroblasts were obtained from ATCC (Manassas, VA) and maintained in 4 parts of Dulbecco's Modified Eagle's Medium containing 4 mM L-glutamine, 4.5 g/L glucose and 1.5 g/L sodium bicarbonate, 1 part of Medium 199 supplemented with 0.01 mg/ml hygromycin B and 10% fetal bovine serum. Human breast tumor-associated endothelial cells (hBTECs) were obtained from Cell Biologics (Chicago, IL) and were maintained in Human Endothelial Cell Medium (500ml) (Cell Biologics, Chicago, IL) supplemented with 0.5 ml VEGF, 0.5 ml heparin, 0.5 ml EGF, 0.5 ML hydrocortisone, 5.0 ml L-gutamine, 5.0 ml antibiotic-antimycotic solution, 10.0 ml endothelial cell supplement and 50.0 ml FBS.

5.2.3 Establishment of Lumenized Vasculature

Fabricated microfluidic chips were initially degassed and coated with human fibronectin solution (Sigma-Aldrich) (100 μg/ml) for 3 hours and with a gelatin-based coating solution (Cell Biologics) for 30 minutes prior to cell seeding. hBTECs cultured in 2D flasks were trypsinized with 0.05% trypsin-EDTA solution (Cell Biologics) and resuspended in endothelial media at 50×10^6 cells/ml. The hBTECs were loaded into a 1 ml syringe and manually flowed in through the inlet port of the chips and allowed to attach overnight. Subsequently, the cells were

maintained under continuous flow conditions (0.1 μl/min) via syringe pump (KD Scientific, Holliston, MA) for at least two days to form complete lumenization with 360° coverage of the vascular channels.

Immunostaining of hBTEC vasculature was conducted post lumenization according to previous protocols. Briefly, media was removed and cells were washed with PBS through the vascular channels. 4% paraformaldehyde solution in PBS was flowed in for 10 minutes to fix the cells. The cells were further permeabilized by with PBS-T for 10 mins and blocked with blocking buffer for three hours at room temperature. CD31-FITC (Invitrogen, 1:50 dilution) in blocking buffer was perfused and staining was done overnight in the dark. Alexa Fluor 568 Phalloidin (Invitrogen, 1:200 dilution) and Hoechst 33342 (1:200 dilution) in blocking buffer were flowed in and cells allowed to stain for 2 hours in the dark. The staining solution was washed away with PBS and fluorescence images were obtained using confocal microscopy (Nikon AI Confocal Scanning Laser Microscope) to obtain z-stacks. Fluorescence images were analyzed using ImageJ software (NIH) to obtain morphological characteristics of endothelial cells.

5.2.4 Long-term 3D Co-culture of Cancer Cells and Fibroblasts

PEG-fibrinogen (PF) was synthesized and characterized as described previously in Section 4.2.2. Microfluidic devices vascularized with hBTECs were used for co-culture of cancer cells (MCF7, MDA-MB-231) with BJ-5ta human fibroblast within PF hydrogels. MCF7 and MDA-MB-231 cells cultured in 2D flasks were trypsinized and resuspended individually with BJ-5ta cells in PF precursor at a density of 50×10^6 cells/ml (for cancer cells) and 10×10^6 cells/ml (for fibroblasts). The cancer-fibroblast-precursor mixture was perfused through the central tumor loading port and allowed to occupy the entire central tumor chamber. Some cancer

cells/fibroblasts which initially escaped into the surrounding vasculature were washed away with media immediately after cell perfusion. The perfused cells were allowed to settle in the central chamber for 1 hour, after which the precursor was crosslinked with exposure to visible light for 2 minutes. Fresh media was perfused every 6 hours to replenish the small volume of media within the microfluidic chips. Seeded cells were imaged every seven days under phase contrast microscopy and these images were analyzed with ImageJ software to determine morphological features representative of the two cancer cell lines. A minimum of three independent chips were imaged and analyzed for each condition. At least 15 colonies for MCF7 cells and 50 cells for MDA-MB-231 cells were analyzed per time point.

In order to assess long-term viability of seeded cells within microfluidic chips, cancer cells and fibroblasts maintained in co-culture through 28 days were stained with Live/Dead® cell viability stain (Invitrogen, Carlsbad, CA) for 20 minutes and fluorescence images were obtained via a Nikon Ti inverted microscope. The number of live and dead cells were manually counted using ImageJ software. A minimum of 5 images from 3 independent chips were analyzed for viability assessment.

The extravasation and migration of MDA-MB-231 cells from the primary tumor region into the surrounding vasculature was also quantified over time. Phase contrast images of cancer cells in the vicinity of vascular networks were acquired every seven days and analyzed via ImageJ for cells which had extravasated into the surrounding microvasculature and further invaded into the secondary sites reminiscent of metastasis. A minimum of 5 images from 3 independent chips were analyzed for this purpose.

5.2.5 Diffusion Testing within Microfluidic Chips

The diffusion of bioactive molecules from the vascular network to the interior regions of the central tumor chamber was analyzed in order to understand the impact of diffusional heterogeneity and resulting impact on cell morphology. Briefly, microfluidic chips were coated with fibronectin, seeded with hBTECs and maintained under dynamic perfusion to form lumenized vasculature. MCF7 cells and BJ-5ta fibroblasts were co-encapsulated in the PF hydrogel matrix within the central tumor chamber and maintained in culture overnight.). Fluorescent TRITC-dextran (Sigma-Aldrich) was perfused through cell-seeded microfluidic devices (Molecular weight: 4400 Da) at 1µl/min for 2 hours using a syringe pump. The chips were imaged under fluorescence microscope and the images were analyzed using ImageJ software to generate heat maps of the concentration profile within the microfluidic chips. In addition, the images were also analyzed to estimate the diffusion profile in specific local regions of the two microfluidic chips using MS Excel. Phase contrast images of various regions of the cell-seeded microfluidic devices were also obtained to visualize the morphological heterogeneity due to diffusional differences.

5.2.6 Anti-cancer Drug Testing

Two common drugs, doxorubicin and paclitaxel, were tested on the microfluidic chips seeded with endothelial cells, cancer cells and fibroblasts. Briefly, vascularized microfluidic chips were seeded with cancer cells and fibroblasts within the PF hydrogel matrix and maintained in culture for 2 days. Doxorubicin and paclitaxel (Euroasian Chemicals, India) were dissolved in DMSO as solvent at 10 mM concentration. The drug solutions were diluted to 10 µM in hBTEC media prior to infusion in the microfluidic chips. The drugs were perfused via syringe pump at 1µl/min for 19 minutes (for high perfusion chip) or 7.5 minutes (for low

perfusion chip) and maintained in culture for 4 hours. After 4 hours, fresh media was infused in the chips to flush out all drug components. The chips were maintained in culture for a further 48 hours and Live/Dead cell viability staining was conducted on the chips to ascertain cell death. Fluorescence images of stained regions of the chips were taken and analyzed by ImageJ software to determine viable cell density and viable tumor area. The number of live cells (stained green) within the field of view was manually counted to obtain viable cell density. The area occupied by the live cells (viable tumor area) within the primary tumor chamber was demarcated by drawing a line around region of interest and the area was calculated by the ImageJ software. The values obtained were normalized to that from the control chips with no drug treatment. Microfluidic chips with media perfusion were run as controls and chips with 0.1% DMSO were run as vehicular controls. A minimum of three chips were analyzed per condition.

5.2.7 Statistical Analysis

All statistical analysis was performed using Minitab 17 Statistical Software (Minitab Inc.). After checking for normality of distribution, One-way ANOVA with Tukey's family error rate of 5% was used to evaluate statistical significance between multiple groups, assuming equal variance and equal sample size of compared groups. In case of unequal variance between groups, the Games-Howell post-hoc test was employed following the ANOVA analysis. Unless otherwise indicated, $p < 0.05$ was considered statistically significant.

5.3 Results and Discussion

5.3.1 Geometry-dependent Variation in Shear Rates

The shear flow rates within the microfluidic channels of the cancer-on-a-chip platform were analyzed via Computational Fluid Dynamics software (Autodesk) to obtain the variations of vascular flow that is closely reminiscent of physiological flow patterns in *in vivo* and native

tumors. The high perfusion chip had a higher tumor chamber volume (127.10 μl) and a higher average shear rate compared to the low perfusion chip (tumor chamber volume: 77.85 μl). Native and *in vivo* tumors are characterized by abnormal blood flow in the surrounding vasculature with the presence of closed loops, branchings, bifurcations and other complex patterns. Traditional microfluidic systems rely on very simplistic designs and geometries for modeling of vascular flow surrounding the central tissue chamber. However, in order to recapitulate native, dynamic shear flow characteristics in these systems, it is necessary to incorporate increased degrees of complexity in vascular patterns and networks.

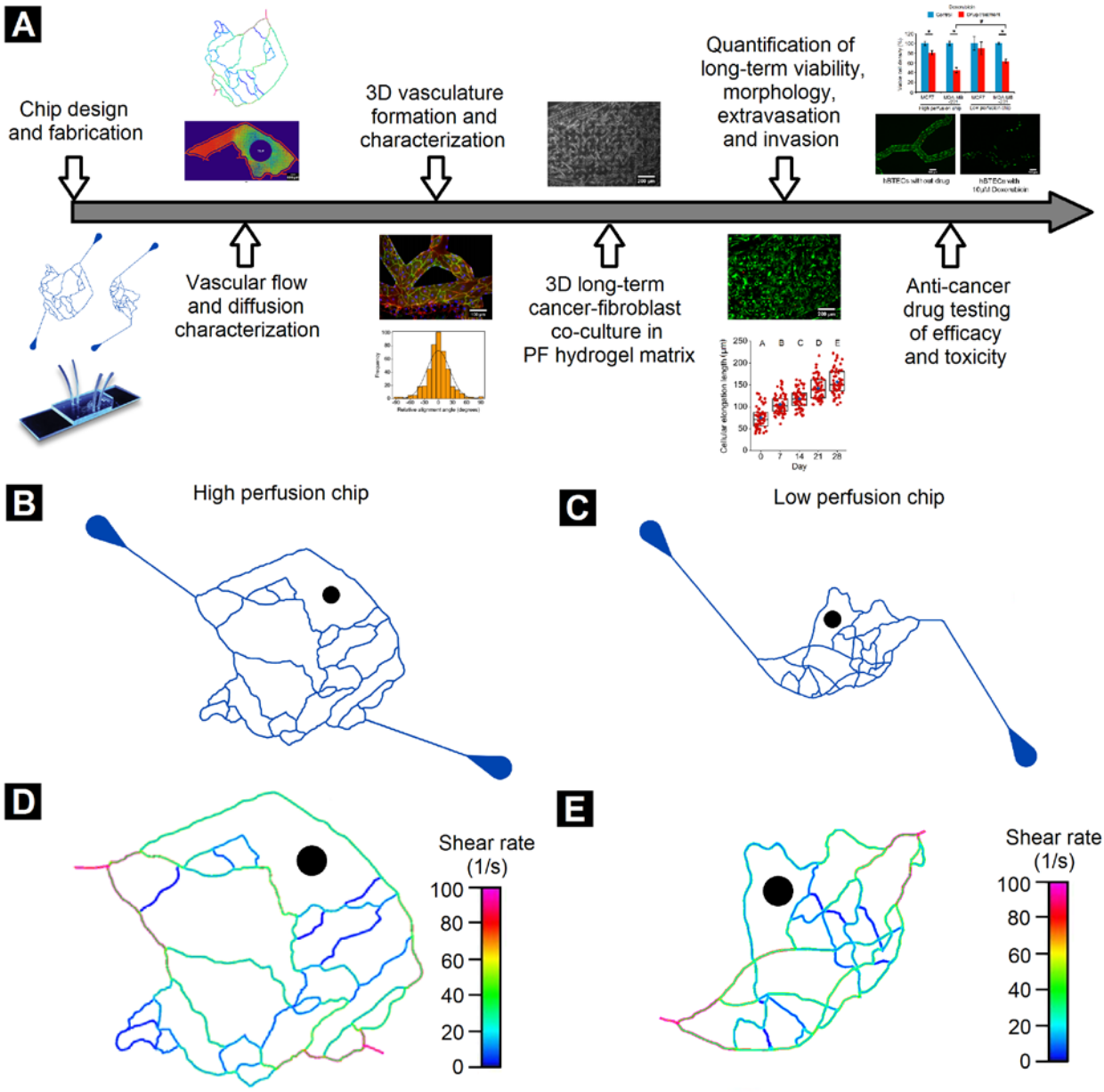

Figure 5.1: Experimental timeline and design of microfluidic chips. (A) Experimental timeline of different steps involved in the cancer-on-a-chip platform starting from chip design and fabrication to final drug-testing stage. AutoCAD design of the (B) high and (C) low perfusion microfluidic chips used for experiments (black circle denote the tumor loading port). Shear rate maps of the (D) high and (E) low perfusion chips reveal vastly different patterns and regional variations in shear flow rate dependent on the vascular geometry of the designs.

5.3.2 Formation of 3D Mature, Lumenized Vasculature

hBTECs seeded within fibronectin-coated microfluidic channels were maintained under continuous perfusion culture to form complete lumenized vasculature with 360° coverage (Fig. 5.2E), indicating high degree of maturity. Immunostaining of this microvascular network revealed high degree of CD31 expression, specifically at cell-cell junctions, which is characteristic of native endothelium. Various sections of the microfluidic channels including linear sections, bifurcations, X-junctions, loops and bends were imaged and consistent immunostaining patterns were observed throughout the network (Fig. 5.2 A-D). Specific morphological characteristics of the endothelial cells were quantified from fluorescence images and are reported as follows: Mean surface area: 2220 ± 794 μm^2, Mean geometric diameter: 53 ± 10 μm, Mean circularity: 0.6 ± 0.1, Mean aspect Ratio: 2.5 ± 0.8, Mean cell density: 285 ± 24 cells/mm^2, Mean elongation length: 92 ± 21 μm. In addition, the directionality of endothelial in different sections of the microfluidic network was also analyzed. Cells were highly aligned in the direction of flow, with majority of cells being in the range of 0°-30° and 150°-180° of flow channel direction (Fig. 5.2F, Fig. 5.3). A minor fraction of cells located in some of the junction regions experienced flow from multiple directions and hence did not show preferential alignment in a single direction.

Establishment of a complex, intricate vascular network is an essential step towards modeling of the native tumor microvasculature. The added presence of this level of complexity is a determining factor in the investigation of a number of different pathophysiological aspects, namely: 1) exchange of media and cellular metabolites between the tumor region and surrounding microvasculature, 2) diffusion and penetration of drug components from the vasculature to the tumor mass, 3) presence of leaky vasculature and abnormal flow patterns

(backflow, closed loops) that is characteristic of native tumors and 4) endothelial-cancer cell communications and bidirectional signaling mechanisms that promote tumorigenesis and malignant growth.

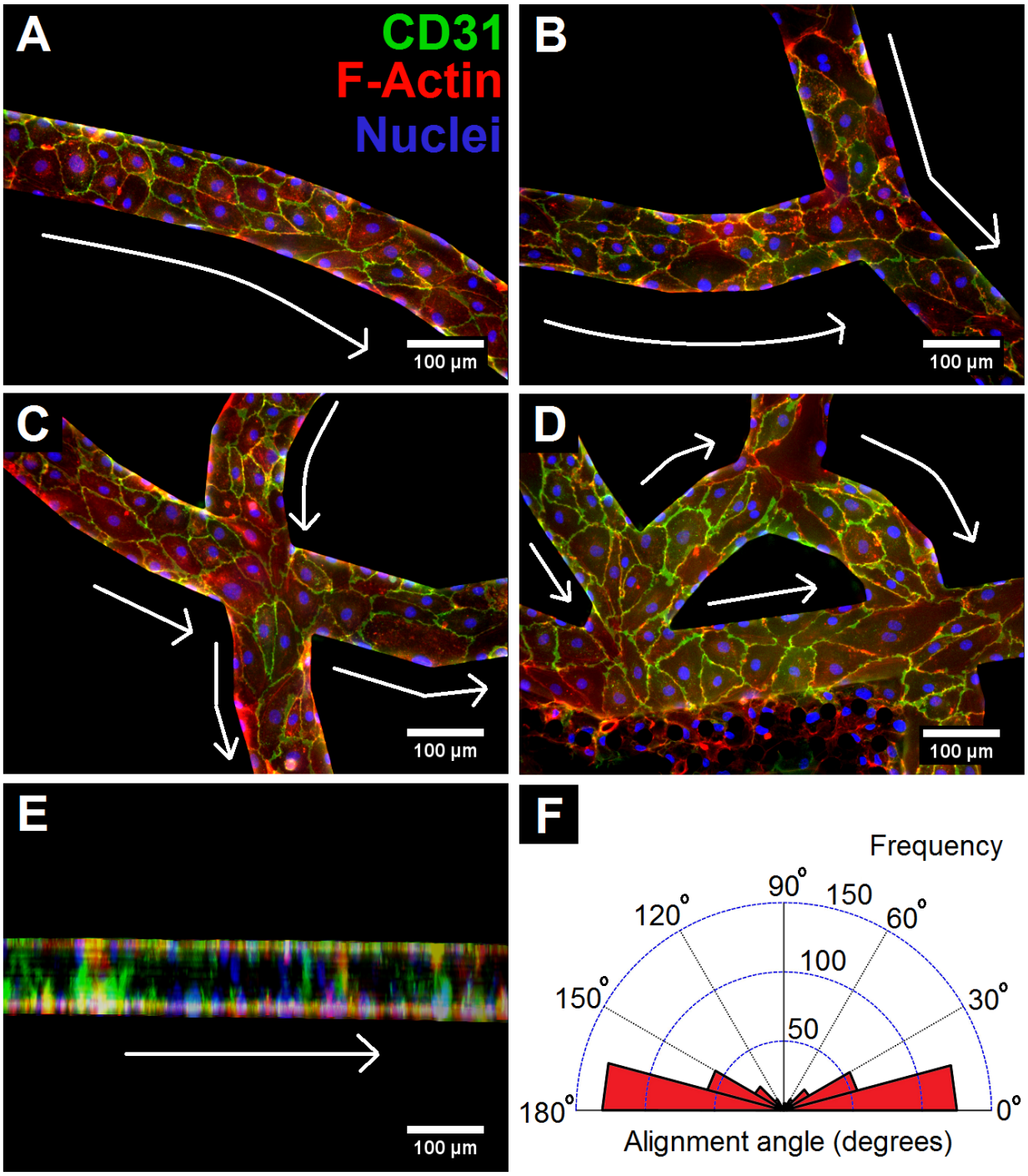

Figure 5.2: Vascular immunostaining and characterization. hBTECs seeded on fibronectin-coated microfluidic channels and maintained under continuous perfusion flow are stained for CD31, F-actin and nuclei in various regions of the network including (A) linear sections, (B) bifurcations, (C) X-junctions and (D) branching loops. (E) Side view of the linear section of the microfluidic channel demonstrating uniform coverage of the microfluidic channels. (F) hBTECs are aligned in the flow direction when maintained under continuous flow.

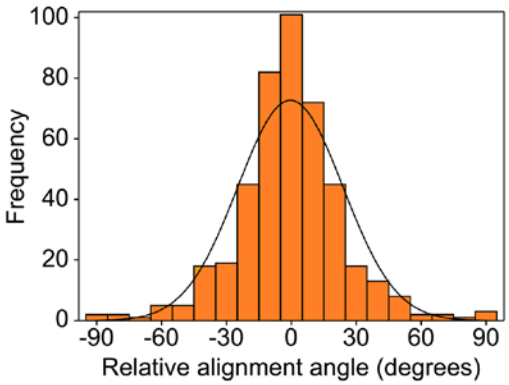

Figure 5.3: Flow alignment of hBTECs. Relative alignment angle of hBTECs in microfluidic channels reveals high degree of alignment with flow direction.

5.3.3 Long-term Co-culture and High Viability within Microfluidic Chips

MCF7 and MDA-MB-231 cells were individually co-encapsulated with BJ-5ta fibroblasts within PF hydrogel matrix in the endothelialized microfluidic chips and maintained in 3D culture for 28 days for observation of morphology and viability. Both cancer cell lines were uniformly distributed throughout the central tumor chamber on day 0 (Fig. 5.4A,D). MCF7 cells formed distinct local colonies with tight cellular packing through 28 days in culture reminiscent of their epithelial phenotype (Fig. 5.4B). MDA-MB-231 cells formed elongated and invasive morphologies as is characteristic of their native metastatic nature (Fig. 5.4E). Staining of the cultured cells with the live/dead dyes revealed high cell viability for both cell types within the

microfluidic devices with quantification revealing over 90% live cells at the end of 28 days Fig. 5.4C, F, G).

Morphological quantification of cellular features was conducted from phase contrast images every seven days post encapsulation of cancer cells. For MCF7 cells co-encapsulated with fibroblasts, there was an increase in colony area (~1900 μm^2 on day 0 vs. ~4200 μm^2 on day 28), increase in colony diameter (50 μm on day 0 vs. 80 μm on day 28), decrease in colony circularity (0.65 on day 0 vs. 0.55 on day 28) and no significant change in colony aspect ratio (~1.5-2.0) over time (Fig. 5.5 A-D). Increases in colony area and diameter are indicators of cell spreading and growth while decrease in colony circularity and increase in aspect ratio are indicators of invasive morphology of MCF7 cell type. For MDA-MB-231 cells co-encapsulated with fibroblasts, there was an increase in cellular area (~600 μm^2 on day 0 vs. ~1500 μm^2 on day 28), increase in cellular diameter (28 μm on day 0 vs. 42 μm on day 28), decrease in cellular circularity (0.30 on day 0 vs. 0.20 on day 28) and increase in cellular aspect ratio over time (4.0 on day 0 vs. 10.0 on day 28) (Fig. 5.5 E-H). In addition, there was also increase in cellular elongation length (60 μm on day 0 to 150 μm on day 28) over time (Fig. 5.6). These changes are indicative of cellular spreading and progression towards invasive morphologies.

In addition to gas exchange via the endothelialized microvasculature within the chips, gas exchange is also permissible through other surfaces on the chips. Specifically, the PDMS structures supporting the microvascular networks and cancer chamber is permeable to oxygen and hence would allow diffusion of oxygen from the outside ambient atmosphere to the interior regions, in a thickness dependent manner (Firpo et al. 2015, Markov et al. 2014). Given that the PDMS thickness was uniform throughout the entire area of the microfluidic chips (and hence oxygen permeability was also uniform), any variation in cell viability and growth can be

attributed to differences in media perfusion resulting from shear rate and microfluidic geometry variations. In addition, the distance of the MCF7 colonies from the surrounding vasculature was approximately within a 500-600 μm range. Cells seeded beyond this region did not form distinct colonies and remained as single cells throughout the culture period, possibly in a quiescent state. No difference in viability of cell colonies was observed within this 500-600 μm distance. Cell viability beyond this distance could not be quantified due to the inability of the Live/Dead dye to perfuse to the innermost regions of the tumor chamber and due to autofluorescence effects from the chip itself making it difficult to quantify fluorescently labelled cells.

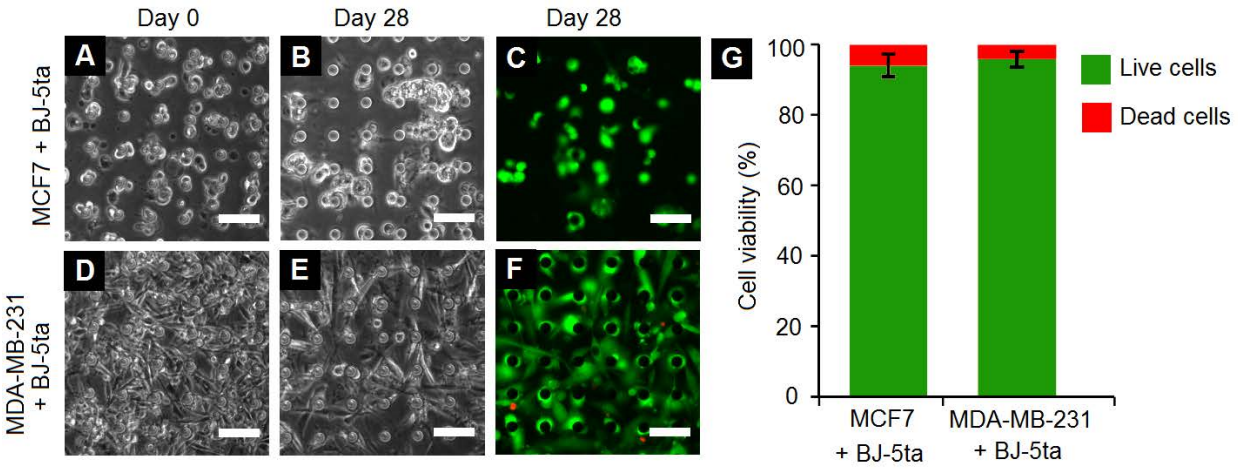

Figure 5.4: Long-term culture and viability of cancer cells within microfluidic chips. MCF7 and BJ-5ta cells (A-C) and MDA-MB-231 and BJ-5ta cells (D-F) co-encapsulated in the PF hydrogel matrix within microfluidic devices on day 0 (A, D) and day 28 (B, E) post seeding. Viability staining (C, F) and quantification (G) of two cell types within chips reveal high viability of cells maintained within microfluidic chips. Scale bars = 50 μm

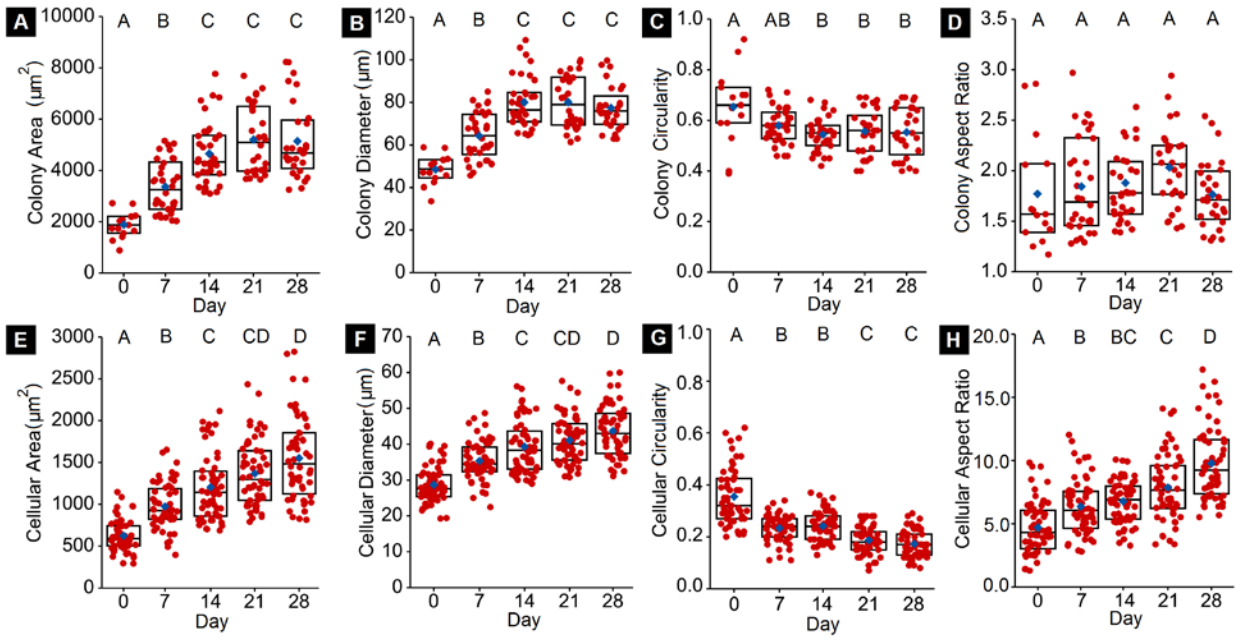

Figure 5.5: Morphological quantification of cells within microfluidic chips. Quantification of MCF7 morphology (co-encapsulated with fibroblasts) reveals (H) increase in colony area, (I) increase in colony diameter, (J) decrease in colony circularity and (K) no change in colony aspect ratio over time. Quantification of MDA-MB-231 morphology (co-encapsulated with fibroblasts) reveals (L) increase in cellular area, (M) increase in cellular diameter, (N) decrease in cellular circularity and (O) increase in cellular aspect ratio over time. Groups having different letters have significantly different means ($p<0.05$). Red points denote individual colonies (for MCF7 cells)/cells (for MDA-MB-231 cells) and blue dots represent mean of group. Rectangular boxes represent upper quartile, median and lower quartile of the group.

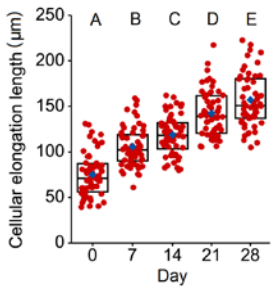

Figure 5.6: MDA-MB-231 elongation length in microfluidic chips. Cellular elongation length of MDA-MB-231 cells increases in long-term culture within microfluidic chips. Groups having different letters have significantly different means ($p<0.05$). Red points denote individual colonies/cells and blue dots represent mean of group. Rectangular boxes represent upper quartile, median and lower quartile of the group.

5.3.4 Extravasation and Migration within Microfluidic Chips

In addition to quantification of morphological parameters, the invasiveness and migratory behavior of cancer cell types were also analyzed. For MDA-MB-231 cells, cellular migration and invasion was observed in long-term culture over 28 days. Cells initially seeded in the primary tumor region were observed to be intravasating into the adjacent endothelialized vascular channels (Fig. 5.7A). These intravasated cells further migrated into the secondary region after crossing the endothelial barrier and by day 28, these cells had completely occupied the secondary region with increased cell density over time (Fig. 5.7B, C). Quantification of cellular intravasation revealed relative increase in intravasation from day 0 to 7, beyond which there was a drop in the relative values, possibly due to cell death in the primary tumor region caused by lack of diffusion of media (Fig. 5.7D). There was also an increase in invasive cell density in the secondary tumor region (~50 cells/mm^2 to ~400 cells/mm^2 on day 28) and increase in the distance covered by the invading cell front (~200 µm on day 0 to ~3000 µm on day 28) over time (Fig. 5.7E, F). These parameters are indicative of the invasive and migratory behavior of the

MDA-MB-231 cancer cells as is observed in *in vivo* systems. These observations highlight the usefulness of the cancer-on-a-chip system to study the invasiveness and aggressive behavior of metastatic MDA-MB-231 cells. In contrast, MCF7 cells remained localized within the primary tumor chamber without any tendency of migrating to secondary chambers or extravasating to adjoining endothelial channels (Fig. 5.8). The differences in these cell behaviors demonstrate the potential ability of the cancer-on-a-chip platform in assessing the invasiveness and metastatic potential of cancer cells in future work.

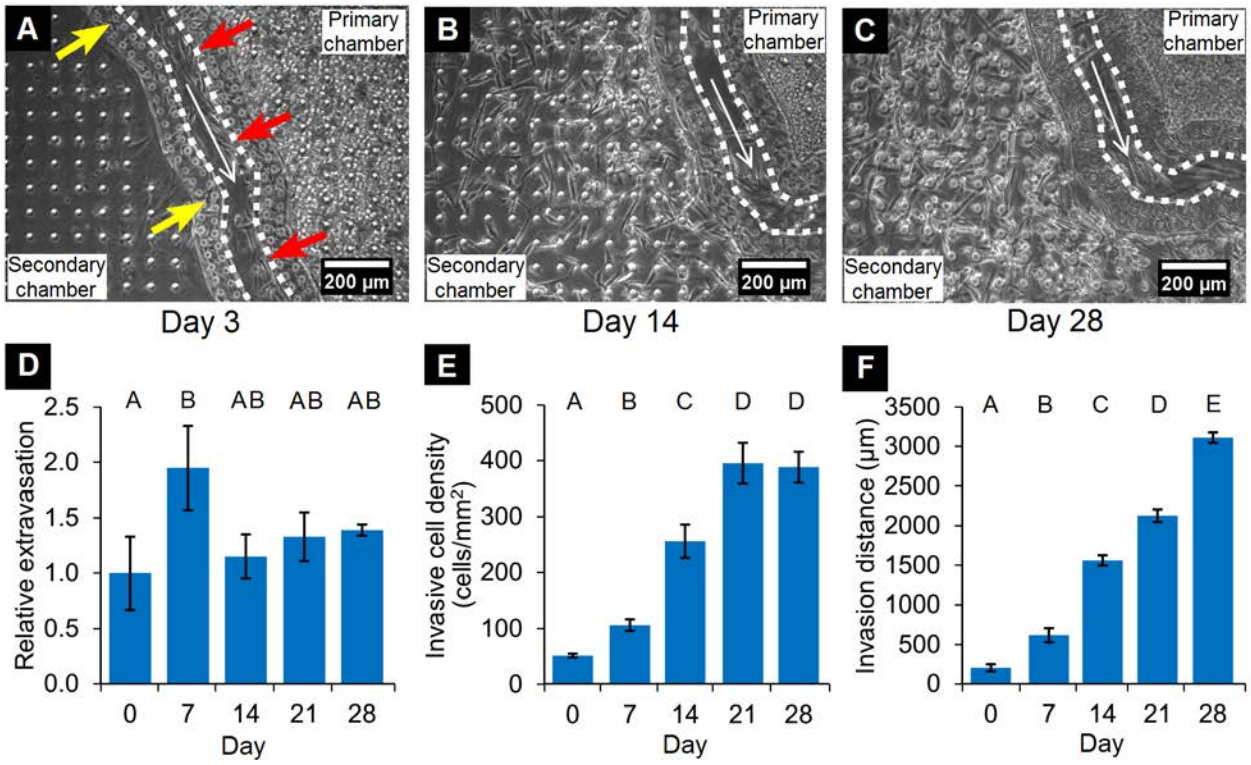

Figure 5.7: Intravasation and cell migration of MDA-MB-231 cells. (A) MDA-MB-231 cells (co-encapsulated with fibroblasts) extravasate from the primary tumor region into the adjacent vascular channels (white dotted lines) by day 3 (denoted by red arrows) and further migrate towards the secondary region (denoted by yellow arrows). (B) Cells invade into the secondary region by day 14 and (C) by day 28, there is increase of cell density in the secondary region.

White arrow indicates diection of vascular flow. (D) Relative extravasation, (E) increase of cell density and (F) increase in distance of the invasive cell front of MDA-MB-231 cells. Groups having different letters have significantly different means ($p<0.05$).

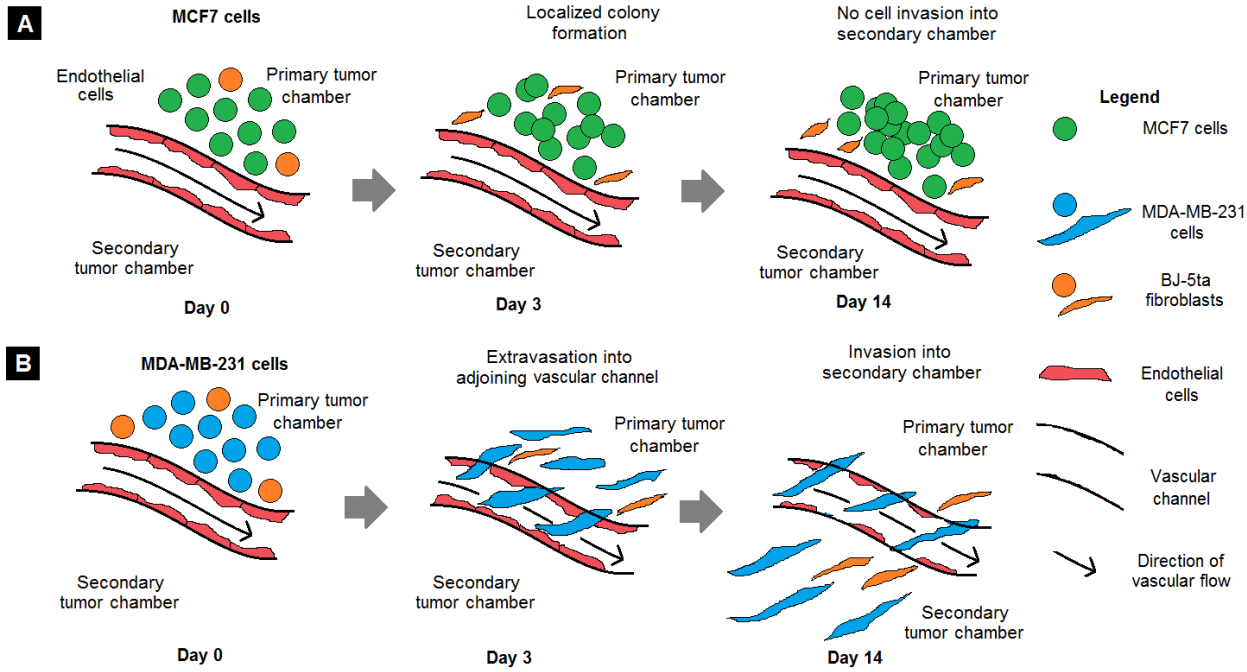

Figure 5.8: Differences in cancer cell aggressiveness in microfluidic chips. (A) MCF7 cells co-encapsulated with fibroblasts remain localized in the primary tumor region forming cell colonies without invading into the secondary chamber, thereby displaying non-aggressive behavior. (B) MDA-MB-231 cells co-encapsulated with fibroblasts are able to extravasate from the primary tumor chamber into the adjoining vascular channels by day 3 and invade into the secondary tumor chamber by day 14, thereby displaying aggressive behavior.

5.3.5 Geometry-dependent Variation in Diffusion and Cellular Morphology

In role to assess the role of the microvascular geometry and shear variation in the diffusion profile within the central tumor chamber, fluorescent TRITC-dextran was used to as a probe to quantify concentration gradients in different locations within the central tumor chamber. The TRITC-dextran (molecular weight: 4.4 kDa) used in this study was not specifically meant to

model a particular bioactive moiety but rather used to highlight differences in diffusion gradients within the central tumor chamber. It can be assumed by extrapolation that bioactive moieties of other molecular weights might also display such gradients to varying degrees depending on their molecular weight and diffusive abilities. In the high perfusion chip, higher degree of TRITC-dextran diffusion was observed compared to the low perfusion chip (Fig. 5.9A, B). A greater area of the tumor chamber was represented by the red, orange and yellow regions in the heat map in the high perfusion chip. This observation could be attributed to the higher shear rates of the surrounding microvascular flow in the high perfusion chip compared to the low perfusion chip. However, locational differences in diffusion were observed for both the chips. Accordingly, these regions of the tumor chamber regions were denoted as high diffusion region of interest (ROI) and low diffusion ROI. In the high perfusion chip, the high diffusion ROI was located closer to the inlet port of the chip. Analysis of the diffusion profile (denoted by blue, green and red arrows) revealed a relatively high concentration gradient with increasing distance from vascular channel (Fig. 5.9E). However, in the low diffusion ROI (denoted by the magenta, cyan and orange arrows), there was a sharp drop in concentration with increasing distance from the vascular channel (Fig. 5.9G). Similar concentration gradients were also observed in the low perfusion chip. In this chip, the drop in concentration gradient in both the high diffusion ROI and low diffusion ROI was even higher compared to the high perfusion chip, possibly due to effects of low shear flow rates in the adjacent vascular channels (Fig. 5.9F, H).

Due to the effect of the diffusional gradients of media and cellular metabolites, morphological differences in seeded cancer cells were also visualized within microfluidic chips (Fig. 5.10A). In the high diffusion ROI regions, MCF7 cells were able to form local colonies characteristic of their 3D phenotype (Fig. 5.10B, C) while MDA-MB-231 cells were able to form

elongated and invasive morphologies indicative of cell spreading (Fig. 5.10D, E). However, in the low diffusion ROI, both cell types appeared rounded, dark and unhealthy indicative of either dormant, quiescent state or a state of cell death due to lack of sufficient media diffusion (Fig. 5.10F, G, H, I). Fibroblasts present in the high diffusion ROI regions were able to form elongated and spread out morphologies but those present in the low diffusion ROI appeared rounded and dormant.

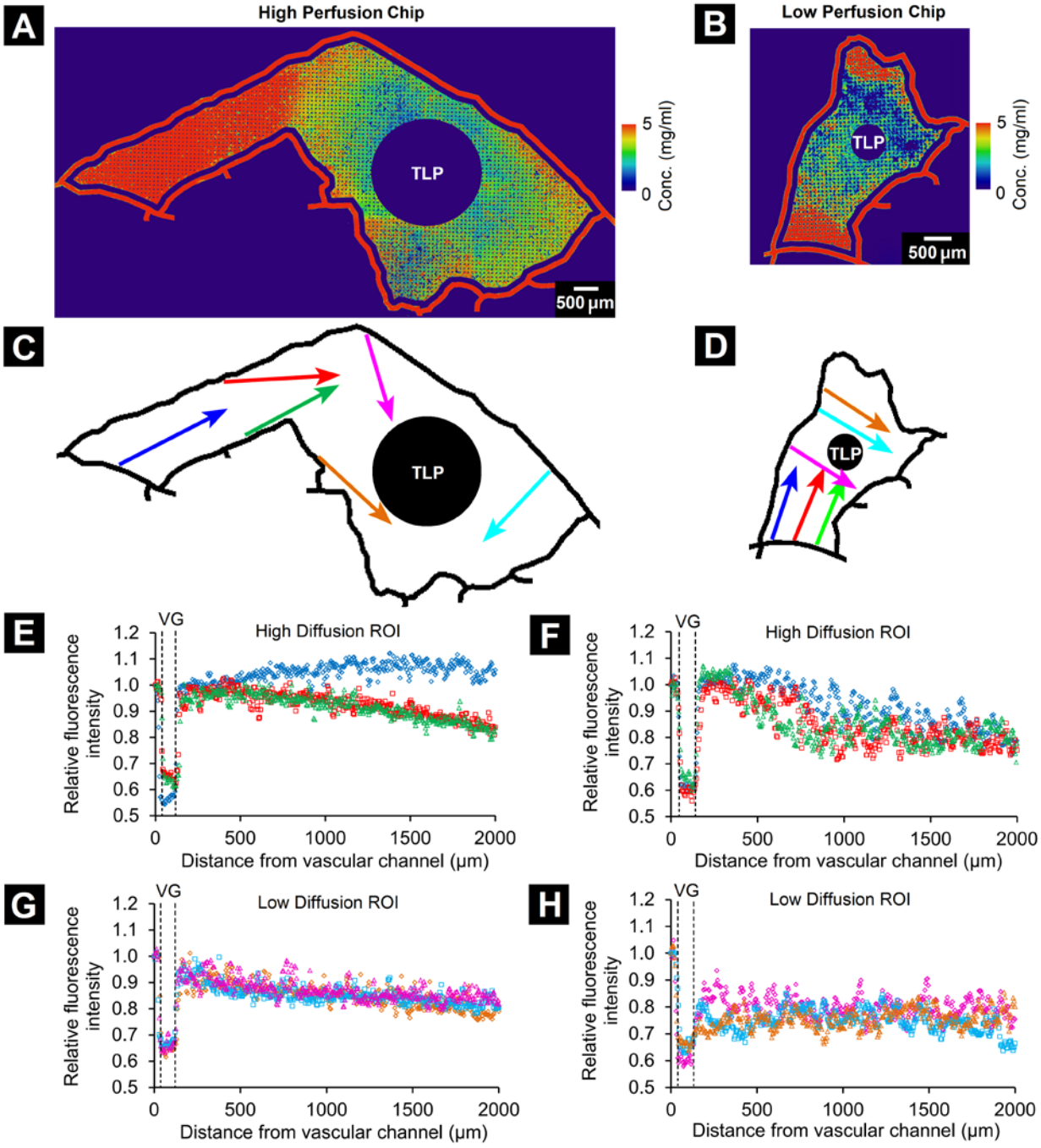

Figure 5.9: Diffusional variation within microfluidic chips. Heat maps of (A) high and (B) low perfusion chips reveal variation in concentration of TRITC-dextran after 2 hours of continuous flow. Schematic of the analyzed diffusion profile directions of the (C) high and (D) low perfusion chips. Relative fluorescence intensity of the analyzed images in the (E, G) high

perfusion chip and (F, H) low perfusion chip reveals decreasing concentration with increasing distance from vascular channel. VG (vascular gap) represents the distance between vascular network and tumor chamber. Though the differences in relative fluorescence intensity due to distance from vascular channel may not appear significantly different between the two different designs, even these small variations within the first 500 μm distance were pronounced enough to cause differences in encapsulated cell behavior and morphology.

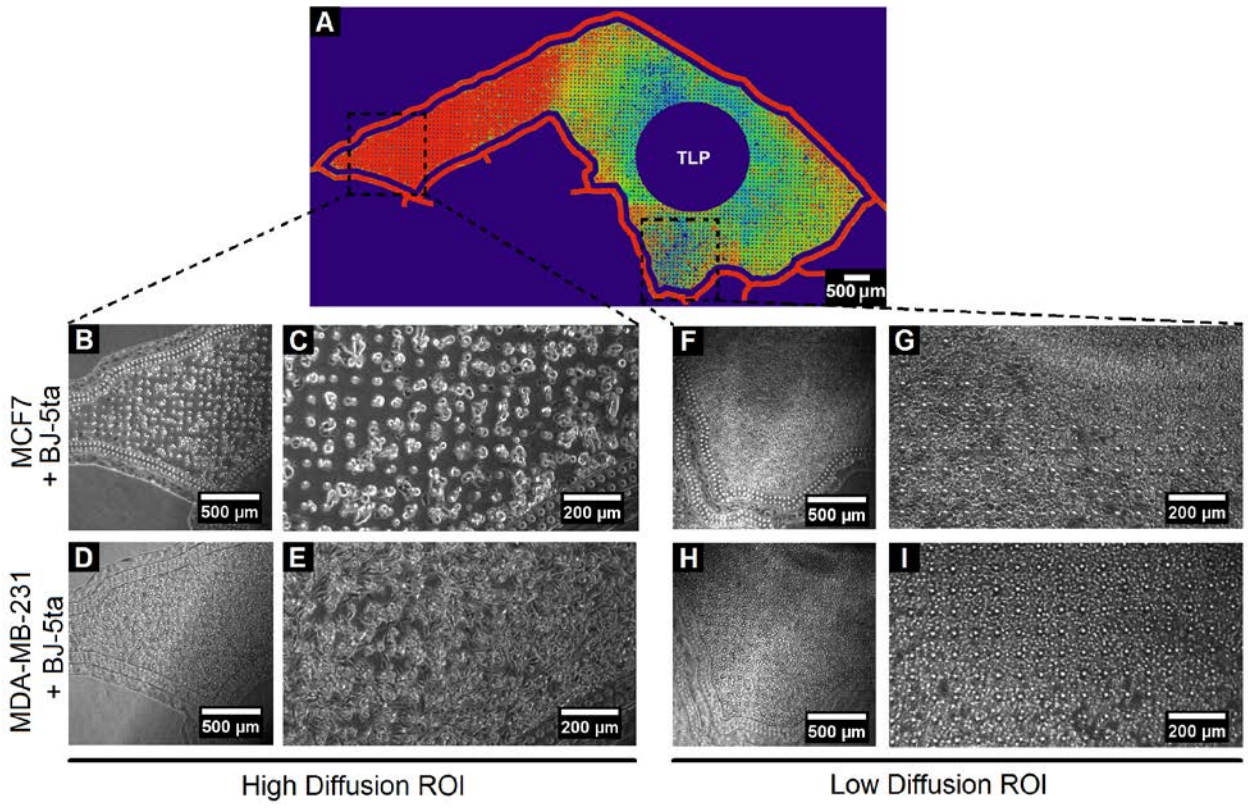

Figure 5.10: Tumor heterogeneity within microfluidic chips. (A) Representative heat map of the high perfusion chip reveals locational heterogeneity within the microfluidic chips. (B, C) MCF7+BJ-5ta cells in the high diffusion region of interest (ROI) are able to form distinct colonies in long-term culture and (D, E) MDA-MB-231+BJ-5ta cells are able to form invasive morphologies characteristic of their metastatic phenotype. However, MCF7 cells (F, G) and

MDA-MB-231 cells (H, I) are unable to survive long-term in the low diffusion ROI and appear rounded and unhealthy in those regions.

5.3.6 Drug Testing within Microfluidic Chips

In order to test the efficacy of anti-cancer drugs on cancer cells encapsulated within the microfluidic chips, doxorubicin and paclitaxel were perfused through the vascular channel and resulting cell viability was tested 48 hours post drug treatment. In general doxorubicin appeared to have a higher cytotoxic effect on the cancer cells compared to paclitaxel in terms of viable cell density (Fig. 5.11A, B). In the high perfusion chips, viable cell density was considerably reduced by both drugs on both cell lines, possibly due to higher penetration of drugs into the respective central tumor regions of the microfluidic chips. However, in the low perfusion chips, only doxorubicin had an appreciable effect on reduction of cell density of MDA-MB-231 cells. In addition, the cell density of MDA-MB-231 cells was considerably lowered in the high perfusion chip compared to the low perfusion chip. In terms of the viable tumor area (area occupied by the viable cancer cells), significant reduction compared to the control was observed across all tested conditions (Fig. 5.11C, D). Specifically, in response to doxorubicin, viable tumor area of MCF7 and MDA-MB-231 cells were significantly reduced in the high perfusion chip compared to the low perfusion chip, possibly due to higher diffusion of drug in the interior regions of the high perfusion chip. Assessment of the cytotoxic effects on endothelial cells also revealed higher cytotoxicity of doxorubicin compared to paclitaxel on both high and low perfusion chips (Fig. 5.11E).

These drug studies were also conducted in parallel with static 3D well plate cultures where cancer cells co-encapsulated with BJ-5ta fibroblasts within PF hydrogels were treated with drug, but without the effect of flow or diffusional resistances. Interestingly, both doxorubicin and

paclitaxel had a much higher cytotoxic effect on both the cancer cell lines in the static 3D culture conditions compared to that under the microfluidic flow conditions (Fig. 5.11F).

The drug studies were conducted with co-cultures of cancer cells and fibroblasts which were initially encapsulated within the PF matrix in a 5:1 ratio of cancer cells:fibroblasts. So the drug efficacy data presented here represents the combined action of the drug on both cancer cells and fibroblasts. In order to distinguish the effects of drug action on cancer cells from that on fibroblasts, it would be necessary to run separate drug testing experiments on vascularized chips seeded with only cancer cells or only fibroblasts in the central tumor chamber.

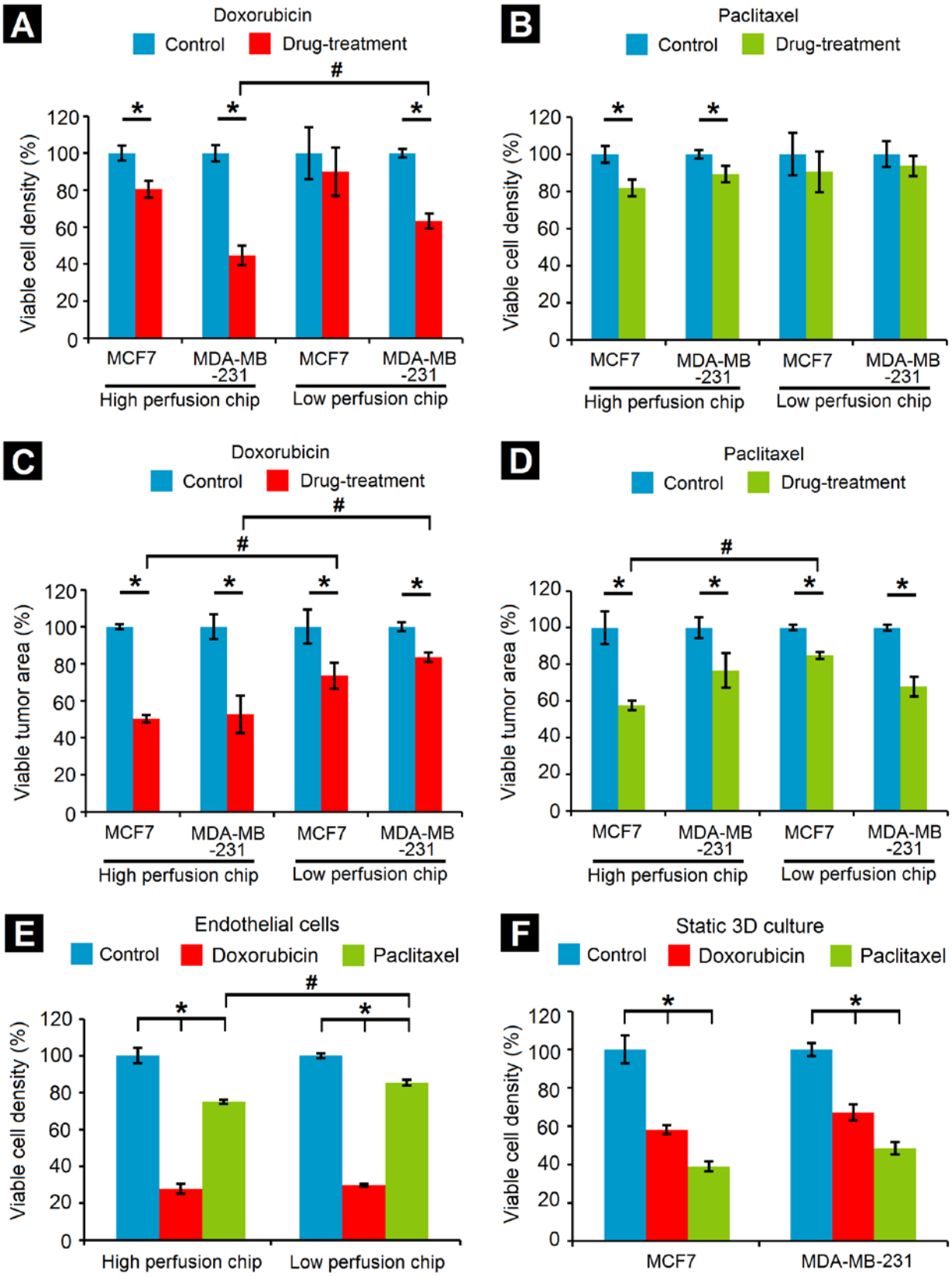
A
Doxorubicin
Control
Drug-treatment
Viable cell density (%)
MCF7
MDA-MB -231
High perfusion chip
Low perfusion chip
B
Paclitaxel
C
Viable tumor area (%)
D
E
Endothelial cells
Paclitaxel
F
Static 3D culture
MDA-MB-231

Figure 5.11: Drug-testing in microfluidic chips. Reduction in viable cell density due to (A) doxorubicin and (B) paclitaxel in high and low perfusion chips for both MCF7 and MDA-MB-231 cells co-encapsulated with fibroblasts. Reduction in viable tumor area (area occupied by viable cells) due to (C) doxorubicin and (D) paclitaxel in high and low perfusion chips for both the cell lines. (E) Drug cytotoxicity on endothelial cells in both high and low perfusion chips. (F) Decrease in viable cell density of both cell lines in static 3D hydrogel well plate culture (* Significant difference between control and drug treatment groups, $p<0.05$; # Significant difference between same cell type in different chips, $p<0.05$).

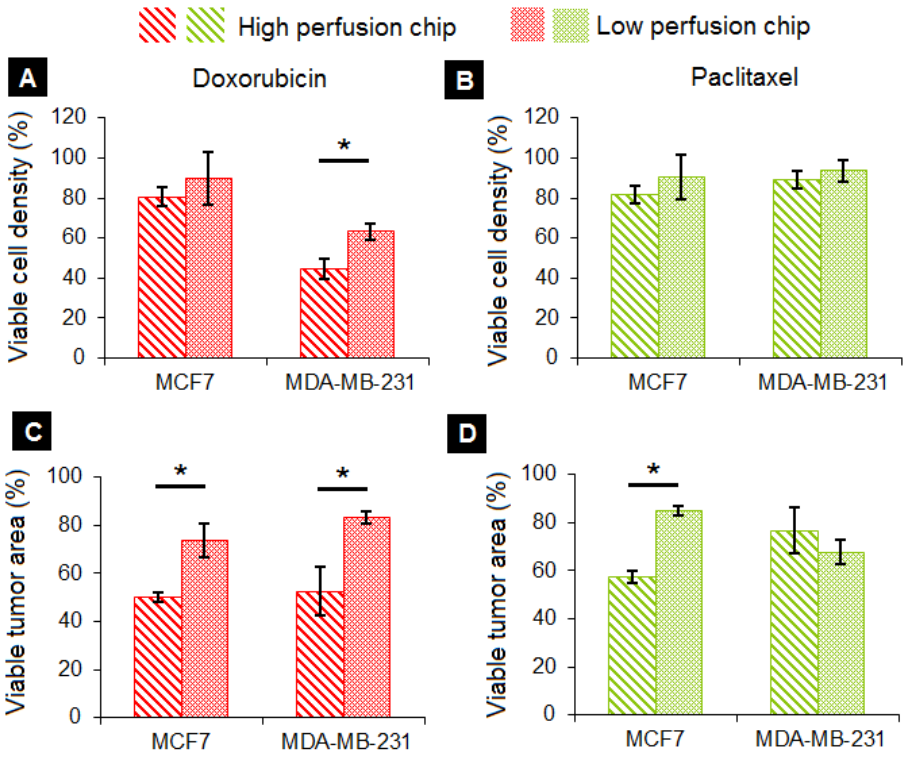

Figure 5.12: Comparison of high and low perfusion chip with respect to drug action. In terms of cell viability, (A) doxorubicin has a significant reduction in MDA-MB-231+fibroblast viable cell density in the high perfusion chip compared to the low perfusion chip, but this trend is not visible in the MCF7+fibroblast cells. (B) Paclitaxel does not exhibit any differences in viable cell

density in either chip design. In terms of viable tumor area, (C) doxorubicin causes significant reduction in viable tumor area for both MCF7 and MDA-MB-231 cells, co-encapsulated with fibroblasts in the high perfusion chip compared to the low perfusion chip. However, (D) paclitaxel causes significant reduction of viable tumor area only in MCF7 cells but not in MDA-MB-231 cells, co-encapsulated with fibroblasts.

These differences in the drug action can be attributed to a number of factors as stated: 1) the design and geometry-dependent variation of shear flow and diffusional profiles within the microfluidic chips that regulates the concentration of drug that is ultimately experienced by the cancer cells in different locations of the central tumor chamber, 2) the state of proliferation and activity of the two cell types (MDA-MB-231 cells are more proliferative than MCF7 cells and hence are more susceptible to drug action that is dependent on inhibiting cell division processes), 3) the differences in mechanism of drug action between doxorubicin and paclitaxel. Specifically, doxorubicin is known to intercalate with the DNA (irrespective of cell type), leading to stabilization of the topoisomerase II complex necessary for DNA replication. As a result, cells are forced into a state of quiescence and further on to apoptosis due to prolonged inhibition of DNA activity. In contrast, paclitaxel targets tubulin and stabilizes the microtubule polymer, preventing it from disassembly during metaphase spindle formation. Thus mitotic progression is blocked and prolonged activation of the mitotic checkpoint triggers apoptosis or reversion to the G-phase of the cell cycle without cell division. In the chip system, the observations of drug action were somewhat different from the expected observations. Paclitaxel had a much lower cytotoxic effect on the cancer cells compared to effect of doxorubicin. This could be attributed to the comparative ability of paclitaxel and doxorubicin to diffuse through the endothelial layer and through the PF hydrogel matrix encapsulating cancer cells. The state of proliferation and active

cell division of encapsulated cancer cells could also be a determining factor behind the responsiveness to drugs. It can be surmised that cancer cells seeded in the PF matrix within the microfluidic chips might not have been in an active of proliferation (or might have been in an quiescent state), hence not being as sensitive to paclitaxel as compared to doxorubicin. It is also possible that paclitaxel might have had some unexpected side interactions with PDMS structures that make up the microfluidic system. This would also explain the differences in cytotoxicity of the drugs observed on endothelial cells. hBTECs are fully lumenized and stabilized in the microvasculature of the chips and hence not in a state of active cell division. Hence, these cells are affected by paclitaxel to a much lesser degree than doxorubicin. Overall, these cancer-on-chip platforms facilitate the investigation of anti-cancer drug efficacy and cytotoxicity with a greater degree of physiological context (in the presence of dynamic and geometry-dependent flow) than that available in static 3D systems.

Due to the differences in perfusion capacities of the two different chip designs with respect to TRITC-dextran, it can be surmised that doxorubicin and paclitaxel might also experience different perfusion profiles within the chips based on both the nature of the drug molecules and also the vascular network geometries. Hence standardization of drug action should be done either based on drug-to-drug on the same chip design or chip-to-chip design based on the same drug. Overall, the use of this cancer-on-a-chip model provides a more realistic and relevant prediction of drug action on *in vivo* tumors, by incorporating a multiple important elements of the TME that synergistically act to recapitulate key features on *in vivo* tumors. The presence of an intricate network of complex and abnormal microvasculature, that is found surrounding tumor tissues, provides shear flow variances and perfusion differences in the flow of metabolites and drugs. The presence of the PF matrix simulates native tumor ECM matrices that

provide mass-transfer limitations to the diffusion of different molecules. The presence of fibroblasts as supportive cell types for cancer cells provides greater degree of physiological context with regards to *in vivo* tumors. Specifically, the microfluidic platform can provide important information regarding the ability of drug compounds to perfuse through the vascular network and into the central tumor chamber and subsequent effects of drug action on encapsulated cancer cells. Comprehensively, the synergistic influence of all these parameters significantly enhance the ability of this platform to provide predictive information of drug action with higher degree of accuracy compared to traditional 2D and static 3D model systems.

The primary objective of this project was the establishment of a cancer-on-a-chip microfluidic platform for the 3D co-culture of cancer cells and associated cell types and subsequent demonstration of the ability to test common breast cancer drugs within the platform as a preliminary proof-of-concept for future drug testing applications. In future studies, improved models would be developed that incorporate tumor cells derived from patient-derived xenografts and more targeted anti-cancer drugs would be used to assess their therapeutic potential.

5.4 Conclusions

This study established a novel cancer-on-a-chip platform for the investigation of 3D long-term co-culture of cancer cells and fibroblasts within a biomimetic PF hydrogel matrix in the presence of an intricate microvasculature. The vascular network formed from hBTECs was mature, lumenized and aligned in the direction of flow, as is observed in *in vivo* and native systems. Breast cancer cells were able to be maintained in long-term co-culture with fibroblasts with high cell viability through 28 days. Further these cells also displayed their characteristic morphologies indicative of cell spreading, proliferation, invasion and metastasis. Specifically, MDA-MB-231 cells were observed to extravasate form the primary seeded region into the

adjoining vascular space and further migrate and invade into secondary tumor regions with the progress of time. Geometry-dependent variation in shear flow rates and diffusion profiles were quantified in the chips and resulting variation in cellular morphologies indicative of tumor heterogeneity were also observed. Finally, testing of anti-cancer drug efficacy and cytotoxicity revealed prominent differences in drug action based on geometry and design of microfluidic chips, types of cancer cell lines tested and the mechanism of drug action in general. Overall, this cancer-on-a-chip platform can be used in the future of investigation of larger number of potential drug candidates and for detailed investigation of various tumorigenic mechanisms related to EMT, metastasis, and tumor-related angiogenesis.

CHAPTER 6: Summary and Conclusions

This work presents the use of polymeric biomimetic materials and biofabrication techniques for establishing 3D *in vitro* tissue-engineered cancer models and recapitulation of specific aspects of the tumor microenvironment, which can be potentially used for investigation of 3D cancer cell behavior and for evaluating efficacies of anti-cancer drugs. The results from this work demonstrate that the use of photocrosslinkable, PEG-based hydrogels modified with suitable bioactive factors that facilitate 3D long-term culture, maintenance and investigation of cancer cells *in vitro*. Further, novel fabrication techniques based on water-oil emulsification, microfluidics and PDMS photolithography have been employed to recreate 3D tumor models of desired shape, size and geometries. In addition to cancer cells, a range of other influential factors present in the tumor microenvironment including fibroblasts, abnormal vasculature comprised of tumor-associated endothelial cells have also been incorporated into the fabricated tumor models with increased degrees of complexity. The combination of all these elements ultimately help establish novel *in vitro* platforms for evalution of anti-cancer drug efficacies prior to *in vivo* or pre-clinical translation.

The work presented here describes four specific studies for the development and investigation of 3D tumor models. In the first study, the establishment of PEGDA tumor millibeads using a surface-tension based, dual-phase technique facilitated the recreation of native tumor microenvironment within millimeter-scale tumor constructs with core regions of cell death surrounded by viable, peripheral cell layers. The tumor millibead model can be potentially used an *in vitro* tool to mimic large tumors in a scalable and reproducible fashion. In conjuction with the tumor millibeads, pre-formed tumor-mimic vasculature could also be incorporated in future

models with higher degrees of complexity to more closely mimic the native physiology of large tumors.

In the second study, the primary objective was to develop and optimize a fabrication technique that would enable the encapsulation of various cancer cell types within PEG-fibrinogen microspheres which could potentially be used in the future in 96 or 384 well plate formats for high-throughput screening assays. The use of a water-in-oil emulsion technique for generation of PEG-fibrinogen hydrogel microspheres enabled the fabrication of the tumor microsphere model and investigation of the role of PEG-fibrinogen on the growth and morphology of MCF7 cells. With future improvement and optimization of fabrication techniques, this microsphere model could be used for the simultaneous testing and validation of large number of drug compounds, which could potentially provide closer physiologically relevant drug-efficacy information than that provided by current 2D assays.

In the third study, the effects of modulation of physico-mechanical characteristics of PEG-fibrinogen matrix on 3D breast cancer cell behavior, morphology and proliferation was explored. The *in vitro* model developed in this study focuses on the comparative study of three different cell lines representative of the major breast cancer subtypes and their 3D behavior in response to varying matrix characteristics. This model could be used in the future to investigate aggressiveness and behavior of various other cancer cell types in a 3D context and under varying matrix characteristics, while also incorporating more complex elements of the tumor microenvironment in conjunction with cancer cells.

Finally, in the fourth study, the establishment of a microfluidic cancer-on-a-chip system provided a combinatorial platform for co-culture of cancer cells and fibroblasts within PEG-fibrinogen hydrogel matrix along with an intricate network of endothelialized tumor

microvasculature for the recapitulation of the native tumor microenvironment and evaluation of anti-cancer drug efficacies. This microfluidic system brings together specific elements of the TME into a single platform and facilitates the investigation of the synergistic effects of 3D cancer cell behavior with secondary cell types under tumor-mimic fluidic conditions. This platorm could be potentially used in the future to evaluate their degree of aggressiveness of cancer cells under a complex 3D microfluidic environment and also assess the ability of drug molecules to perfuse through the tumor-mimic vasculature and cause cell death in the tumor region. In addition, this platform could also be used for mechanistic examination of therapeutic particle uptake by investigation of particle flow through the tumor vasculature, particle diffusion through the vascular barrier and cellular uptake in the central tumor region. In future studies, this platform could be further validated using chemotherapeutics that were found to differ in their effectiveness between *in vivo* models and 2D assays. The following schematic (Fig. 6.1) provides a brief overview of the scope of this work in relation to the overall drug development process.

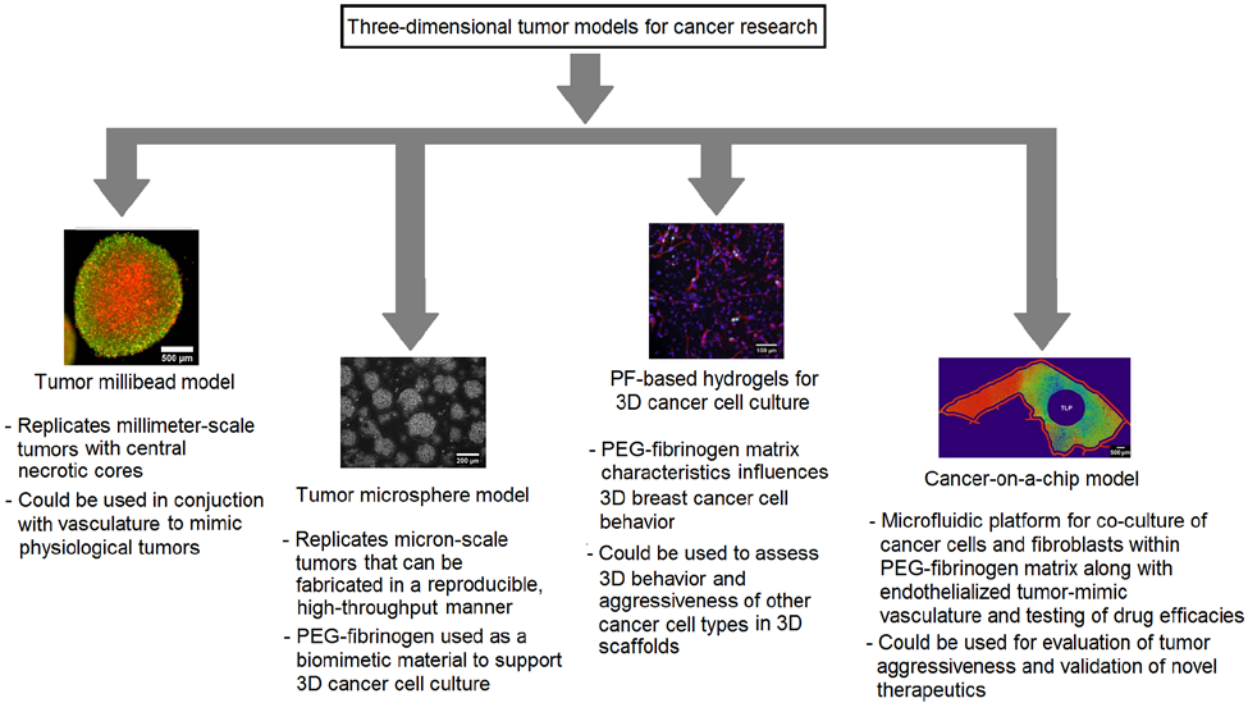

Fig. 6.1. Overview of models fabricated in relation to cancer research. The current work presents four different strategies for investigation of cancer cells in 3D culture via different biofabrication techniques that can be suitably used to replicate specific aspects of cancer biology and could be used selectively in the future in different phases of the drug discovery process to test or validate the efficacies of anti-cancer therapeutics.

Each *in vitro* model is designed to answer specific questions regarding cancer biology and/or subsequent chemotherapeutic treatment. Hence, comparison of the suitability of different models to native tumors and assessment of physiological relevance of these models need to be made with care. Microtissue-scale models of all organ types are physically limited in their ability to recapitulate the physiological complexities of the entire organs or organ systems, but are more suited to simulate specific key features representative of the organs. A similar approach has been adopted in the design and fabrication of the tumor models described in the above studies. Some of the current assays in use require the use of small, replicable and reproducible tumors in a high throughput fashion. These model tumors may not be positioned to capture the entire gamut of physiological complexities of native tumors including hypoxia, interaction with secondary cell types and other factors, owing to inherent physical limitations of biofabrication techniques. However, compared to standard 2D models, novel 3D tumor models offer dimensional complexity (including cell-cell and cell matrix interactions, influence of mechanical stiffness) owing to contextual presentation of cancer cells in 3D microenvironments. In addition, small, uniform 3D tumor models could be adapted for use in high-throughput screening assays. Whereas the size of the tumor models developed in these studies are representative of small localized tumors that are generally undiagnosed or treated by surgery rather than by chemotherapy, yet the contextual cues provided in these models present a subunit view of the

larger tumor tissue and is one of the preliminary steps towards building more complex and intricate cancer tissue which would be more closely replicative of the native TME. Various elements of the native TME inclusing hypoxia, changes in pH levels, presence of cancer-associated fibroblats or macrophages contribute synergistically to disease progression mechanisms. Each of these aspects is important in promoting aggressive and chemo-resistant behavior of cancer cells. The tissue-engineered tumor models developed in these studies can help replicate specific aspects of cancer biology and can provide information about specific aspects of drug testing processes. The specific physical and biological limitations of each developed model must be kept in mind while making subsequent interpretations regarding physiological relevance or therapeutic drug action.

Overall, these investigations provide a foundation for further work and specific toolsets to better understand the role of the tumor microenvironment in the malignant progression of cancer, metastasis and tumor-related angiogenesis. In addition, the use of these bioengineered platforms for recreating the tumor microenvironment can provide greater physiological context than current *in vitro* 2D models of cancer and provide more relevant information with regards to disease progression and treatment mechnisms.

References:

1. Achilli, T. M., J. Meyer, and J. R. Morgan. 2012. "Advances in the formation, use and understanding of multi-cellular spheroids." *Expert Opin Biol Ther* 12 (10):1347-60. DOI: 10.1517/14712598.2012.707181.

2. Agastin, Sivaprakash, Ut-Binh T. Giang, Yue Geng, et al. 2011. "Continuously perfused microbubble array for 3D tumor spheroid model." *Biomicrofluidics* 5 (2):24110-24110. DOI: 10.1063/1.3596530.

3. Alemany-Ribes, M., and C. E. Semino. 2014. "Bioengineering 3D environments for cancer models." *Advanced Drug Delivery Reviews* 79-80:40-49. DOI: 10.1016/j.addr.2014.06.004.

4. Allen, M., and J. Louise Jones. 2011. "Jekyll and Hyde: the role of the microenvironment on the progression of cancer." *J Pathol* 223 (2):162-76. DOI: 10.1002/path.2803.

5. Almany, L., and D. Seliktar. 2005. "Biosynthetic hydrogel scaffolds made from fibrinogen and polyethylene glycol for 3D cell cultures." *Biomaterials* 26 (15):2467-77. DOI: 10.1016/j.biomaterials.2004.06.047.

6. Alt-Holland, Addy, Yulia Shamis, Kathleen N. Riley, et al. 2008. "E-cadherin suppression directs cytoskeletal rearrangement and intraepithelial tumor cell migration in 3D human skin equivalents." *The Journal of investigative dermatology* 128 (10):2498-507. DOI: 10.1038/jid.2008.102.

7. Apostolopoulou, M., and L. Ligon. 2012. "Cadherin-23 mediates heterotypic cell-cell adhesion between breast cancer epithelial cells and fibroblasts." *PLoS One* 7 (3):e33289. DOI: 10.1371/journal.pone.0033289.

8. Appelman, T. P., J. Mizrahi, J. H. Elisseeff, et al. 2011. "The influence of biological motifs and dynamic mechanical stimulation in hydrogel scaffold systems on the phenotype of chondrocytes." *Biomaterials* 32 (6):1508-16. DOI: 10.1016/j.biomaterials.2010.10.017.

9. Arya, N., V. Sardana, M. Saxena, et al. 2012. "Recapitulating tumour microenvironment in chitosan-gelatin three-dimensional scaffolds: an improved in vitro tumour model." *Journal of the Royal Society Interface* 9 (77):3288-3302. DOI: 10.1098/rsif.2012.0564.

10. Asakawa, N., T. Shimizu, Y. Tsuda, et al. 2010. "Pre-vascularization of in vitro three-dimensional tissues created by cell sheet engineering." *Biomaterials* 31 (14):3903-9. DOI: 10.1016/j.biomaterials.2010.01.105.

11. Bae, S. N., G. Arand, H. Azzam, et al. 1993. "Molecular and cellular analysis of basement membrane invasion by human breast cancer cells in Matrigel-based in vitro assays." *Breast Cancer Research and Treatment* 24 (3):241-255.

12. Baker, B. M., and C. S. Chen. 2012. "Deconstructing the third dimension: how 3D culture microenvironments alter cellular cues." *J Cell Sci* 125 (Pt 13):3015-24. DOI: 10.1242/jcs.079509.

13. Bal, T., B. Kepsutlu, and S. Kizilel. 2013. "Characterization of protein release from poly(ethylene glycol) hydrogels with crosslink density gradients." *J Biomed Mater Res A.* DOI: 10.1002/jbm.a.34701.

14. Bearzi, C., C. Gargioli, D. Baci, et al. 2014. "PlGF-MMP9-engineered iPS cells supported on a PEG-fibrinogen hydrogel scaffold possess an enhanced capacity to repair damaged myocardium." *Cell Death Dis.* 5:e1053. DOI: 10.1038/cddis.2014.12.

15. Beck, Jennifer N., Anirudha Singh, Ashley R. Rothenberg, et al. 2013. "The independent roles of mechanical, structural and adhesion characteristics of 3D hydrogels on the regulation of cancer invasion and dissemination." *Biomaterials* 34 (37):9486-9495. DOI: http://dx.doi.org/10.1016/j.biomaterials.2013.08.077.

16. Benton, G., I. Arnaoutova, J. George, et al. 2014. "Matrigel: from discovery and ECM mimicry to assays and models for cancer research." *Advanced Drug Delivery Reviews* 79-80:3-18. DOI: 10.1016/j.addr.2014.06.005.

17. Bersini, S., J. S. Jeon, G. Dubini, et al. 2014. "A microfluidic 3D in vitro model for specificity of breast cancer metastasis to bone." *Biomaterials* 35 (8):2454-2461. DOI: 10.1016/j.biomaterials.2013.11.050.

18. Bing, Yu, Cong Hailin, Liu Xuesong, et al. 2013. "Preparation of monodisperse PEG hydrogel composite microspheres via microfluidic chip with rounded channels." *Journal of Micromechanics and Microengineering* 23 (9):095016.

19. Bischel, L. L., D. J. Beebe, and K. E. Sung. 2015. "Microfluidic model of ductal carcinoma in situ with 3D, organotypic structure." *BMC Cancer* 15:12. DOI: 10.1186/s12885-015-1007-5.

20. Bischel, L. L., E. W. Young, B. R. Mader, et al. 2013. "Tubeless microfluidic angiogenesis assay with three-dimensional endothelial-lined microvessels." *Biomaterials* 34 (5):1471-7. DOI: 10.1016/j.biomaterials.2012.11.005.

21. Bissell, M. J., D. C. Radisky, A. Rizki, et al. 2002. "The organizing principle: microenvironmental influences in the normal and malignant breast." *Differentiation* 70 (9-10):537-46. DOI: 10.1046/j.1432-0436.2002.700907.x.

22. Bordeleau, F., L. N. Tang, and C. A. Reinhart-King. 2013. "Topographical guidance of 3D tumor cell migration at an interface of collagen densities." *Physical Biology* 10 (6):065004. DOI: 10.1088/1478-3975/10/6/065004.

23. Bourhis, Xuefen, Rodrigue Romon, and Hubert Hondermarck. 2010. "Role of endothelial progenitor cells in breast cancer angiogenesis: from fundamental research to clinical ramifications." *Breast Cancer Research and Treatment* 120 (1):17-24. DOI: 10.1007/s10549-009-0686-5.

24. Boussommier-Calleja, A., R. Li, M. B. Chen, et al. 2016. "Microfluidics: A new tool for modeling cancer-immune interactions." *Trends Cancer* 2 (1):6-19. DOI: 10.1016/j.trecan.2015.12.003.

25. Braet, F., R. De Zanger, and E. Wisse. 1997. "Drying cells for SEM, AFM and TEM by hexamethyldisilazane: a study on hepatic endothelial cells." *J Microsc* 186 (Pt 1):84-7.

26. Brandt, Burkhard, Christoph Heyder, Eva Gloria-Maercker, et al. 2005. "3D-extravasation model – selection of highly motile and metastatic cancer cells." *Seminars in Cancer Biology* 15 (5):387-395. DOI: http://dx.doi.org/10.1016/j.semcancer.2005.06.006.

27. Bray, L. J., M. Binner, A. Holzheu, et al. 2015. "Multi-parametric hydrogels support 3D in vitro bioengineered microenvironment models of tumour angiogenesis." *Biomaterials* 53:609-20. DOI: 10.1016/j.biomaterials.2015.02.124.

28. Bruce, A., R. Evans, R. Mezan, et al. 2015. "Three-Dimensional Microfluidic Tri-Culture Model of the Bone Marrow Microenvironment for Study of Acute Lymphoblastic Leukemia." *PLoS One* 10 (10):e0140506. DOI: 10.1371/journal.pone.0140506.

29. Bulysheva, A. A., G. L. Bowlin, S. P. Petrova, et al. 2013. "Enhanced chemoresistance of squamous carcinoma cells grown in 3D cryogenic electrospun scaffolds." *Biomedical Materials* 8 (5):055009. DOI: 10.1088/1748-6041/8/5/055009.

30. Burdett, E., F. K. Kasper, A. G. Mikos, et al. 2010. "Engineering Tumors: A Tissue Engineering Perspective in Cancer Biology." *Tissue Engineering Part B-Reviews* 16 (3):351-359. DOI: 10.1089/ten.teb.2009.0676.

31. Butcher, D. T., T. Alliston, and V. M. Weaver. 2009. "A tense situation: forcing tumour progression." *Nat Rev Cancer* 9 (2):108-22. DOI: 10.1038/nrc2544.

32. Carlsson, J., and H. Acker. 1988. "Relations between Ph, Oxygen Partial-Pressure and Growth in Cultured-Cell Spheroids." *International Journal of Cancer* 42 (5):715-720. DOI: DOI 10.1002/ijc.2910420515.

33. Carlsson, J., and Thore Nederman. 1989. "Tumor spheroid technology in cancer therapy & research." *European Journal of Cancer Clinical Oncology* 25 (8):1127-1133.

34. Carvalho, M. R., D. Lima, R. L. Reis, et al. 2015. "Evaluating Biomaterial- and Microfluidic-Based 3D Tumor Models." *Trends Biotechnol* 33 (11):667-78. DOI: 10.1016/j.tibtech.2015.09.009.

35. Cassereau, L., Y. A. Miroshnikova, G. Ou, et al. 2015. "A 3D tension bioreactor platform to study the interplay between ECM stiffness and tumor phenotype." *Journal of Biotechnology* 193:66-69. DOI: 10.1016/j.jbiotec.2014.11.008.

36. Chaudhuri, O., S. T. Koshy, C. Branco da Cunha, et al. 2014. "Extracellular matrix stiffness and composition jointly regulate the induction of malignant phenotypes in mammary epithelium." *Nature Materials* 13 (10):970-978. DOI: 10.1038/nmat4009.

37. Chen, L., Z. Xiao, Y. Meng, et al. 2012. "The enhancement of cancer stem cell properties of MCF-7 cells in 3D collagen scaffolds for modeling of cancer and anti-cancer drugs." *Biomaterials* 33 (5):1437-44. DOI: 10.1016/j.biomaterials.2011.10.056.

38. Chen, Michael C. W., Madhuja Gupta, and Karen C. Cheung. 2010. "Alginate-based microfluidic system for tumor spheroid formation and anticancer agent screening." *Biomedical microdevices* 12 (4):647-54. DOI: 10.1007/s10544-010-9417-2.

39. Chen, Q. K., K. Lee, D. C. Radisky, et al. 2013. "Extracellular matrix proteins regulate epithelial-mesenchymal transition in mammary epithelial cells." *Differentiation* 86 (3):126-32. DOI: 10.1016/j.diff.2013.03.003.

40. Chung, B. G., K. H. Lee, A. Khademhosseini, et al. 2012. "Microfluidic fabrication of microengineered hydrogels and their application in tissue engineering." *Lab Chip* 12 (1):45-59. DOI: 10.1039/c1lc20859d.

41. Chwalek, K., L. J. Bray, and C. Werner. 2014. "Tissue-engineered 3D tumor angiogenesis models: Potential technologies for anti-cancer drug discovery." *Advanced Drug Delivery Reviews* 79-80:30-39. DOI: 10.1016/j.addr.2014.05.006.

42. Costantini, V., L. R. Zacharski, V. A. Memoli, et al. 1991. "Fibrinogen Deposition without Thrombin Generation in Primary Human Breast-Cancer Tissue." *Cancer Research* 51 (1):349-353.

43. Cruise, G. M., D. S. Scharp, and J. A. Hubbell. 1998. "Characterization of permeability and network structure of interfacially photopolymerized poly(ethylene glycol) diacrylate hydrogels." *Biomaterials* 19 (14):1287-94.

44. Cuchiara, M. P., A. C. Allen, T. M. Chen, et al. 2010. "Multilayer microfluidic PEGDA hydrogels." *Biomaterials* 31 (21):5491-7. DOI: 10.1016/j.biomaterials.2010.03.031.

45. Culver, J. C., J. C. Hoffmann, R. A. Poche, et al. 2012. "Three-dimensional biomimetic patterning in hydrogels to guide cellular organization." *Adv Mater* 24 (17):2344-8. DOI: 10.1002/adma.201200395.

46. Dang, T. T., A. M. Prechtl, and G. W. Pearson. 2011. "Breast cancer subtype-specific interactions with the microenvironment dictate mechanisms of invasion." *Cancer Res* 71 (21):6857-66. DOI: 10.1158/0008-5472.CAN-11-1818.

47. Das, V., F. Bruzzese, P. Konecny, et al. 2015. "Pathophysiologically relevant in vitro tumor models for drug screening." *Drug Discov Today* 20 (7):848-55. DOI: 10.1016/j.drudis.2015.04.004.

48. David, L., V. Dulong, D. Le Cerf, et al. 2004. "Reticulated hyaluronan hydrogels: a model for examining cancer cell invasion in 3D." *Matrix Biology* 23 (3):183-193. DOI: 10.1016/j.matbio.2004.05.005.

49. Deforest, Cole a, Evan a Sims, and Kristi S. Anseth. 2010. "Peptide-Functionalized Click Hydrogels with Independently Tunable Mechanics and Chemical Functionality for 3D Cell Culture." *Chemistry of materials : a publication of the American Chemical Society* 22 (16):4783-4790. DOI: 10.1021/cm101391y.

50. DelNero, P., M. Lane, S. S. Verbridge, et al. 2015. "3D culture broadly regulates tumor cell hypoxia response and angiogenesis via pro-inflammatory pathways." *Biomaterials* 55:110-118. DOI: 10.1016/j.biomaterials.2015.03.035.

51. DeLong, S. A., J. J. Moon, and J. L. West. 2005. "Covalently immobilized gradients of bFGF on hydrogel scaffolds for directed cell migration." *Biomaterials* 26 (16):3227-34. DOI: 10.1016/j.biomaterials.2004.09.021.

52. Derda, R., A. Laromaine, A. Mammoto, et al. 2009. "Paper-supported 3D cell culture for tissue-based bioassays." *Proceedings of the National Academy of Sciences of the United States of America* 106 (44):18457-18462. DOI: 10.1073/pnas.0910666106.

53. Dhiman, H. K., A. R. Ray, and A. K. Panda. 2005. "Three-dimensional chitosan scaffold-based MCF-7 cell culture for the determination of the cytotoxicity of tamoxifen." *Biomaterials* 26 (9):979-86. DOI: 10.1016/j.biomaterials.2004.04.012.

54. Dhiman, Harpreet K., Alok R. Ray, and Amulya K. Panda. 2004. "Characterization and evaluation of chitosan matrix for in vitro growth of MCF-7 breast cancer cell lines." *Biomaterials* 25 (21):5147-5154. DOI: 10.1016/j.biomaterials.2003.12.025.

55. Dickinson, Laura E., Cornelis Lutgebaucks, Daniel M. Lewis, et al. 2012. "Patterning microscale extracellular matrices to study endothelial and cancer cell interactions in vitro." *Lab on a Chip* 12 (21):4244-4248. DOI: 10.1039/C2LC40819H.

56. Dikovsky, D., H. Bianco-Peled, and D. Seliktar. 2006. "The effect of structural alterations of PEG-fibrinogen hydrogel scaffolds on 3-D cellular morphology and cellular migration." *Biomaterials* 27 (8):1496-506. DOI: 10.1016/j.biomaterials.2005.09.038.

57. do Amaral, J. B., P. Rezende-Teixeira, V. M. Freitas, et al. 2011. "MCF-7 cells as a three-dimensional model for the study of human breast cancer." *Tissue Eng Part C Methods* 17 (11):1097-107. DOI: 10.1089/ten.tec.2011.0260.

58. do Amaral, Jônatas Bussador, Marcel Shiniti Urabayashi, and Gláucia Maria Machado-Santelli. 2010. "Cell death and lumen formation in spheroids of MCF-7 cells." *Cell biology international* 34 (3):267-74. DOI: 10.1042/CBI20090024.

59. Draget, K. I., G. Skjak-Braek, and O. Smidsrod. 1997. "Alginate based new materials." *International Journal of Biological Macromolecules* 21 (1-2):47-55.

60. Edmondson, R., J. J. Broglie, A. F. Adcock, et al. 2014. "Three-dimensional cell culture systems and their applications in drug discovery and cell-based biosensors." *Assay Drug Dev Technol* 12 (4):207-18. DOI: 10.1089/adt.2014.573.

61. Ehrbar, Martin, Andrew Metters, Prisca Zammaretti, et al. 2005. "Endothelial cell proliferation and progenitor maturation by fibrin-bound VEGF variants with differential susceptibilities to local cellular activity." *Journal of Controlled Release* 101 (1–3):93-109. DOI: http://dx.doi.org/10.1016/j.jconrel.2004.07.018.

62. Elbert, D. L. 2011. "Liquid-liquid two-phase systems for the production of porous hydrogels and hydrogel microspheres for biomedical applications: A tutorial review." *Acta Biomater* 7 (1):31-56. DOI: 10.1016/j.actbio.2010.07.028.

63. Elliott, N. T., and F. Yuan. 2011. "A review of three-dimensional in vitro tissue models for drug discovery and transport studies." *J Pharm Sci* 100 (1):59-74. DOI: 10.1002/jps.22257.

64. Elliott, N. T., and F. Yuan. 2012. "A microfluidic system for investigation of extravascular transport and cellular uptake of drugs in tumors." *Biotechnol Bioeng* 109 (5):1326-35. DOI: 10.1002/bit.24397.

65. Engberg, K., and C. W. Frank. 2011. "Protein diffusion in photopolymerized poly(ethylene glycol) hydrogel networks." *Biomed Mater* 6 (5):055006. DOI: 10.1088/1748-6041/6/5/055006.

66. Estrada, M. F., S. P. Rebelo, E. J. Davies, et al. 2016. "Modelling the tumour microenvironment in long-term microencapsulated 3D co-cultures recapitulates phenotypic features of disease progression." *Biomaterials* 78:50-61. DOI: 10.1016/j.biomaterials.2015.11.030.

67. Fang, J. Y., S. J. Tan, Z. Yang, et al. 2014. "Tumor bioengineering using a transglutaminase crosslinked hydrogel." *PLoS One* 9 (8):e105616. DOI: 10.1371/journal.pone.0105616.

68. Faratian, D., A. Munro, C. Twelves, et al. 2009. "Membranous and cytoplasmic staining of Ki67 is associated with HER2 and ER status in invasive breast carcinoma." *Histopathology* 54 (2):254-7. DOI: 10.1111/j.1365-2559.2008.03191.x.

69. Farhat, F. S., A. Tfayli, N. Fakhruddin, et al. 2012. "Expression, prognostic and predictive impact of VEGF and bFGF in non-small cell lung cancer." *Crit Rev Oncol Hematol* 84 (2):149-60. DOI: 10.1016/j.critrevonc.2012.02.012.

70. Felton, E. J., C. R. Copeland, C. S. Chen, et al. 2012. "Heterotypic cell pair co-culturing on patterned microarrays." *Lab Chip* 12 (17):3117-26. DOI: 10.1039/c2lc40349h.

71. Feng, S., X. Duan, P. K. Lo, et al. 2013. "Expansion of breast cancer stem cells with fibrous scaffolds." *Integr Biol (Camb)* 5 (5):768-77. DOI: 10.1039/c3ib20255k.

72. Fenner, J., A. C. Stacer, F. Winterroth, et al. 2014. "Macroscopic stiffness of breast tumors predicts metastasis." *Sci Rep* 4:5512. DOI: 10.1038/srep05512.

73. Firpo, G., E. Angeli, L. Repetto, et al. 2015. "Permeability thickness dependence of polydimethylsiloxane (PDMS) membranes." *Journal of Membrane Science* 481:1-8. DOI: http://dx.doi.org/10.1016/j.memsci.2014.12.043.

74. Fischbach, C., R. Chen, T. Matsumoto, et al. 2007. "Engineering tumors with 3D scaffolds." *Nature methods* 4 (10):855-860.

75. Fischbach, C., H. J. Kong, S. X. Hsiong, et al. 2009. "Cancer cell angiogenic capability is regulated by 3D culture and integrin engagement." *Proc Natl Acad Sci U S A* 106 (2):399-404. DOI: 10.1073/pnas.0808932106.

76. Fischer, Robert S., Kenneth A. Myers, Margaret L. Gardel, et al. 2012. "Stiffness-controlled three-dimensional extracellular matrices for high-resolution imaging of cell behavior." *Nature protocols* 7 (11):10.1038/nprot.2012.127. DOI: 10.1038/nprot.2012.127.

77. Florczyk, S. J., G. Liu, F. M. Kievit, et al. 2012. "3D porous chitosan-alginate scaffolds: a new matrix for studying prostate cancer cell-lymphocyte interactions in vitro." *Advanced Healthcare Materials* 1 (5):590-599. DOI: 10.1002/adhm.201100054.

78. Fong, E. L., S. E. Lamhamedi-Cherradi, E. Burdett, et al. 2013. "Modeling Ewing sarcoma tumors in vitro with 3D scaffolds." *Proceedings of the National Academy of Sciences of the United States of America* 110 (16):6500-6505. DOI: 10.1073/pnas.1221403110.

79. Franco, C. L., J. Price, and J. L. West. 2011. "Development and optimization of a dual-photoinitiator, emulsion-based technique for rapid generation of cell-laden hydrogel microspheres." *Acta Biomater* 7 (9):3267-76. DOI: 10.1016/j.actbio.2011.06.011.

80. Frisman, I., D. Seliktar, and H. Bianco-Peled. 2011. "Nanostructuring PEG-fibrinogen hydrogels to control cellular morphogenesis." *Biomaterials* 32 (31):7839-7846. DOI: 10.1016/j.biomaterials.2011.06.078.

81. Frisman, I., D. Seliktar, and H. Bianco-Peled. 2012. "Nanostructuring biosynthetic hydrogels for tissue engineering: a cellular and structural analysis." *Acta Biomater* 8 (1):51-60. DOI: 10.1016/j.actbio.2011.07.030.

82. Fu, Y., and W. J. Kao. 2009. "Drug release kinetics and transport mechanisms from semi-interpenetrating networks of gelatin and poly(ethylene glycol) diacrylate." *Pharm Res* 26 (9):2115-24. DOI: 10.1007/s11095-009-9923-1.

83. Fukuda, Junji, Ali Khademhosseini, Yoon Yeo, et al. 2006. "Micromolding of photocrosslinkable chitosan hydrogel for spheroid microarray and co-cultures." *Biomaterials* 27 (30):5259-67. DOI: 10.1016/j.biomaterials.2006.05.044.

84. Geum, T. Dongil, Jun Beum Kim, E. Audrey Chang, et al. 2016. "Epidermal growth factor promotes a mesenchymal over an amoeboid motility of MDA-MB-231 cells embedded within a 3D collagen matrix." *The European Physical Journal Plus* 131 (1):1-10. DOI: 10.1140/epjp/i2016-16008-8.

85. Ghajar, C. M., and M. J. Bissell. 2010. "Tumor engineering: the other face of tissue engineering." *Tissue Engineering Part A* 16 (7):2153-6. DOI: 10.1089/ten.TEA.2010.0135.

86. Gill, B. J., D. L. Gibbons, L. C. Roudsari, et al. 2012. "A synthetic matrix with independently tunable biochemistry and mechanical properties to study epithelial morphogenesis and EMT in a lung adenocarcinoma model." *Cancer Res* 72 (22):6013-6023. DOI: 10.1158/0008-5472.CAN-12-0895.

87. Gill, B. J., and J. L. West. 2014. "Modeling the tumor extracellular matrix: Tissue engineering tools repurposed towards new frontiers in cancer biology." *Journal of Biomechanics* 47 (9):1969-1978. DOI: 10.1016/j.jbiomech.2013.09.029.

88. Godde, N. J., R. C. Galea, I. A. Elsum, et al. 2010. "Cell Polarity in Motion: Redefining Mammary Tissue Organization Through EMT and Cell Polarity Transitions." *Journal of Mammary Gland Biology and Neoplasia* 15 (2):149-168. DOI: 10.1007/s10911-010-9180-2.

89. Godugu, C., A. R. Patel, U. Desai, et al. 2013. "AlgiMatrix (TM) Based 3D Cell Culture System as an In-Vitro Tumor Model for Anticancer Studies." *Plos One* 8 (1):e53708. DOI: ARTN e5370810.1371/journal.pone.0053708.

90. Gomez-Sjoberg, R., A. A. Leyrat, D. M. Pirone, et al. 2007. "Versatile, fully automated, microfluidic cell culture system." *Anal Chem* 79 (22):8557-63. DOI: 10.1021/ac071311w.

91. Gong, Xue, Chao Lin, Jian Cheng, et al. 2015. "Generation of Multicellular Tumor Spheroids with Microwell-Based Agarose Scaffolds for Drug Testing." *PLoS ONE* 10 (6):e0130348. DOI: 10.1371/journal.pone.0130348.

92. Grzanka, A., R. Sujkowska, A. Janiak, et al. 2000. "Immunogold labelling of PCNA and Ki-67 antigen at the ultrastructural level in laryngeal squamous cell carcinoma and its correlation with lymph node metastasis and histological grade." *Acta Histochemica* 102 (2):139-149. DOI: Doi 10.1078/S0065-1281(04)70023-9.

93. Gu, L., and D. J. Mooney. 2015. "Biomaterials and emerging anticancer therapeutics: engineering the microenvironment." *Nat Rev Cancer* 16 (1):56-66. DOI: 10.1038/nrc.2015.3.

94. Gurski, L. A., X. Xu, L. N. Labrada, et al. 2012. "Hyaluronan (HA) interacting proteins RHAMM and hyaluronidase impact prostate cancer cell behavior and invadopodia formation in 3D HA-based hydrogels." *PLoS One* 7 (11):e50075. DOI: 10.1371/journal.pone.0050075.

95. Guzman, A., M. J. Ziperstein, and L. J. Kaufman. 2014. "The effect of fibrillar matrix architecture on tumor cell invasion of physically challenging environments." *Biomaterials* 35 (25):6954-6963. DOI: 10.1016/j.biomaterials.2014.04.086.

96. Hahn, M. S, J. S Miller, and J. L West. 2005. "Laser Scanning Lithography for Surface Micropatterning on Hydrogels." *Advanced Materials* 17 (24):2939-2942. DOI: 10.1002/adma.200500184.

97. Hakanson, M., S. Kobel, M. P. Lutolf, et al. 2012. "Controlled breast cancer microarrays for the deconvolution of cellular multilayering and density effects upon drug responses." *PLoS One* 7 (6):e40141. DOI: 10.1371/journal.pone.0040141.

98. Hall, C. E., and H. S. Slayter. 1959. "The fibrinogen molecule: its size, shape, and mode of polymerization." *J Biophys Biochem Cytol* 5 (1):11-6.

99. Hanahan, D., and L. M. Coussens. 2012. "Accessories to the crime: functions of cells recruited to the tumor microenvironment." *Cancer Cell* 21 (3):309-22. DOI: 10.1016/j.ccr.2012.02.022.

100. Hanahan, Douglas, and Robert A. Weinberg. 2000. "The Hallmarks of Cancer." *Cell* 100 (1):57-70. DOI: http://dx.doi.org/10.1016/S0092-8674(00)81683-9.

101. Hanahan, Douglas, and Robert A Weinberg. 2011. "Hallmarks of Cancer: The Next Generation." *Cell* 144 (5):646-674. DOI: http://dx.doi.org/10.1016/j.cell.2011.02.013.

102. Hazan, R. B., G. R. Phillips, R. F. Qiao, et al. 2000. "Exogenous expression of N-cadherin in breast cancer cells induces cell migration, invasion, and metastasis." *J Cell Biol* 148 (4):779-90.

103. Helczynska, K., A. Kronblad, A. Jogi, et al. 2003. "Hypoxia promotes a dedifferentiated phenotype in ductal breast carcinoma in situ." *Cancer Research* 63 (7):1441-1444.

104. Hickman, J. A., R. Graeser, R. de Hoogt, et al. 2014. "Three-dimensional models of cancer for pharmacology and cancer cell biology: capturing tumor complexity in vitro/ex vivo." *Biotechnol J* 9 (9):1115-28. DOI: 10.1002/biot.201300492.

105. Hielscher, A. C., C. Qiu, and S. Gerecht. 2012. "Breast cancer cell-derived matrix supports vascular morphogenesis." *Am J Physiol Cell Physiol* 302 (8):C1243-56. DOI: 10.1152/ajpcell.00011.2012.

106. Hirschhaeuser, F., H. Menne, C. Dittfeld, et al. 2010a. "Multicellular tumor spheroids: an underestimated tool is catching up again." *J Biotechnol* 148 (1):3-15. DOI: 10.1016/j.jbiotec.2010.01.012.

107. Hirschhaeuser, Franziska, Heike Menne, Claudia Dittfeld, et al. 2010b. "Multicellular tumor spheroids: An underestimated tool is catching up again." *Journal of Biotechnology* 148 (1):3-15. DOI: http://dx.doi.org/10.1016/j.jbiotec.2010.01.012.

108. Ho, Wan Yong, Swee Keong Yeap, Chai Ling Ho, et al. 2012. "Development of Multicellular Tumor Spheroid (MCTS) Culture from Breast Cancer Cell and a High Throughput Screening Method Using the MTT Assay." *PLoS ONE* 7 (9):e44640. DOI: 10.1371/journal.pone.0044640.

109. Ho, Won Jin, Edward a Pham, Jun W. Kim, et al. 2010. "Incorporation of multicellular spheroids into 3-D polymeric scaffolds provides an improved tumor model for screening anticancer drugs." *Cancer science* 101 (12):2637-43. DOI: 10.1111/j.1349-7006.2010.01723.x.

110. Hoffman, A. S. 2012. "Hydrogels for biomedical applications." *Advanced Drug Delivery Reviews* 64:18-23. DOI: 10.1016/j.addr.2012.09.010.

111. Horch, R. E., A. M. Boos, Y. Quan, et al. 2013. "Cancer research by means of tissue engineering--is there a rationale?" *J Cell Mol Med* 17 (10):1197-206. DOI: 10.1111/jcmm.12130.

112. Hsu, T. H., Y. L. Kao, W. L. Lin, et al. 2012. "The migration speed of cancer cells influenced by macrophages and myofibroblasts co-cultured in a microfluidic chip." *Integr Biol (Camb)* 4 (2):177-82. DOI: 10.1039/c2ib00112h.

113. Huang, Y. J., and S. H. Hsu. 2014. "Acquisition of epithelial-mesenchymal transition and cancer stem-like phenotypes within chitosan-hyaluronan membrane-derived 3D tumor

spheroids." *Biomaterials* 35 (38):10070-10079. DOI: 10.1016/j.biomaterials.2014.09.010.

114. Huebner, R. J., and A. J. Ewald. 2014. "Cellular foundations of mammary tubulogenesis." *Semin Cell Dev Biol* 31:124-31. DOI: 10.1016/j.semcdb.2014.04.019.

115. Hutmacher, D. W., D. Loessner, S. Rizzi, et al. 2010. "Can tissue engineering concepts advance tumor biology research?" *Trends Biotechnol* 28 (3):125-33. DOI: 10.1016/j.tibtech.2009.12.001.

116. Hutmacher, Dietmar W. 2010. "Biomaterials offer cancer research the third dimension." *Nature Materials* 9 (2):90-93.

117. Hutmacher, Dietmar W., Raymund E. Horch, Daniela Loessner, et al. 2009. "Translating tissue engineering technology platforms into cancer research." *Journal of Cellular and Molecular Medicine* 13 (8a):1417-1427. DOI: 10.1111/j.1582-4934.2009.00853.x.

118. Imamura, Y., T. Mukohara, Y. Shimono, et al. 2015. "Comparison of 2D- and 3D-culture models as drug-testing platforms in breast cancer." *Oncol Rep* 33 (4):1837-43. DOI: 10.3892/or.2015.3767.

119. Infanger, D. W., M. E. Lynch, and C. Fischbach. 2013. "Engineered culture models for studies of tumor-microenvironment interactions." *Annu Rev Biomed Eng* 15:29-53. DOI: 10.1146/annurev-bioeng-071811-150028.

120. Ivascu, A., and M. Kubbies. 2007. "Diversity of cell-mediated adhesions in breast cancer spheroids." *Int J Oncol* 31 (6):1403-13.

121. Jabbari, E., S. K. Sarvestani, L. Daneshian, et al. 2015. "Optimum 3D Matrix Stiffness for Maintenance of Cancer Stem Cells Is Dependent on Tissue Origin of Cancer Cells." *PLoS One* 10 (7):e0132377. DOI: 10.1371/journal.pone.0132377.

122. Jeon, J. S., S. Bersini, M. Gilardi, et al. 2015. "Human 3D vascularized organotypic microfluidic assays to study breast cancer cell extravasation." *Proc Natl Acad Sci U S A* 112 (1):214-9. DOI: 10.1073/pnas.1417115112.

123. Jessup, J. M., and Marylin Frantz. 2000. "Microgravity culture reduces apoptosis and increases the differentiation of a human colorectal carcinoma cell line." *In Vitro Cellular & Developmental Biology - Animal* 36 (June):367-373.

124. Jimenez Valencia, A. M., P. H. Wu, O. N. Yogurtcu, et al. 2015. "Collective cancer cell invasion induced by coordinated contractile stresses." *Oncotarget* 6 (41):43438-51. DOI: 10.18632/oncotarget.5874.

125. Kalluri, R., and M. Zeisberg. 2006. "Fibroblasts in cancer." *Nat Rev Cancer* 6 (5):392-401. DOI: 10.1038/nrc1877.

126. Kang, S. W., and Y. H. Bae. 2009. "Cryopreservable and tumorigenic three-dimensional tumor culture in porous poly(lactic-co-glycolic acid) microsphere." *Biomaterials* 30 (25):4227-4232. DOI: 10.1016/j.biomaterials.2009.04.025.

127. Keller, D., C. Guilfoyle, and J. Sariego. 2011. "Geographical influence on racial disparity in breast cancer presentation in the United States." *Am Surg* 77 (7):933-6.

128. Kelm, J. M., N. E. Timmins, C. J. Brown, et al. 2003a. "Method for generation of homogeneous multicellular tumor spheroids applicable to a wide variety of cell types." *Biotechnol Bioeng* 83 (2):173-80. DOI: 10.1002/bit.10655.

129. Kelm, Jens M., Nicholas E. Timmins, Catherine J. Brown, et al. 2003b. "Method for generation of homogeneous multicellular tumor spheroids applicable to a wide variety of cell types." *Biotechnology and bioengineering* 83 (2):173-80. DOI: 10.1002/bit.10655.

130. Kenny, Hilary A., Madhu Lal-Nag, Erin A. White, et al. 2015. "Quantitative high throughput screening using a primary human three-dimensional organotypic culture predicts in vivo efficacy." *Nat Commun* 6. DOI: 10.1038/ncomms7220.

131. Kenny, P. A., G. Y. Lee, C. A. Myers, et al. 2007. "The morphologies of breast cancer cell lines in three-dimensional assays correlate with their profiles of gene expression." *Mol Oncol* 1 (1):84-96. DOI: 10.1016/j.molonc.2007.02.004.

132. Kerscher, P., I. C. Turnbull, A. J. Hodge, et al. 2016. "Direct hydrogel encapsulation of pluripotent stem cells enables ontomimetic differentiation and growth of engineered human heart tissues." *Biomaterials* 83:383-95. DOI: 10.1016/j.biomaterials.2015.12.011.

133. Kesselman, D., O. Kossover, I. Mironi-Harpaz, et al. 2013. "Time-dependent cellular morphogenesis and matrix stiffening in proteolytically responsive hydrogels." *Acta Biomater* 9 (8):7630-9. DOI: 10.1016/j.actbio.2013.04.030.

134. Kievit, F. M., S. J. Florczyk, M. C. Leung, et al. 2010. "Chitosan-alginate 3D scaffolds as a mimic of the glioma tumor microenvironment." *Biomaterials* 31 (22):5903-10. DOI: 10.1016/j.biomaterials.2010.03.062.

135. Kievit, F. M., S. J. Florczyk, M. C. Leung, et al. 2014. "Proliferation and enrichment of CD133(+) glioblastoma cancer stem cells on 3D chitosan-alginate scaffolds." *Biomaterials* 35 (33):9137-9143. DOI: 10.1016/j.biomaterials.2014.07.037.

136. Kim, J., and K. Tanner. 2015. "Recapitulating the Tumor Ecosystem Along the Metastatic Cascade Using 3D Culture Models." *Front Oncol* 5:170. DOI: 10.3389/fonc.2015.00170.

137. Kim, Jong Bin, Robert Stein, and Mike J. O'Hare. 2004. "Three-dimensional in vitro tissue culture models of breast cancer - a review." *Breast Cancer Research and Treatment* 85 (3):281-91. DOI: 10.1023/B:BREA.0000025418.88785.2b.

138. Kimlin, Lauren C., Giovanna Casagrande, and Victoria M. Virador. 2011. "In vitro three-dimensional (3D) models in cancer research: An update." *Molecular carcinogenesis* (August). DOI: 10.1002/mc.21844.

139. King, W. J., M. W. Toepke, and W. L. Murphy. 2011. "Facile formation of dynamic hydrogel microspheres for triggered growth factor delivery." *Acta Biomater* 7 (3):975-85. DOI: 10.1016/j.actbio.2010.10.026.

140. Kingsley, D. M., A. D. Dias, D. B. Chrisey, et al. 2013. "Single-step laser-based fabrication and patterning of cell-encapsulated alginate microbeads." *Biofabrication* 5 (4):045006. DOI: 10.1088/1758-5082/5/4/045006.

141. Kleinman, Hynda K., and George R. Martin. 2005. "Matrigel: basement membrane matrix with biological activity." *Seminars in Cancer Biology* 15 (5):378-386. DOI: 10.1016/j.semcancer.2005.05.004.

142. Kloxin, A. M., A. M. Kasko, C. N. Salinas, et al. 2009a. "Photodegradable hydrogels for dynamic tuning of physical and chemical properties." *Science* 324 (5923):59-63. DOI: 10.1126/science.1169494.

143. Kloxin, A. M., M. W. Tibbitt, and K. S. Anseth. 2010. "Synthesis of photodegradable hydrogels as dynamically tunable cell culture platforms." *Nature Protocols* 5 (12):1867-1887. DOI: 10.1038/nprot.2010.139.

144. Kloxin, April M., Andrea M. Kasko, Chelsea N. Salinas, et al. 2009b. "Photodegradable hydrogels for dynamic tuning of physical and chemical properties." *Science (New York, N.Y.)* 324 (5923):59-63. DOI: 10.1126/science.1169494.

145. Knop, K., R. Hoogenboom, D. Fischer, et al. 2010. "Poly(ethylene glycol) in drug delivery: pros and cons as well as potential alternatives." *Angew Chem Int Ed Engl* 49 (36):6288-308. DOI: 10.1002/anie.200902672.

146. Kolodziejczyk, J., and M. B. Ponczek. 2013. "The role of fibrinogen, fibrin and fibrin(ogen) degradation products (FDPs) in tumor progression." *Contemp Oncol (Pozn)* 17 (2):113-9. DOI: 10.5114/wo.2013.34611.

147. Kong, Hyunjoon, Youyun Liang, Jaehyun Jeong, et al. 2011. "A cell-instructive hydrogel to regulate malignancy of 3D tumor spheroids with matrix rigidity." *Biomaterials* 32 (35):9308-9315. DOI: 10.1016/j.biomaterials.2011.08.045.

148. Koutsilieris, M., A. Sourla, G. Pelletier, et al. 1994. "Three-dimensional type I collagen gel system for the study of osteoblastic metastases produced by metastatic prostate

cancer." *Journal of Bone Mineral Research* 9 (11):1823-1832. DOI: 10.1002/jbmr.5650091120.

149. Kraehenbuehl, T. P., L. S. Ferreira, P. Zammaretti, et al. 2009. "Cell-responsive hydrogel for encapsulation of vascular cells." *Biomaterials* 30 (26):4318-24. DOI: 10.1016/j.biomaterials.2009.04.057.

150. Kramer, R. H., K. G. Bensch, and Johnson Wong. 1986. "Invasion of reconstituted basement membrane matrix by metastatic human tumor cells." *Cancer Research* 46:1980-1989.

151. Krause, S., M. V. Maffini, A. M. Soto, et al. 2010. "The microenvironment determines the breast cancer cells' phenotype: organization of MCF7 cells in 3D cultures." *BMC Cancer* 10:263. DOI: 10.1186/1471-2407-10-263.

152. Kundu, Banani, Paramita Saha, Kasturi Datta, et al. 2013. "A silk fibroin based hepatocarcinoma model and the assessment of the drug response in hyaluronan-binding protein 1 overexpressed HepG2 cells." *Biomaterials* 34 (37):9462-9474. DOI: http://dx.doi.org/10.1016/j.biomaterials.2013.08.047.

153. Kunz-Schughart, L. A., J. P. Freyer, F. Hofstaedter, et al. 2004. "The use of 3-D cultures for high-throughput screening: the multicellular spheroid model." *J Biomol Screen* 9 (4):273-85. DOI: 10.1177/1087057104265040.

154. Kwon, H., H. J. Kim, W. L. Rice, et al. 2010a. "Development of an in vitro model to study the impact of BMP-2 on metastasis to bone." *Journal of Tissue Engineering and Regenerative Medicine* 4 (8):590-599. DOI: 10.1002/term.268.

155. Kwon, H., H. J. Kim, W. L. Rice, et al. 2010b. "Development of an in vitro model to study the impact of BMP-2 on metastasis to bone." *J Tissue Eng Regen Med* 4 (8):590-9. DOI: 10.1002/term.268.

156. Ladekarl, M. 1995. "Quantitative Histopathology in Ductal Carcinoma of the Breast - Prognostic Value of Mean Nuclear Size and Mitotic Counts." *Cancer* 75 (8):2114-2122. DOI: Doi 10.1002/1097-0142(19950415)75:8<2114::Aid-Cncr2820750814>3.0.Co;2-W.

157. Langley, R. R., and I. J. Fidler. 2011. "The seed and soil hypothesis revisited--the role of tumor-stroma interactions in metastasis to different organs." *Int J Cancer* 128 (11):2527-35. DOI: 10.1002/ijc.26031.

158. Laurent, T. C., and J. R. Fraser. 1992. "Hyaluronan." *FASEB Journal* 6 (7):2397-2404.

159. Lawlor, E. R., C. Scheel, J. Irving, et al. 2002. "Anchorage-independent multi-cellular spheroids as an in vitro model of growth signaling in Ewing tumors." *Oncogene* 21 (2):307-18. DOI: 10.1038/sj.onc.1205053.

160. Le Bras, G. F., K. J. Taubenslag, and C. D. Andl. 2012. "The regulation of cell-cell adhesion during epithelial-mesenchymal transition, motility and tumor progression." *Cell Adh Migr* 6 (4):365-73. DOI: 10.4161/cam.21326.

161. Lee, B. H., S. P. Tin, S. Y. Chaw, et al. 2014. "Influence of soluble PEG-OH incorporation in a 3D cell-laden PEG-fibrinogen (PF) hydrogel on smooth muscle cell morphology and growth." *Journal of Biomaterial Science Polymer Edition* 25 (4):394-409. DOI: 10.1080/09205063.2013.862401.

162. Lee, H., W. Park, H. Ryu, et al. 2014. "A microfluidic platform for quantitative analysis of cancer angiogenesis and intravasation." *Biomicrofluidics* 8 (5):054102. DOI: 10.1063/1.4894595.

163. Lee, J. S., and J. Feijen. 2012. "Polymersomes for drug delivery: design, formation and characterization." *J Control Release* 161 (2):473-83. DOI: 10.1016/j.jconrel.2011.10.005.

164. Leight, J. L., E. Y. Tokuda, C. E. Jones, et al. 2015. "Multifunctional bioscaffolds for 3D culture of melanoma cells reveal increased MMP activity and migration with BRAF kinase inhibition." *Proc Natl Acad Sci U S A* 112 (17):5366-71. DOI: 10.1073/pnas.1505662112.

165. Leslie-Barbick, J. E., J. E. Saik, D. J. Gould, et al. 2011. "The promotion of microvasculature formation in poly(ethylene glycol) diacrylate hydrogels by an immobilized VEGF-mimetic peptide." *Biomaterials* 32 (25):5782-9. DOI: 10.1016/j.biomaterials.2011.04.060.

166. Leslie-Barbick, J. E., C. Shen, C. Chen, et al. 2011. "Micron-scale spatially patterned, covalently immobilized vascular endothelial growth factor on hydrogels accelerates endothelial tubulogenesis and increases cellular angiogenic responses." *Tissue Eng Part A* 17 (1-2):221-9. DOI: 10.1089/ten.TEA.2010.0202.

167. Levental, K. R., H. Yu, L. Kass, et al. 2009. "Matrix crosslinking forces tumor progression by enhancing integrin signaling." *Cell* 139 (5):891-906. DOI: 10.1016/j.cell.2009.10.027.

168. Li, L., and Y. Lu. 2011. "Optimizing a 3D Culture System to Study the Interaction between Epithelial Breast Cancer and Its Surrounding Fibroblasts." *J Cancer* 2:458-66.

169. Li, Q., C. Chen, A. Kapadia, et al. 2011. "3D models of epithelial-mesenchymal transition in breast cancer metastasis: high-throughput screening assay development, validation, and pilot screen." *Journal of Biomolecular Screening* 16 (2):141-54. DOI: 10.1177/1087057110392995.

170. Liang, Y., J. Jeong, R. J. DeVolder, et al. 2011. "A cell-instructive hydrogel to regulate malignancy of 3D tumor spheroids with matrix rigidity." *Biomaterials* 32 (35):9308-9315. DOI: 10.1016/j.biomaterials.2011.08.045.

171. Liao, D., Y. Luo, D. Markowitz, et al. 2009. "Cancer associated fibroblasts promote tumor growth and metastasis by modulating the tumor immune microenvironment in a 4T1 murine breast cancer model." *PLoS One* 4 (11):e7965. DOI: 10.1371/journal.pone.0007965.

172. Lin, R. Z., and H. Y. Chang. 2008. "Recent advances in three-dimensional multicellular spheroid culture for biomedical research." *Biotechnol J* 3 (9-10):1172-84. DOI: 10.1002/biot.200700228.

173. Liu, C., Y. Liu, H. G. Xie, et al. 2015. "Role of three-dimensional matrix stiffness in regulating the chemoresistance of hepatocellular carcinoma cells." *Biotechnol Appl Biochem* 62 (4):556-62. DOI: 10.1002/bab.1302.

174. Liu, C., Y. Liu, X. X. Xu, et al. 2015. "Potential effect of matrix stiffness on the enrichment of tumor initiating cells under three-dimensional culture conditions." *Exp Cell Res* 330 (1):123-34. DOI: 10.1016/j.yexcr.2014.07.036.

175. Liu, J., Y. Tan, H. Zhang, et al. 2012. "Soft fibrin gels promote selection and growth of tumorigenic cells." *Nat Mater* 11 (8):734-41. DOI: 10.1038/nmat3361.

176. Liu, T., M. Winter, and B. Thierry. 2014. "Quasi-spherical microwells on superhydrophobic substrates for long term culture of multicellular spheroids and high throughput assays." *Biomaterials* 35 (23):6060-8. DOI: 10.1016/j.biomaterials.2014.04.047.

177. Liu, W., and C. Chen. 2005. "Engineering biomaterials to control cell function." *Materials Today* 8 (12):28-35. DOI: citeulike-article-id:6372672

doi: 10.1016/s1369-7021(05)71222-0.

178. Loessner, D., K. S. Stok, M. P. Lutolf, et al. 2010. "Bioengineered 3D platform to explore cell-ECM interactions and drug resistance of epithelial ovarian cancer cells." *Biomaterials* 31 (32):8494-8506. DOI: 10.1016/j.biomaterials.2010.07.064.

179. Long, T. J., C. C. Sprenger, S. R. Plymate, et al. 2014. "Prostate cancer xenografts engineered from 3D precision-porous poly(2-hydroxyethyl methacrylate) hydrogels as models for tumorigenesis and dormancy escape." *Biomaterials* 35 (28):8164-8174. DOI: 10.1016/j.biomaterials.2014.04.090.

180. Lu, P., V. M. Weaver, and Z. Werb. 2012. "The extracellular matrix: a dynamic niche in cancer progression." *J Cell Biol* 196 (4):395-406. DOI: 10.1083/jcb.201102147.

181. Lutolf, M. P., G. P. Raeber, A. H. Zisch, et al. 2003. "Cell-Responsive Synthetic Hydrogels." *Advanced Materials* 15 (11):888-892. DOI: 10.1002/adma.200304621.

182. Mao, Y., E. T. Keller, D. H. Garfield, et al. 2013. "Stromal cells in tumor microenvironment and breast cancer." *Cancer Metastasis Rev* 32 (1-2):303-15. DOI: 10.1007/s10555-012-9415-3.

183. Markov, D. A., E. M. Lillie, S. P. Garbett, et al. 2014. "Variation in diffusion of gases through PDMS due to plasma surface treatment and storage conditions." *Biomed Microdevices* 16 (1):91-6. DOI: 10.1007/s10544-013-9808-2.

184. Markovitz-Bishitz, Y., Y. Tauber, E. Afrimzon, et al. 2010. "A polymer microstructure array for the formation, culturing, and high throughput drug screening of breast cancer spheroids." *Biomaterials* 31 (32):8436-44. DOI: 10.1016/j.biomaterials.2010.07.050.

185. Martin, T. A., and W. G. Jiang. 2009. "Loss of tight junction barrier function and its role in cancer metastasis." *Biochim Biophys Acta* 1788 (4):872-91. DOI: 10.1016/j.bbamem.2008.11.005.

186. Martinez-Ramos, C., and M. Lebourg. 2015. "Three-dimensional constructs using hyaluronan cell carrier as a tool for the study of cancer stem cells." *Journal of Biomedical Materials Research Part B Applied Biomaterials* 103 (6):1249-1257. DOI: 10.1002/jbm.b.33304.

187. Masci, V. L., A. R. Taddei, G. Gambellini, et al. 2016. "Ultrastructural investigation on fibroblast interaction with collagen scaffold." *J Biomed Mater Res A* 104 (1):272-82. DOI: 10.1002/jbm.a.35563.

188. Melero-Martin, J. M., and A. C. Dudley. 2011. "Concise review: Vascular stem cells and tumor angiogenesis." *Stem Cells* 29 (2):163-8. DOI: 10.1002/stem.583.

189. Miki, Y., K. Ono, S. Hata, et al. 2012. "The advantages of co-culture over mono cell culture in simulating in vivo environment." *J Steroid Biochem Mol Biol* 131 (3-5):68-75. DOI: 10.1016/j.jsbmb.2011.12.004.

190. Miller, J. S., K. R. Stevens, M. T. Yang, et al. 2012. "Rapid casting of patterned vascular networks for perfusable engineered three-dimensional tissues." *Nat Mater* 11 (9):768-74. DOI: 10.1038/nmat3357.

191. Moon, J. J., M. S. Hahn, I. Kim, et al. 2009. "Micropatterning of poly(ethylene glycol) diacrylate hydrogels with biomolecules to regulate and guide endothelial morphogenesis." *Tissue Eng Part A* 15 (3):579-85. DOI: 10.1089/ten.tea.2008.0196.

192. Moon, J. J., J. E. Saik, R. A. Poche, et al. 2010. "Biomimetic hydrogels with pro-angiogenic properties." *Biomaterials* 31 (14):3840-7. DOI: 10.1016/j.biomaterials.2010.01.104.

193. Mooney, R., S. Haeger, R. Lawal, et al. 2011. "Control of neural cell composition in poly(ethylene glycol) hydrogel culture with soluble factors." *Tissue Eng Part A* 17 (21-22):2805-15. DOI: 10.1089/ten.tea.2010.0654.

194. Morales, Jorge, and Mary L. Alpaugh. 2009. "Gain in cellular organization of inflammatory breast cancer: A 3D in vitro model that mimics the in vivo metastasis." *BMC cancer* 9:462-462. DOI: 10.1186/1471-2407-9-462.

195. Mosesson, M. W. 2005. "Fibrinogen and fibrin structure and functions." *J Thromb Haemost* 3 (8):1894-904. DOI: 10.1111/j.1538-7836.2005.01365.x.

196. Muraoka, M., T. Shimizu, K. Itoga, et al. 2013. "Control of the formation of vascular networks in 3D tissue engineered constructs." *Biomaterials* 34 (3):696-703. DOI: 10.1016/j.biomaterials.2012.10.009.

197. Nandakumar, V., L. Kelbauskas, K. F. Hernandez, et al. 2012. "Isotropic 3D nuclear morphometry of normal, fibrocystic and malignant breast epithelial cells reveals new structural alterations." *PLoS One* 7 (1):e29230. DOI: 10.1371/journal.pone.0029230.

198. Nandakumar, V., L. Kelbauskas, R. Johnson, et al. 2011. "Quantitative Characterization of Preneoplastic Progression Using Single-Cell Computed Tomography and Three-Dimensional Karyometry." *Cytometry Part A* 79A (1):25-34. DOI: 10.1002/cyto.a.20997.

199. Neve, R. M., K. Chin, J. Fridlyand, et al. 2006. "A collection of breast cancer cell lines for the study of functionally distinct cancer subtypes." *Cancer Cell* 10 (6):515-27. DOI: 10.1016/j.ccr.2006.10.008.

200. Nguyen, K. T., and J. L. West. 2002. "Photopolymerizable hydrogels for tissue engineering applications." *Biomaterials* 23 (22):4307-4314.

201. Nichols, M. D., E. A. Scott, and D. L. Elbert. 2009. "Factors affecting size and swelling of poly(ethylene glycol) microspheres formed in aqueous sodium sulfate solutions without surfactants." *Biomaterials* 30 (29):5283-91. DOI: 10.1016/j.biomaterials.2009.06.032.

202. Nikkhah, M., J. S. Strobl, E. M. Schmelz, et al. 2011. "MCF10A and MDA-MB-231 human breast basal epithelial cell co-culture in silicon micro-arrays." *Biomaterials* 32 (30):7625-32. DOI: 10.1016/j.biomaterials.2011.06.041.

203. Nyga, A., U. Cheema, and M. Loizidou. 2011. "3D tumour models: novel in vitro approaches to cancer studies." *Journal of Cell Communication and Signaling* 5 (3):239-248. DOI: 10.1007/s12079-011-0132-4.

204. Olabisi, R. M., Z. W. Lazard, C. L. Franco, et al. 2010. "Hydrogel microsphere encapsulation of a cell-based gene therapy system increases cell survival of injected cells, transgene expression, and bone volume in a model of heterotopic ossification." *Tissue Eng Part A* 16 (12):3727-36. DOI: 10.1089/ten.TEA.2010.0234.

205. Olsen, C. J., J. Moreira, E. M. Lukanidin, et al. 2010. "Human mammary fibroblasts stimulate invasion of breast cancer cells in a three-dimensional culture and increase stroma development in mouse xenografts." *BMC Cancer* 10:444. DOI: 10.1186/1471-2407-10-444.

206. Orimo, A., P. B. Gupta, D. C. Sgroi, et al. 2005. "Stromal fibroblasts present in invasive human breast carcinomas promote tumor growth and angiogenesis through elevated SDF-1/CXCL12 secretion." *Cell* 121 (3):335-48. DOI: 10.1016/j.cell.2005.02.034.

207. Oskarsson, T. 2013. "Extracellular matrix components in breast cancer progression and metastasis." *Breast* 22 Suppl 2:S66-72. DOI: 10.1016/j.breast.2013.07.012.

208. Ota, Hiroki, and Norihisa Miki. 2011. "Microfluidic experimental platform for producing size-controlled three-dimensional spheroids." *Sensors & Actuators: A. Physical* 169 (2):266-273. DOI: 10.1016/j.sna.2011.03.051.

209. Oudar, Olivier. 2000. "Spheroids: relation between tumour and endothelial cells." *Critical Reviews in Oncology/Hematology* 36 (2–3):99-106. DOI: http://dx.doi.org/10.1016/S1040-8428(00)00080-9.

210. Palumbo, J. S., and J. L. Degen. 2001. "Fibrinogen and tumor cell metastasis." *Haemostasis* 31 Suppl 1:11-5.

211. Pan, T., E. L. Fong, M. Martinez, et al. 2015. "Three-dimensional (3D) culture of bone-derived human 786-O renal cell carcinoma retains relevant clinical characteristics of bone metastases." *Cancer Letters* 365 (1):89-95. DOI: 10.1016/j.canlet.2015.05.019.

212. Peela, N., F. S. Sam, W. Christenson, et al. 2016. "A three dimensional micropatterned tumor model for breast cancer cell migration studies." *Biomaterials* 81:72-83. DOI: 10.1016/j.biomaterials.2015.11.039.

213. Peyton, S. R., P. D. Kim, C. M. Ghajar, et al. 2008. "The effects of matrix stiffness and RhoA on the phenotypic plasticity of smooth muscle cells in a 3-D biosynthetic hydrogel system." *Biomaterials* 29 (17):2597-607. DOI: 10.1016/j.biomaterials.2008.02.005.

214. Peyton, S. R., C. B. Raub, V. P. Keschrumrus, et al. 2006. "The use of poly(ethylene glycol) hydrogels to investigate the impact of ECM chemistry and mechanics on smooth muscle cells." *Biomaterials* 27 (28):4881-93. DOI: 10.1016/j.biomaterials.2006.05.012.

215. Phan-Lai, V., S. J. Florczyk, F. M. Kievit, et al. 2013. "Three-dimensional scaffolds to evaluate tumor associated fibroblast-mediated suppression of breast tumor specific T cells." *Biomacromolecules* 14 (5):1330-1337. DOI: 10.1021/bm301928u.

216. Pickl, M., and C. H. Ries. 2009. "Comparison of 3D and 2D tumor models reveals enhanced HER2 activation in 3D associated with an increased response to trastuzumab." *Oncogene* 28 (3):461-8. DOI: 10.1038/onc.2008.394.

217. Pienta, K. J., and D. S. Coffey. 1991. "Correlation of Nuclear Morphometry with Progression of Breast-Cancer." *Cancer* 68 (9):2012-2016. DOI: Doi 10.1002/1097-0142(19911101)68:9<2012::Aid-Cncr2820680928>3.0.Co;2-C.

218. Pietras, K., and A. Ostman. 2010. "Hallmarks of cancer: interactions with the tumor stroma." *Exp Cell Res* 316 (8):1324-31. DOI: 10.1016/j.yexcr.2010.02.045.

219. Pinto, M. P., W. W. Dye, B. M. Jacobsen, et al. 2014. "Malignant stroma increases luminal breast cancer cell proliferation and angiogenesis through platelet-derived growth factor signaling." *BMC Cancer* 14:735. DOI: 10.1186/1471-2407-14-735.

220. Plotkin, M., S. R. Vaibavi, A. J. Rufaihah, et al. 2014. "The effect of matrix stiffness of injectable hydrogels on the preservation of cardiac function after a heart attack." *Biomaterials* 35 (5):1429-38. DOI: 10.1016/j.biomaterials.2013.10.058.

221. Pradhan, S., C. S. Chaudhury, and E. A. Lipke. 2014. "Dual-phase, surface tension-based fabrication method for generation of tumor millibeads." *Langmuir* 30 (13):3817-3825. DOI: 10.1021/la500402m.

222. Provenzano, P. P., D. R. Inman, K. W. Eliceiri, et al. 2008. "Collagen density promotes mammary tumor initiation and progression." *BMC Medicine* 6:11. DOI: 10.1186/1741-7015-6-11.

223. Raeber, G. P., M. P. Lutolf, and J. A. Hubbell. 2005. "Molecularly engineered PEG hydrogels: a novel model system for proteolytically mediated cell migration." *Biophysical Journal* 89 (2):1374-1388. DOI: 10.1529/biophysj.104.050682.

224. Raghavan, S., R. A. Desai, Y. Kwon, et al. 2010. "Micropatterned dynamically adhesive substrates for cell migration." *Langmuir* 26 (22):17733-8. DOI: 10.1021/la102955m.

225. Raghavan, S., C. M. Nelson, J. D. Baranski, et al. 2010. "Geometrically controlled endothelial tubulogenesis in micropatterned gels." *Tissue Eng Part A* 16 (7):2255-63. DOI: 10.1089/ten.TEA.2009.0584.

226. Rainaldi, G., A. Calcabrini, G. Arancia, et al. 1999. "Differential expression of adhesion molecules (CD44, ICAM-1 and LFA-3) in cancer cells grown in monolayer or as multicellular spheroids." *Anticancer Res* 19 (3A):1769-78.

227. Raof, N. A., W. K. Raja, J. Castracane, et al. 2011. "Bioengineering embryonic stem cell microenvironments for exploring inhibitory effects on metastatic breast cancer cells." *Biomaterials* 32 (17):4130-4139. DOI: 10.1016/j.biomaterials.2011.02.035.

228. Räsänen, Kati, and Antti Vaheri. 2010. "Activation of fibroblasts in cancer stroma." *Experimental Cell Research* 316 (17):2713-2722. DOI: http://dx.doi.org/10.1016/j.yexcr.2010.04.032.

229. Ren, Yu Min, Bing Yu, Hai Lin Cong, et al. 2012. "Preparation of Monodisperse PEG Microspheres by a T-Junction Microfluidic Chip." *Advanced Materials Research* 465:178-181.

230. Revzin, A., R. J. Russell, V. K. Yadavalli, et al. 2001. "Fabrication of poly(ethylene glycol) hydrogel microstructures using photolithography." *Langmuir* 17 (18):5440-7.

231. Rhee, H. W., H. E. Zhau, and S. Pathak. 2001. "Permanent phenotypic and genotypic changes of prostate cancer cells cultured in a three-dimensional rotating-wall vessel." *In Vitro Cellular & Developmental Biology - Animal* 37:127-140.

232. Ricci, C., L. Moroni, and S. Danti. 2013. "Cancer tissue engineering-new perspectives in understanding the biology of solid tumours-a critical review." *OA Tissue Engineering* 1 (1):4.

233. Ricci, C., C. Mota, S. Moscato, et al. 2014. "Interfacing polymeric scaffolds with primary pancreatic ductal adenocarcinoma cells to develop 3D cancer models." *Biomatter* 4:e955386. DOI: 10.4161/21592527.2014.955386.

234. Rijal, G., and W. Li. 2016. "3D scaffolds in breast cancer research." *Biomaterials* 81:135-56. DOI: 10.1016/j.biomaterials.2015.12.016.

235. Roskoski, R., Jr. 2007. "Vascular endothelial growth factor (VEGF) signaling in tumor progression." *Crit Rev Oncol Hematol* 62 (3):179-213. DOI: 10.1016/j.critrevonc.2007.01.006.

236. Rybarczyk, B. J., and P. J. Simpson-Haidaris. 2000. "Fibrinogen assembly, secretion, and deposition into extracellular matrix by MCF-7 human breast carcinoma cells." *Cancer Research* 60 (7):2033-2039.

237. Sahni, A., and C. W. Francis. 2000. "Vascular endothelial growth factor binds to fibrinogen and fibrin and stimulates endothelial cell proliferation." *Blood* 96 (12):3772-8.

238. Sahni, A., P. J. Simpson-Haidaris, S. K. Sahni, et al. 2008. "Fibrinogen synthesized by cancer cells augments the proliferative effect of fibroblast growth factor-2 (FGF-2)." *J Thromb Haemost* 6 (1):176-83. DOI: 10.1111/j.1538-7836.2007.02808.x.

239. Sahoo, Sanjeeb K., Amulya K. Panda, and Vinod Labhasetwar. 2005. "Characterization of porous PLGA/PLA microparticles as a scaffold for three dimensional growth of breast cancer cells." *Biomacromolecules* 6 (2):1132-1139. DOI: 10.1021/bm0492632.

240. Sakai, S., S. Ito, and K. Kawakami. 2010. "Calcium alginate microcapsules with spherical liquid cores templated by gelatin microparticles for mass production of multicellular spheroids." *Acta Biomater* 6 (8):3132-7. DOI: 10.1016/j.actbio.2010.02.003.

241. Sakai, Shinji, Kazuya Inamoto, Yang Liu, et al. 2011. "Multicellular tumor spheroid formation in duplex microcapsules for analysis of chemosensitivity." *Cancer science*:2-7. DOI: 10.1111/j.1349-7006.2011.02187.x.

242. Samani, A., J. Zubovits, and D. Plewes. 2007. "Elastic moduli of normal and pathological human breast tissues: an inversion-technique-based investigation of 169 samples." *Phys Med Biol* 52 (6):1565-76. DOI: 10.1088/0031-9155/52/6/002.

243. Sant, S., M. J. Hancock, J. P. Donnelly, et al. 2010. "Biomimetic Gradient Hydrogels for Tissue Engineering." *Can J Chem Eng* 88 (6):899-911. DOI: 10.1002/cjce.20411.

244. Sapudom, J., S. Rubner, S. Martin, et al. 2015. "The phenotype of cancer cell invasion controlled by fibril diameter and pore size of 3D collagen networks." *Biomaterials* 52:367-375. DOI: 10.1016/j.biomaterials.2015.02.022.

245. Sasser, A. K., B. L. Mundy, K. M. Smith, et al. 2007. "Human bone marrow stromal cells enhance breast cancer cell growth rates in a cell line-dependent manner when evaluated in 3D tumor environments." *Cancer Lett* 254 (2):255-264. DOI: 10.1016/j.canlet.2007.03.012.

246. Schmidt, M. H., R. Broll, H. P. Bruch, et al. 2004. "Proliferation marker pKi-67 occurs in different isoforms with various cellular effects." *J Cell Biochem* 91 (6):1280-92. DOI: 10.1002/jcb.20016.

247. Schneider, B. P., and K. D. Miller. 2005. "Angiogenesis of breast cancer." *J Clin Oncol* 23 (8):1782-90. DOI: 10.1200/jco.2005.12.017.

248. Seib, F. P., J. E. Berry, Y. Shiozawa, et al. 2015. "Tissue engineering a surrogate niche for metastatic cancer cells." *Biomaterials* 51:313-319. DOI: 10.1016/j.biomaterials.2015.01.076.

249. Seo, B. R., P. DelNero, and C. Fischbach. 2014. "In vitro models of tumor vessels and matrix: Engineering approaches to investigate transport limitations and drug delivery in cancer." *Advanced Drug Delivery Reviews* 69:205-216. DOI: 10.1016/j.addr.2013.11.011.

250. She, Zhending, Chenrui Jin, Zhi Huang, et al. 2008. "Silk fibroin/chitosan scaffold: preparation, characterization, and culture with HepG2 cell." *Journal of Materials Science: Materials in Medicine* 19 (12):3545-3553. DOI: 10.1007/s10856-008-3526-y.

251. Shieh, Adrian C. 2011. "Biomechanical Forces Shape the Tumor Microenvironment." *Annals of Biomedical Engineering* 39 (5):1379-1389. DOI: 10.1007/s10439-011-0252-2.

252. Shweiki, D., M. Neeman, A. Itin, et al. 1995. "Induction of vascular endothelial growth factor expression by hypoxia and by glucose deficiency in multicell spheroids: implications for tumor angiogenesis." *Proceedings of the National Academy of Sciences of the United States of America* 92 (3):768-72.

253. Sieh, Shirly, Anna V. Taubenberger, Simone C. Rizzi, et al. 2012. "Phenotypic Characterization of Prostate Cancer LNCaP Cells Cultured within a Bioengineered Microenvironment." *PLoS ONE* 7 (9):e40217. DOI: 10.1371/journal.pone.0040217.

254. Simpson-Haidaris, P. J., and B. Rybarczyk. 2001. "Tumors and fibrinogen. The role of fibrinogen as an extracellular matrix protein." *Annals of the New York Academy of Sciences* 936:406-25.

255. Singh, S. P., M. P. Schwartz, J. Y. Lee, et al. 2014. "A peptide functionalized poly(ethylene glycol) (PEG) hydrogel for investigating the influence of biochemical and biophysical matrix properties on tumor cell migration." *Biomater Sci* 2 (7):1024-1034. DOI: 10.1039/C4BM00022F.

256. Smalley, K. S., M. Lioni, and M. Herlyn. 2006. "Life isn't flat: taking cancer biology to the next dimension." *In Vitro Cell Dev Biol Anim* 42 (8-9):242-7. DOI: 10.1290/0604027.1.

257. Smith, A. W., C. E. Segar, P. K. Nguyen, et al. 2012. "Long-term culture of HL-1 cardiomyocytes in modular poly(ethylene glycol) microsphere-based scaffolds crosslinked in the phase-separated state." *Acta Biomater* 8 (1):31-40. DOI: 10.1016/j.actbio.2011.08.021.

258. Smith, B. H., L. S. Gazda, B. L. Conn, et al. 2011. "Three-dimensional culture of mouse renal carcinoma cells in agarose macrobeads selects for a subpopulation of cells with cancer stem cell or cancer progenitor properties." *Cancer Research* 71 (3):716-724. DOI: 10.1158/0008-5472.CAN-10-2254.

259. Smith, B. H., L. S. Gazda, B. L. Conn, et al. 2011. "Hydrophilic agarose macrobead cultures select for outgrowth of carcinoma cell populations that can restrict tumor growth." *Cancer Research* 71 (3):725-735. DOI: 10.1158/0008-5472.CAN-10-2258.

260. Soman, Pranav, Jonathan A. Kelber, Jin Woo Lee, et al. 2012. "Cancer cell migration within 3D layer-by-layer microfabricated photocrosslinked PEG scaffolds with tunable

stiffness." *Biomaterials* 33 (29):7064-7070. DOI: http://dx.doi.org/10.1016/j.biomaterials.2012.06.012.

261. Soysal, S. D., A. Tzankov, and S. E. Muenst. 2015. "Role of the Tumor Microenvironment in Breast Cancer." *Pathobiology* 82 (3-4):142-52. DOI: 10.1159/000430499.

262. Staton, C. A., N. J. Brown, and C. E. Lewis. 2003. "The role of fibrinogen and related fragments in tumour angiogenesis and metastasis." *Expert Opin Biol Ther* 3 (7):1105-20. DOI: 10.1517/14712598.3.7.1105.

263. Stroock, Abraham D., and Claudia Fischbach. 2010. "Microfluidic culture models of tumor angiogenesis." *Tissue engineering. Part A* 16 (7):2143-2146. DOI: 10.1089/ten.TEA.2009.0689.

264. Subia, B., T. Dey, S. Sharma, et al. 2015. "Target specific delivery of anticancer drug in silk fibroin based 3D distribution model of bone-breast cancer cells." *ACS Appl Mater Interfaces* 7 (4):2269-2279. DOI: 10.1021/am506094c.

265. Subik, K., J. F. Lee, L. Baxter, et al. 2010. "The Expression Patterns of ER, PR, HER2, CK5/6, EGFR, Ki-67 and AR by Immunohistochemical Analysis in Breast Cancer Cell Lines." *Breast Cancer (Auckl)* 4:35-41.

266. Sung, K. E., and D. J. Beebe. 2014. "Microfluidic 3D models of cancer." *Adv Drug Deliv Rev* 79-80:68-78. DOI: 10.1016/j.addr.2014.07.002.

267. Sutherland, R. M., and R. E. Durand. 1984. "Growth and cellular characteristics of multicell spheroids." *Recent Results Cancer Res* 95:24-49.

268. Sutherland, R. M., J. A. Mccredie, and W. R. Inch. 1971. "Growth of Multicell Spheroids in Tissue Culture as a Model of Nodular Carcinomas." *Journal of the National Cancer Institute* 46 (1):113-&.

269. Szot, C. S., C. F. Buchanan, J. W. Freeman, et al. 2011a. "3D *in vitro* bioengineered tumors based on collagen I hydrogels." *Biomaterials* 32 (31):7905-7912. DOI: 10.1016/j.biomaterials.2011.07.001.

270. Szot, C. S., C. F. Buchanan, J. W. Freeman, et al. 2013. "In Vitro Angiogenesis Induced by Tumor-Endothelial Cell Co-Culture in Bilayered, Collagen I Hydrogel Bioengineered Tumors." *Tissue Engineering Part C Methods*. DOI: 10.1089/ten.TEC.2012.0684.

271. Szot, Christopher S., Cara F. Buchanan, Joseph W. Freeman, et al. 2011b. "3D in vitro bioengineered tumors based on collagen I hydrogels." *Biomaterials* 32 (31):7905-12. DOI: 10.1016/j.biomaterials.2011.07.001.

272. Talukdar, S., M. Mandal, D. W. Hutmacher, et al. 2011. "Engineered silk fibroin protein 3D matrices for in vitro tumor model." *Biomaterials* 32 (8):2149-2159. DOI: 10.1016/j.biomaterials.2010.11.052.

273. Tan, P. H., K. Z. Aung, S. L. Toh, et al. 2011. "Three-dimensional porous silk tumor constructs in the approximation of in vivo osteosarcoma physiology." *Biomaterials* 32 (26):6131-6137. DOI: 10.1016/j.biomaterials.2011.04.084.

274. Tan, W., and T. A. Desai. 2005. "Microscale multilayer cocultures for biomimetic blood vessels." *J Biomed Mater Res A* 72 (2):146-60. DOI: 10.1002/jbm.a.30182.

275. Tan, Y., A. Tajik, J. Chen, et al. 2014. "Matrix softness regulates plasticity of tumour-repopulating cells via H3K9 demethylation and Sox2 expression." *Nature Communications* 5:4619. DOI: 10.1038/ncomms5619.

276. Thao, T. T. V., C. Lim, and M. Lim. 2012. "Characterization of leukemic cell behaviors in a soft marrow mimetic alginate hydrogel." *Journal of Biomedical Materials Research Part B-Applied Biomaterials* 100b (7):1980-1988. DOI: 10.1002/jbm.b.32765.

277. Théry, Manuel. 2010. "Micropatterning as a tool to decipher cell morphogenesis and functions." *Journal of Cell Science* 123 (24):4201-4213.

278. Thouas, G. A., M. C. Thompson, K. G. Contreras, et al. 2008. "Improved oxygen diffusion and mechanical aggregation of tumor colonies in a novel stirred mini-bioreactor." *Conf Proc IEEE Eng Med Biol Soc* 2008:3586-9. DOI: 10.1109/iembs.2008.4649981.

279. Tibbitt, Mark W., and Kristi S. Anseth. 2009. "Hydrogels as extracellular matrix mimics for 3D cell culture." *Biotechnology and bioengineering* 103 (4):655-63. DOI: 10.1002/bit.22361.

280. Topley, P., D. C. Jenkins, E. a Jessup, et al. 1993. "Effect of reconstituted basement membrane components on the growth of a panel of human tumour cell lines in nude mice." *British journal of cancer* 67 (5):953-8.

281. Torisawa, Yu-suke, Airi Takagi, Yuji Nashimoto, et al. 2007. "A multicellular spheroid array to realize spheroid formation, culture, and viability assay on a chip." *Biomaterials* 28 (3):559-66. DOI: 10.1016/j.biomaterials.2006.08.054.

282. Torre, L. A., F. Bray, R. L. Siegel, et al. 2015. "Global cancer statistics, 2012." *CA Cancer J Clin* 65 (2):87-108. DOI: 10.3322/caac.21262.

283. Tsuda, Y., T. Shimizu, M. Yamato, et al. 2007. "Cellular control of tissue architectures using a three-dimensional tissue fabrication technique." *Biomaterials* 28 (33):4939-46. DOI: 10.1016/j.biomaterials.2007.08.002.

284. Ulrich, Theresa a, Amit Jain, Kandice Tanner, et al. 2010. "Probing cellular mechanobiology in three-dimensional culture with collagen-agarose matrices." *Biomaterials* 31 (7):1875-1884. DOI: 10.1016/j.biomaterials.2009.10.047.

285. Vantangoli, M. M., S. J. Madnick, S. M. Huse, et al. 2015. "MCF-7 Human Breast Cancer Cells Form Differentiated Microtissues in Scaffold-Free Hydrogels." *PLoS One* 10 (8):e0135426. DOI: 10.1371/journal.pone.0135426.

286. Verbridge, S. S., N. W. Choi, and Y. Zheng. 2010. "Oxygen-controlled three-dimensional cultures to analyze tumor angiogenesis." *Engineering Part A*.

287. Verbridge, Scott S., Emily M. Chandler, and Claudia Fischbach. 2010. Tissue-engineered three-dimensional tumor models to study tumor angiogenesis.

288. Wang, C., X. Tong, and F. Yang. 2014. "Bioengineered 3D brain tumor model to elucidate the effects of matrix stiffness on glioblastoma cell behavior using PEG-based hydrogels." *Molecular Pharmaceutics* 11 (7):2115-2125. DOI: 10.1021/mp5000828.

289. Wang, Ruoxiang, Jianchun Xu, Lisa Juliette, et al. 2005. "Three-dimensional co-culture models to study prostate cancer growth, progression, and metastasis to bone." *Seminars in cancer biology* 15 (5):353-64. DOI: 10.1016/j.semcancer.2005.05.005.

290. Weiss, Michael S., Beatriz Peñalver Bernabé, Ariella Shikanov, et al. 2012. "The impact of adhesion peptides within hydrogels on the phenotype and signaling of normal and cancerous mammary epithelial cells." *Biomaterials* 33 (13):3548-3559. DOI: http://dx.doi.org/10.1016/j.biomaterials.2012.01.055.

291. West, J. L. 2011. "Protein-patterned hydrogels: Customized cell microenvironments." *Nat Mater* 10 (10):727-9. DOI: 10.1038/nmat3132.

292. White, F. H., Y. Jin, and L. Yang. 1997. "An evaluation of the role of nuclear cytoplasmic ratios and nuclear volume densities as diagnostic indicators in metaplastic, dysplastic and neoplastic lesions of the human cheek." *Histology and Histopathology* 12 (1):69-77.

293. Wohl-Bruhn, S., A. Bertz, J. Kuntsche, et al. 2013. "Variations in polyethylene glycol brands and their influence on the preparation process of hydrogel microspheres." *Eur J Pharm Biopharm*. DOI: 10.1016/j.ejpb.2013.02.018.

294. Workman, V. L., L. B. Tezera, P. T. Elkington, et al. 2014. "Controlled Generation of Microspheres Incorporating Extracellular Matrix Fibrils for Three-Dimensional Cell Culture." *Advanced Functional Materials* 24 (18):2648-2657. DOI: 10.1002/adfm.201303891.

295. Wu, L. Y., D. Di Carlo, and L. P. Lee. 2008. "Microfluidic self-assembly of tumor spheroids for anticancer drug discovery." *Biomed Microdevices* 10 (2):197-202. DOI: 10.1007/s10544-007-9125-8.

296. Wu, M., M. Cao, Y. He, et al. 2015. "A novel role of low molecular weight hyaluronan in breast cancer metastasis." *FASEB Journal* 29 (4):1290-1298. DOI: 10.1096/fj.14-259978.

297. Wu, P. H., J. M. Phillip, S. B. Khatau, et al. 2015. "Evolution of cellular morpho-phenotypes in cancer metastasis." *Sci Rep* 5:18437. DOI: 10.1038/srep18437.

298. Xu, F., and K. J. Burg. 2007. "Three-dimensional polymeric systems for cancer cell studies." *Cytotechnology* 54 (3):135-143. DOI: 10.1007/s10616-007-9065-4.

299. Xu, R., M. B. Taskin, M. Rubert, et al. 2015. "hiPS-MSCs differentiation towards fibroblasts on a 3D ECM mimicking scaffold." *Sci Rep* 5:8480. DOI: 10.1038/srep08480.

300. Xu, X., L. A. Gurski, C. Zhang, et al. 2012. "Recreating the tumor microenvironment in a bilayer, hyaluronic acid hydrogel construct for the growth of prostate cancer spheroids." *Biomaterials* 33 (35):9049-9060. DOI: 10.1016/j.biomaterials.2012.08.061.

301. Xu, X., C. R. Sabanayagam, D. A. Harrington, et al. 2014. "A hydrogel-based tumor model for the evaluation of nanoparticle-based cancer therapeutics." *Biomaterials* 35 (10):3319-3330. DOI: 10.1016/j.biomaterials.2013.12.080.

302. Xu, X. X., C. Liu, Y. Liu, et al. 2014. "Enrichment of cancer stem cell-like cells by culture in alginate gel beads." *Journal of Biotechnology* 177:1-12. DOI: 10.1016/j.jbiotec.2014.02.016.

303. Yamada, K. M., and E. Cukierman. 2007. "Modeling tissue morphogenesis and cancer in 3D." *Cell* 130 (4):601-610. DOI: 10.1016/j.cell.2007.08.006.

304. Yang, X., S. K. Sarvestani, S. Moeinzadeh, et al. 2013a. "Effect of CD44 binding peptide conjugated to an engineered inert matrix on maintenance of breast cancer stem cells and tumorsphere formation." *PLoS One* 8 (3):e59147. DOI: 10.1371/journal.pone.0059147.

305. Yang, X., S. K. Sarvestani, S. Moeinzadeh, et al. 2013b. "Three-dimensional-engineered matrix to study cancer stem cells and tumorsphere formation: effect of matrix modulus." *Tissue Eng Part A* 19 (5-6):669-84. DOI: 10.1089/ten.TEA.2012.0333.

306. Yeung, T. M., S. C. Gandhi, J. L. Wilding, et al. 2010. "Cancer stem cells from colorectal cancer-derived cell lines." *Proceedings of the National Academy of Sciences of the United States of America* 107 (8):3722-3727. DOI: 10.1073/pnas.0915135107.

307. Yonet-Tanyeri, N., M. H. Rich, M. Lee, et al. 2013. "The spatiotemporal control of erosion and molecular release from micropatterned poly(ethylene glycol)-based hydrogel." *Biomaterials* 34 (33):8416-23. DOI: 10.1016/j.biomaterials.2013.07.026.

308. Yoshii, Yukie, Atsuo Waki, Kaori Yoshida, et al. 2011. "The use of nanoimprinted scaffolds as 3D culture models to facilitate spontaneous tumor cell migration and well-regulated spheroid formation." *Biomaterials* 32 (26):6052-8. DOI: 10.1016/j.biomaterials.2011.04.076.

309. Yu, Linfen, Michael C. W. Chen, and Karen C. Cheung. 2010. "Droplet-based microfluidic system for multicellular tumor spheroid formation and anticancer drug testing." *Lab on a chip* 10 (18):2424-32. DOI: 10.1039/c004590j.

310. Yu, Xinzi, and Laura M. Machesky. 2012. "Cells assemble invadopodia-like structures and invade into matrigel in a matrix metalloprotease dependent manner in the circular invasion assay." *PloS one* 7 (2):e30605-e30605. DOI: 10.1371/journal.pone.0030605.

311. Yuhas, J. M., and A. P. Li. 1978. "Growth fraction as the major determinant of multicellular tumor spheroid growth rates." *Cancer Research* 38 (6):1528-1528.

312. Zaytseva-Zotova, Daria S., Olga O. Udartseva, Elena R. Andreeva, et al. 2011. "Polyelectrolyte microcapsules with entrapped multicellular tumor spheroids as a novel tool to study the effects of photodynamic therapy." *Journal of biomedical materials research. Part B, Applied biomaterials* 97 (2):255-62. DOI: 10.1002/jbm.b.31808.

313. Zhang, Xulang Xiaohui, Wei Wang, Weiting Yu, et al. 2005. "Development of an in vitro multicellular tumor spheroid model using microencapsulation and its application in anticancer drug screening and testing." *Biotechnology Progress* 21 (4):1289-1296. DOI: 10.1021/bp050003l.

314. Zheng, C., L. Zhao, G. Chen, et al. 2012. "Quantitative study of the dynamic tumor-endothelial cell interactions through an integrated microfluidic coculture system." *Anal Chem* 84 (4):2088-93. DOI: 10.1021/ac2032029.

315. Zhu, J. 2010. "Bioactive modification of poly(ethylene glycol) hydrogels for tissue engineering." *Biomaterials* 31 (17):4639-4656. DOI: 10.1016/j.biomaterials.2010.02.044.

316. Zhu, J., L. Liang, Y. Jiao, et al. 2015. "Enhanced invasion of metastatic cancer cells via extracellular matrix interface." *PLoS One* 10 (2):e0118058. DOI: 10.1371/journal.pone.0118058.

317. Zhu, W., M. Wang, Y. Fu, et al. 2015. "Engineering a biomimetic three-dimensional nanostructured bone model for breast cancer bone metastasis study." *Acta Biomater* 14:164-74. DOI: 10.1016/j.actbio.2014.12.008.

318. Zhu, Xin Hao, Lai Yeng Lee, Jie Sheng Hong Jackson, et al. 2008. "Characterization of porous poly(D,L-lactic-co-glycolic acid) sponges fabricated by supercritical CO2 gas-foaming method as a scaffold for three-dimensional growth of Hep3B cells." *Biotechnology and Bioengineering* 100 (5):998-1009. DOI: 10.1002/bit.21824.

319. Zustiak, S. P., and J. B. Leach. 2010. "Hydrolytically degradable poly(ethylene glycol) hydrogel scaffolds with tunable degradation and mechanical properties." *Biomacromolecules* 11 (5):1348-1357. DOI: 10.1021/bm100137q.